THE POTENTIAL MOLECULAR MECHANISMS OF VARIOUS TREATMENT COMBINATIONS BETWEEN CISPLATIN, CANNABIDIOL, CANNABIS EXTRACTS, AND INTERMITTENT SERUM STARVATION ON COLORECTAL CANCER CELL LINES

VIKTORIIA CHERKASOVA
Medical Doctor, Ivano-Frankivsk State Medical University, 2008

A thesis submitted
in partial fulfilment of the requirements for the degree of

DOCTOR OF PHILOSOPHY

in

BIOMOLECULAR SCIENCES

Department of Biological Sciences
University of Lethbridge
LETHBRIDGE, ALBERTA, CANADA

THE POTENTIAL MOLECULAR MECHANISMS OF VARIOUS TREATMENT COMBINATIONS BETWEEN CISPLATIN, CANNABIDIOL, CANNABIS EXTRACTS, AND INTERMITTENT SERUM STARVATION ON COLORECTAL CANCER CELL LINES

VIKTORIIA CHERKASOVA

Date of defence: April 20, 2023

Dr. I. Kovalchuk	Professor	M.D., Ph.D.
Dr. O. Kovalchuk	Professor	M.D., Ph.D
Thesis Co-Supervisors		
Dr. R. Golsteyn	Professor	Ph.D.
Thesis Examination Committee Member		
Dr. N. Thakor	Associate Professor	Ph.D.
Thesis Examination Committee Member		
Dr. R. McDonald	Professor	Ph.D.
Internal External Examiner		
Dr. P. Bose	Professor	Ph.D.
External Examine		
Dr. R. Laird	Professor	Ph.D.
Chair, Thesis Examination Committee		

DEDICATION

I dedicate this thesis to my wonderful parents, who fought cancer with high dignity and unimaginable bravery. And to my beloved husband, who always supported me in this journey with patience, care, and love.

ABSTRACT

Colorectal cancer is the third most common cancer worldwide. The mortality rates remain high despite the wide variety of multiple preventive and treatment options.

Platinum-derived chemotherapy medications are often combined with other conventional therapies for treating different tumors, including colorectal cancer. However, the development of drug resistance and multiple adverse effects remain common in clinical settings. Thus, there is a necessity to find novel treatments and drug combinations that could effectively target colorectal cancer cells without affecting normal tissues and lower the probability of disease relapse.

To find potential synergistic interaction, I tried multiple different combinations between cisplatin, cannabidiol, cannabis extracts, and intermittent serum starvation on colorectal cancer cell lines. Based on the cell viability assay, we found that combinations between cannabidiol and intermittent serum starvation, cisplatin and intermittent serum starvation, as well as cisplatin, cannabidiol and intermittent serum starvation, can work in a synergistic fashion on different colorectal cancer cell lines. I analyzed differentially expressed genes and affected pathways in two colorectal cancer cell lines to further understand the potential molecular mechanisms behind the treatments and their interactions.

ACKNOWLEDGEMENTS

I would like to express my sincerest gratitude to my thesis supervisor Dr. Igor Kovalchuk for providing me with this remarkable opportunity to complete my Ph.D. degree. This work would not be possible without his constant guidance, knowledge, and tremendous encouragement. His mentorship has greatly aided me during experiments and in writing this thesis.

I would like to extend my appreciation to Dr. Olga Kovalchuk for her great support and guidance in understanding cancer biology. I would also like to thank my committee members, Dr. Roy Golsteyn and Dr. Thakor Nehalkumar, for their support, insightful comments, and challenging questions that helped me to explore my research from different perspectives. Dr. Golsteyn, your advice and guidance greatly impacted my work. Dr. Thakor, thank you for always providing me with knowledge and practical advice.

I would like to thank Dr. Yaroslav Ilnytskyy for the bioinformatic analysis of my data. Many thanks to Dr. Bo Wang, Dr. Dongping Li, and Dr. Andrey Golubov for numerous advice and suggestions. I appreciate your time and effort. Many thanks to my lab mates Rommy Rodriguez Juarez and Rocio Rodriguez Juarez for providing me with technical support.

I thank the funding agency MITACS and InPlanta Biotechnology Inc. for the financial support and the possibility of working with cannabinoid extracts.

TABLE OF CONTENTS

LIST OF TABLES

LIST OF FIGURES

LIST OF ABBREVIATIONS

ABCA1 – ATP binding subfamily A member 1
ABL1 – ABL proto-oncogene 1
ACADM – Medium-chain acyl-CoA dehydrogenase
ACFcf – Aberrant cryptic foci
ADAM – A disintegrin and metalloproteinase with thrombospondin motif
AEA – Anandamide
AHRR – Aryl hydrocarbon receptor repressor
AKT – Protein kinase B
ALK – ALK receptor tyrosine kinase
AMP – Adenosine monophosphate
AMPK – AMP protein kinase
ANGPT2 – Angiopoietin 2
ANGPTL4 – Angiopoietin-like 4
AOM - Azoxymethane
APC – Adenomatosis polyposis coli
AREG - Amphiregulin
ATF – Activating transcription factor
ATM – Ataxia telangiectasia mutated
ATP – Adenosine triphosphate
ATR – Ataxia telangiectasia and Rad3-related
AURKB – Aurora B kinase
BAD – Bcl2-associated agonist of cell death
BAX – Bcl2-associated X
BCL2 – B-cell CLL/lymphoma 2
BCRP – Breast cancer resistance protein
BDNF – Brain-derived neurotrophic factor
BER – Base excision repair
BHLHE40 - Basic helix-loop-helix family member E40
BIP – Binding immunoglobulin protein
BLM – Bloom syndrome RecQ helicase
BMP4 – Bone morphogenic protein 4
BRAF – V-Raf murine sarcoma viral oncogene homolog B1
BTC - Betaleucin
BTG – B-cell translocation gene
BUB1 – Budding uninhibited by benzimidazoles 1
CACac – Colitis-associated cancer
CAPN8 – Caspase 8
CARD – Caspase recruitment domain-containing protein 5
CARS – Cysteinyl-tRNA sythetase
CB1 – Cannabinoid receptor 1
CB13 - N-cyclopentyl-7-methyl-1-(2-morpholin-4-ylethyl)-1,8-naphthyridin-4(1H)-on-3-carboxamide
CB1R – Cannabinoid receptor 1
CB2 – Cannabinoid receptor 2
CBD – Cannabidiol

CBGA – Cannabigerolic Acid
CBN - Cannabinol
CBR – Cannabinoid Receptor
CCNB1 – Cyclin B1
CCNB2 – Cyclin B2
CCND3 – Cyclin D3
CCNE2 – Cyclin E2
CD22 – Cluster Differentiation 22
CD8 – Cluster Differentiation 8
CDC20 – Cell Division Cycle 20
CDC25A - Cell Division Cycle 25a
CDH11 – Cadherin 11
CDK – Cyclin-Dependent Kinase
CDKN1A - Cyclin-Dependent Kinase Inhibitor 1 A
CDKN1C - Cyclin-Dependent Kinase Inhibitor 1 C
CEACAM1 – CEA Cell Adhesion Molecule 1
CEBPA – CCAAT Enhancer Binding Protein Alpha
CHD4 – Chromodomain Helicase DNA Binding Protein 4
CHEK2 – Checkpoint Kinase 2
CHK1 – Checkpoint Kinase 1
CHK2 – Checkpoint Kinase 2
CHOP – C/EBP Homologous Protein
CHUK – Component Of Inhibitor Of NFkB
CI – Combination Index
CIN – Chromosomal Instability
CLASP1 – Cytoplasmic Linker Associated Protein 1
CLIP1 – Cap-Gly Domain Containing Linker Protein 1
CLTC – Clathrin Heavy Chain
CNOT3 – CCR4-Not Transcription Complex Subunit 3
CNTRL - Centriolin
COL13A1 – Collagen Type XIII Alpha 1 Chain
COL1A1 – Collagen Type I Alpha 1 Chain
COL3A1 – Collagen Type III Alpha 1 Chain
COL4A3 – Collagen Type IV Alpha 3 Chain
COL5A2 – Collagen Type V Alpha 2 Chain
COX - Cyclooxygenase
CRC – Colorectal Cancer
CREB1 – cAMP Responsive Binding Protein 1
CREBBP – CREB Binding Protein
CRK – CT10 Regulator Of Kinase
CRKL – Crk-Like Protein
CSF – Colony Stimulating Factor
CTNNB1 – Catenin Beta 1
CTSK – Cathepsin K
CUX1 – Cut Like Homeobox 1
CXCR4 – CXC Motif Chemokine Receptor 4

CYP1A1 – Cytochrome P450 Family 1 Subfamily A Member 1
DAD – Defender Against Cell Death
DAF – Decay Accelerating Factor
DCTN1 – Dynactin Subunit 1
DDR2 – Discoidin Domain Receptor Tyrosine Kinase 2
DEG – Differentially Expressed Genes
DICER1 – Dicer Ribonuclease III
DMSO – Dimethyl Sulfoxide
DNM2 – Dynamin 2
DNM3 – Dynamin 3
DR4 – Death Receptor 4
DR5 – Death Receptor 5
DRI – Dose Reduction Index
DROSHA – Double-Stranded RNA-Specific Endoribonuclease III
DUSP – Dual Specific Phosphatase
E2F1 – E2F Transcription Factor 1
EBF1 – EBF Transcription Factor 1
EBP – EBP Cholestenol Delta-Isomerase
ECM – Extracellular Matrix
ECS – Endocannabinoid System
EFEMP2 – EGF Containing Fibulin Extracellular Matrix Protein 2
EGF – Epidermal Growth Factor
EGFR – Epidermal Growth Factor Receptor
EML4 – Emap Like 4
EMT – Epithelial To Mesenchymal Transition
ER – Endoplasmic Reticulum
ERBB – Erythroblastic Leukemia Viral Oncogene Homolog
ERCC5 – Ercc Excision Repair 5 Endonuclease
EREG - Epiregulin
ERK – Extracellular Regulated Kinase
EZH2 – Enhancer Of Zeste Polycomb Repressive Complex 2 Subunit
FAAH – Fatty Acid Amid Hydrolase
FANCC – Fanconi Anemia Complementation Group C
FAS – Fas Cell Surface Death Receptor
FAT1 – Fat Atypical Cadherin 1
FBLN2 – Fibulin 2
FBN1 – Fibrillin 1
FBS – Fetal Bovine Serum
FBXO11 – F-Box Protein 11
FCGR2B – Fc Gamma Receptor Iib
FGF – Fibroblast Growth Factor
FGFR1 – Fibroblast Growth Factor Receptor 1
FLIP – Flice-Inhibitory Protein
FLT3 – Fms Related Receptor Tyrosine Kinase 3
FN1 – Fibronectin 1Fos – Fos Proto-Oncogene

FOSL1 – Fos Like 1
FOXO3 – Forkhead Box O3
FOXP1 – Forkhead Box P1
FZD8 – Frizzled Class Receptor 8
GAB1 – Grb2 Associated Binding Protein 1
GADD34 – Growth Arrest And Dna-Damage Growth Inducible Protein 34
GADD45 - Growth Arrest And Dna-Damage Growth Inducible Protein 45
GAPDH – Glyceraldehyde 3-Phosphate Dehydrogenase
GATA2 – Gata Binding Protein 2
GBP2 – Guanylate Binding Protein 2
GEF – Guanine Nucleotide Exchange Factor
GIT – Gastro-Intestinal Tract
GNAQ – G Protein Subunit Alpha 2
GNAS – Gnas Complex Locus
GOLGA5 – Golgin A5
GPCR– G Protein-Coupled Receptor
GPHN - Gephyrin
GPI - Glucose-6-Phosphate Isomerase
GPR119 – G-Protein Coupled Receptor 119
GRB2 – Growth Factor Receptor Bound Protein 2
GSH - Glutathione
GTP – Guanine Triphosphate
HBEGF – Heparin Binding Egf Like Growth Factor
HER – Human Epidermal Growth Factor Receptor 2
HIF1 – Hypoxia-Inducible Factor 1
HK2 – Hexokinase 2
HLA – Human Leukocyte Antigen
HMGCS1 – 3-Hydroxy-3-Methylglutaryl-Coa Synthase 1
HOXD11 – Homeobox D11
HT1 – Histamine Receptor 1
IAP – Inhibitor O Apoptosis
IBD – Inflammatory Bowel Diseases
ICAM – Intracellular Adhesion Molecule
ICMT – Isoprenylcysteine Carboxyl Methyltransferase
ID2 – Inhibitor Of Dna Binding 2
IDH1 – Isocitrate Dehydrogenase 1
IF– Intermittent Fasting
IFIT1 – Interferon-Induced Protein With Tetratricopeptide Repeats 1
IFN - Interferon
IFNAR1 – Interferon Alpha And Beta Receptor Subunit 1
IFNGR1 – Interferon Gamma Receptor 1
IGF – Insulin Growth Factor
IGFBP3 - Insulin-Like Growth Factor Binding Protein 3
IKK – I Kappa B Kinase
IL - Interleukin
IL1RAP – Interleukin 1 Receptor Accessory Protein

IL21R – Interleukin 21 Receptor
INPP5D – Inositol Polyphosphate-5-Phosphatase D
IRE1 – Inositol-Requiring Enzyme 1
ISS – Intermittent Serum Starvation
ITGA1 – Integrin Subunit Alpha 1
JAK – Janus Kinase
JNK – C-Jun N-Terminal Kinase
JUN – Jun Proto-Oncogene
KAT6B – Lysine Acetyltransferase 6b
KDM5A – Lysine Demethylase 5a
KEGG – Kyoto Encyclopedia Of Genes
KIF5b – Kinesin Family Member 5b
KMT2C – Lysine Methyltransferase 2c
KRAS – K-Ras Proto-Oncogene, GTPase
KSR2 – Kinase Suppressor Of Ras 2
KTN1- Kinectin 1
LAMA2 – Laminin Subunit Alpha 2
LAMA4 – Laminin Subunit Alpha 4
LAMB3 – Laminin Subunit Beta 3
LAMC1 – Laminin Subunit Gamma 1
LAMC2 – Laminin Subunit Gamma 2
LCK – Lck Proto-Oncogene, Src Family Tyrosine Kinase
LEF – Lymphoid Enhancer Factor
LOXl2 – Lysyl Oxidase Like 2
LPP – Lim Domain Containing Preferred Translocation Partner In Lipoma
LPS – Lipopolysaccharide
LRP1B – LDL Receptor Related Protein 1b
LTBP3 – Latent Transforming Growth Factor Beta Binding Protein 3
MAD2l1 – Mitotic Arrest Deficient 2 Like 1
MAGL – Monoacylglycerol Lipase
MAP2K1 – Mitogen-Activated Protein Kinase Kinase 1
MAP3K1 - Mitogen-Activated Protein Kinase Kinase Kinase 1
MAP3K8 - Mitogen-Activated Protein Kinase 1
MAPK – Mitogen-Activated Protein Kinase
MCM – Minichromosome Maintenance Complex
MDM2 – Mdm2 Proto-Oncogene
MEK1 – Map2k1
MEN1 – Multiple Endocrine Neoplasia Type 1
MHC – Major Histocompatibility Complex
MITF– Melanocyte Inducing Transcription Factor
MKK4 – Map2k4
MLH1 – Mutl Homolog 1
MMP – Matrix Metalloproteinase
MMR – Mismatch Repair
MN1 – Mn1 Proto-Oncogene
MRX – Mre11, Rad50, And Xrs2 Complex

MSH2 – Muts Homolog 2
MSH6 – Muts Homolog 6
MSI – Microsatellite Instability
MSN – Moesin
MTOR – Mammalian Target Of Rapamycin
MTORC1 – Mammalian Target Of Rapamycin Complex 1
MX1 – Mx Dynamin Like Gtpase
MYH11 – Myosin Heave Chain 11
MYO5A – Myosin 5a
MYOD1 – Myogenic Differentiation 1
NAB2 – Ngfi-A Binding Protein 1
NAPE-PLD – N-Acetylphosphatidylethanolamine Phospholipase D
NCOA1 – Nuclear Receptor Coactivator 1
NCOR1 – Nuclear Receptor Corepressor 1
NDRG1 – N-Myc Downstream Regulated 1
NF1 – Neurofibromin 1
NFATC2 – Nuclear Factor Of Activated T Cell 2
NFIL3 – Nuclear Factor Interleukin 3 Regulated
NFKB2 – Nuclear Factor Kappa B Subunit 2
NFKIAB - Nuclear Factor Kappa B Inhibitor Alpha
NGF – Nerve Growth Factor
NIK – NFkB-Inducing Kinase
NK – Natural Killer
NLR – Nod-Like Receptor
NOD1 – Nucleotide Binding Oligomerization Domain Containing 1
NOS3 – No Synthase 3
NOTCH1 – Notch Receptor 1
NR1D1 – Nuclear Receptor Subfamily 1 Group D Member 1
NRAS – Neuroblastoma Ras
NRF – Nuclear Respiratory Factor
NRG1 – Neuregulin 1
NSD3 – Nuclear Receptor Binding Set Domain Protein 3
NTN4 – Netrin 4
NTRK1 – Neurotrophic Receptor Tyrosine Kinase 1
NUF2 – Nuf2 Component Of Ndc80 Kinetochore Complex
OAS1 – 2’ – 5’ -Oligoadenylate Synthetase 1
OASl – 2’ – 5’ -Oligoadenylate Synthetase Like
P4HA1 – Prolyl 4-Hydroxylase Subunit Alpha 1
PAK1 – P21 (Rac1) Activated Kinase 1
PARP – Poly(Adp-Ribose) Polymerase 1
PAX3 – Paired Box 2
PBX1 – Pbx Homeobox 1
PCM1 – Pericentriolar Material 1
PCNA – Proliferating Cell Nuclear Antigen
PCR – Polymerase Chain Reaction
PDE4DIP – Phosphodiesterase 4d Interacting Protein

PDGF – Platelet-Derived Growth Factor
PDGFA – Platelet Derived Growth Factor Subunit A
PDGFRB - Platelet Derived Growth Factor Receptor Beta
PDK1 – Pyruvate Dehydrogenase Kinase 1
PEA - Palmitoylethanolamide
PER1 – Period Circadian Regulator 1
PERK – Protein Kinase Rna-Like Er Kinase
PERP – P53 Apoptosis Effector Related To Pmp22
PFKFB4 – 6-Phosphofructo-2-Kinase/Fructose-2, 6-Biphosphatase 4
PGE2 – Prostaglandin E2
PI3K – Phosphatidylinositol 3-Kinase
PICALM – Phosphatidylinositol Binding Clathrin Assembly Protein
PIK3AP1 – Phosphoinositide-3-Kinase Adaptor Protein 1
PIK3CA – Phosphatidylinositol-4, 5-Bisphosphate 3-Kinase Catalytic Subunit Alpha
PIK3R3 – Phosphoinositide-3-Kinase Regulatory Subunit 3
PIM – Pim-1 Proto-Oncogene, Serine/Threonine Kinase
PKB – Protein Kinase B
PKC – Protein Kinase C
PLC – Phospholipase C
PLCG1 - Phospholipase C Gamma 1
PLK1 – Polo Like Kinase 1
PLOD1 – Procollagen-Lysine, 2-Oxoglutarate 5-Dioxygenase 1
PMAIP1 – Phorbol-12-Myristate-13-Acetate-Induced Protein 1
PMP22 – Peripheral Myelin Protein 22
POLQ – DNA Polymerase Theta
PPAR – Peroxisome Proliferator Activated Receptor
PPFIA4 – PTRF Interacting Protein Alpha 4
PPFIBP1 – PPFIA Binding Protein 1
PPP2R1A – Protein Phosphatase 2 Scaffold Subunit Alpha
PRCC – Proline Rich Mitotic Checkpoint Control Factor
PRDM1 – Pr/Set Domain 1
PREX2 - Phosphatidylinositol-3,4,5-Trisphosphate Dependent Rac Exchange Factor 2
PRKACA - Protein Kinase Camp-Activated Catalytic Subunit Alpha
PRKCA – Protein Kinase C Alpha
PSEN – Presenilin
PSMB10 – Proteasome 20s Subunit Beta 10
PSMB9 – Proteasome 20s Subunit Beta 9
PTCH1 – Patched 1
PTEN – Phosphatase And Tensin Homolog
PTK6 – Protein Tyrosine Kinase 6
PTPRB – Protein Tyrosine Phosphatase Receptor Type B
PTPRT – Protein Tyrosine Phosphatase Receptor Type T
PUMA – P53 Upregulated Modulator Of Apoptosis
RAC1 – Rac Family Small Gtpase 1
RAD21 – Rad21 Cohesin Complex Component
RAF – Raf-1 Proto-Oncogene, Serine/Threonine Kinase

RASGRP1 – Ras Guanyl Releasing Protein 1
RFC – Replication Factor C
RGCC – Regulator Of Cell Cycle
RIT1 – Ras Like Without Caax 1
RNA – Ribonucleic Acid
RNF43 – Ring Finger Protein 43
ROS – Reactive Oxygen Species
RPA – Replication Protein A
RPL5 – Ribosomal Protein L5
RPS27L – Ribosomal Protein S27 Like
RUNX1 – Runx Family Transcription Factor 1
RUNX1T1 – Runx Partner Transcriptional Co-Repressor 1
RXR – Retinoid X Receptor Alpha
SALL4 – Splat-Like Transcription Factor 4
SAPK – Stress-Activated Protein Kinase
SDC1 – Syndecan 1
SERPINE1 – Serpin Family E Member 1
SESN1 – Sestrin 1
SETBP1 – Set Binding Protein 1
SETD2 – Set Domain Containing 2, Histone Lysine Methyltransferase
SFN - Stratifin
SLC34A2 – Solute Carrier Family 34 Member 2
SLC45A3 – Solute Carrier Family 45 Member 3
SMAD – Mothers Against Decapentaplegic Homolog
SMO – Smoothened, Frizzled Class Receptor
SNAIL1 – Snail Family Transcriptional Repressor 1
SND1 – Staphylococcal Nuclease And Tudor Domain Containing 1
SNF – Swi/Snf Complex
SOD – Superoxide Dismutase
SOX – Sry-Box Transcription Factor
SPEN – Spen Family Transcriptional Repressor
SPOCK3 – Sparc (Osteonectin), CWCV and Kazal Like Domains Proteoglycan 3
SRF – Serum Response Factor
SRI - Sorcin
SS18 – Ss18 Subunit Of Baf Chromatin Remodeling Complex
SS18L1 – Ss18l1 Subunit Of Baf Chromatin Remodeling Complex
STAT – Signal Transducer And Activator Of Transcription
STIL – Stil Centriolar Assembly Protein
STK11 – Serine/Threonine Kinase 11
SUFU – Sufu Negative Regulator Of Hedgehog Signaling
TACE – Tumor Necrosis Factor Alpha Converting Enzyme
TCF – Transcription Factor
TCFZl2 – T-Cell Factor/Lymphoid Enhancer Factor 2
TENT5c – Terminal Nucleotidyltransferase 5c
TGF – Transforming Growth Factor
THBS1 – Thrombospondin 1

THC – Tetrahydrocannabinol
THCA – Tetrahydrocannabinolic Acid
TIAM – T-Cell Lymphoma Invasion And Metastasis
TLL1 – Tolloid-Like 1
TLR – Toll-Like Receptor
TNF – Tumor Necrosis Factor
TNFAIP3 – TNF Alpha Induced Protein 3
TNFR – TNF Receptor
TNFRSF10C – TNF Receptor Superfamily Member 10c
TNFRSF1B – TNF Receptor Superfamily Member 1b
TP53 – Tumor Protein P53
TP53I3 – Tp53 Inducible Protein 3
TP53INP1 – Tp53 Inducible Nuclear Protein 1
TP63 – Tumor Protein 63
TPR– Translocated Promoter Region, Nuclear Basket Protein
TRAF6 – Tnf Receptor Associated Factor 6
TRAIL – Tumor Necrosis Factor-Related Apoptosis-Inducing Ligand
TRIAP – Tp53 Induced Nuclear Protein 1
TRIB1 – Tribbles Pseudokinase 1
TRIB3 – Tribbles Pseudokinase 3
TRIM24 – Tripartite Motif Containing 24
TRIP11 – Thyroid Hormone Receptor Interactor 11
TRP– Transient Receptor Ion Channels
TRPA1 – Transient Receptor Potential Cation Channel Subfamily A Member 1
TRPM8 – Transient Receptor Potential Cation Channel Subfamily M Member 8
TRPV1 – Transient Receptor Potential Cation Channel Subfamily V Member 1
TRPV2 – Transient Receptor Potential Cation Channel Subfamily V Member 2
TRRAP – Transformation/Transcription Domain Associated Protein
TRVP2 – Transient Receptor Potential Vanilloid 2
TSC1 – Tuberous Sclerosis 1 Protein
TSHR – Thyroid Stimulating Hormone Receptor
U2AF1 – U2 Small Nuclear RNA Auxiliary Factor 1
UBE2l6 – Ubiquitin Conjugating Enzyme E2 L6
UBR5 – Ubiquitin Protein Ligase E3 Component N-Recognin 5
UPR – Unfolded Protein Response
USP28 – Ubiquitin Specific Peptidase 28
VDAC – Voltage Dependent Anion Channel
VEGF – Vascular Endothelial Growth Factor
VGF– Vgf Nerve Growth Factor Inducible
WNT – Wingless/Integrated
WRN– Wrn Recq Like Helicase
XIAP – X-Linked Inhibitor of Apoptosis
XPC – Xeroderma Pigmentosum, Complementation Group C
ZFHX3 – Zinc Finger Homeobox 3
ZMYM2 – Zinc Finger Mym-Type Containing 2
ZNF331 – Zinc Finger Protein 331

CHAPTER 1: THE EFFECTS OF CISPLATIN, CANNABIDIOL AND INTERMITTENT SERUM STARVATION ON COLORECTAL CANCER CELL LINES

1.1. Introduction

This part was mainly described in our review article by Cherkasova et al. (2020).

1.1.1. Epidemiological data and molecular mechanisms of CRC

Statistical data

According to the Canadian Cancer Society, cancer is Canada's leading cause of death. Researchers estimated that there would be 233,900 new cancer cases in Canada and 85,100 cancer-related deaths in 2022. More than 220,000 new cases were recorded in 2019, with lung, breast, colon, and prostate cancers as the most common (1). Colorectal cancer (CRC) is the third leading cancer worldwide in men and women, with a 5-year survival rate of 67% (2). About one million individuals are newly diagnosed with CRC each year (3). It is estimated that disease-related mortality in developed countries is around 33% (4). Most sporadic cases occur in patients over 50, with 75% occurring in those over 60. The lifetime risk of developing CRC is 3–4% in Western populations; however, the risk is doubled if there is a family history of CRC (5).

CRC is not a single disease but a group of molecularly heterogeneous pathologies with standard features primarily affecting the colorectal region (4). The "classic" steps in CRC "evolution" start from a polyp or aberrant cryptic foci (ACF) developing into an early adenoma (<1 cm) followed by a late adenoma (>1 cm), eventually transforming into adenocarcinoma, which takes around 10–15 years to develop (4). The conventional adenoma-to-carcinoma model proposed by Fearon and Vogelstein (1990) was one of the first to explain the step-by-step processes of CRC development and is true for about 60–65% of colon cancers (5). In this model, the primary initiation of the mutation is the downregulation of the APC gene leading to an overgrowth of intestinal epithelial cells and the formation of colon adenomas. Further development in the model consists of mutations and epimutations in KRAS and NRAS, affecting the mitogen-activated protein kinase (MAPK) pathway; then SMAD4 or SMAD6 genes, affecting the phosphoinositil-3-kinase (PI3K) pathway; and finally, downregulation of "guardian of the genome" p53, causing adenocarcinoma to progress (5).

Molecular mechanisms of CRC development

Despite a wide variety of conventional chemotherapy for CRC patients, the tumor eventually becomes drug-resistant in many cases, and treatments are ineffective. Another crucial limitation of CRC therapy is that these tumors are a genetically heterogeneous group of oncological pathology (6). In 2014, four consensus molecular subtypes (CMSs) of CRC have been

developed based on genetic alterations affecting colonic epithelium: CMS1 - microsatellite instability (MSI) immune (CpG island methylation phenotype, and BRAF mutation associated with immune cell infiltrates); CMS2 - canonical (WNT and MAPK associated, characterized by high proliferation); CMS3 - metabolic (KRAS associated); and CMS4 - mesenchymal (somatic copy number alteration of TGF-β associated with stromal invasion and angiogenesis) (7,8). Therefore, there is no "best" drug for CRC treatment, and different therapeutic approaches should be undertaken based on the stage, subtype, and the pathogenesis of CRC (6,9,10).

There is also so-called colitis-associated cancer (CAC) (12), which develops in 20% of inflammatory bowel disease (IBD) patients approximately after 30 years of disease onset (11)(12). Despite considerable similarities in the pathogenesis of CAC and “classical” CRC, some differences remain. A persistent chronic inflammatory response in IBDs with increased levels of TNF, IL-17, IL-23, IFN-γ, and IL-6 due to the activation of NFkB and STAT3 can lead to the formation of ACFs and adenomas. Moreover, continuous activation of COX-2 increases KRAS signalling and promotes tumor survival, progression, and metastatic potential (13–15). Increased levels of PGE2, which is produced from arachidonic acid, and protein kinase B (AKT) signalling increase produced from arachidonic acid, and protein kinase B (AKT) signalling increased intranuclear levels of transcription factor β-catenin that stimulate the proliferation of enterocytes (16,17). Activating genetic alterations leading to nuclear accumulation of β-catenin (TCFZL2, FZD8, AX1N1) is seen in 41% of these neoplasms (18). Additionally, in intestinal adenomas, there areis a higher TGF-β receptor (19,20). In many CRC tumors, there are infiltrations of natural killers, neutrophils, dendritic cells, and macrophages (21). A vital difference between CAC and “classical” CRC is the infiltration in the intestinal wall, with T-cells that react with tumour-specific antigens in the classical type. However, in CAC, many T-cells are reactive against intestinal microflora. That is why, in CACs, CD8+ cells can stimulate tumor proliferation with their cytokines (15). In this case, the immuno-suppressive effect of cannabinoids may have a protective role against cancer development and progression.

Despite the multiple preventive measures, screening procedures, and a wide variety of treatment options, CRC holds one of the most significant positions in world disease and mortality rates. The development of novel, more effective preventive measures and treatment approaches isare critically needed, and based on recent experimental data, cannabinoids could potentially become good candidates (22–30).

1.1.2. Cancer and cannabinoids

For many centuries, cannabis plants have been used empirically to treat different diseases, including cancer (31). Cannabinoids are commonly used as a treatment for insomnia, as an appetite stimulator or as an antinociceptive agent to alleviate chemo- and radiotherapy-induced nausea and vomiting (11). Since cannabinoids regulate CB1 expression, reduce the motility of the GI tract, and decrease proinflammatory mediators, they could potentially become one of the treatments for IBDs (30,32–34). Presently, there is broad scientific support regarding cannabinoid cytotoxicity in intestinal malignancies (22,26,35–37). Some experiments indicated a higher potency of whole-plant extracts rich in phytocannabinoids, such as cannabidiol (CBD), over purified cannabinoids (38). Cannabinoids may reduce colonic polyp formation and intestinal inflammation and reduce cancer cells growth via cannabinoid 1 (CB1), cannabinoid 2 (CB2) receptors, transient receptor potential cation channel subfamily V member 1 (TRPV1) receptors, and G-coupled protein receptor 55 (GPR55) (22,30,37,39–45). The mechanisms of anticancer effects of cannabinoids include the activation of apoptosis, endoplasmic reticulum (ER) stress response, downregulation of survivin (inhibitor of apoptosis), a decrease of RAS/MAPK and PI3K/AKT signalling (22,26,35,37,40). Despite the multiple possibilities of clinical applications for cannabinoids, there are data regarding the anticancer effects of cannabinoid compounds in case reports (37–39).

Classes of cannabinoids

Currently, there are three main known classes of cannabinoids: endocannabinoids present in the human body, phytocannabinoids extracted from the cannabis plant, and synthetic cannabinoids (31). To accomplish their action, cannabinoids mainly bind to seven transmembrane $G_{i/o}$-coupled receptors (GPCRs), usually the inhibitory type (31,49,50). When cannabinoids bind to CB1 or CB2 receptors, there is a decrease in cyclic adenosine monophosphate (cAMP) and expression of adenylate cyclase (49,50). CB1 and CB2 receptors share only 44% of the protein homology and 68% in the transmembrane domains with binding sites for cannabinoids (51).

In *in situ* receptor/G protein reconstruction techniques, the activation of CB1 receptors results in high-affinity interactions with both G_i and G_o, whereas CB2 activation results in high-affinity interaction with G_o (52). Ionic channels are placed in the membrane as multimeric complexes that form passage pathways for selected molecules triggered by mechanical or chemical signals. Cannabinoids can stimulate A-type potassium channels, which causes an increased efflux of potassium from the cell. Moreover, by binding to CB1 receptors, cannabinoids may inhibit N-

and P/Q-types of voltage-dependent calcium channels and activate inwardly, rectifying potassium channels, which results in decreased calcium influx and increased potassium efflux from the cells (53–57). The ionic channels that respond to cannabinoids are transient receptor ion channels (TRPs), such as TRPV1, TRPV2, TRPM8, and TRPA1 (54–58). In addition to CB1 and CB2, multiple other receptors may respond to cannabinoids (49). The most studied receptors are GPR119, GPR55, peroxisome proliferating activated receptor α (PPAR α), and PPAR γ (44,58,59).

The endocannabinoid system

The endocannabinoid system (ECS) includes CB receptors, cannabinoid enzymes, and endocannabinoids. Endocannabinoids are mostly represented by arachidonoyl ethanolamine, or anandamide (AEA), and 2-arachidonoylglycerol (2-AG), which are derivatives of membrane phospholipids (31,49) and are produced by multiple pathways. Thus, inhibiting enzymes that participate in their synthesis will not always result in changes in endocannabinoid levels and may affect the amounts of other cell mediators (60,61). Endocannabinoids are synthesized from the cell membrane's phospholipids on demand due to the intracellular calcium elevation. Both endocannabinoids, AEA and 2-AG, signal through GPCRs, ion channels (TRPs), and nuclear receptors (PPARs) (62). PPARs are the subfamily receptors that act with retinoic X receptors of the nuclear hormone receptor superfamily, regulating the expression of target genes by binding to peroxisome proliferator response elements in the genes (63).

1.1.3. Cannabinoids in the gastrointestinal tract

Both types of CB receptors are present within the gut but with various expression levels and different distribution in epithelial cells, lamina propria, smooth muscle cells, and enteric nervous plexuses. Importantly, the expression of cannabinoid receptors and endocannabinoid system vary in whether tissue is intact or diseased (64).

In the gastrointestinal tract (GIT), the CB1 receptors are mainly present in excitatory motor neurons, interneurons, and intrinsic primary afferent neurons (65). Additionally, the endocannabinoid system takes part in neuronal proliferation, differentiation, axon guidance, and synaptogenesis in many organs in embryonic and early postnatal periods, including large intestines (66). On the contrary, CB2 receptors are expressed by subepithelial immune cells such as macrophages and plasma cells, while they are usually absent in normal epithelial cells of the intestinal mucosa (67). Interestingly, the CB1 expression is higher in the epithelial cells of the

crypts, goblet cells, and absorptive cells of the apical surface. The CB2 are expressed at the higher levels in Paneth cells (64). Another study showed that both CB1 and CB2 receptors are highly expressed in enteric nervous plexuses, especially myenteric and submucosal (68). Additionally, endocannabinoids AEA, acylethanolamide, and OEA are ligands for TRVP1 receptors (69). The highest density of TRVP1 is in myenteric plexus and interganglionic fibers (70).

GIT maintains the endogenous regulation of the ECS according to its needs (71). Endocannabinoids AEA and 2-AG are synthesized on demand from membrane lipids by intracellular calcium influx (72). ECS plays an essential role in maintaining the GIT homeostatic function by ECS maintaining epithelial integrity, interactions with gut microbiota (73), and suppresses chronic stress-induced visceral hyperalgesia (74). Typically, 2-AG and palmitoylethanolamide (PEA) - another endocannabinoid - are the "gatekeepers" of the intestines. Their actions are achieved by increasing intestinal barrier functions. On the other hand, AEA can work as a "gate opener" (73) that increases intestinal permeability.

1.1.4. Changes in the cannabinoid system in CRC

Intact enterocytes express CB1 receptors; however, during intestinal inflammation or carcinogenesis, levels of CB1 receptors progressively decrease due to CpG island hypermethylation of the *CB1R* promoter's transcription sites (67). In contrast, CB2 receptors expression increases, which in some cases is associated with poor prognosis of CRC patients (67). Wang et al. (2009) performed experiments on 10 CRC cell lines (HCT-116, HT-29, LS-174T, SW-480, Colo-201, DLD-1, Caco-2, HCT-15, HCA-7, LoVo) showed that HCT-116, HT-29, and LS-174T have low CB1 expression. In the SW-480 cell line or normal colon tissues, there was no CB1 receptor change. Additionally, CB1 receptor loss was indicated in 8 out of 13 human tumor samples, showing that in human biopsies of the second and third grade of CRC, there was a loss of expression of CB1 receptors, often via CpG island promoter hypermethylation (26). The transcriptome analysis of 566 CRC patients showed a reduction of CB1 expression in the TNM-I stage. However, with the disease's progression, CB1 expression was again elevated. In contrast, GPR55 expression decreased with disease progression compared to healthy colon samples (45). Moreover, CpG methylation of the CB1 promoter site was hypomethylated in most healthy intestinal tissues and CRC patients – a cohort of 86 (45). These findings suggest that translational regulation of miRNAs may be the critical point of CB1 receptor expression changes in CRC patients (45). Additionally, CB1-deficient APC-mutated mice had 2.5–3.8-fold elevated polyp

formation compared to the control mice (75). However, the deletion of CB2 receptors did not significantly affect the formation of preneoplastic intestinal lesions in animal models (75). The DLD-1 CRC xenograft model had higher CB2 levels of expression, and treatment with CB2 agonist such as N-cyclopentyl-7-methyl-1-(2-morpholin-4-ylethyl)-1,8-naphthyridin-4(1H)-on-3-carboxamide (CB13) significantly decreased tumors in size (188).

The study provided by Tutino et al. (2019), which involved samples from 59 CRC patients, showed low expression of CB1 receptors in primary tumors and adjacent mucosa, especially in those with diagnosed metastatic disease. In metastatic CRC, downregulation of CB1 expression was associated with decreased p38/MAPK and ERK1/2 signalling in both tumor tissue and adjacent normal mucosa. Additionally, there was significant upregulation of the pro-survival AKT pathway in the same samples, especially in the surrounding tumor tissues that were intact. Moreover, patients with metastatic disease had significantly lower levels of Bcl-2-associated-X protein (BAX), which is responsible for the stimulation of apoptosis (27).

Some studies showed that CB receptor expression changes play a pro-cancer role in colon carcinogenesis (78–80). Analyses of CRC samples (both tumor front and interior) for CB1 expression from 487 patients that underwent surgical resection showed that the levels of CB1 presence are associated with tumor grade. Additionally, the authors suggested that high CB1 expression is associated with poorer prognosis in stage II microsatellite stable tumors (79). The data comparison set included gender, tumor site, radiotherapy, stage, tumor differentiation, type, microsatellite stability, lymphocyte infiltration, and frequency of tumor aggregates at the invasion front. Surprisingly, the significant differences associated with CB1 receptor expression were histological tumor grade and microsatellite stability. In both tumor front and center samples, the CB1 receptor expression was higher in patients with moderate-poorly/poorly differentiated microsatellite-stable CRCs (79). One of the explanations for the relationship between poor patients' prognosis and high CB1 expression was proposed by studies on glioblastoma cell lines (80). This study suggested that at low levels of expression, CB receptors are mainly coupled with ERK, thus, their activation caused apoptosis. It was also shown that high CB1 expression could cause additional AKT signalling activation that switches proapoptotic signalling to survival mechanisms. Endocannabinoid levels could protect intestinal mucosa from damage; however, they may also exacerbate cancer cell survival (79). Thus, alterations in CB receptor expression can be used as a prognostic marker in different molecular subtypes of CRC.

The data provided by Hasenoehrl et al. (2018) showed that cannabinoid receptor GPR55 activation has pro-cancer effects by stimulating tumor invasiveness and promoting metastatic potential (45). Moreover, there is evidence that blocking GPR55 with CBD activates MAPK/p53 signalling and stimulates ERK1/2, which can cause apoptotic cell death (81). GPR55 is a Gα12/13 and Gq lysophosphatidylinositol type of receptor, stimulating proliferation, invasion, and angiogenesis of cancer cells (82,83). GPR55 can activate a cascade of reactions involving calcium mobilization (84), ERK1/2 phosphorylation (85), adhesion, and migration of colon cancer cells that may lead to liver metastasis (86). Besides cancer cells, GPR55 is expressed by macrophages, neutrophils, and lymphocytes (82,87,88).

The research performed by Raup-Konsavage et al. (2018) showed the sensitivity of different molecular subtypes of CRC cell lines (SW480, SW620, HT-29, DLD-1, HCT-116, LS-174T, RKO) to 370 different cannabinoid compounds (25). It was found that cell lines SW480, SW620, HT-29, and DLD-1 had APC mutations and HCT-116 and LS-174T had activating mutations in CTNNB1, the β-catenin encoding gene. SW620 is derived from lymph metastases. The identified synthetic cannabinoids that suppressed CRC cell viability most effectively were – HU-331; CP 55,940; 5-epi-CP 55,940; CP 47,497; 3-epi-CP 47,497 C-8 Homolog; CP 47,497 C-8 Homolog; PTI-1; PTI2; and NPB-22. The selected compounds did not work through canonical signalling, including CB1, CB2, GPR55, and TRPV1 (25). The most significant result was the cell lines with APC mutations (SW480, HT-29, DLD-1). They were more sensitive to CBD than the cells mutated in the β-catenin pathway (HCT-116, LS-174T) (25). These results suggest that various molecular subtypes of CRC may react differently to cannabinoid treatment and that the antitumor action of cannabinoid compounds is not always CB1- or GPR55-dependent.

Because of the high variety of receptors that are involved in cannabinoid effects on cancers, we did not prioritize the action of specific receptors on tested colorectal cancer cell lines. In this work, we focused more on the effects of treatment combinations on colorectal cancer cell lines with different genetic landscapes. However, to better understand the pathways affected, the next step would be to evaluate the expression and activation of various cannabinoid receptors under the chosen most effective treatments.

1.1.5. Molecular mechanisms of anti-CRC effects of cannabinoids

Over the recent years, multiple experimental data have provided evidence of the antioncogenic impact of cannabinoids on CRC (35,76,78,89–91). Phytocannabinoids reduce CRC

cell growth by multiple mechanisms of action (35,71,76,91,92), which are discussed in this subsection (Figure 1).

Ceramide is a neutral lipid backbone of complex sphingolipids. Its *de novo* synthesis can be activated by chemotherapy, ionizing radiation, and enzyme sphingomyelinase. Ceramide action is specific to its carbon chain lengths (93,94). Ceramide can trigger apoptosis and inhibit cancer cell proliferation by causing cell cycle arrest. It can also activate autophagy in cancer cells. The main pathways in ceramide interaction are protein phosphatase 2A, p38/MAPK, JNK, AKT, protein kinase C, and survivin (95). Some cancers upregulate ceramide-degrading enzymes to avoid death or even promote mutagenicity (95).

One of the best-explained anticancer mechanisms of cannabinoids is activating the *de novo* synthesis of ceramide via CB receptor activation (76,96). Due to the intensive synthesis of ceramide, the production of ROS is enhanced, leading to the ER stress response. Next, ER stress-related signalling events may cause CRC cell death. First, eukaryotic translation initiation factor 2α (eIF2α) is downregulated, decreasing the global translation of proteins. Simultaneously, the C/EBP homology protein (CHOP) is activated. It acts on pseudokinase tribbles-homologue 3 (TRIB3), which stimulates the release of proapoptotic BAD and BAX proteins (97). Moreover, AKT is downregulated by CHOP. AKT inhibition causes major intracellular changes, such as the downregulation of the mammalian target of rapamycin (mTOR) and the activation of autophagy. In addition, AKT can directly activate caspase 3 and caspase 9 and stimulate G1 cell cycle arrest through cyclin-dependent kinase inhibitors, such as p21 and p27. The anti-tumor mechanism of cannabinoids also involves the upregulation of AMP protein kinase (AMPK), which, along with low mTOR, strongly stimulates the macroautophagy of CRC cells (35,36,76,81,98–100).

Cianchi et al. (2008) performed a study regarding CB receptor expression in human specimens (24 samples of primary sporadic adenocarcinoma and adjacent tissues), DLD-1, and HT-29 CRC cell lines, which showed CB1 expression mainly in normal colonic epithelial tissue samples (76). In addition, the tumor tissues highly expressed CB2 receptors. The activation of CB1 by the synthetic agonist arachinodyl-2'-chloroethylamide and the CB2 agonist CB13 caused the stimulation of apoptosis by *de novo* ceramide synthesis in intestinal cancer cells. This study also showed that TNF-α connects CB receptor activation and ceramide synthesis in CRC cell lines, which activate apoptosis. CB1 receptor activation elevates intracellular ceramide levels via sphingomyelin hydrolysis by coupling with factors associated with neutral sphingomyelinase

activation that bind to TNF receptors, resulting in sphingomyelin breakdown and ceramide *de novo* production (76,101). This signalling is antiproliferative and proapoptotic to CRCs (76).

Chen et al. investigated the connection between cannabinoid signalling and ceramide. They described the profiles of the main endocannabinoids AEA and 2-AG, ceramides, free fatty acids, and the critical enzymes of cannabinoid metabolism in 47 pairs of human CRC samples and adjacent non-cancerous tissues (90). Results showed that AEA and its metabolite, arachidonic acid, are elevated in CRC tissues and are mainly associated with lymphatic node metastases. In the CRC samples, the ceramide levels have different expression patterns, with elevated C16 and C24 and decreased C18 and C20. In addition, the mRNA levels of NAPE-PLD, FAAH, and ceramide synthases, such as CerS2, CerS5, and CerS6, are higher in cancer tissues (90). Other experiments have shown that C16 and C24 ceramides promote apoptosis of CRC cells (102,103). In summary, elevated levels of AEA, ceramides, and CB1 receptors have been shown to have protective effects against colon carcinogenesis (90).

In CRCs, the RAS-MAPK pathway is overactivated, with KRAS and BRAF being overexpressed in approximately 50% and 15% of cases (104,105). PI3K/AKT signalling is upregulated in almost 40% of colon malignancies (106). This makes these pathways relevant in our research due to their changes in CRC and the fact that they are affected by the action of cannabinoids.

In 2007, Greenhough et al. (2007) reported that *in vitro* THC-treated adenoma (AA/C1, AN/C1, BH/C1, RG/C2, AAC1/SB/10C) and CRC (SW480, HCT-15, HT-29, Caco2, HCT-116, LS-174t, SW620, and JW2) cell lines induce apoptosis via proapoptotic BAD activation by its dephosphorylation on serine 112 and 136 (35). These effects are achieved by inhibiting the major cancer survival pathways—RAS/MAPK, ERK1/2, and PI3K/AKT via CB1 receptor activation (35). However, THC does not affect p38/MAPK and JNK signalling (35). The provided data showed that the induction of CB1, but not CB2 receptors, by THC can result in CRC cell death (35). On the contrary, glioblastoma and lung carcinoma cell line treatment with nanomolar concentrations of THC may even promote cancer cell growth, which depends on metalloproteinase and EGFR activity. EGFR receptor signalling is the mechanistic link with cannabinoid receptors. It can activate the pro-survival AKT pathway via the shedding of pro-amphiregulin and pro-heparin-binding epidermal growth factor-like growth factor by the TNF-α converting enzyme TACE/ADAM17. The experimental results showed that THC leads to the phosphorylation of

EGFR, the phosphorylation of adaptor protein Src homology 2 domain-containing, and the subsequent activation of ERK1/2 and AKT/PKB pathways. EGFR transactivation with CB1/2 receptors requires EGFR tyrosine kinase and metalloproteinase activity. As a result, higher THC concentrations can induce apoptosis in multiple cell lines, although THC can accelerate cancer cell progression in nanomolar concentrations (107).

CBD is a partial agonist of CB1 and CB2 receptors (108,109); it stimulates TRPV1, TRVP2, 5-HT1A, and PPARγ, inhibits GPR55, and increases endogenous AEA concentration by blocking its hydrolysis (110). One of the best-described anticancer effects of CBD is the activation of NOXA, suppressing mTOR/AKT signalling and MAPK pathways (91). Recent studies on HCT-116 and DLD-1 CRC cell lines indicated that CBD could induce apoptosis via the significant upregulation of NOXA-ROS signalling (91). ROS can induce ER stress by triggering unfolded protein response (UPR) (111,112). The ER stress can stimulate UPR to restore protein homeostasis. UPR is guided by the signalling proteins inositol-requiring protein-1α (IRE1α), protein kinase RNA-like ER kinase (PERK) and activating transcription factor 6 (ATF6). Usually, PERK and ATF6 are kept inactive by binding to the binding immunoglobulin protein (BIP) chaperone. IRE1α is activated directly under unfolded proteins and then starts to accumulate. When UPR is activated, all three proteins are signalled to increase the levels of chaperones, decrease translation, and transport misfolded proteins back into the cytosol for ubiquitination and subsequent degradation (112). In CBD-treated CRC cells, the expression of the stress-related ER gene is decreased, with further activation of NOXA (91). Activating transcription factor 3 (ATF3) and ATF4 may be involved in CHOP and NOXA stimulation (113). Adding CBD stimulates ER response, resulting in ATF3 and ATF4 binding directly to the ATF/cAMP response element in the NOXA and CHOP promoter region (91). As a result, NOXA migration into mitochondria causes the release of cytochrome c, the further activation of caspase 3, caspase 8, and caspase 9; the cleavage of PARP, and the initiation of apoptosis in CRC *in vivo* and *in vitro* models (91). In addition, CBD may enhance the phosphorylation of p38 stress protein kinase, eventually leading to apoptosis (92).

The combination of CBD with TNF-related inducing apoptosis ligand (TRAIL) causes a synergistic effect of the two molecules on CRC *in vivo*. CBD treatment activates ER stress response with CHOP release and phosphorylated protein kinase RNA-like ER kinase (PERK). In addition, CBD stimulates the expression of molecules responsible for the extrinsic apoptotic

pathway by stimulating DR5 expression. The addition of 4 μM CBD to 10 ng/mL TRAIL potentiates the effect of TRAIL by sensitizing CRC cells to undergo TRAIL-induced apoptosis in a xenograft mouse model (114). Moreover, CBD suppresses the expression of apoptosis (IAPs) inhibitors c-FLIP and survivin (114). IAPs are a group of antiapoptotic molecules that suppress caspase activity (115). One of the IAPs, survivin, is overexpressed in merely every tested tumor and may serve as a promising target molecule for CRC treatment (116). CBD may exhibit a protective role against CRC by stimulating CB1 receptors, which causes the inhibition of cAMP-dependent protein kinase. This process leads to the reduction of the cdc2 (Wee1/cdc25C-cdc2 cascade), which leads to the destabilization of survivin, the activation of caspase 3, and apoptosis (26). These findings show that cannabinoids can become efficient preventive agents in canonical molecular subtypes of CRCs (26).

Extracellular vesicles are classified into exosomes, microvesicles, and apoptotic bodies (117). Exosomes and microvesicles mediate intercellular communications by carrying molecules from parental cells to recipient cells. These lipid-bilayer vesicles can affect the physiology of cancer cells' migration, differentiation, and angiogenesis (118–120). The vesicular release is regulated by membrane receptors, apoptotic signals, and intracellular calcium release (121). It was shown that apoptotic bodies could transfer oncogenes horizontally, resulting in cancer cell survival (122). Thus, tumor-derived exosomes prepare a pre-metastatic niche in specific organs (123). Kosgodage et al. (2018) showed that CBD could inhibit cancer-derived extracellular vesicle release in a dose-dependent fashion. The effect is associated with alterations in mitochondrial functions, the modulation of STAT3 signalling, and changes in prohibitin expression (124). As a result, CBD may sensitize cancer cells to chemotherapy drugs by altering the biogenesis of extracellular vesicles (124).

Autophagy is the self-consumption mechanism that eliminates intracellular waste, attenuates stressful factors, and exhibits anti-carcinogenic effects (125). One of the conventional chemotherapy drugs used in CRCs is oxaliplatin, which causes the formation of DNA crosslinks, usually between guanines and guanine-adenine, effectively killing cancer cells (126). However, 40% of patients with CRC may develop resistance to it (127). Jeong et al. (2019) showed that CBD could overcome oxaliplatin resistance by activating autophagy and inhibiting superoxide dismutase 2, a main antioxidant enzyme within a cell (128). Moreover, the authors observed decreased phosphorylation of nitric oxide synthase 3 (NOS3), resulting in reduced NO and ROS

production (128). The study suggested that NOS3 phosphorylation is indispensable for developing oxaliplatin resistance. Oxaliplatin resistance can be overcome by adding CBD to the treatment, which results in autophagy-mediated cell death and the formation of free radicals by dysfunctional mitochondria in resistant cells (128). Combined CBD treatment with oxaliplatin causes the activation of the microtubule-associated protein 1A/1B light chain 3B and the increased expression of p63 (128). These markers are commonly used to assess autophagy (129). In addition, the combination of CBD and oxaliplatin decreases the number of mitochondria in the resistant cells and reduces the levels of cardiolipin and NADH dehydrogenase 1α subcomplex subunit 9 (mitochondrial complex I), resulting in abnormal oxidative phosphorylation and autophagy-mediated cancer cell death (128). This data was one of the reasons why we decided to combine platinum drug cisplatin with cannabinoids. Other studies regarding drug resistance and cannabinoids indicated that THC, CBD, and CBN could inhibit ATP-binding cassette family transporters, P-glycoprotein, and the breast cancer resistance protein (BCRP) (130), resulting in the potential chemosensitizing effect of cannabinoids in resistant CRCs (131–133).

Cannabinoids can inhibit the invasion and metastasis of cancer cells by downregulating vascular endothelial growth factor (VEGF), matrix metalloproteinase 2 (MMP2), MMP9, and the adhesion molecule E-cadherin (134). In a xenograft and AOM model of colon carcinogenesis, Pagano et al. (2017) showed that 2-AG and MAGL, a serine hydrolase that degrades 2-AG, are highly expressed in aggressive colon cancers. The inhibition of MAGL by URB602 decreases xenograft tumor volume by downregulating VEGF and fibroblast growth factor-2 (FGF-2). This study has shown that 2-AG exerts an anti-tumor effect on colon cancer via the inhibition of angiogenesis (VEGF) and cell proliferation (cyclin D1). Moreover, in a mouse AOM model of colon carcinogenesis, URB602 attenuates the formation of preneoplastic lesions, such as polyps, thus supporting the chemopreventive role of endocannabinoid 2-AG in CRC (134). The *in vitro* experiments provide evidence that 17β-estradiol stimulates CB1 expression via the activation of the estrogen receptors ERα and ERβ in the primary tumor CRC cell lines DLD-1 and HT-29 and the lymph node metastatic cell line SW620. The authors suggested the antiproliferative effect of estrogens on primary and metastatic CRCs via interaction with polyamine and growth factors in the tumor (134,260).

In another study, the strong antiangiogenic effect of the cannabinoid-like compound LYR-8 was demonstrated on a xenograft model using chorioallantoic chick membranes. The mechanism

behind cannabinoid action is the suppression of VEGF, COX-2, and hypoxia-inducible factor α (HIF α) (136). One of the synthetic cannabinoids, HU-311, a quinone of CBD, shows antiangiogenic effects by stimulating apoptosis in endothelial cells and inhibiting topoisomerase II (137). Some experiments have also demonstrated that 12 μM CBD may induce the migration of HUVECs. CBD inhibits MMP 2, MMP 9, and tissue inhibitor of metalloproteinase 1, which results in the suppression of cell motility and the invasion of endothelial cells; also, CBD inhibits urokinase-type plasminogen activator (uPA) and serpin E1/plasminogen activator inhibitor 1, which are involved in the degradation of the extracellular matrix and contribute to cancer cell invasiveness. Moreover, CBD downregulates HIF1α in U87 cells, which suggests the suppression of cell survival, motility, and angiogenesis (138); endothelin 1, PDGF-A (139); and the reduction of STAT5-induced vasorelaxation (138,140). In addition, the antimetastatic action of CB receptor agonists have been shown on SW480 cell lines. AEA, HU-210 (non-selective CB agonists), and docosatetraenoylethanolamide (CB1 selective agonist) suppress the norepinephrine-induced migration of human CRC cells (77,141).

Overall, we observe a tremendous variety of the anti-cancer mechanisms of cannabinoids in different tumors. It was one of the reasons why we looked at the mRNA expression in CRC cell lines to better understand the entire picture of cannabinoids' antiproliferative effects. Despite the existence of substantial data on anticancer effect of cannabinoids in preclinical studies, we decided to test combination of cannabinoids with conventional chemotherapeutics such as cisplatin. The rationale behind it would be the insufficient clinical data regarding cannabinoid action on CRC and no data on combination of the treatment with chemotherapy drugs. Moreover, clinical protocols involve platinum drugs for multiple cancer treatments and many patients ingest cannabis for symptom relief. It would be relevant to test if cannabinoids may affect the action of platinum medications in a synergistic or antagonistic way.

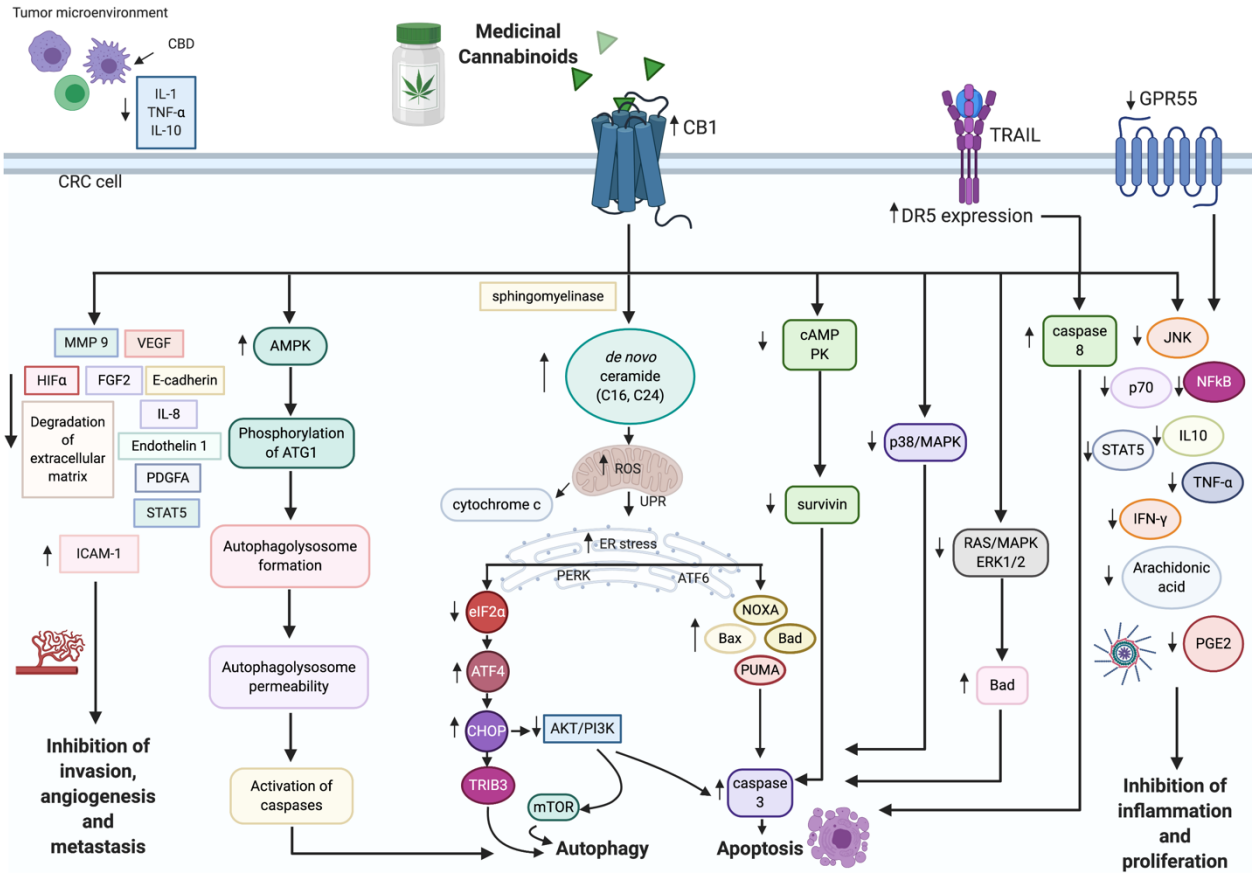

Figure 1. The effects of cannabinoids on colorectal cancer. See text for discussion. Created with BioRender.com

Abbreviations: AMPK – AMP kinase; ATF4 – activated transcription factor 4; AKT – protein kinase B; CBR – cannabinoid receptor; cdc2 – cell division control 2; cAMP PK – cyclic AMP protein kinase; CBD – cannabidiol; CHOP – C/EBP homologous protein; DR5 – death receptor 5; eIF2α – eukaryotic initiation factor 2α; ERK1/2 – extracellular regulated kinase 1/2; FGF2 – fibroblast growth factor 2; GPR55 – G protein coupled receptor 55; HIF α – hypoxia inducible factor α; ICAM-1 – intercellular adhesion molecule 1; IFN-γ – interferon γ; IL-1 – interleukin 1; IL-8 – interleukin 8; IL-10 – interleukin 10; MAPK – mitogen-activated protein kinase; MMP 9 – matrix metalloproteinase 9; STAT-5 – signal transducer and activator of transcription 5; mTOR – mammalian target of rapamycin; PDGFA – platelet-derived growth factor A; PGE2 – prostaglandin 2; PI3K – phosphoinositide-3 kinase; TNF-α – tumor necrosis factor α; TRAIL – Tumor necrosis factor-related apoptosis-inducing ligand; TRIB3 – tribbles homolog 3; VEGF – vascular endothelial growth factor.

1.1.6. Cisplatin in cancer therapy

Mechanism of cisplatin's action

The potential application of cisplatin (cis-dichlorodiammineplatinum II) as a chemotherapy agent arose when Rosenberg et al., 1965 (142) observed that the products of platinum mesh electrodes inhibited the growth of *E. coli.* FDA first approved cisplatin in 1978 (143) then, it has shown effectiveness in fighting different types of cancer, including cancers of the ovaries, testes, head and neck cancers, sarcomas, CRC, and many other types of tumors (144). Cisplatin is used in multiple combination therapies with paclitaxel, tegafur-uracil, doxorubicin, gemcitabine, and vitamin D (145). Unfortunately, any chemotherapy, including cisplatin, has a narrow therapeutic window and multiple adverse effects. The main side effects of cisplatin are nephrotoxicity, nausea, and vomiting (146,147).

The cytotoxic effects of cisplatin start once it enters the cell. Water molecules substitute the chloride ions from cisplatin. Next, the formed electrophile reacts with sulfhydryl groups on proteins and nitrogen donor atoms on nucleic acids, which leads to DNA crosslinks of purine bases with cisplatin causing DNA damage and apoptosis (144).

Cancer cells are adapted to higher oxidative stress conditions due to increased metabolism and mitochondrial dysfunction. Cisplatin induces oxidative stress mainly in mitochondria, causing membrane potential reduction (148). The formation of ROS under cisplatin treatment depends on intracellular redox homeostasis maintained by thiol group (-SH) molecules. Under cisplatin exposure, a thiol group can form thiyl radicals that interact with molecular oxygen and produce ROS, which consequently causes apoptosis (149). In low intracellular concentrations of Cl ion, cisplatin may hydrolyze into monoaqua and diaqua forms that are 1000 times more reactive than cisplatin. These forms can uncouple oxidative phosphorylation and result in Ca release from mitochondria, which eventually contributes to the activation of apoptosis (150). Cannabinoids could possibly potentiate the effects of cisplatin on oxidative phosphorylation. This could be one of the rationales for combining two treatments together.

Additionally, cisplatin can affect antioxidant systems such as glutathione (GSH), leading to its nephrotoxic effect (151). Another mechanism of cisplatin action is the activation of the MAPK pathway via ERK. However, due to cisplatin-mediated activation of DNA-damage response, activation of ERK may lead to cell cycle arrest via p21, which allows the cell to repair DNA damage (152).

The ability to generate DNA crosslinks culminates in activating cell cycle checkpoints. Cisplatin temporarily induces S phase arrest facilitated with p16. G2/M cell cycle arrest is more

prominent due to potent inhibition of Cdc2-cyclin A or B kinase. Cisplatin also activates ATM and ATR, which causes the phosphorylation of the p53 protein. Cisplatin-induced ATR activation results in the upregulation of CHK1 kinase and directly CHK2, which is independent of ATM. One of the major cascades activated by ATR is MAPK. MAPK signalling cascade includes ERK, JNK, SAPK, and p38, which regulate cell proliferation, differentiation, cell survival, and apoptosis (153), with ERK being one of the most prominent inducers of apoptosis (154).

As already mentioned, one of the crucial pathways of cisplatin-induced apoptotic death is the activation of p38 MAPK, which causes transcription of PUMA and NOXA through p53 activation (155,156). Hayakawa et al. (2000) (157) demonstrated that cisplatin-induced DNA damage leads to the phosphorylation of BAD via the prosurvival AKT pathway. Later studies have also shown that BAD protein was phosphorylated with the help of ERK cascade under cisplatin treatment (158). Inhibition of AKT or ERK cascades caused sensitization of ovarian cancer cells to cisplatin (157). These mechanisms are also commonly affected by cannabinoids, which could justify the attempt to combine the treatments with seeingto see if we could achieve synergistic interaction on CRC cells.

Resistance to cisplatin

Sadly, resistance to cisplatin is a common phenomenon. According to Zahid, 2003, there are multiple mechanisms involved in inhibiting apoptosis in cisplatin-resistant tumor cells, which include increased efflux transporter, uptake defects, increased drug inactivation, HER-2/neu overexpression, defect in mismatch repair (MMR), enhanced activity of PI3K/AKT, H-Rras overexpression, deregulation of MAPK pathway, increase in DNA damage tolerance, increase in replicative bypass, increase in DNA repair, suppressed caspase activity, increase in Bcl-2 or Bcl-xL, downregulation of Bax or Bad, reduced Fas expression, and finally, loss of p53 function (153). Nucleotide excision repair is a major pathway for removing cisplatin DNA adducts and DNA damage repair. The basal activity of the PI3K /AKT pathway facilitates the induction of p21 under cisplatin action in a p53-dependent fashion (159). AKT may also attenuate Mdm2 phosphorylation and downregulation of p53, which can assist in resistance to cisplatin (160). Additionally, AKT can be upregulated by XIAP, which causes inhibition of caspases resulting in cell survival (161).

Due to similar molecular targets between cisplatin and cannabinoids, we decided to test whether combining cisplatin and cannabinoids could act in synergy. This would allow to widen

the therapeutic window of cisplatin, maintain its cytotoxic effects on cancer cells yet reduce potential adverse effects.

1.1.7. Serum starvation and cisplatin

It was shown that serum starvation sensitized cancer cells to cisplatin while protecting normal cells. In normal cells, serum starvation caused cell cycle arrest in G0/G1 phase due to p53/p21 activation, which depended on AMPK but not on the activation of ATM. In cancer cells, serum starvation-activated p53 was both AMPK- and ATM-dependent. Furthermore, the combination of cisplatin with serum starvation led to the activation of the ATM/CHK2/p53 pathway, compared to cisplatin alone, which indicated that the combination therapy sensitized cancer cells to chemotherapy. As a result, short-term starvation sensitized tumor xenografts to cisplatin, as indicated by significant tumor growth delay and the induction of complete remission in 60% of mesotheliomas and 40% of lung carcinoma xenografts. Thus, combining starvation with cisplatin may enhance the therapeutic index of cisplatin-based chemotherapy (162).

1.1.8. Intermittent fasting and cancer

Humanity has been practicing fasting for centuries. However, only recent years' discoveries have shown the health benefits of simple time-adapted food consumption and calorie deprivation. Fasting helps reprogram cellular stress-related adaptation mechanisms and energy metabolism and boosts cellular defence mechanisms. It was shown in animal models that intermittent fasting (IF) could protect against diabetes mellitus, cardiovascular pathologies, neurodegeneration, and cancer. Recent human trials showed that IF helps fight obesity, hypertension, asthma, and rheumatoid arthritis. Fasting may expand the lifespan of bacteria, yeast, worms, and mice (163–166).

Research showed that serum starvation *in vitro* and short-term food starvation *in vivo* reduced levels of growth factor stimulation (167–169). In normal cells, the depletion of growth signals decreases the activity of proliferation-stimulating signalling and reduces metabolism (170). However, in cancer cells, starvation increases cellular stress due to their metabolism reprogramming to maintain continuous proliferation (171) and activates the DNA damage response (162).

Fasting has shown potential in the prevention and treatment of cancer. In rodent models and humans, fasting for 2 or 5 days can lead to more than 50% decreased insulin growth factor 1 (IGF-1), around 30% decreased glucose levels and an almost 10-fold increase in IGF-1 binding protein (172–176). Elevated levels of IGF-1 have been associated with certain types of tumors

(177,178). It was shown that IGF-1 and other hormones and growth factors might regulate energy metabolism, cell proliferation, and differentiation in response to calorie and protein availability (179–181). IGF-1 has a tumorigenic effect on cancer cells by stimulating proliferation and inhibiting apoptosis (179,182). IGF-1 can reduce Ras, Akt/mTOR and MAPK signalling. These endocrinological changes cause the expression of hundreds of genes, leading to decreased proliferation and increased stress resistance. Multiple oncogenic pathways play a role in decreased stress resistance in cancer cells, which results in their inability to switch into a stress-protective mode (183). The reduction of IGF-1, insulin, and glucose levels could lead to the activation of protective mechanisms in cells, decreasing DNA damage and creating an unfavorable environment for carcinogenesis.

Adding serum deprived of IGF-1 protects human cells from oxidative DNA damage. However, once the DNA became damaged, cells were more likely to activate apoptosis (184). In mice models, short-term fasting protected normal cells while sensitizing malignant cells to chemotherapy drugs. This depends on reduced levels of IGF-1 and glucose. Interestingly, only the complete short-term protein deficiency reduced IGF-1 levels. Short-term 50% calorie restriction combined with protein deficiency or a ketogenic diet improved chemotoxicity resistance (185).

Another animal study, including fasting, showed that alternate-day fasting in mice reduced the incidence of lymphomas (186). The same study also presented that the significant reduction in the formation of ROS in mitochondria was associated with the upregulation of superoxide dismutase (SOD) activity (186). Fasting 1 day a week could delay spontaneous tumorigenesis in p53-deficient mice (187). The mechanism of cancer delay was p53-independent, and IGF-1 related. These studies identified possible energy balance interventions in humans to prevent cancer development (187). However, refeeding may cause abnormally high cell proliferation (188). In some mice models, periodic fasting can be as effective as chemotherapy (175). Periodic fasting may also sensitize some tumors to chemotherapy medications because, in contrast to normal cells, cancer cells cannot adapt to fasting due to the accumulation of mutations responsible for cell growth enhancement in normal environmental conditions called differential stress sensitization (175).

Lee et al. showed that short-term cycles of starvation could protect normal cells from chemotherapy-induced side effects (175). In their study, starvation sensitized RAS2 expressing yeast cells to oxidative stress and 15 of 17 tested mammalian cancer cell lines to chemotherapeutic

drugs. Cycles of fasting were as effective as chemotherapy alone in delaying tumor progression and increased chemotherapy sensitivity in melanoma, glioma, and breast cancer cells. The combination of fasting cycles with chemotherapy resulted in long-term cancer survival in mouse models of neuroblastoma. Moreover, starvation of the breast cancer cell line increased the phosphorylation of AKT and S6 kinases, stimulating oxidative stress and DNA damage, which resulted in apoptosis. The differential stress resistance during fasting may be attributed to the redistribution of energy from growth and proliferation into protection and maintenance in normal but not in cancer cells (189) due to different regulations of mTOR signalling in cancer cells (190). These results may indicate that multiple cycles of starvation that stimulate differential stress sensitization of cancer cells could potentially find their way into clinical practice (175).

In metastatic animal models, the combination of fasting and chemotherapy resulted in 20-60% cancer-free survival compared to chemotherapy or fasting alone (162,175). Additionally, studies on neuronal protection showed that IF might boost antioxidant defence and heat shock proteins and decrease levels of proinflammatory factors such as TNF-α, IL-1β, and IL-6 (191). Thus, inhibition of the mTOR pathway, activation of autophagy, and ketogenesis also benefit the human body, which would help fight cancer (192,193).

Despite the notable cytotoxic effects of fasting in animal models, few human trials were studying fasting effects in cancer patients. The clinical trial that involved ten subjects with different malignancies reported that fasting during chemotherapy reduced common chemotherapy-induced side effects (194). Case studies where cancer patients voluntarily fasted before (48-140 hours) and after (5-56 hours) chemotherapy reported a reduction in fatigue, weakness, and gastrointestinal side effects caused by chemotherapy. Thus, fasting helped to ameliorate chemotherapy-induced side effects in cancer patients (194).

Some of the literature indicated that shift work with nighttime eating was associated with higher risks of breast cancer (195,196). The prospective data analysis of breast cancer survivors with follow-up for seven years showed that patients who fasted less than 13 hours per night had an increased recurrence risk (197). According to Patterson et al. (2017), IF could influence metabolic regulation via circadian rhythms, gut microbiota, and modifiable lifestyle behaviour (198).

Fasting also has a notable anti-inflammatory effect. As the study showed, alternate-day fasting significantly reduced levels of TNF-α and ceramides in asthma patients (199). As

previously mentioned, ceramides are released from membrane sphingomyelin in response to inflammation and oxidative stress. Johnson et al. provided evidence that markers of oxidative stress (protein carbonyls, nitrotyrosine, and 8-isoprostane), as well as TNF-α, BDNF, and ceramides C16:0, C18:0, C22:0, and C24:1 was significantly decreased in alternate-day caloric restriction trial, which suggests that this diet reduces inflammation and oxidative injury in asthma patients (199). There are a few mechanisms that could explain the results. First, during calorie restriction, there is a decrease in energy intake. Thus, the production of free radicals is decreased. Second, cells under fasting may respond by up-regulation of antioxidant systems to increase cellular stress resistance (199). The anti-inflammatory effect of fasting and increased ceramide production with the help of cannabinoids can be one of the joining pieces of the puzzle of how the combination of CBD and IF may synergistically interact with cancer cells but not on normal cells.

1.1.9. Oncogenic and non-oncogenic stress in cancer cells

There are a few types of stress encountered by the tumor cells. This includes metabolic, proteotoxic, mitotic, oxidative and stresses due to DNA damage.

DNA damage happens when cancer cells pass through extreme genomic instability, generating multiple mutations, deletions, chromosomal rearrangements, and aneuploidy (200). These changes activate the DNA damage stress response pathway (201). Thus, mutations in DNA repair systems such as ATM and p53 cause increased rates of DNA damage, cell-cycle progression, and genomic instability (202). Proteotoxic stress can result from the aneuploidies often present in cancers (203), which can lead to the excessive formation of protein complex subunits and increased production of truncated proteins (202). Regarding mitotic stress, many tumors exhibit chromosome missegregation; such tumors have a name of a CIN phenotype. Cancer cells rely on stress-support pathways for proper chromosome segregation. Thus, they are more sensitive to catastrophic genomic instability in case of stress overload (204).

In 1926, Otto Warburg discovered that cancer cells produce their ATP mostly via glycolytic pathway even when the oxygen supply is sufficient (205). Surprisingly, the mechanisms of the Warburg effect are still unclear. It was suggested that such adaptation allows cancer cells to divert resources for biosynthesis and reduce ROS production (206,207).

As one of the major hallmarks of cancer is rapid proliferation, it often puts cancer cells to experience hypoxia and nutrient deprivation. However, due to low p53 levels, apoptosis is not induced as it would be in normal cells (208). The stimulation of the proliferation of cancer cells

requires an excess of nutrients in the environment because each passage through the cell cycle yields two daughter cells and requires a doubling of biomass (207). During cell division, activation of the glycolytic pathway provides ATP and intermediates needed for biosynthetic pathways, including ribose sugars, glycerol and citrate for lipids, amino acids and via pentose phosphate pathway, NADPH. Thus, the Warburg effect benefits bioenergetics and biosynthesis overall (207).

The inhibition of the glycolytic pathway in cancer cells could lead to stress overload due to constant proliferative signalling from oncogenes (209). Cancer frequently encounters hypoxia-reperfusion in its microenvironment leading to extreme ROS production, causing mitochondrial damage and apoptosis (210). Thus, tumors learned to alleviate oxidative damage via increased glycolysis and downregulate mitochondrial function (210).

Glycolysis is activated by the PI3K pathway and its downstream target AKT, which can trigger cell hypertrophy, enhances glycolysis, and activates cell survival (211). AKT may regulate post-transcriptionally multiple glycolytic steps, such as the localization of glucose transporters in the cell membrane and stimulation of hexokinase function without growth-stimulating signals. High glucose uptake by tumor cells compensates for mitochondrial dysfunction and is required for proliferation. Stimulation of glycolysis enables cells to redirect accumulated pyruvate toward the biosynthesis of lipids, which is needed for membrane assembly (212).

Additionally, during nutrient deprivation, one of the mechanisms of tumor cell adaptation is autophagy. Thus, impaired autophagy could contribute to stimulating genomic instability and the release of cytokines (213). Autophagy is critical for survival when apoptosis-resistant cancer cells encounter severe nutrient deprivation. In this case, inhibition of autophagy would sensitize tumor cells to metabolic stress and promote necrosis.

Above-mentioned metabolic changes in cancer cells might become one of the targets for anticancer therapy. As we discussed before, fasting affects metabolism in cancer cells leading to differential stress sensitization. Additionally, cannabinoids are also known to regulate stress survival pathways in cancer cells. Thus, it makes sense to test these treatments individually and in combination to assess if there is a cytotoxic effect on CRC cells and whether these treatments can act in synergy.

1.1.10. Metabolic changes in cancer cells and AKT signalling

Cancer cells are highly exposed to oncogene-mediated genotoxic stress (214), oxidative damage (215), and metabolic stress (216), which are usually not present in normal cells. As a

result, tumor cells are highly dependent on stress-support pathways for their survival. Thus, therapy targeting stress pathways, for example, fasting in cancer cells, would more specifically affect tumors while sparing the normal cells (202). Previous research showed that interfering with the cellular response to oxidative damage selectively killed cancer cells (217), and targeting the replicative stress response killed oncogene-driven tumors (218).

Cancer cells usually have excessive proliferative signalling that is not coordinated with the rest of cellular metabolism. This creates excessive free radicals and additional metabolic stress on tumor cells. Consequently, to survive, cancer cells heavily rely on the activity of stress-defensive pathways such as ATR and CHK1. The replicative stress in cancer cells originates in the deregulation of the S-phase progression, mainly driven by upregulated oncogenes such as Myc (202,218), which accounts for multiple genomic rearrangements in tumor cells. Myc can promote entry into the S phase by stimulating cyclin E-Cdk2 and E2F1 activity (219) or directly stimulating replication (220). In tumors, the oncogene-induced replicative stress activates ATR and CHK1. For instance, mice with deficient ATR completely prevented the development of myc-induced lymphomas and pancreatic tumors, which have a high replicative turnover (218). Thus, adding CHK1 inhibitors to myc-induced lymphomas promoted a strong increase in γH2AXax and apoptosis in lymphoma cells but not in normal cells (218).

The therapeutic perspective of tumor metabolic modulation has yet to be extensively studied. There are a few ways to influence tumor cell metabolism that could have therapeutic implications and normalize cell metabolism. First, inhibition of HIF-1α, which can inhibit angiogenesis. Next is the re-establishment of p53, which can activate apoptosis, and lastly, suppression of the PI3K/AKT/mTOR signalling pathway, inhibiting cell growth and proliferation (206). Thus, in glucose-addicted cancer cells that have overactivated oncogenes, low-nutrient conditions and inhibitors of glycolysis may enhance the activation of apoptosis.

As previously mentioned, many cancer cells have higher glucose uptake rates and rely on glycolysis and lactic acid fermentation even when there is an oxygen source, known as the Warburg effect (216). The metabolic effects of the PI3K/AKT/mTOR pathway involve enhanced glucose uptake, essential amino acids, and translation of proteins. The PI3K/AKT/mTOR pathway is a master regulator of aerobic glycolysis and cellular biosynthesis (207). In cancers, the hyperactivation of AKT prevents apoptosis and boosts uncontrolled cell proliferation (221).

The signalling from growth factors and cytokine receptors are major determinants for cell survival via opposing the basal intrinsic and extrinsic proapoptotic stimuli (222). It has been demonstrated that PI3K/AKT/PKB signalling mediated cell survival by various growth factors and cytokines and can inhibit the activation of apoptosis (223,224). When growth factors bind to cell surface receptors, it activates PI3K with phosphorylation of phosphatidylinositol lipids in a plasma membrane. AKT is activated by PI3K, stimulating its downstream effector, the mTOR. Subsequently, it enhances multiple biosynthetic pathways. Stimulation of the PI3K/AKT/mTOR results in increased expression of nutrient transporters (225–229), increased glycolysis and lactate production, the so-called Warburg effect (205,230,231).

Additionally, AKT causes enhancement of lipogenesis, whereas mTOR is mainly responsible for protein translation (232). Mutations in the AKT pathway are usually one of the most significant metabolic dysregulating events in cancer cells, which enables them to drive aerobic glycolysis and suppress macromolecular degradation (231,233). mTOR is a complex kinase that coordinates cell growth with the availability of nutrients, energy, and growth factors. It was shown that the inhibition of mTOR leads to the induction of PPARα, which activates ketogenesis (193).

Activated AKT requires glucose and its metabolic pathways to maintain mitochondrial integrity and inhibit apoptosis. AKT increased the coupling of oxidative phosphorylation to glucose metabolism and regulated PT pore opening via activation of hexokinase-voltage-dependent anion channel (VDAC) at the outer membrane in mitochondria (234). Inhibition of apoptosis by AKT does not require *de novo* protein synthesis. Thus, AKT provided posttranslational regulation via phosphorylation of downstream effectors. AKT may inhibit apoptosis via the activation of mitochondria-bound hexokinase (234).

One of AKT's most evolutionally conserved functions is the control of energy metabolism (211). AKT may directly phosphorylate DAF-16 and its mammalian homolog FOXO, which excludes this transcription factor from the nucleus and its transcriptional activation (235). Thus, activation of FOXO happens when AKT activity is reduced. FOXO transcription factors play a role in the regulation of ROS via the activation of antioxidants such as catalase and SOD (235).

The FOXO transcription factors are one of the major substrates of the AKT during growth factor and insulin presence. Insulin and growth factors lead to the re-localization of FOXO from the nucleus to the cytoplasm, where they are degraded via ubiquitination. On the contrary, when

the growth factors are scarce, FOXOs are localized to the nucleus, where they upregulate a series of genes, such as growth arrest and DNA-damage-inducible protein 45 (GADD45), cyclin-dependent kinase inhibitor p27, manganese superoxide dismutase (MnSOD), BIM and Fas ligand (FasL), which results in cell cycle arrest, stress resistance, or apoptosis. Thus, FOXO plays a tumor suppressor role in cancers (235). Moreover, the MAPK signalling protein JNK is sufficient to overcome the inhibition of FOXO by AKT. Furthermore, it was shown that β-catenin might bind FOXO and inhibit cell cycle progression (236).

Overall, AKT increases oxygen consumption and oxidative phosphorylation, consequently increasing ROS production (234). AKT may increase ROS production by two mechanisms. First, it increases oxidative phosphorylation. Second, AKT decreases scavenging ROS by inhibiting FOXO transcription factors (237).

Depletion of AKT caused resistance to replicative senescence, oxidative damage, Ras-induced premature senescence, and ROS-induced apoptosis. On the contrary, activation of AKT induced cell senescence and increased free radical production via increased oxygen consumption. Furthermore, AKT inhibited ROS scavengers downstream of FOXO and sestrin 3 and sensitized cells to ROS-induced apoptosis. Moreover, treatment with rapamycin led to AKT activation hypersensitized cells to ROS-mediated apoptosis. In general, AKT suppresses apoptosis activation. However, it fails to inhibit ROS-mediated apoptosis (237).

Moreover, PI3K/AKT/mTOR pathway can control levels of HIF-1α, which also can stimulate glycolysis. Mitogen stimulation can also increase levels of c-Myc in the G1 phase, enhancing entry into the S phase by activating the expression of cyclins and CDK4 (238).

Based on the literature search, we decided to test if the addition of intermittent serum starvation to cisplatin and cannabinoids could result in synergistic interactions on CRC cell lines.

1.2. Hypotheses

Based on the literature review and initial data from our laboratory, we formulated the following hypotheses:

1. The antiproliferative effect of CBD is attributed to its modulation of CRC cell metabolism and stress survival pathways.
2. The combined application of CBD and cisplatin demonstrates synergistic inhibition of CRC cell proliferation through DNA damage and metabolic alterations.

3. Intermittent serum starvation induces cytotoxicity in CRC cells via metabolic reprogramming and activation of stress survival pathways.

4. Combining cisplatin and ISS has a synergistic effect. The synergistic effect of cisplatin and ISS is due to their combined induction of DNA damage and excessive stress response in CRC cells.

5. Combining CBD and ISS has a synergistic effect on cell cytotoxicity. CBD and ISS synergistically affect CRC cells by targeting cancer cell metabolism and stress response.

6. Combining cisplatin, CBD, and ISS has a synergistic effect. CBD, cisplatin and ISS synergistically affect CRC cell viability by targeting cancer cell metabolism, abnormal stress response, and DNA damage.

1.3. Materials and methods

1.3.1. Main reagents

Cisplatin was obtained from Sigma-Aldrich (CAS 15663-27-1), CBD from Sigma-Aldrich (Cerilliant, C -045 Lot: FE01271601), and Δ9-THC from Sigma-Aldrich (Cerilliant, T4764, Lot: SLBQ8309V). DMSO (Dimethyl sulfoxide anhydrous) was purchased from Thermo Fisher Scientific (Cat#D12345). Cannabinoids (10 mg/ml) were dissolved in methanol and stored at -20℃. The stock solution of cisplatin (100 μM) was dissolved in DMSO and kept in -20℃ for no longer than 3 weeks.

1.3.2. Cell culture and maintenance

The experiments were performed on three human CRC cell lines, HT-29 (HTB-38™), HCT-116 (CCL-247™), and LS-174T (CL188™), and immortalized human colonic epithelial cell line HCEC-1CT (abm catalogue N# T0715). The CRC cell lines HCT-116 (CCL-247™) and LS-174T (CL188™) were purchased from ATCC (Rockvile, MD, USA). The HT-29 (HTB-38™) was a kind gift from Dr. Roy Golsteyn's Laboratory at the University of Lethbridge. The mutational background of CRC cell lines is represented in Table 1.

The HCEC-1CT (abm catalogue N# T0715) cell line was cultured in Complete Human Epithelial Cell Medium (cat. # H6621) with a supplement kit. The HT-29 (HTB-38™) was cultured in RPMI-1640 medium (30-2001^{TM}), the HCT-116 (CCL-247™) – in McCoy's 5A Medium (30-2007^{Tm}), and LS-174T (CL188™) – in Eagle's Minimum Essential Medium (30-2003^{TM}). All cell lines were grown as adherent cells supplemented with a final concentration of

10% heat-activated fetal bovine serum (FBS) (ATCC® 30-2020™) and 100 U/mL penicillin/streptomycin (ATCC® 30-2300™). All cell lines were incubated at 37°C in a humidified atmosphere of 5% CO_2. Every experiment was repeated at least three times. The culture medium was replaced with a fresh complete medium every 2 days until cell confluency reached 85-90% for further experiments.

Table 1. CRC cell lines used with the list of driver mutations and corresponding possible molecular subtypes

Cell line	Pathogenic mutations Census TIER1	References	The molecular subtype of CRC
HT-29	APC, BCL9L, BRAF, BRD3, CAMTA1, EBF1, FAT4, FCGR2B, FLT3, GOLGA5, KAT6B, PAX3, PIK3CA, POLQ, PRDM16, PTCH1, SMAD4, SPEN, TP53, TP63, TRIM24, ZFHX3	https://cancer.sanger.ac.uk/cell_lines/sample/overview?fathmm=PATHOGENIC&genes=census&id=905939#muts	Classical subtype with APC, P53 and PI3K mutations
HCT-116	ABL1, ABL2, ACSL3, ATIC, ATM, BCL11A, BCOR, CACNA1D, CALR, CAMTA1, CDK12, CHCHD7, CHD4, CHEK2, CLIP1, COL1A1, CREBBP, CUX1, CXCR4, DCTN1, DDR2, DICER1, DNM2, DROSHA, ERBB3, ERCC5, FAT1, FAT4, FGFR1, FGFR2, FLT3, FLT4, FOXO3, GNAQ, GNAS, GPHN, HSP90AA1,	https://cancer.sanger.ac.uk/cell_lines/sample/overview?fathmm=PATHOGENIC&genes=census&id=905936#muts	Microsatellite unstable with MLH1 and PI3K mutations

	IDH1, IL21R, KAT6B, KDM6A, KIF5B, KMT2C, KMT2D, KRAS, KTN1, LCK, LPP, LRP1B, MAP3K1, MITF, MLH1, MN1, MYH11, MYO5A, MYOD1, NCOA1, NCOA2, NCOR1, NCOR2, NF1, NFATC2, NOTCH1, NOTCH2, NSD3, NTRK3, PAX7, PDE4DIP, PDGFB, PICALM, PIK3CA, PLCG1, PPFIBP1, PPP2R1A, PRCC, PRDM1, PREX2, PTPRB, PTPRT, RNF43, ROS1, RUNX1, SALL4, SETD2, SLC34A2, SLC45A3, SMO, SOX, SS18, SS18L1, STAT5B, TENT5C, TP63, TRIM24, TRIP11, TRRAP, TSC1, TSHR, UBR5, WRN, ZFHX3, ZMYM2, ZNF331		
LS-174T	AFF1, APC, ATIC, AXIN2, BCL11A, BRAF, BRIP1, CARS, CBFB, CCND3, CDH11, CDK6, CEBPA, CIC, CLTC, CNOT3, CNTRL, CREB1, CTNNB1, CUX1, DDR2, DROSHA, EP300, ERBB4, EZH2,	https://cancer.sanger.ac.uk/cell_lines/sample/overview?fathmm=PATHOGENIC&genes=census&id=998189#muts	Canonical or microsatellite unstable with APC, BRAF, MLH1, PI3K mutations

	FANCC, FAT4, FBXO11, FGFR1, FLT4, FOXP1, GATA2, GATA3, HOXD11, JAK1, JAK2, KDM5A, KDM6A, KRAS, LRP1B, MECOM, MEN1, MLH1, MN1, MSN, MYH9, MYO5A, NCOR1, NSD3, PBX1, PCM1, PDE4DIP, PDGFRB, PIK3CA, POLQ, PRKACA, PTCH1, PTPRB, PTPRT, RNF43, RPL5, RUNX1T1, SETBP1, SND1, SPEN, STIL, STK11, SUFU, TNFAIP3, TPR, TRIP11, TSC1, TSHR, U2AF1, XPC, ZFHX3		

1.3.3. Treatments

Exposure of CRC cells to cisplatin

To establish IC50s, a range of concentrations (1-15 μM) of cisplatin were obtained by diluting the cannabinoids in the fresh complete media and tested on CRC and normal colon epithelial cell line.

Exposure of CRC cells to cannabinoids

To establish IC50s, a range of concentrations (2-12 μM) of pure THC and CBD were obtained by diluting the cannabinoids in the fresh complete media and were tested on CRC and normal cell lines.

Exposure of CRC cells to intermittent serum starvation

To maintain the same nutritional supply for each CRC cell line, the cells were cultivated in RPMI-1640 medium (30-2001^{TM}). The intermittent serum starvation was recreated by depriving

cells with FBS for 16 hours and reintroducing media with FBS for 8 hours. The experiments lasted for 5 consecutive days in HT-29, HCT-116, and HCEC, and for 10 days in LS-174T cells.

All the treatment samples were filtered with 0.22 μm filter after being diluted in the growth media and were kept at 4°C.

Exposure of cells to different combinational treatments is represented in Table 2.

Table 2. Experimental treatments in normal and CRC cell lines.

Treatments		
Complete media for 24 h	Addition of FBS for 8 h	Serum starvation for 16 h
Cisplatin and CBD in different doses	-	-
Cisplatin in different doses for 8 h	-	-
CBD in different doses for 16 h	-	-
-	Cisplatin in different doses	-
-	-	CBD in different doses
-	Cisplatin in different doses	CBD in different doses

1.3.4. Cell viability assay (MTT)

Cell viability was determined by MTT [3-(4, 5-dimethylthiazol-2-Yl)-2, 5-diphenyltetrazolium bromide] assay. An MTT assay (Roche, Sigma-Aldrich, Germany) was used to evaluate the effect of cisplatin, cannabis extracts, CBD, and THC on CRC and normal epithelial colon cell viability.

Cells were incubated to 80-90% confluency in 10 cm Petri dishes. Next, cells were trypsinized by TRYPSIN/EDTA (0.25% Trypsin and 2.21 mM EDTA-4Na; Cat#325-043-EL; WISENT Inc., Quebec, Canada). After trypsinization and centrifuging, fresh media was added to the cells, and one (for experiments with complete media) or three (for ISS experiments) thousand cells per well were plated in triplicate into flat-bottom 96-well plates in 100 μl of the appropriate medium. The cells were allowed to adhere to the plate surface overnight and were exposed to treatment for five (HT-29, HCT-116, and HCEC) and ten days (LS-174T). Cells were then maintained at 37°C in a humidified atmosphere containing 5% CO_2 for 24 hours. Treatments were changed daily with the normalized concentrations of methanol and DMSO.

Every 24 hours of treatment, for instance, 0, 1, 2, 3, 4 and 5 days, 10 µl of MTT kit I (#11465007001, Roche, Ontario, Canada) was added and plates were incubated at 37°C in the CO2 incubator for 4 hours. At 4 h after incubation, 100 µl of MTT solution was added to each well and the plate continued to incubate at 37°C overnight. Absorbance was measured at 595 nm using a FLUOstar Omega microplate reader (BMG Labtech Ortenberg, Germany). Results were calculated by comparing the treatments to the appropriate controls. All treatments were in triplicate, and each test was performed in at least three independent experiments. Cell morphologies were assessed daily by light microscopy.

1.3.5. RNA extraction and Gene Expression Analysis

RNA isolation of HT-29 and HCT-116 cell lines

Once grown to 85-90% confluency in a Petri dish, cells were detached using TRYPSIN/EDTA (0.25% Trypsin and 2.21 mM EDTA-4Na, Cat#325-043-EL, WISENT INC., Quebec, Canada) and re-plated in 6-well plates at a density of 6 x 10^5 cells/well for HCT-116, and 3 x 10^5 cells/well for HT-29 experiments. After 24 h after incubation, cells were exposed to treatments for 72 h. The culture medium was replaced with a fresh treatment medium every 24 hours for HT-29 and at specific time points for ISS (at the 16^{th} and 8^{th} hour during 24 h) experiments on the HCT-116 cell line. At the endpoint, cells were washed twice with ice-cold PBS and harvested using the TRIzol™ Reagent (Invitrogen). Total RNA extraction followed the TRIzol Reagent protocol (https://assets.thermofisher.com/TFS-Assets/LSG/manuals/trizol_reagent.pdf). Immediately after the isolation, the quality and quantity of the extracted RNA waswere assessed using a NanoDrop 2000/2000c Spectrophotometer (Thermo-Fisher Scientific Company, Wilmington, DE). Additionally, the RNA integrity of RNA samples was assessed by agarose gel electrophoresis.

The RNA samples from the HCT-116 CRC cell line were shipped to Génome Québec (Montréal, Québec) for mRNA library preparation and next-generation sequencing. The stranded mRNA libraries were prepared using NEBNext® Ultra™ RNA Library Prep Kit for Illumina® (New England BioLabs). Massive parallel sequencing was performed using Illumina NovaSeq6000 S4 PE 100 bp – 25M reads, number of sequencing units – 30.00. Basecalling and demultiplexing were done by the Sequencing provider (Genome Quebec).

Pathway analysis for HCT-116 CRC cell line

Library construction, basecalling and demultiplexing. Libraries were generated from 250 ng of total RNA using the kit Illumina® Stranded mRNA Prep, Ligation (Illumina) as per the manufacturer's recommendations. Adapters and PCR primers were purchased from Illumina. Libraries were quantified using the KAPA Library Quantification Kits - Complete kit (Universal) (Kapa Biosystems). Average size fragment was determined using a LabChip GXII (PerkinElmer) instrument. The libraries were normalized and pooled and then denatured in 0.05N NaOH and neutralized using HT1 buffer. The pool was loaded at 175pM and 200pM on an Illumina NovaSeq S4 lane using Xp protocol as per the manufacturer's recommendations. The run was performed for 2x100 cycles (paired-end mode). A phiX library was used as a control and mixed with libraries at 1% level. Base calling was performed with RTA v3.4.4. Program bcl2fastq2 v2.20 was then used to demultiplex samples and generate fastq reads.

Initial quality control

Initial quality control was conducted using FastQC v0.11.9 https://www.bioinformatics.babraham.ac.uk/projects/fastqc/. The base qualities were excellent across the board, and no quality issues were detected at this stage.

Adapter and quality trimming

Sequencing reads were trimmed of adapter sequences and low-quality bases using Trimmomatic. (239). Trimmed sequence files were examined with FastQC to verify the trimming results. Trimmed reads were saved in the trimmed_reads folder, and trimmed FastQC reports can be found in the fastqc_results/ directory.

Read mapping

Trimmed sequencing reads were mapped to Human genome (GRCh37, Ensembl) downloaded from illuminaIllumina iGenome website.

Counting reads mapping to features (genes)

Differentially expressed genes are detected based on counts of reads mapping to genes after appropriate normalization. The counts if reads mapping to features (genes) were counted using FeatureCounts v.2.0.1 software. The files containing raw counts data and corresponding summaries are located in read_counts/ directory.

Integrating quality information

Output summaries and quality report from various software used in the analysis were integrated into a single report using multiqc v.1.13 https://multiqc.info/. MultiQC report is located

in multiqc_results/ directory and can be viewed in any web browser. Qualimap integrates various statistics from sequencing files, QualiMap, HISAT2, FeatureCounts, Trimmomatic, and FastQC. All graphs and tables present in MultiQC report can be exported.

Differential expression analysis

Data exploration, visualization and statistical comparisons were conducted using R language version 4.2.2. Pair-wise comparisons between experimental groups were done using DESeq2 v.2.1.36 as described in the package manual. To decrease computational time, only the genes with at least 5 reads across 3 samples were kept in the analysis. In addition to hard threshold filtering mentioned above, DESeq2 implements independent filtering based on mean of normalized count as a filter statistic. The purpose of independent filtering is to remove lowly expressed genes that cannot produce a reliable measure of significance. This in turn allows to decrease overall number of the statistical tests and increase the power to detect truly differentially expressed genes (DEGs).

We used hierarchical clustering (HC) and principal components analysis (PCA) to investigate the relationship between samples and detect potential outliers. Prior to HC and PCA analysis, DESeq2 normalized values underwent variance stabilizing transformation with using vst() function from DESeq2. HC was done using hclust() function implemented in R, with the clustering method set as “complete” for the matrices of sample-to-sample distances, and “Ward.D2” in case of the sample and gene clustering based on top 500 most variable genes. The distance measure in HC analysis was set to “euclidean”. Principal components analysis, applied to top 500 highly variable genes, was conducted using prcomp() function implemented in R with default options.

DEGs were detected with DESeq2 function results() with default options. DESeq2 uses Wald test to determine significantly changed genes between groups. The independent filtering option was set to TRUE with alpha threshold kept at 0.1. Multiple comparison adjustment was done using Bejamini-Hochberg procedure. Significantly changed genes were visualized as MA plots, volcano plots and heatmaps built using pheatmap v.1.0.12 and ggplot2 v.3.4.0. The genes involved in the analysis were annotated with entrez ids, descriptions, using BiomaRt 2.54.0. Genes with adjusted p.values below 0.05 and absolute log2 fold change over 0.59 were considered significant. Additionally, we prepared the result reports that with summaries in the form of graphs and tables using regionReport Bioconductor package 1.32.0.

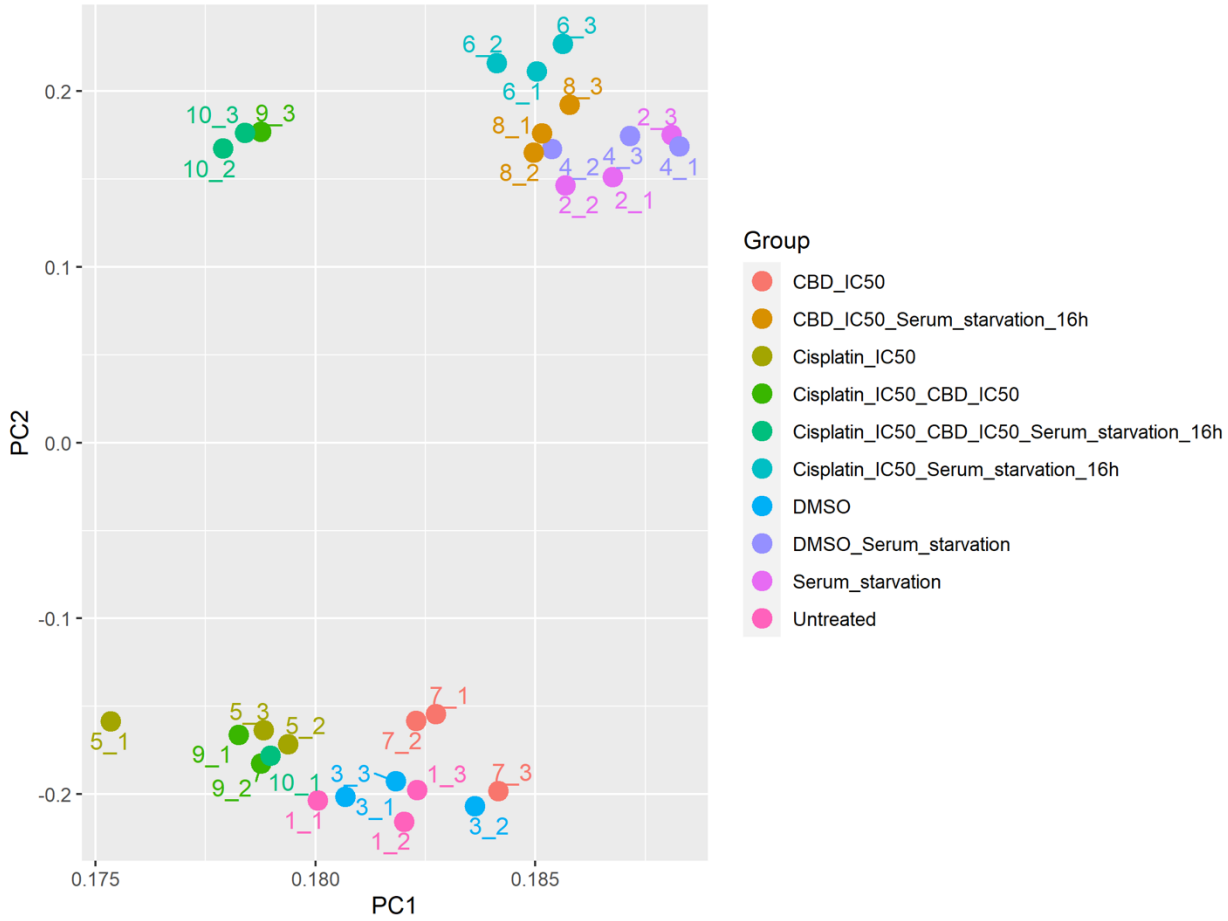

Figure 2. Principal component analysis (PCA) plot based on the top 500 genes with the highest variance for multiple treatments in the HCT-116 CRC cell line. Each treatment group (biological triplicate) is represented in a different colour. The x-axis represents the values of the first principal component (PC1), and the y-axis represents values for the second principal component (PC2). The PCA plot was generated using R software version 4.2.2.

We expected the biological replicates to cluster closely in the PCA plot, which reflected the similarity of their gene expression profiles. Since inter-individual variance is not expected within the same cell line, the biological replicates belonging to separate clusters in the case of cell lines indicate a high degree of technical variance. Most of the samples clustered perfectly according to the experimental treatments, except for 9.3 and 10.1., which were excluded as statistical outliers (Figure 2).

Differentially expressed genes were detected with DESeq2. Genes with adjusted p-values below 0.05 and absolute log2 fold change over 0.59 were considered significantly changed.

GO term enrichment analysis

PathfindR analysis. Gene ontology (GO) and Reactome pathways enrichment analysis was conducted using pathfindR v.1.64.0 (240), an R package that identifies significantly enriched biological terms utilizing active subnetworks. This tool detects active subnetworks in protein-protein interaction networks using a user-provided list of genes with associated p-values. In this case, the user-selected list included significant genes with adjusted p-values less than 0.05 and absolute log2 fold change over 0.59. In addition, pathfindR functionality was used to cluster enriched GO categories by similarity and identify representative terms. The main pathfindR function was used with the following options: gene_sets = "GO-All" (use all GO categories), adj_method = "fdr", enrichment_threshold = 0.05, pin_name_path = "STRING", search_method = "GR", max_gset_size = 500. The same options were applied to pathfindR enrichment of Reactome analysis. PathfindR output includes a table with enriched terms, a table of enriched term clusters, dot plots, gene-term maps, and upset plots. Clustering analysis and corresponding plots were prepared using corresponding pathfindR functions with default settings.

Additionally, SPIA analysis was performed. Pathway topology analysis was performed with the Signaling Pathway Impact Analysis (SPIA) tool (version 2.50.0). Reactome pathways were used as the reference database. Results with Padj < 0.05 were considered statistically significant.

Pathway analysis for the HT-29 CRC cell line was described in chapter 2.

The analysis of the pathway results, including gene functions and interactions, was performed with the help of GeneCards – the human gene database www.genecards.org (241,242).

1.3.6. Statistical analysis

GraphPad Prizm 9.0 software was used to calculate two- and one-way analysis of variance (ANOVA), and the two-tailed Student's t-test to determine the statistical significance between treatment groups for cell viability experiments. Results were presented as the mean ± SD of data. The $p < 0.05$ was considered statistically significant.

1.3.7. Calculation of combination index (CI)

To determine synergism, additivity, or antagonism, we performed drug combination analysis based on the Chou-Talalay method using CompuSyn software (243–245). In Chou's approach, the scattering data points fit the median-effect principle with mass-action law. The

combination index (CI) was calculated to quantify synergism and antagonism of the drugs, where CI<1 indicates synergism, CI=1 – additive effect, and CI>1 – antagonistic effect (Table 3).

Table 3. Description of synergism or antagonism in drug combination studies analyzed with CI method.

Range of CI	Description
<0.1	Very strong synergism
0.1-0.3	Strong synergism
0.3-0.7	Synergism
0.7-0.85	Moderate synergism
0.85-0.90	Slight synergism
0.90-1.10	Neary additive
1.10-1.20	Slight antagonism
1.20-1.45	Moderate antagonism
1.45-3.3	Antagonism
3.3-10	Strong antagonism
>10	Very strong antagonism

The favourable outcomes of drug synergism could be to increase the efficacy of therapeutic effect, decrease the dosage but maintain the same efficacy, minimize the development of drug resistance, and provide selective synergism against the target.

1.4 Results and discussion

1.4.1 Cisplatin and colorectal cancer cell lines

To establish a time and dose-dependent effect of cisplatin on different CRC cell lines and to calculate IC50s for each tested cell line, I performed a cell viability assay (MTT).

1.a

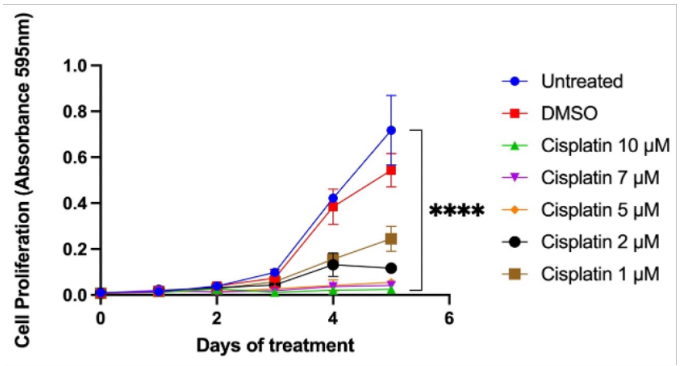

1.b

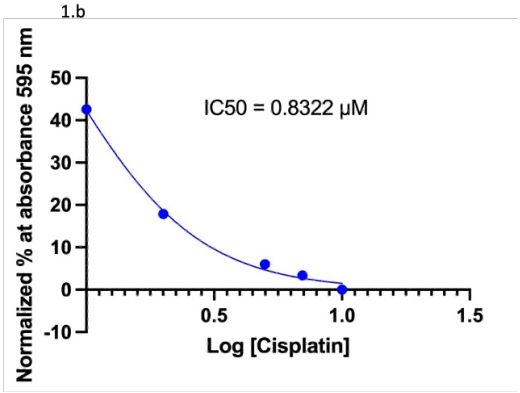

2.a

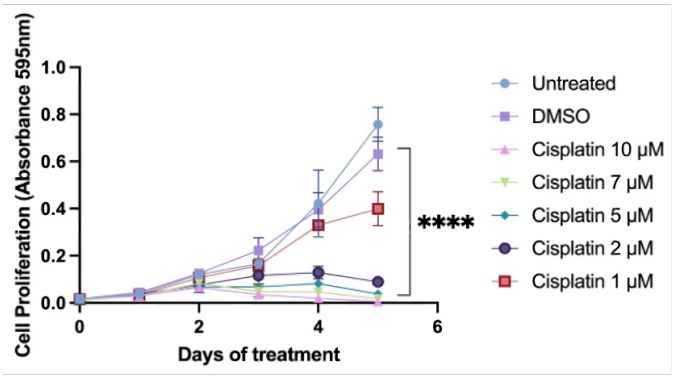

2.b

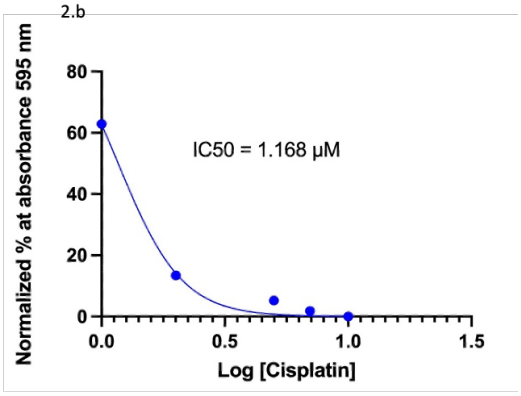

3.a

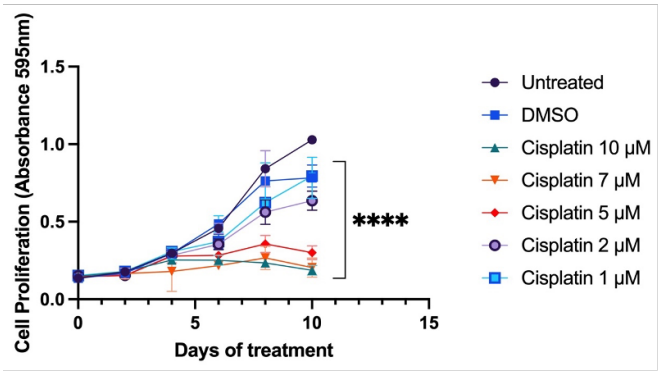

3.b

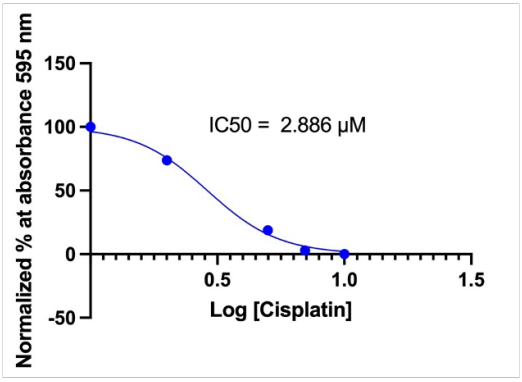

4.a

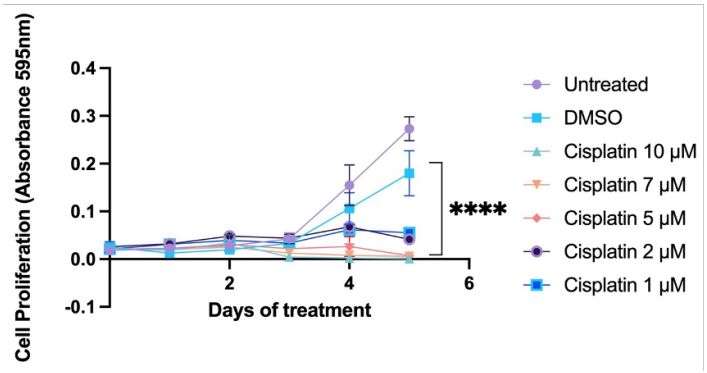

4.b

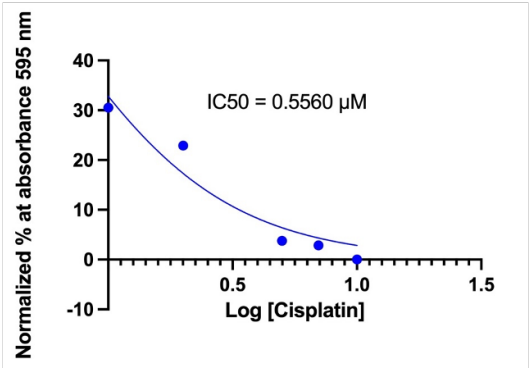

Figure 3. The time-dose-dependent effect and nonlinear regression analysis of the dose-effect curve with calculated IC50 values of cisplatin on HCT-116 (1.a, 1.b), HT-29 (2.a, 2.b), LS-174T (3.a, 3.b), and HCEC (4.a, 4.b) cell lines based on MTT results. Results are expressed as means of calculated cell viability ± standard deviations of each group in triplicate at absorbance 595 nm. To calculate time-dose effects, two-way ANOVA was performed using GraphPad Prism version 9.0. Significant differences between groups are marked with ns – non-significant, *p < 0.05, **p < 0.01, ***p < 0.001, ****p <0.0001. A nonlinear fit with log(inhibitor) vs. normalized response–variable slope analysis was performed using GraphPad Prism version 9.0.

We observed cisplatin's time and dose-dependent effect on all tested cell lines during treatment (Figure 3). Cell viability was significantly inhibited throughout tested concentrations. Based on non-linear regression analysis, the IC50 for normal epithelial cell line HCEC was lower than for all tested CRC cell lines, which might indicate higher toxicity of cisplatin on normal cells. This could explain cisplatin's narrow therapeutic window and multiple adverse effects in clinical settings. Although more normal cell lines would need to be tested to support this suggestion, it would be relevant to test cisplatin in combination with different treatments to find if there would be a synergistic effect, which would allow for its dose reduction but maintain its cytotoxic effect.

Next, to understand the underlying effects of cisplatin on APC (HT-29) and MMR (HCT-116) mutated CRC cell lines, we performed mRNA sequencing and bioinformatics analysis of pathways affected by cisplatin. This also helped to choose what treatment combinations could be beneficial to add to cisplatin and achieve potential synergism.

In our experiment, we used the HT-29 CRC cell line, which resembles the classical subtype of CRC. It has mutations in APC, PI3K, and P53 genes, which are common in CRCs.

Exploratory analysis

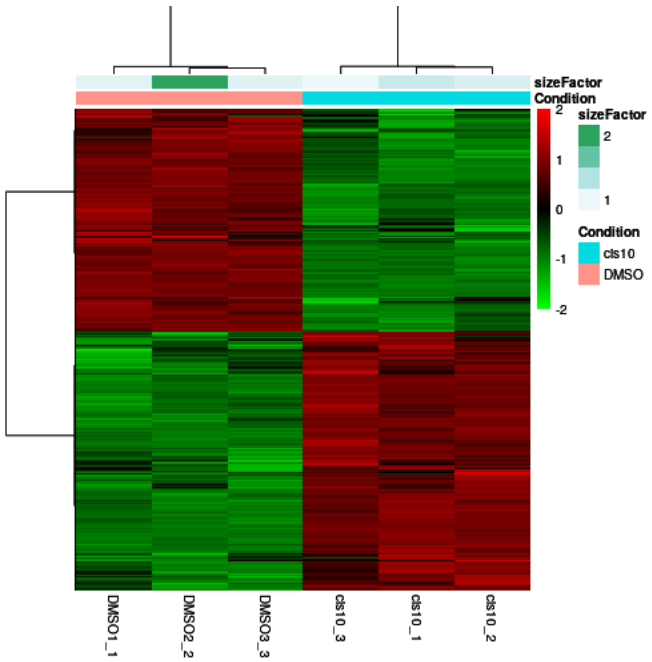

Figure 4. A hierarchical clustering heatmap analysis of the differentially expressed genes with fold change over 1.5 and adjusted p-values < 0.05 for DMSO control versus cisplatin in the HT-29 CRC cell line. The x-axis shows non-supervised clusters between the two treatment groups. The DMSO_1, DMSO_2, and DMSO_3 are independent replicates for DMSO and cis10_1, cis_2, and cis10_3 are for cisplatin 10 μM. The y-axis shows differentially expressed genes. The fold changes of up-regulated genes are in the red spectrum, and the down-regulated genes are represented in the green spectrum. The heatmap was generated using R software.

A heatmap represents differentially expressed genes for DMSO versus cisplatin in the HT-29 CRC cell line (Figure 4). The unsupervised clustering based on the underlying data determined if there were sub-categories within DMSO control and cisplatin treatment. As the figure shows, there were significant differences in gene expression between treatment groups. The differences were not substantial for the biological replicates within the same group, showing the treatment samples' good quality.

A

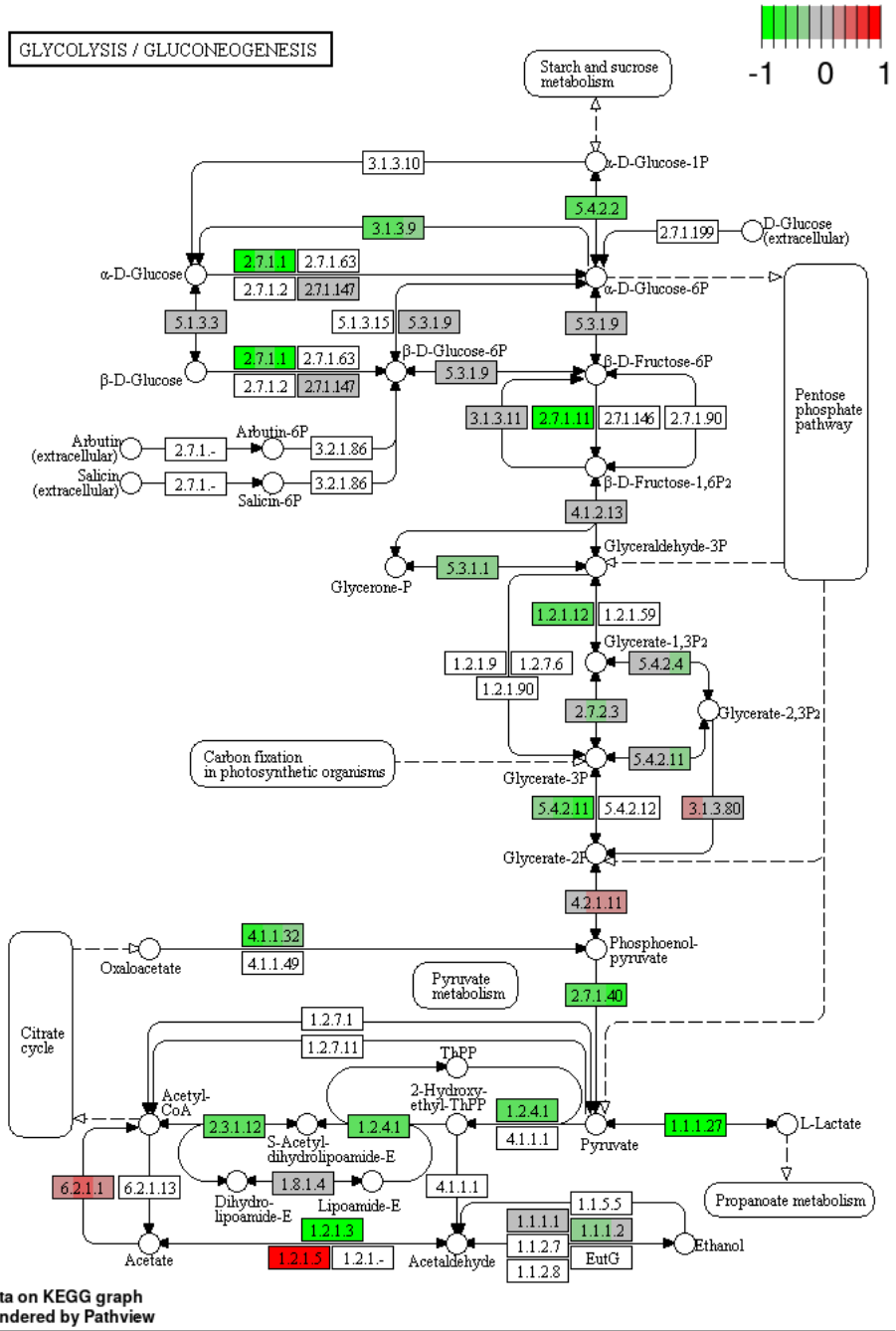

Data on KEGG graph
Rendered by Pathview

B

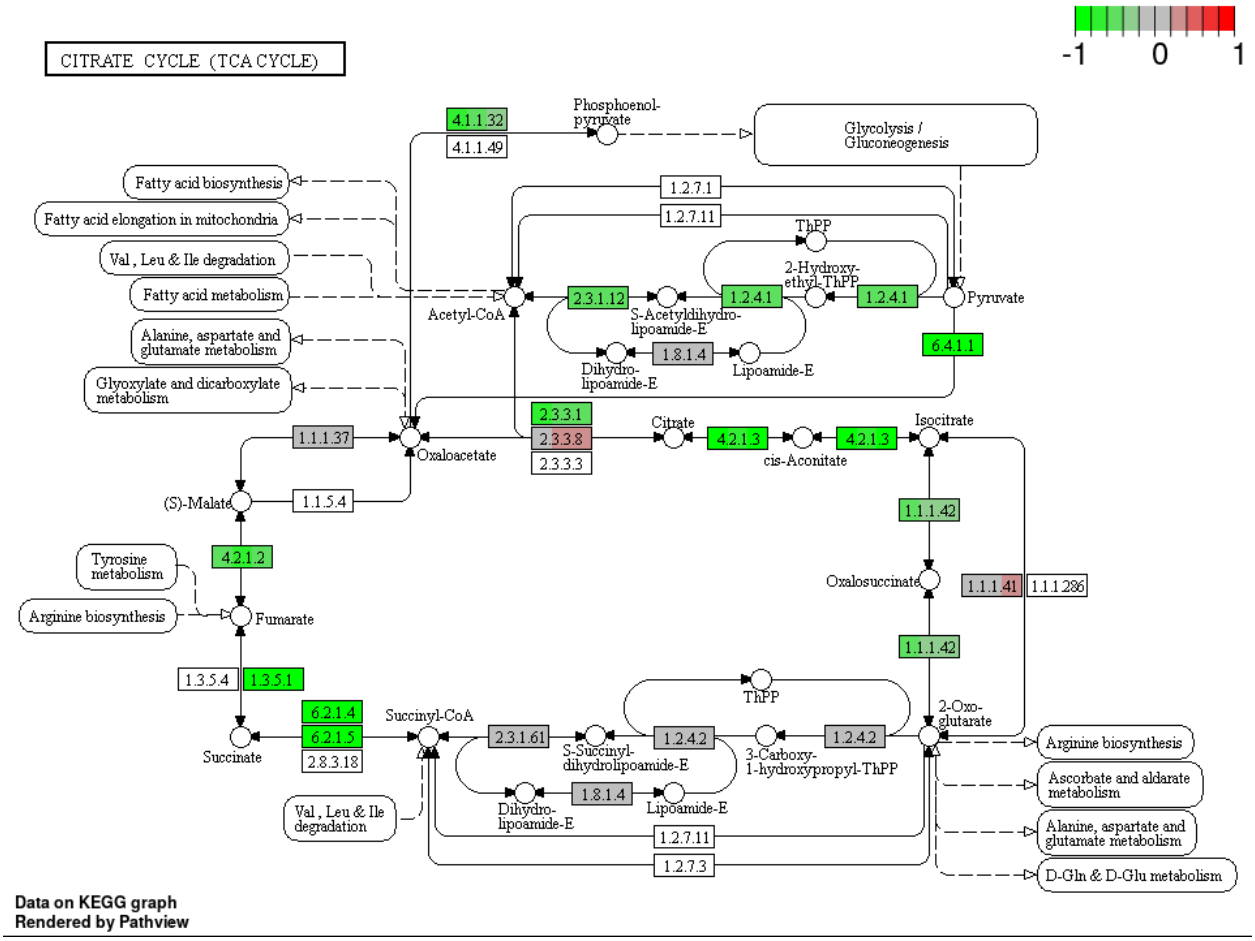

Figure 5. Decreased expression of multiple genes regulating glycolysis/gluconeogenesis (A) and citrate cycle (B) pathways under cisplatin 10 μM compared to DMSO control in HT-29 CRC cell line. The genes are coloured according to the difference in expression level between treatment and control for each individual sample. Red colour shows up- and green down-regulation relative to the treatment group. Data based on GAGE uni-directional analysis.

Cisplatin decreased the expression of multiple genes responsible for the glycolysis, gluconeogenesis, and citrate cycle pathways (Figure 5) in CRC cell line HT-29 compared to DMSO control. This could point out the metabolic effects of cisplatin on the tested CRC cell line, which could deplete the energetic supplies of cancer cells and push them toward cell cycle arrest or even cell death.

A

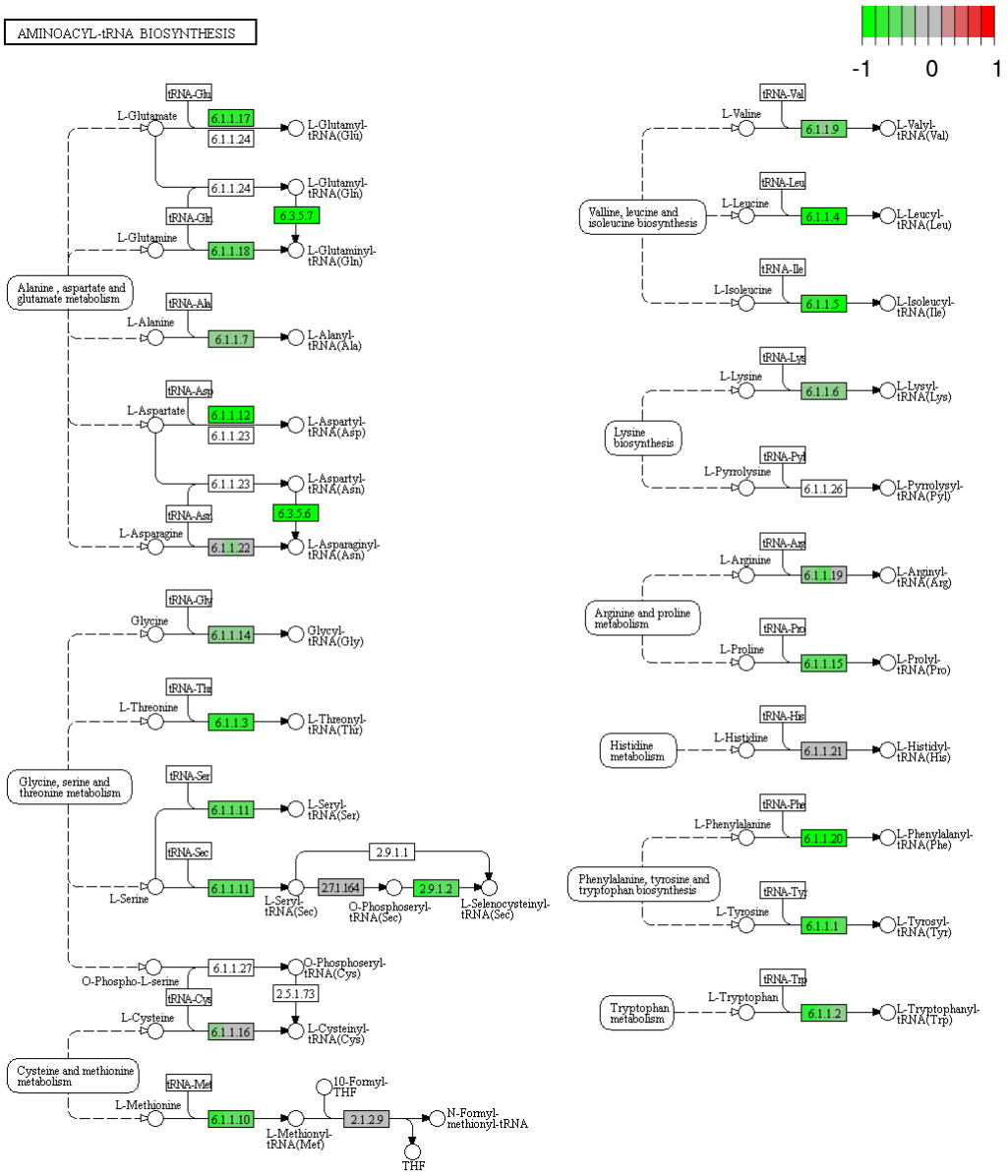

Data on KEGG graph
Rendered by Pathview

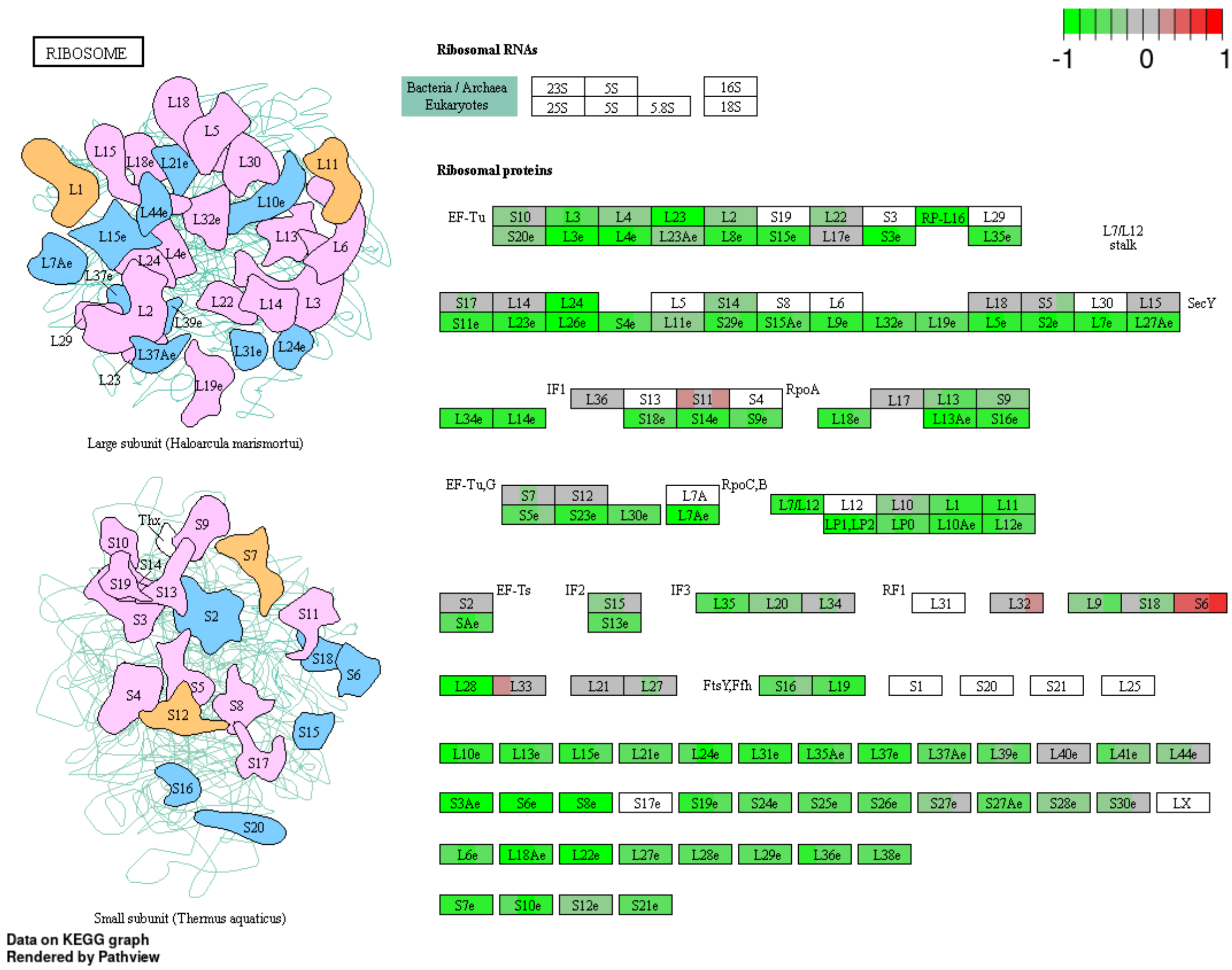

RIBOSOME
-1 0 1
Ribosomal RNAs
Bacteria / Archaea
Eukaryotes
23S 5S 16S
25S 5S 5.8S 18S
Ribosomal proteins
EF-Tu
S10 L3 L4 L23 L2 S19 L22 S3 RP-L16 L29
S20e L3e L4e L23Ae L8e S15e L17e S3e L35e
L7/L12 stalk
S17 L14 L24 L5 S14 S8 L6 L18 S5 L30 L15 SecY
S11e L23e L26e S4e L11e S29e S15Ae L9e L32e L19e L5e S2e L7e L27Ae
IF1 L36 S13 S11 S4 RpoA L17 L13 S9
L34e L14e S18e S14e S9e L18e L13Ae S16e
EF-Tu,G S7 S12 L7A RpoC,B L7/L12 L12 L10 L1 L11
S5e S23e L30e L7Ae LP1,LP2 LP0 L10Ae L12e
S2 EF-Ts IF2 S15 IF3 L35 L20 L34 RF1 L31 L32 L9 S18 S6
SAe S13e
L28 L33 L21 L27 FtsY,Ffh S16 L19 S1 S20 S21 L25
L10e L13e L15e L21e L24e L31e L35Ae L37e L37Ae L39e L40e L41e L44e
S3Ae S6e S8e S17e S19e S24e S25e S26e S27e S27Ae S28e S30e LX
L6e L18Ae L22e L27e L28e L29e L36e L38e
S7e S10e S12e S21e
Large subunit (Haloarcula marismortui)
Small subunit (Thermus aquaticus)
Data on KEGG graph
Rendered by Pathview

C

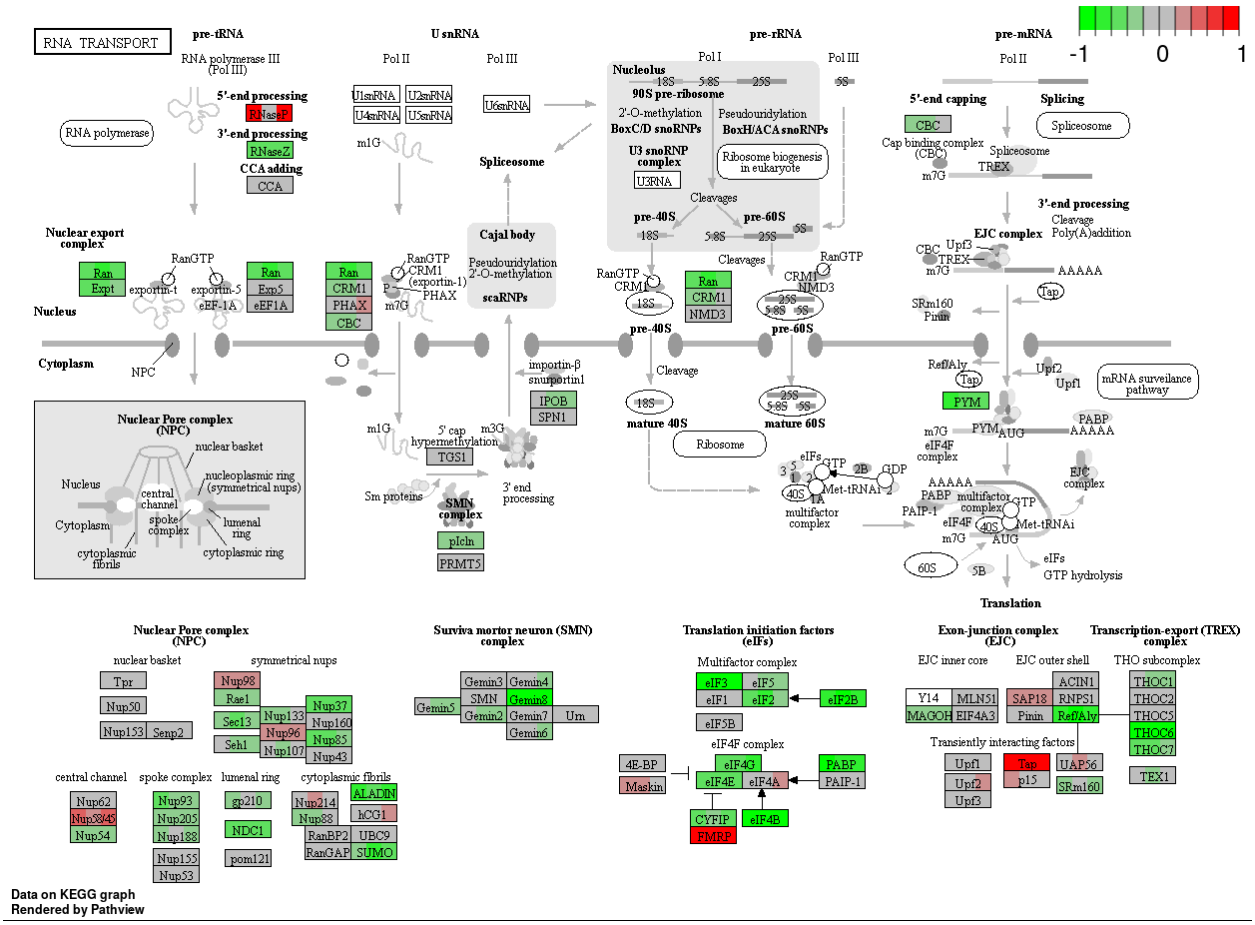

Figure 6. Decreased expression of multiple genes regulating aminoacyl-tRNA synthesis (A), ribosome biosynthesis (B), and genes regulating mRNA transport, maturation, and translation initiation (C) under cisplatin 10 μM compared to DMSO control in HT-29 CRC cell line. The genes are coloured according to the difference in expression level between treatment and control for each individual sample. Red colour shows up- and green down-regulation relative to the treatment group. Data based on GAGE uni-directional analysis.

Based on mRNA sequencing results, cisplatin decreased the expression of multiple genes responsible for translation involving processes such as amino-acyl tRNA synthesis, synthesis of ribosomes, and mRNA transport, maturation, and initiation of translation (Figure 6) in CRC cell line HT-29 compared to DMSO control. The results suggest that cisplatin could stimulate stress pathways that led to global translation inhibition to reduce energy expenditure, thus, increasing the chances of cell survival.

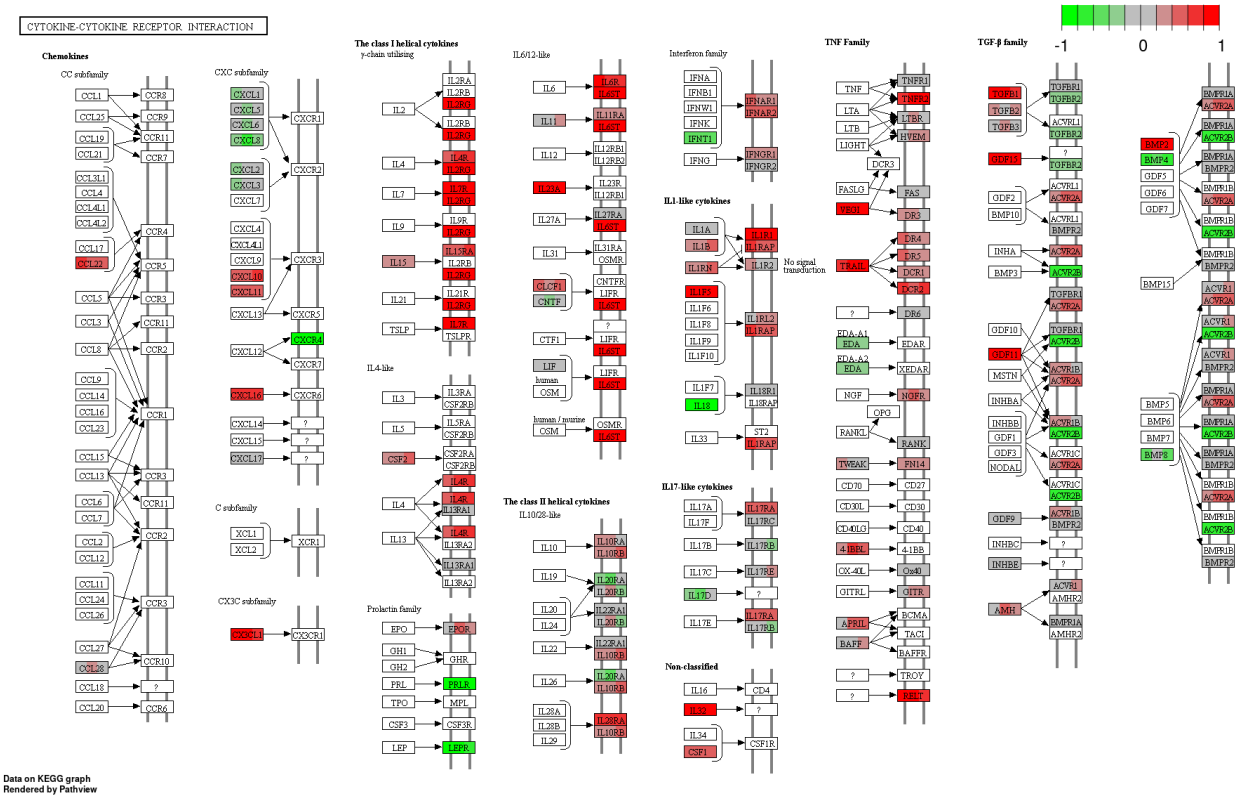

Figure 7. Changes in the expression of multiple genes in cytokine-cytokine interaction under cisplatin 10 μM compared to DMSO control in HT-29 CRC cell line. The genes are coloured according to the difference in expression level between treatment and control for each individual sample. Red colour shows up- and green down-regulation relative to the treatment group. Data based on GAGE uni-directional analysis.

Cisplatin increased the expression of multiple genes responsible for the cytokine-cytokine receptor interaction in CRC cell line HT-29 compared to DMSO control. As Figure 7 presents, mRNAs have increased expression for chemokines CCL22 from the CC subfamily and CXC subfamily with decreased expression of the CXCR4 receptor. Cisplatin upregulated the expression of the receptors for IL2, IL4, IL7, IL9, IL15, IL21 and IL13. There was also an increased expression of multiple class II helical cytokine receptors to which IL10, IL22, IL26, IL28 A and B, and IL29 bind. Additionally, there was increased expression of IFNAR1, IFNAR2, and IFNGR1, which are interferon family receptors. Moreover, cisplatin upregulated IL-1 and many IL17 receptors, TRAIL, and TNF family receptors, including DR4 and DR5, which take part in the extrinsic apoptosis pathway. Interestingly, increased levels of TGF-β could indicate possible

activation of cancer cell invasiveness, but most TGF-β receptors were decreased. Thus, cancer cells could not be able to undergo EMT and achieve their invasive potential.

A

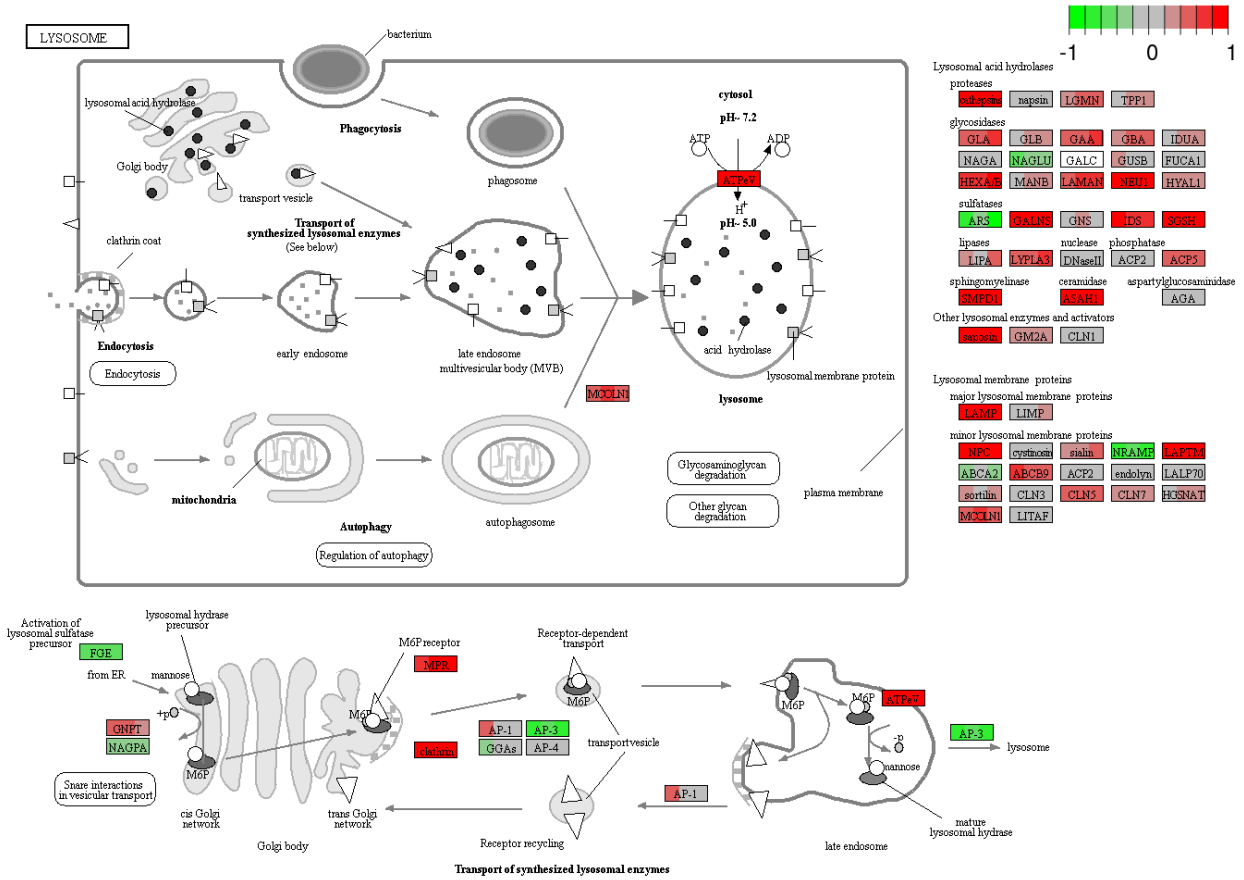

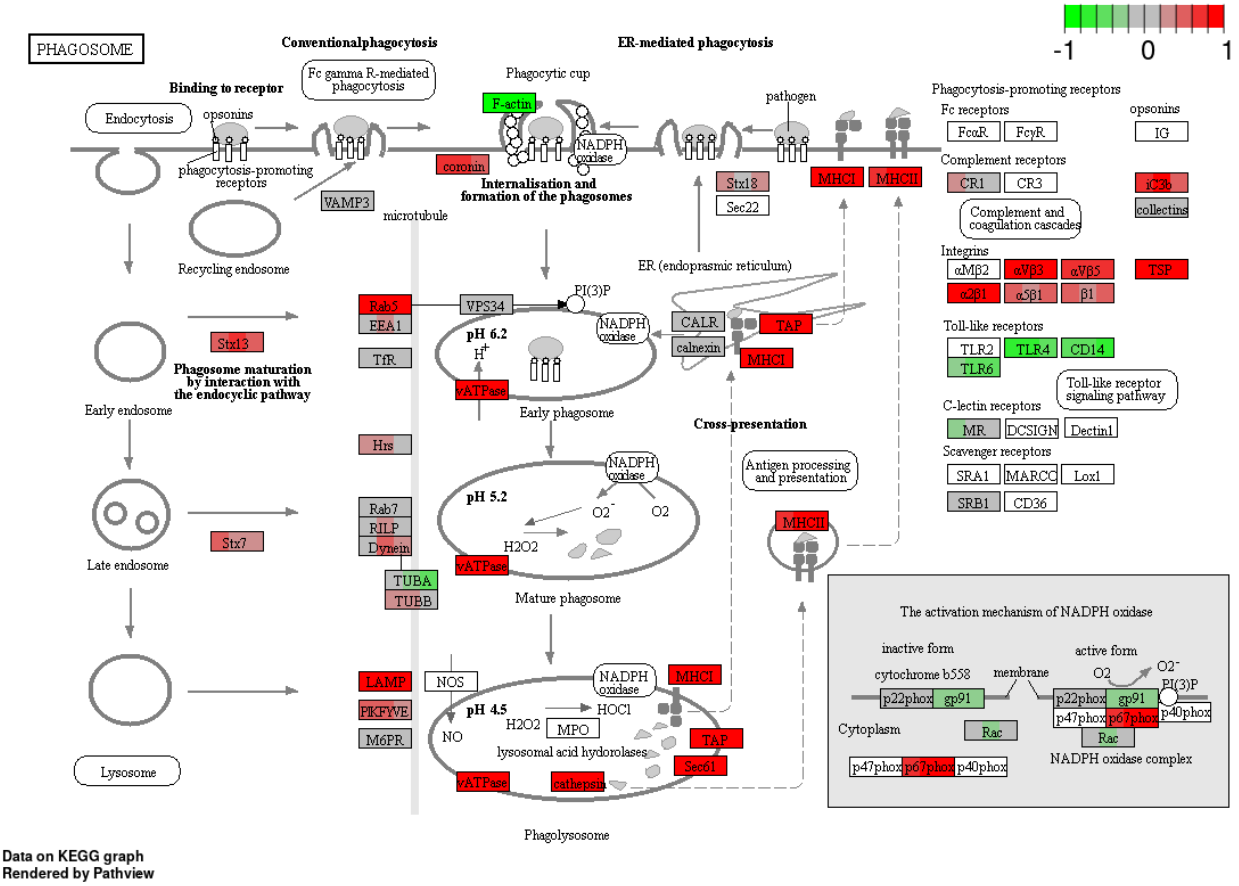

Figure 8. Changes in the expression of multiple genes responsible for lysosomal enzyme biosynthesis (A), and phagosome formation and phagocytosis (B) under cisplatin 10 μM compared to DMSO control in HT-29 CRC cell line. The genes are coloured according to the difference in expression level between treatment and control for each individual sample. Red colour shows up- and green down-regulation relative to the treatment group. Data based on GAGE uni-directional analysis.

Cisplatin increased the expression of most of the lysosomal acid hydrolases, membrane proteins and ATPeV, which may indicate high lysosomal activity in cancer cells leading to cell death (Figure 8). Moreover, cisplatin upregulated multiple genes encoding proteins involved in phagosome formation as well as MHCI and MHCII that are responsible for antigen presentation and recognition by the immune cells.

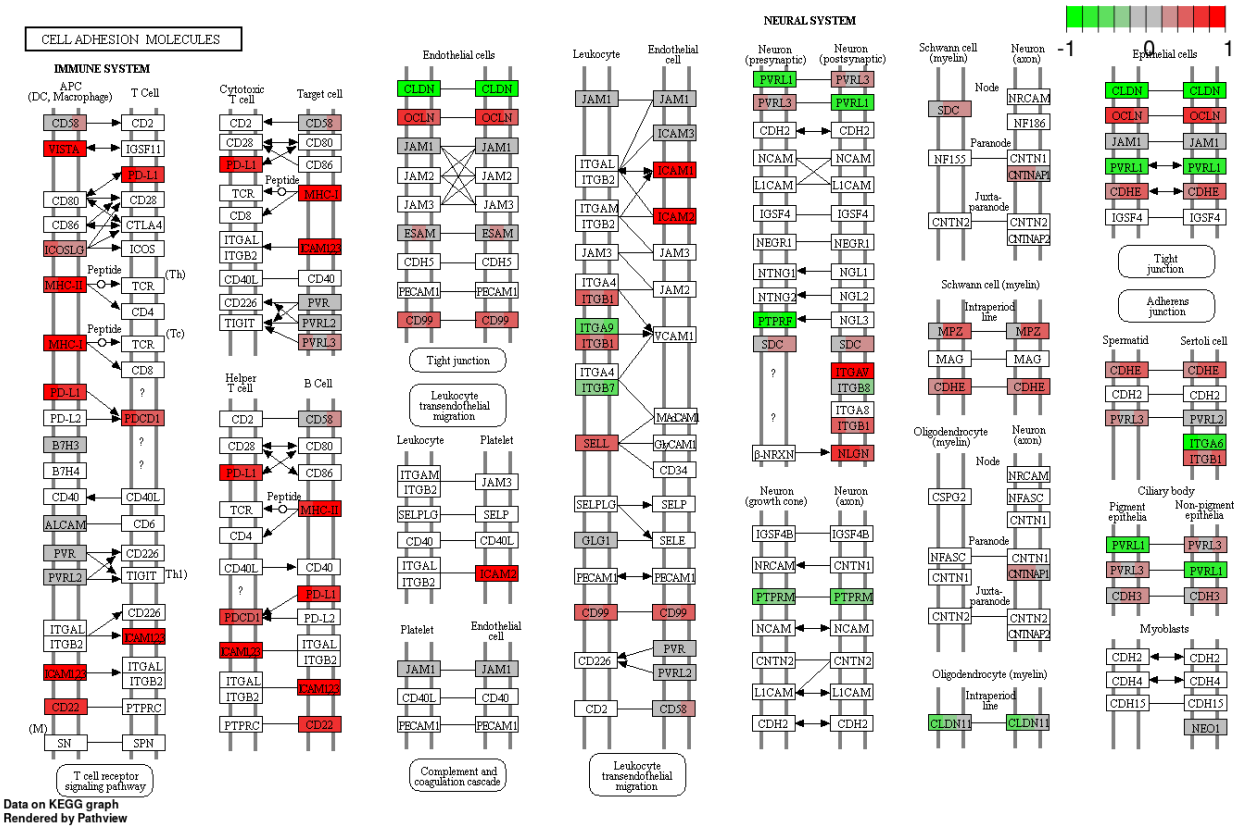

Figure 9. Changes in the expression of multiple genes responsible for cell adhesion molecules under cisplatin 10 μM compared to DMSO control in HT-29 CRC cell line. The genes are coloured according to the difference in expression level between treatment and control for each individual sample. Red colour shows up- and green down-regulation relative to the treatment group. Data based on GAGE uni-directional analysis.

Cisplatin upregulated multiple molecules involved in cell adhesion, which may point out its activities for the stimulation of epithelial-to-mesenchymal transition and invasion of tumor cells. There was also an increased expression of PDL-1 receptors that are targeted during cancer immune therapies, which may improve the therapeutic effectiveness of monoclonal antibodies targeting PDL-1 (Figure 9).

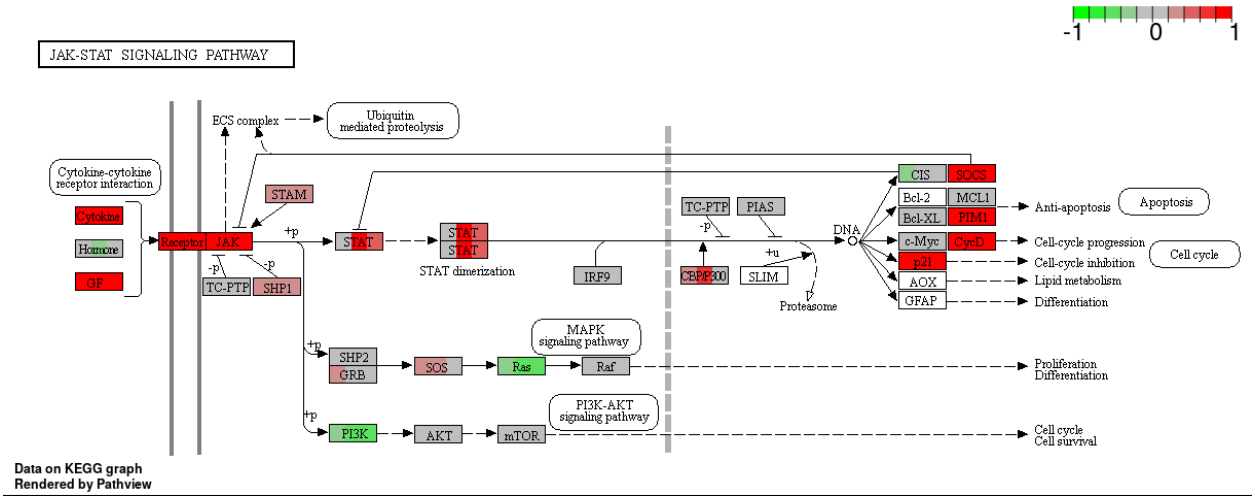

Figure 10. Changes in the expression of multiple genes responsible for JAK/STAT signalling pathway under cisplatin 10 μM compared to DMSO control in HT-29 CRC cell line. The genes are coloured according to the difference in expression level between treatment and control for each individual sample. Red colour shows up- and green down-regulation relative to the treatment group. Data based on GAGE uni-directional analysis.

In the HT-29 cell line, cisplatin downregulated Ras and PI3K expression and upregulated p21, which can be responsible for cell cycle arrest, inhibition of proliferation and cell survival mechanisms (Figure 10). However, it increased the expression of JAK/STAT signalling, which could lead to the inhibition of apoptosis and cell cycle progression via upregulated cyclin D.

A

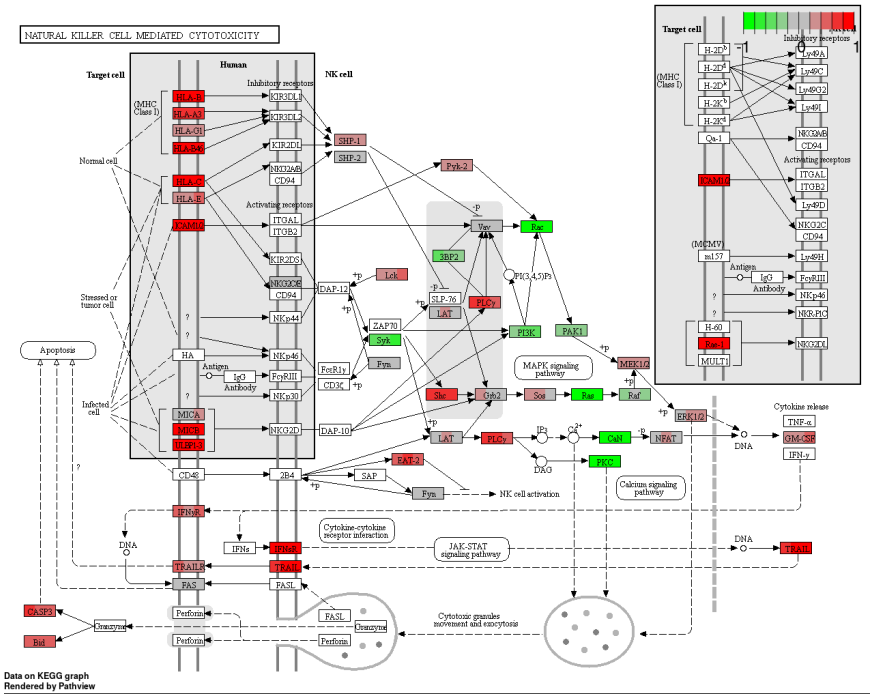

B

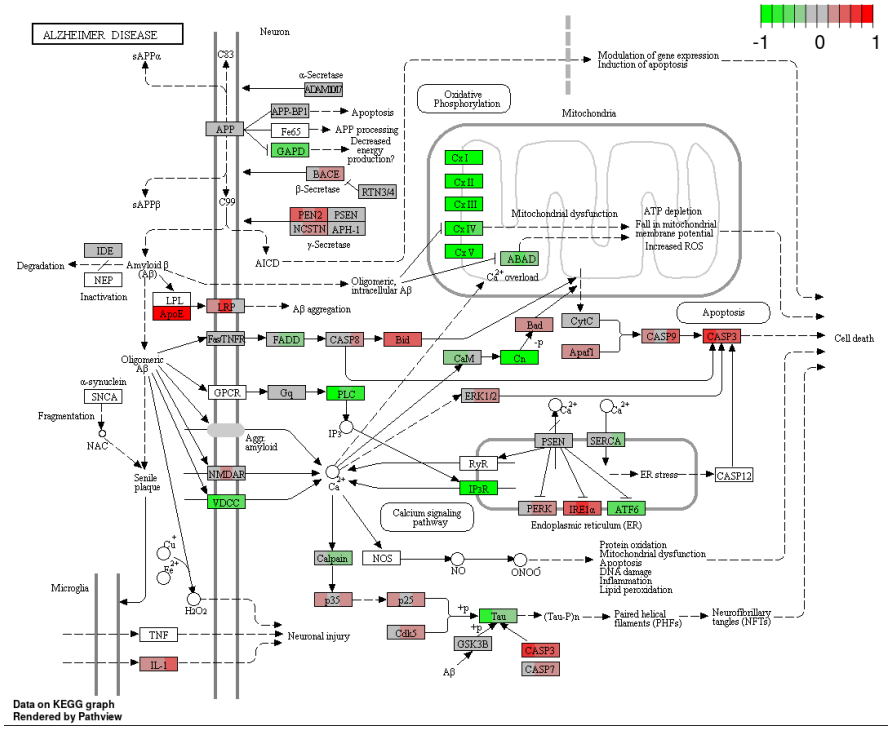

Figure 11. Changes in the expression of multiple genes responsible for natural killer mediated cytotoxicity (A) and pathways involved in cell bioenergetics, ER stress, and apoptosis (B) under cisplatin 10 μM compared to DMSO control in HT-29 CRC cell line. The genes are coloured according to the difference in expression level between treatment and control

for each individual sample. Red colour shows up- and green down-regulation relative to the treatment group. Data based on GAGE uni-directional analysis.

In a figure representing natural killer (NK) cell-mediated cytotoxicity, cisplatin increased MHC I, IFN receptors and integrins that are present on stressed and tumor cells, which can potentially attract cytotoxic immune cells. Additionally, there was increased expression of proapoptotic genes such as ERK1/2, TRAIL, Bid, and caspase 3 and downregulated Rac, PI3K, Ras, and PKC, which assist in cisplatin's antiproliferative and proapoptotic properties (Figure 11).

Cisplatin strongly inhibits oxidative phosphorylation by inhibiting all five complexes, which will would result in substantial ATP reduction in cancer cells. Cisplatin also activated ER stress response via PERK and IRE1α and increased the expression of pro-apoptotic genes, Bid, Bad, Apaf1, and caspases 8, 9, 7, and 3. These mechanisms align with the previously discussed cytotoxic effects of cannabinoids, which we can consider as a combination therapy with cisplatin.

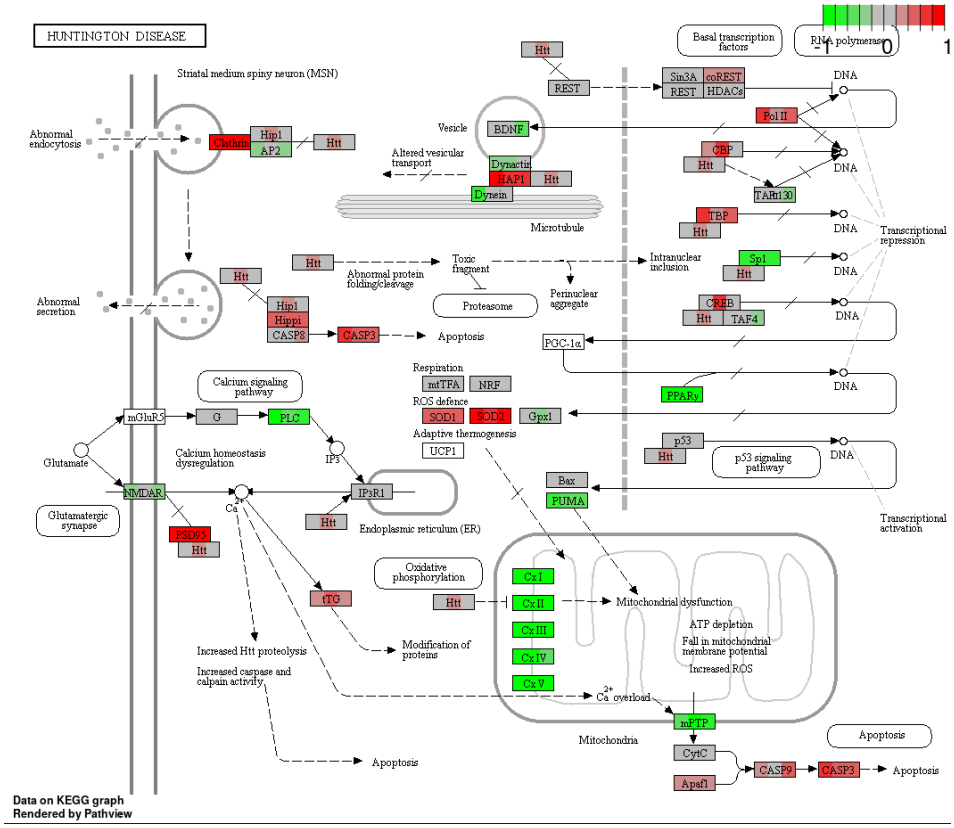

Figure 12. Changes in the expression of multiple genes responsible for endo- and exocytosis, basal transcription factors expression, oxidative phosphorylation, and regulation of apoptosis under cisplatin 10 μM compared to DMSO control in HT-29 CRC cell line. The genes are coloured according to the difference in expression level between treatment and control

for each individual sample. Red colour shows up- and green down-regulation relative to the treatment group. Data based on GAGE uni-directional analysis.

Cisplatin upregulated clathrin and other proteins that caused endo- and exocytosis enhancement in HT-29 CRC cells (Figure 12). There was downregulation of Ca signalling via PLC and upregulation of pro-apoptotic proteins except for PUMA. Cisplatin also increased levels of antioxidants such as superoxide dismutase 1 and 2. It also decreased levels of PPARγ, one of the effectors of CBD.

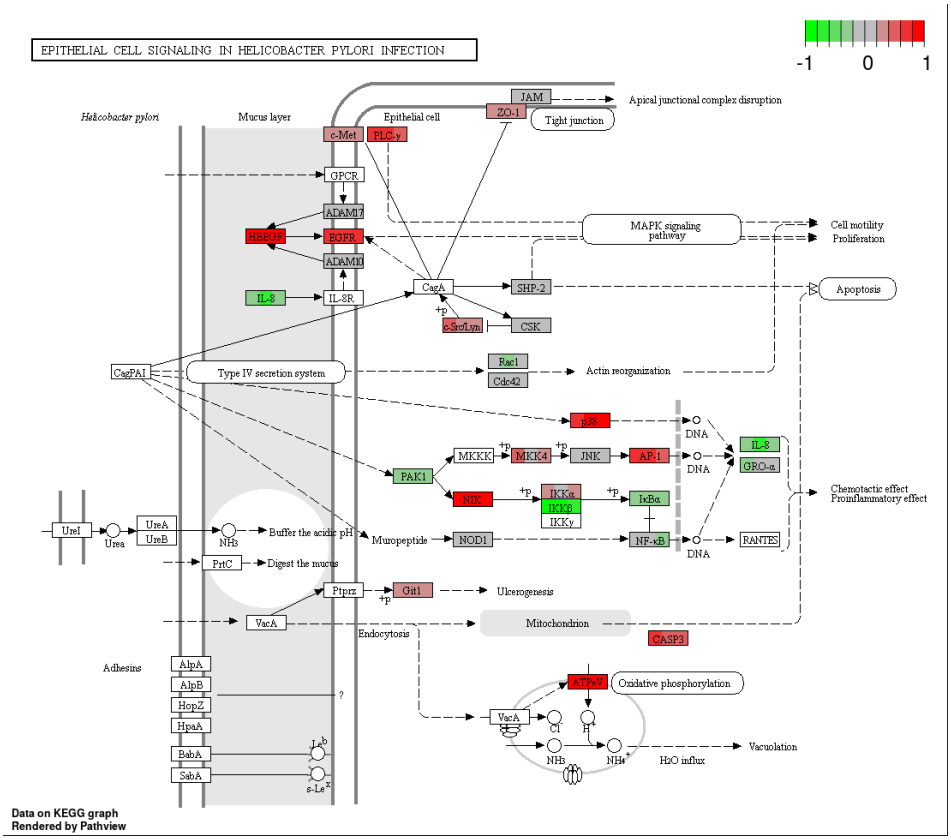

Figure 13. Changes in the expression of multiple genes responsible for growth factor signalling, tight junction maintenance, and inflammation under cisplatin 10 μM compared to DMSO control in HT-29 CRC cell line. The genes are coloured according to the difference in expression level between treatment and control for each individual sample. Red colour shows up- and green down-regulation relative to the treatment group. Data based on GAGE uni-directional analysis.

Under cisplatin action, there was upregulation of EGFR and growth factors release in the HT-29 cell line, which can indicate an autocrine signalling cascade in cancer cells that could be essential for self-initiated proliferation and activation of MAPK cascade (Figure 13). There was

upregulation of ZO-1, which is responsible for maintaining tight junctions in cancer cells that can prevent cancer invasion and metastasis of HT-29 CRC cells.

Moreover, cisplatin upregulated the MAPK pathway by increased expression of p38, MKK4 and transcription factor AP-1. On the other side, there was downregulation of NF-κB with strong suppression of IKKβ. Cisplatin decreased the expression of chemotactic IL-8, which can indicate the anti-chemotactic effect of cisplatin in cancer cells.

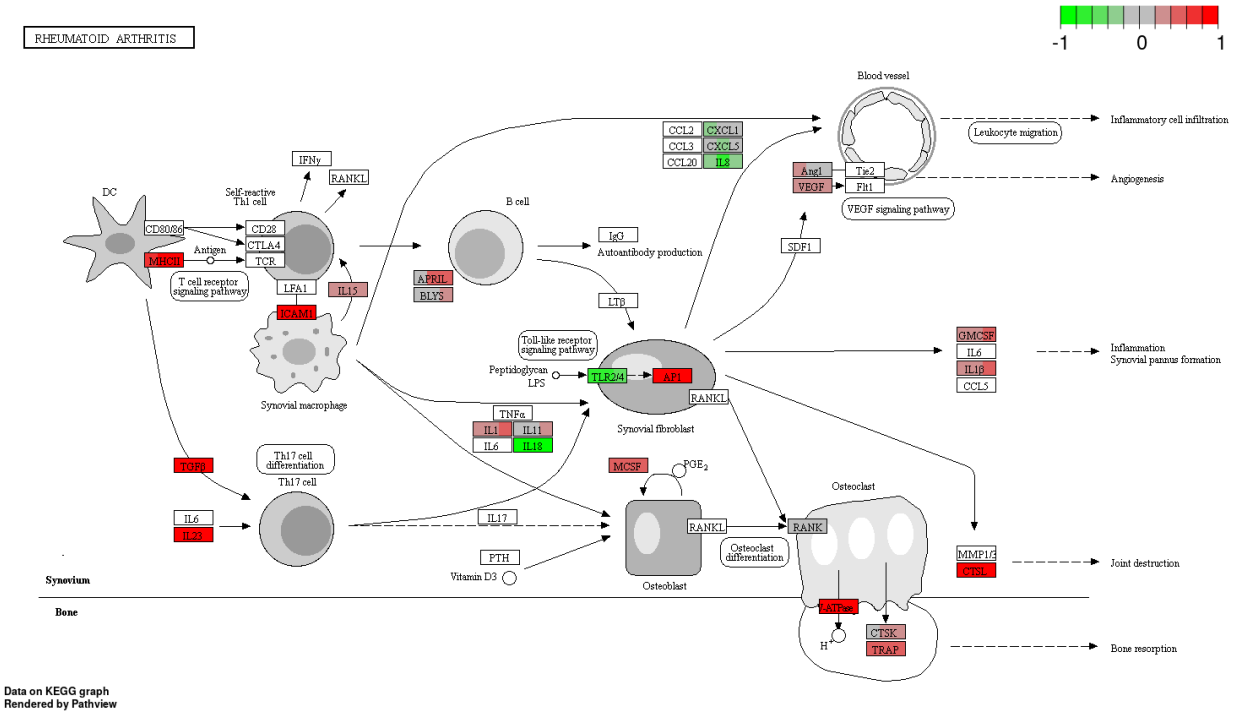

Figure 14. Changes in the expression of multiple genes responsible for immune system response under cisplatin 10 μM compared to DMSO control in HT-29 CRC cell line. The genes are coloured according to the difference in expression level between treatment and control for each individual sample. Red colour shows up- and green down-regulation relative to the treatment group. Data based on GAGE uni-directional analysis.

Figure 14 presents cisplatin action on multiple pathways involved in immune system response. It increases the expression of MHC class II responsible for antigen presentation, ICAM1 enhancing cellular adhesion, and cytokines responsible for inflammatory reactions such as IL-1β and IL-8. There is also upregulation of TGF-β, which may indicate activation of epithelial-to-mesenchymal transition, and VEGF, which is responsible for angiogenesis. This could promote the invasive and metastatic potential of HT-29 cancer cells. TGF-β and IL-23 may stimulate Th17

cells, inhibiting the cellular immune response of cancer cells. The interesting effect of cisplatin was the downregulation of the toll-like receptor signalling pathway, TLR 2/4, together with IL-18 that is required for killer T-cell activation. This may indicate an attempt by cancer cells to avoid immune destruction.

We also did differential gene expression analysis in of the HCT-116 CRC cell line, which resembles the MMR-deficient subtype of CRC.

Exploratory analysis

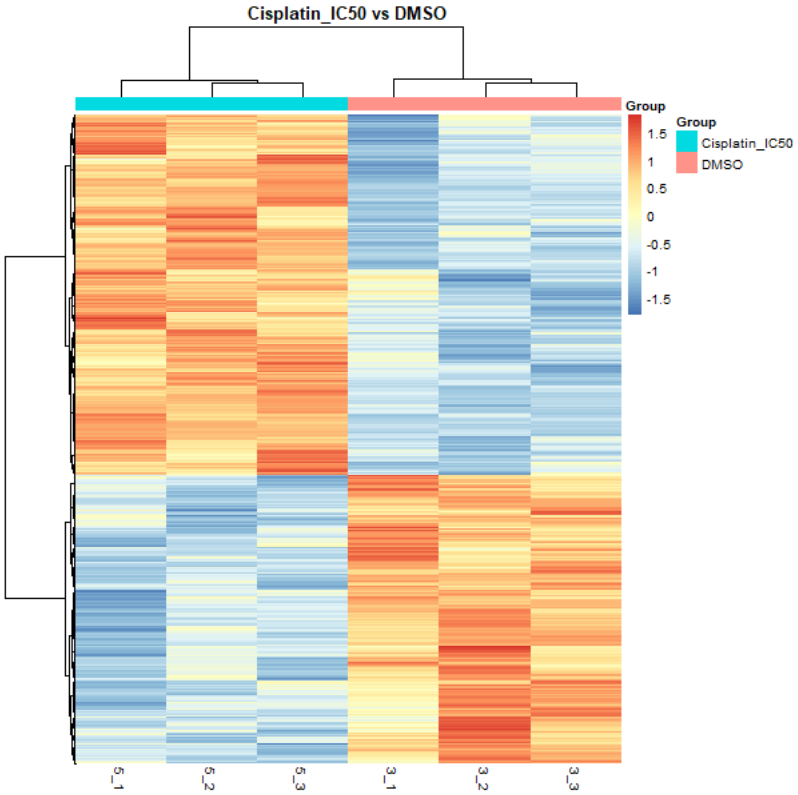

Figure 15. A hierarchical clustering heatmap analysis of the differentially expressed genes with fold change over 1.5 and adjusted p-values < 0.05 for DMSO control versus cisplatin IC50 in the HCT-116 CRC cell line. The x-axis shows non-supervised clusters between the two treatment groups. The 3.1, 3.2, and 3.3 are independent replicates for DMSO and 5.1, 5.2, and 5.3 are for cisplatin IC50. The y-axis shows differentially expressed genes. The fold changes of up-regulated genes are in the red-orange colour spectrum, and the down-regulated genes are represented in the blue colour spectrum. The heatmap was generated using R software version 4.2.2.

A heatmap represents differentially expressed genes for DMSO versus cisplatin IC50 in the HCT-116 CRC cell line. The unsupervised clustering based on the underlying data determined if there were sub-categories within DMSO control and cisplatin IC50 treatment. As the figure shows, there were significant differences in gene expression between treatment groups. The differences were not substantial for the biological replicates within the same group, showing the treatment samples' good quality (Figure 15).

Pathway analysis

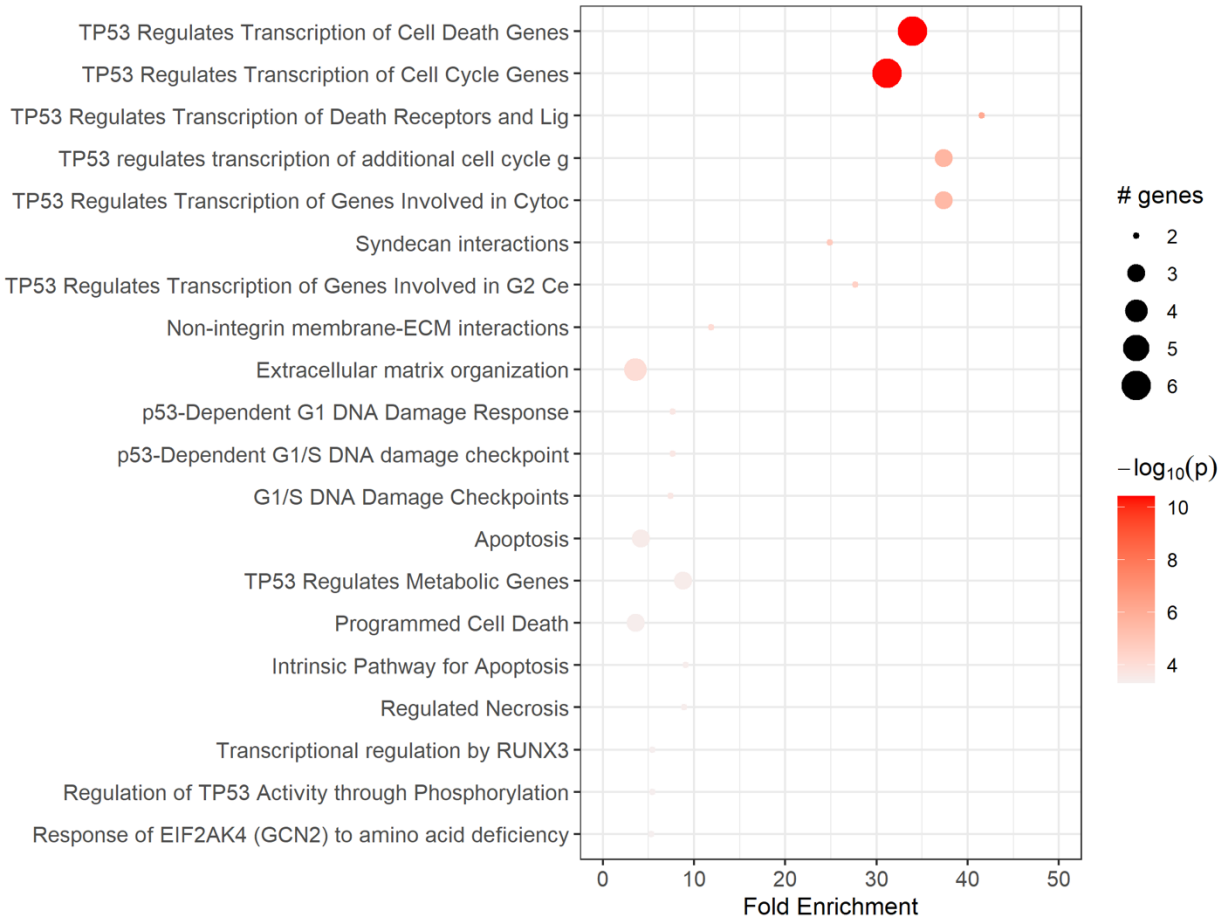

Figure 16. The Reactome dot plot of the top 20 terms for DMSO versus cisplatin IC50 in the HCT-116 CRC cell line. The top 20 terms with the highest fold change are shown in this plot, with their corresponding Reactome pathways on the y-axis. The size of the dots represents the number of genes in each pathway, while the red colour's intensity indicates the enrichment's significance. The most enriched pathways are shown at the top of the plot. The figure was generated using pathfindR enrichment analysis software.

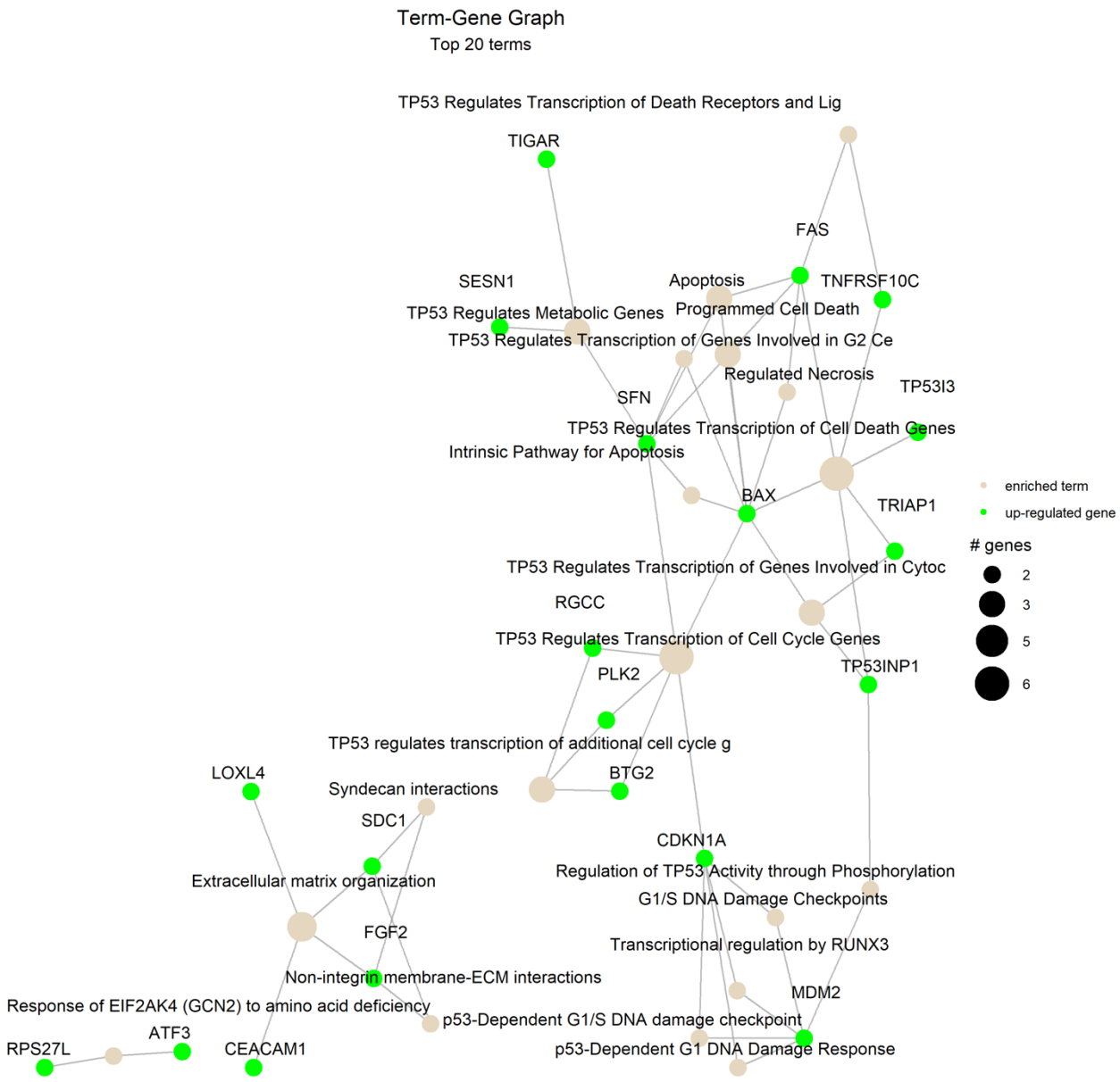

Figure 17. The Reactome Term-Gene Graph for Top 20 terms for DMSO versus cisplatin IC50 treatment in the HCT-116 CRC cell line. The graph displays the top 20 Reactome terms and their corresponding gene sets. Each node represents a Reactome term, and the size of the node is proportional to the number of genes associated with that term. The edges between the nodes represent the overlap in gene sets between the terms. The edge's thickness represents the overlap's magnitude, and the edge's colour represents the direction of the overlap, with green for upregulated and red for downregulated genes. The figure was generated using pathfindR enrichment analysis software.

Based on the Reactome data for differential expression analysis in HCT-116 CRC cells, cisplatin increased expression of genes responsible for p53-mediated cell cycle arrest in G1/S and G2 phases, activation of DNA-damage response including SNF and apoptosis such as BAX and FAS, which is expectable based on the drug action (Figures 16 and 17). There was also upregulation of gene coding for fibroblast growth factor 2, which can be responsible for epithelial-to-mesenchymal transition and tumor progression, and genes taking part in angiogenesis and interaction with the vascular wall (ANGPT2 – angiopoietin 2, CEACAM1 – CEA cell adhesion molecule 1, INPP5D – inositol polyphosphate-5-phosphatase D, SDC1 – Syndecan 1). Moreover, overexpression of MDM2 would also lead to inhibition of p53 activity and its effects.

One of the most enriched terms under cisplatin action on the HCT-116 CRC cell line was TP53-regulated transcription of cell death gene. The increased levels of TP53, BAX, FAS and TNF receptor ligands would strongly indicate that cells were heading toward apoptotic cell death, which is similar to the expression data in the HT-29 CRC cell line. The increased levels of Cyclin-Dependent Kinase inhibitor 1A (CDKN1A) that binds to cyclin-cyclin-dependent kinase 2 or 4 complexes and functions as a regulator of the G1 cell cycle could support the notion of G1/S cell cycle arrest. Increased RGCC gene expression is also responsible for cell cycle regulation and is induced by p53 because of DNA damage. Additionally, higher levels of BTG anti-proliferation factor 2 could have helped with G1/S cell cycle arrest. The increased levels of stratifin (SFN) transcript, which binds to translation initiation factors and functions as a regulator of translation during mitosis, helps prevent DNA errors during mitosis and could correspond to cancer cell survival. The increased transcription of the SESN1 gene, coding for sestrin 1, which is induced by p53 and serves as a potent inhibitor of mTOR, would help in cisplatin's cytotoxic effects. Although the increased levels of polo-like kinase 2 might indicate a strong stimulus for cell proliferation, the weight of antiproliferative signalling was stronger, which supports our MTT results.

The increased levels of fibroblast growth factor 2 (FGF2) and syndecan 1 (SDC1), which are responsible for cell binding, cytoskeletal organization, interactions with ECM, and cell migration, could stimulate EMT and invasiveness of HCT-116 cell line, which are the signs of cancer cell progression.

The ATF3 (activating transcription factor 3) and RPS27L (ribosomal protein S27) were also activated, the genes responsible for eIF2-mediated response to amino acid starvation.

The top 10 up- and 5 down-regulated genes are presented in Table 4.

Table 4. Top 10 up-and 5 down-regulated genes for DMSO versus cisplatin treatment in the HCT-116 CRC cell line based on mRNA expression analysis.

Top 10 up-regulated genes			
Gene name	Gene description	Gene biotype	Log2 Fold Change
ABCA12	ATP binding cassette subfamily A member 12	Protein coding	1.95
PTCHD4	patched domain containing 4	Protein coding	1.60
INPP5D	inositol polyphosphate-5-phosphatase D	Protein coding	1.45
INKA2	Inka box actin regulator 2	Protein coding	1.39
MUC19	mucin 19, oligomeric	Protein coding	1.32
ACTA2	actin alpha 2, smooth muscle	Protein coding	1.28
DRAXIN	dorsal inhibitory axon guidance protein	Protein coding	1.23
CDKN1A	cyclin dependent kinase inhibitor 1A	Protein coding	1.22
SULF2	sulfatase 2	Protein coding	1.14
CEACAM1	CEA cell adhesion molecule 1	Protein coding	1.14
Top 5 down-regulated genes			
Gene name	Gene description	Gene biotype	Log2 Fold Change
DHRS2	dehydrogenase/reductase 2	Protein coding	-0.85
DHFR2	dihydrofolate reductase 2	Protein coding	-0.73
PRAM1	PML-RARA regulated adaptor molecule 1	Protein coding	-0.63
LINC01011	long intergenic non-protein coding RNA 1011	lncRNA	-0.62
KCNQ1	potassium voltage-gated channel subfamily Q member 1	Protein coding	-0.60

Overall, despite cisplatin's ability to activate programmed cell death and cell cycle arrest, there was also activation of the transcripts that could be responsible for the tumour's progression

and development of drug resistance. The mRNA sequencing results of the HCT-116 CRC cell line were similar to the ones we received for the HT-29 CRC cell line.

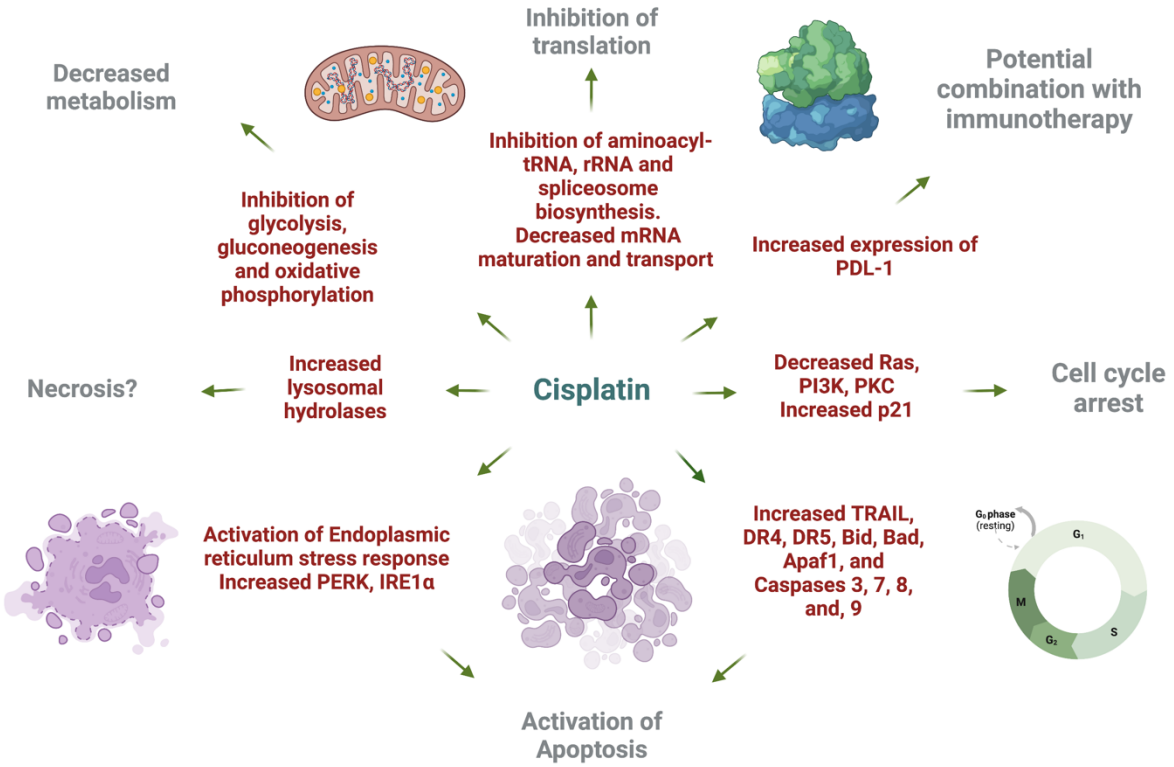

Figure 18. Cytotoxic effect of cisplatin on HT-29 cell line based on gene expression data. Created with BioRender.com

The mRNA expression data on the HT-29 cell line showed that cisplatin might affect cancer cells in multiple ways. As Figure 18 shows, cisplatin inhibited global translation by inhibiting aminoacyl-tRNA, rRNA and spliceosome biosynthetic pathways. It also decreased multiple metabolic pathways cancer cells rely on for growth and proliferation, such as glycolysis, gluconeogenesis, and oxidative phosphorylation. One of the major cytotoxic effects of cisplatin was the increased expression of multiple genes that take part in the activation and execution of extrinsic and intrinsic apoptotic pathways. Additionally, cisplatin increased the expression of p21, which can lead to cell cycle arrest in the G1/S phase. However, cell cycle arrest could also lead to cell survival and is not necessarily a beneficial effect of chemotherapy. Interestingly, cisplatin increased the expression of some genes that take part in endoplasmic reticulum stress response, which can assist the anticancer action of cannabinoids. Moreover, cisplatin increased PDL-1

expression, a known target for cancer immunotherapy. This can be one of the milestones for combining cisplatin with immunotherapy with a possible synergistic effect.

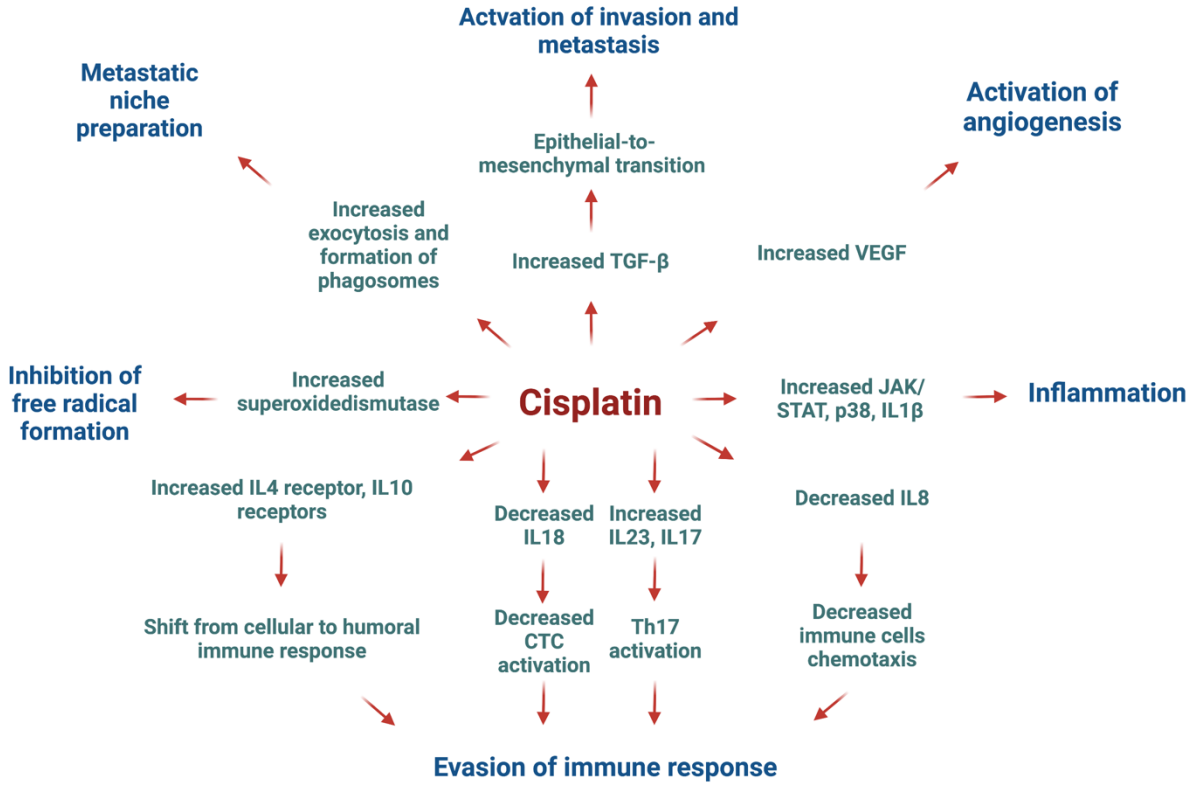

Figure 19. Possible mechanisms of tumor progression in HT-29 CRC cell line under cisplatin treatment. Created with BioRender.com

The Figure 19 represents the undesirable effects of cisplatin on HT-29 CRC cells based on mRNA sequencing results. Cytotoxic T-cells are the ones that may kill cancer cells by binding to death receptors and infusing perforins and granzymes. Multiple cisplatin effects help with immune response evasion. For instance, cisplatin decreased the expression of IL18, which takes part in cytotoxic T-cell activation. At the same time, it increased the expression of IL4 and IL10, which can shift cellular immune response to humoral, as well as could activate regulatory T-cells in tumor microenvironment by increased expression of IL17 and IL23.

Surprisingly, cisplatin may stimulate cancer progression by enhancing invasion and metastasis with the help of TGF-β signalling and increased formation of exosomes, which has been shown to prepare the niche in different organs for successful metastasizing. Moreover, it increased the expression of VEGF, which promotes angiogenesis – another hallmark of cancer progression.

Overall, cisplatin has controversial effects on HT-29 CRC cells. On the one hand, it strongly stimulated apoptosis. Still, the cells that survived may become more adapted to the next rounds of chemotherapy because of the upregulated genes responsible for the tumor progression and evasion by the immune response.

1.4.2. Cannabinoids and colorectal cancer cell lines

To establish a time and dose-dependent effect of THC and CBD on different CRC cell lines and to calculate IC50s for each tested cell line, I performed a cell viability assay (MTT).

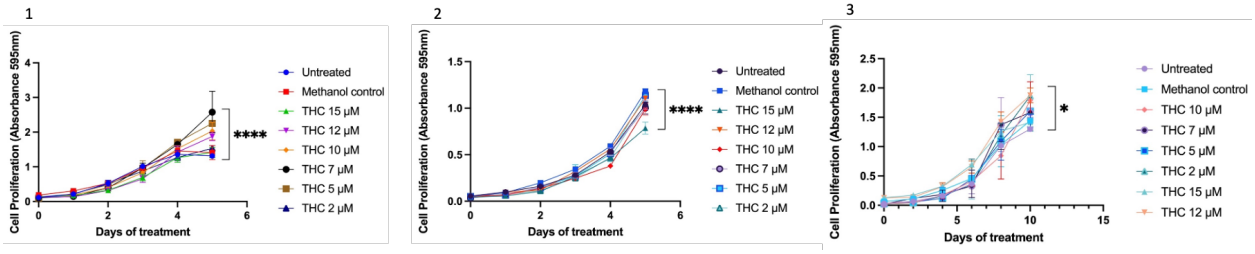

Figure 20. The time-dose-dependent effect of THC on HCT-116 (1), HT-29 (2), and LS-174T (3) cell lines based on MTT results. Results are expressed as means of calculated cell viability ± standard deviations of each group in triplicate at absorbance 595 nm. To calculate time-dose effects, two-way ANOVA was performed using GraphPad Prism version 9.0. Significant differences between groups are marked with ns – non-significant, *p < 0.05, **p < 0.01, ***p < 0.001, ****p <0.0001.

Based on the MTT results, THC did not substantially reduce cell viability in the HT-29, HCT-116, and LS-174T CRC cell lines (Figure 20). We did not continue testing THC as anti-cancer therapy due to its low antiproliferative properties on tested CRC cell lines.

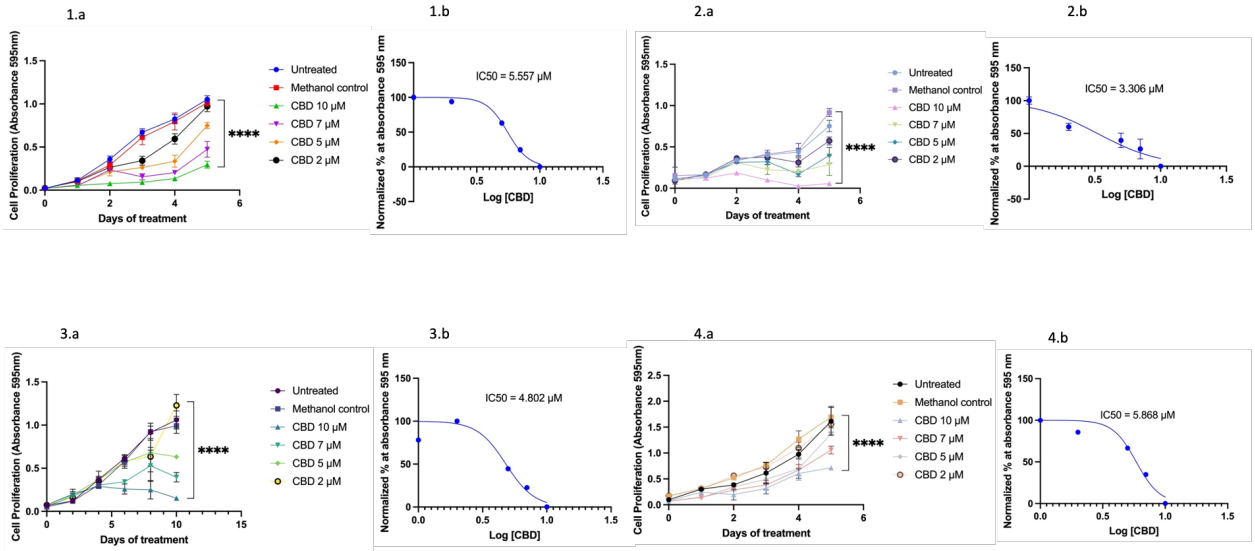

Figure 21. The time-dose-dependent effect and nonlinear regression analysis of dose-effect curve with calculated IC50 values of CBD on HCT-116 (1.a, 1.b), HT-29 (2.a, 2.b), LS-174T (3.a, 3.b), and HCEC (4.a, 4.b) cell lines based on MTT results. Results are expressed as means of calculated cell viability ± standard deviations of each group in triplicate at absorbance 595 nm. To calculate time-dose effects, two-way ANOVA was performed using GraphPad Prism version 9.0. Significant differences between groups are marked with ns – non-significant, *p < 0.05, **p < 0.01, ***p < 0.001, ****p <0.0001. A nonlinear fit with log(inhibitor) vs. normalized response–variable slope analysis was performed using GraphPad Prism version 9.0.

CBD significantly inhibited the cell viability of all tested cell lines in a time and dose-dependent manner (Figure 21). Based on nonlinear regression analysis, the CBD's IC50s for tested CRC cell lines were lower than the IC50 for normal colon epithelial cell line. This means that tested cancer cells were more susceptible to CBD than tested normal cell line. Thus, CBD might have lesser adverse effects than cisplatin.

The next step was to establish the possible molecular mechanisms behind CBD cytotoxicity. For that, we performed mRNA sequencing and pathway analysis for the HCT-116 CRC cell line.

Exploratory analysis

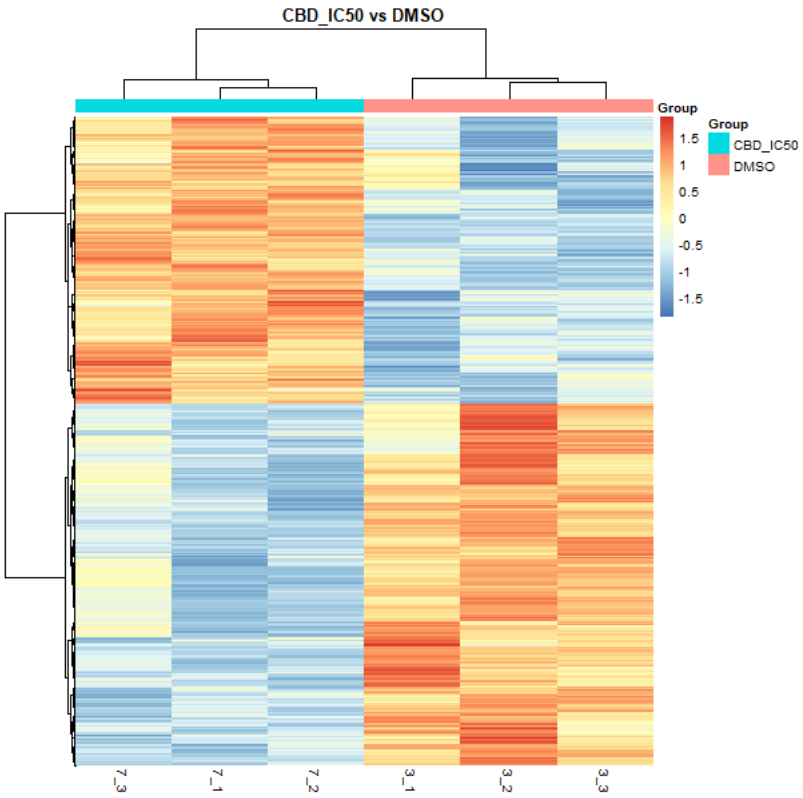

Figure 22. A hierarchical clustering heatmap analysis of the differentially expressed genes with fold change over 1.5 and adjusted p-values < 0.05 for DMSO control versus CBD IC50 in the HCT-116 CRC cell line. The x-axis shows non-supervised clusters between the two treatment groups. The 3.1, 3.2, and 3.3 are independent replicates for DMSO and 7.1, 7.2, and 7.3 are for CBD IC50. The y-axis shows differentially expressed genes. The fold changes of up-regulated genes are in the red-orange colour spectrum, and the down-regulated genes are represented in the blue colour spectrum. The heatmap was generated using R software version 4.2.2.

A heatmap represents differentially expressed genes for DMSO versus CBD IC50 in the HCT-116 CRC cell line. The unsupervised clustering based on the underlying data determined if there were sub-categories within DMSO control and CBD IC50 treatment. As the figure shows, there were significant differences in gene expression between treatment groups. The differences were not substantial for the biological replicates within the same group, showing the treatment samples' good quality (Figure 22).

Pathway analysis

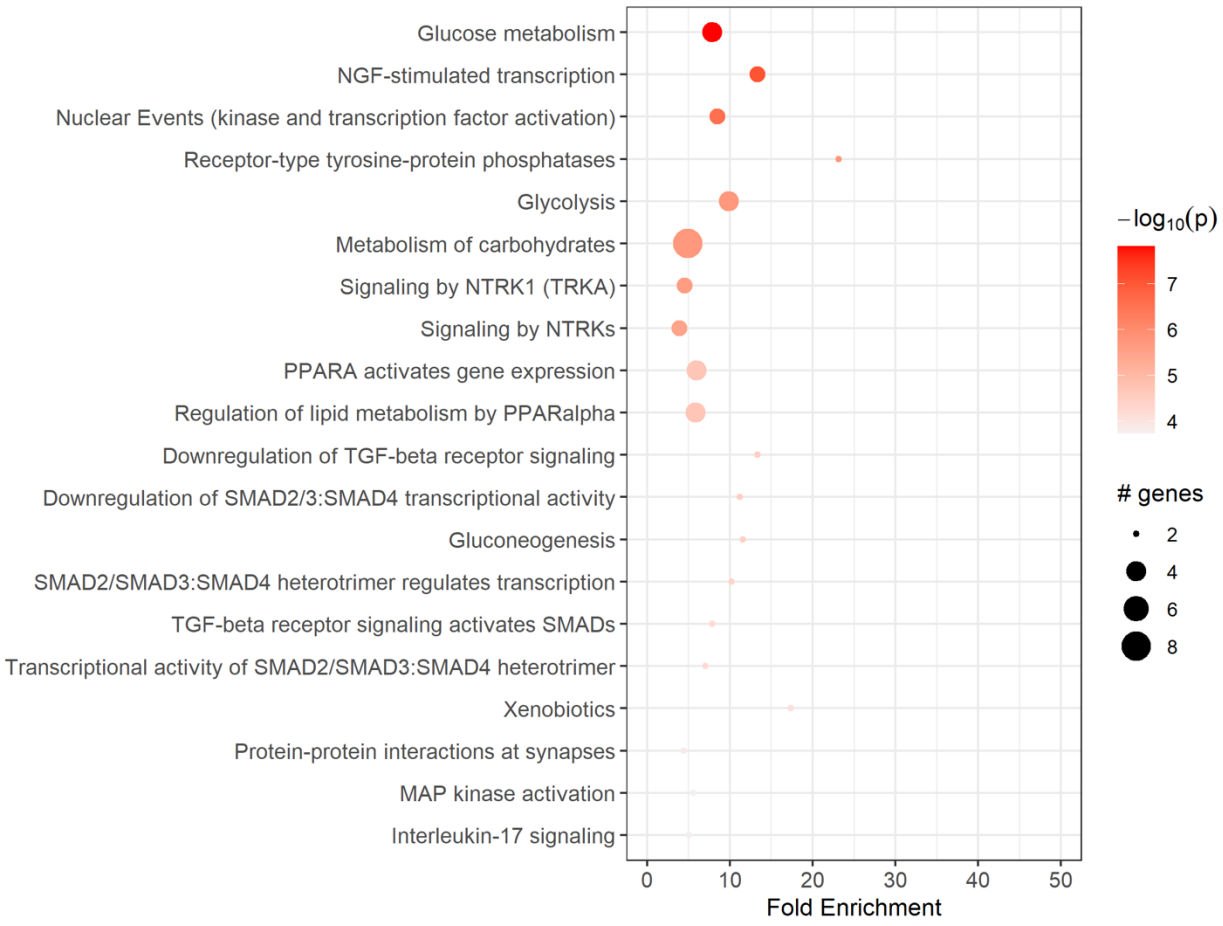

Figure 23. The Reactome dot plot of the top 20 terms for DMSO versus CBD IC50 in the HCT-116 CRC cell line. The top 20 terms with the highest fold change are shown in this plot, with their corresponding Reactome pathways on the y-axis. The size of the dots represents the number of genes in each pathway, while the red colour's intensity indicates the enrichment's significance. The most enriched pathways are shown at the top of the plot. The figure was generated using pathfindR enrichment analysis software.

Based on the dot plot data, CBD significantly affected carbohydrate metabolism, PPAR, TGF-β, and MAPK signalling (Figure 23).

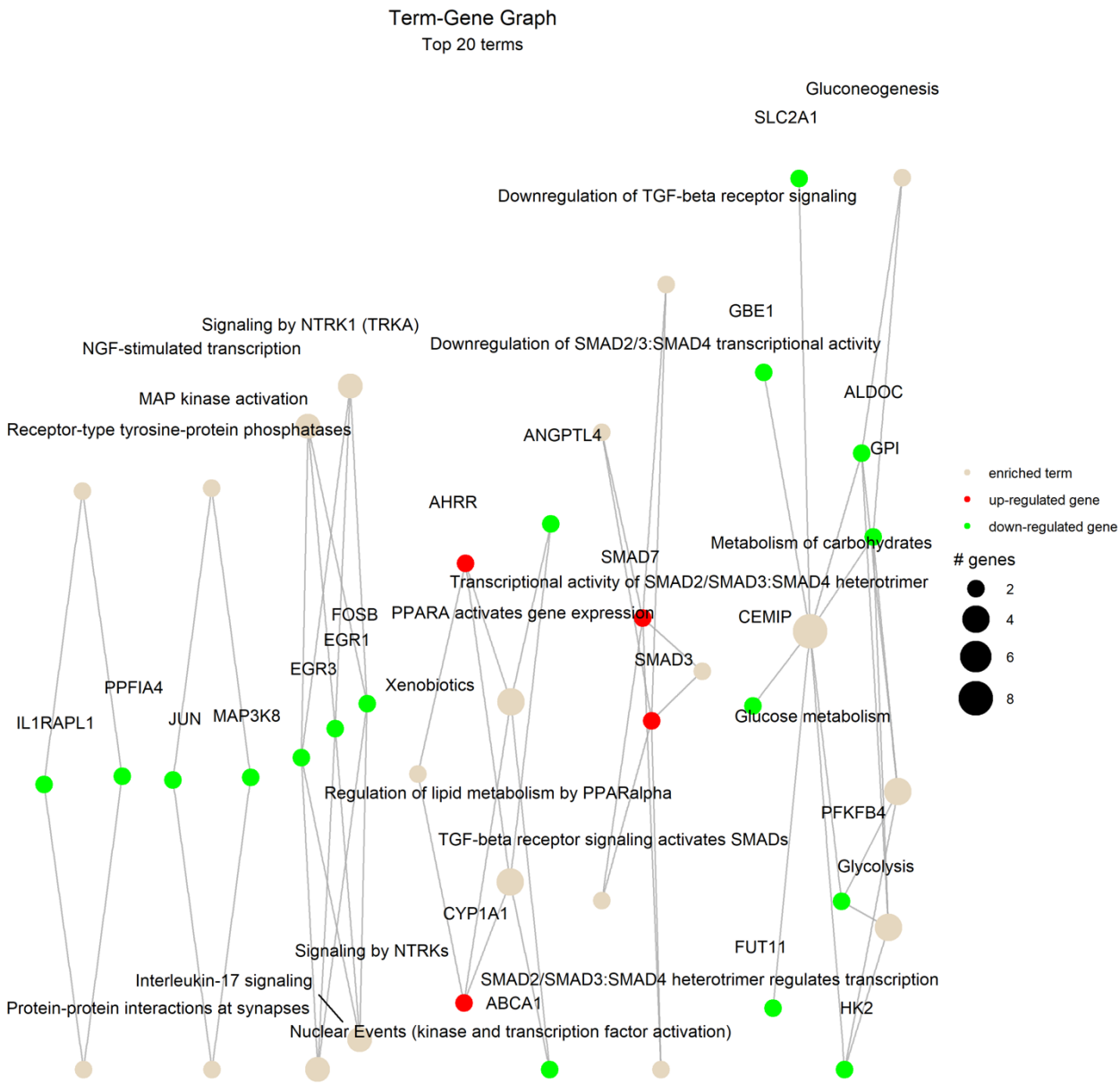

Figure 24. The Reactome Term-Gene Graph for Top 20 terms for DMSO versus CBD IC50 treatment in the HCT-116 CRC cell line. The graph displays the top 20 Reactome terms and their corresponding gene sets. Each node represents a Reactome term, and the size of the node is proportional to the number of genes associated with that term. The edges between the nodes represent the overlap in gene sets between the terms. The edge's thickness represents the overlap's magnitude, and the edge's colour represents the direction of the overlap, with green for downregulated and red for upregulated genes. The figure was generated using pathfindR enrichment analysis software.

Based on the Reactome data for differential expression analysis in HCT-116 CRC cells, CBD decreased the expression of genes responsible for glucose metabolism, glycolysis, and gluconeogenesis, such as PFKFB4 that regulates fructose-2,6-bisphosphate, and responded to hypoxia to help cancer cells produce more ATP (Figure 24). There was also downregulation of hexokinase 2 (HK2) expression that is involved in the rapid activation of glycolysis in cancer cells. The transcript for glucose-6-phosphate isomerase (GPI) was decreased too. The function of GPI, along with the regulation of glucose metabolism, is acting as an autocrine motility factor, a tumor-secreting cytokine, and an inducer of angiogenesis. This shows that the addition of CBD inhibited transcription of factors that help cancer cells in energy and oxygen scarcity and might prevent cancer progression.

Addition of CBD changes NGF-stimulated transcription kinase and transcription factor activation by downregulating genes such as FOSB, EGR3, and EGR1. FOSB gene codes for FosB proto-oncogene, AP-1 transcription factor, which can activate cell proliferation, differentiation, and transformation in cancer cells. EGR3 and EGR1, transcripts for the early growth response 3 and 1, are regulators of cell mitogenesis, and differentiation was higher too.

Adding CBD also modulated pathways involving TGF- β signalling, such as SMAD7 and SMAD3. SMAD7 was shown to antagonize signalling by the TGF- β type 1 receptor and inhibit TGF- β by associating with their receptors and preventing SMAD 2 access. SMAD7 mutations have been associated with CRC. The upregulation of SMAD 3 has a similar effect, which is part of the transcription factor complex and can serve as a tumor suppressor.

There was also downregulation of IL1RAPL1 gene expression, which is a part of the IL-1 receptor family. The gene that takes part in regulating the interaction between the extracellular environment and regulating the disassembly of focal adhesions PPFIA4 was decreased.

CBD decreased expression ABCA1, the ATP binding subfamily A member 1, which functions as a cholesterol efflux pump and is regulated by the PPAR signalling system. The ABC family transporters are commonly responsible for chemotherapy drug resistance. Thus, CBD might reduce the likelihood of drug resistance development. The downregulation of angiopoietin-like 4 (ANGPTL4), which is induced by PPAR signalling, functions as a serum hormone regulating glucose and lipid metabolism and insulin sensitivity. Furthermore, there was upregulation of CYP1A1, a gene coding for monooxygenase enzymes that take part in drug metabolism, and AHRR, which is involved in cytochrome P450 signalling and drug metabolism.

The decreased expression of a transcription factor JUN could inhibit T-cell activation-induced death and reduce transcription in response to Toll-like receptor signalling. JUN transcript is also responsible for KRAS-mediated transcriptional activation of USP28 in CRC. It also takes part in the MyD88-dependent cascade initiated by endosome signalling. Additionally, CBD increased the expression of CD22, which helps in B-cell activation. Finally, there was decreased level of MAP3K8 transcript, an oncogene coding for Mitogen-Activated Protein Kinase Kinase Kinase 8, which can activate both MAP and JNK pathways as well as proinflammatory pathways involving activation of NFκB.

The top 10 up- and 10 down-regulated genes are presented in Table 5.

Table 5. Top 10 up-and 10 down-regulated genes for DMSO versus CBD treatment in the HCT-116 CRC cell line based on mRNA expression analysis.

Top 10 up-regulated genes			
Gene name	Gene description	Gene biotype	Log2 Fold Change
CYP1A1	cytochrome P450 family 1 subfamily A member 1	Protein coding	1.8
AHRR	aryl hydrocarbon receptor repressor	Protein coding	1.8
CYP1B1	cytochrome P450 family 1 subfamily B member 1	Protein coding	1.3
ALDH1A3	aldehyde dehydrogenase 1 family member A3	Protein coding	1.2
HOXA1	homeobox A1	Protein coding	1.1
SMAD7	SMAD family member 7	Protein coding	1.1
GDA	guanine deaminase [	Protein coding	1
LINC00886	long intergenic non-protein coding RNA 886	lncRNA	0.9
VIPR1	vasoactive intestinal peptide receptor 1	Protein coding	0.9
PLA2G7	phospholipase A2 group VII	Protein coding	0.8

Top 10 down-regulated genes			
Gene name	Gene description	Gene biotype	Log2 Fold Change
ANKRD37	ankyrin repeat domain 37	Protein coding	-1.4
FOSB	FosB proto-oncogene, AP-1 transcription factor subunit	Protein coding	-1.3
SUSD2	sushi domain containing 2	Protein coding	-1.2
UPK1A-AS1	UPK1A antisense RNA 1	lncRNA	-1.1
ARRDC4	Arrestin domain containing 4	Protein coding	-1.1
CA9	carbonic anhydrase 9	Protein coding	-1.1
JUN	Jun proto-oncogene, AP-1 transcription factor subunit	Protein coding	-1.1
ABCA1	ATP binding cassette subfamily A member 1	Protein coding	-1.0
FAM13A-AS1	FAM13A antisense RNA 1	lncRNA	-1.0
IGFBP3	insulin like growth factor binding protein 3	Protein coding	-0.9

Overall, based on Reactome data for differential expression analysis in HCT-116 CRC cells, CBD had various effects on gene expression. CBD decreased the expression of genes responsible for glucose metabolism, glycolysis, and gluconeogenesis, which may prevent cancer growth. It could also downregulate cell mitogenesis and differentiation genes, FOSB, EGR3, and EGR1. Additionally, CBD modulated pathways involving TGF- β signalling and could reduce the likelihood of drug resistance development by decreasing the expression of ABCA1 and ANGPTL4. Furthermore, it increased the expression of oncogenes, such as JUN and MAP3K8. In summary, these findings suggest that CBD may have potential therapeutic benefits for treating the MSI subtype of CRC. However, more experimental data would be needed to support this notion, such as apoptosis assay, protein expression of chosen pathways and animal models.

1.4.3 Intermittent serum starvation and colorectal cancer cell lines

To establish a time and dose-dependent effect of ISS on different CRC and normal cell lines and to calculate IC50s for each tested cell line, I performed a cell viability assay (MTT).

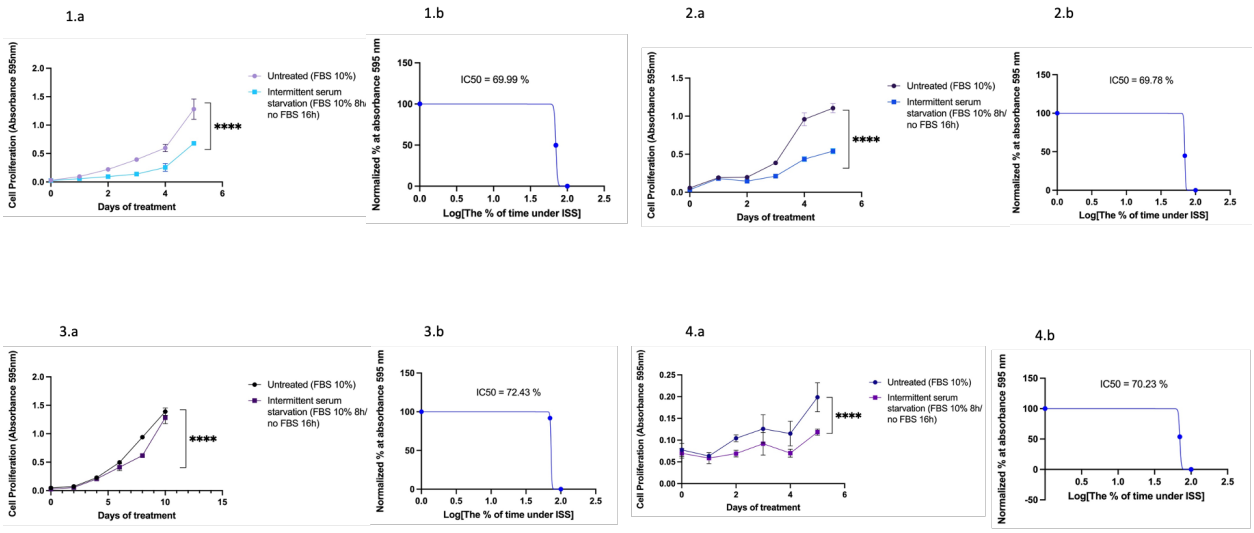

Figure 25. The time-dose-dependent effect and nonlinear regression analysis of the dose-effect curve with calculated IC50 values of ISS (10% FBS for 8 h/ 0% FBS for 16h) in HCT-116 (1.a, 1.b), HT-29 (2.a, 2.b), LS-174T (3.a, 3.b), and HCEC (4.a, 4.b) cell lines based on MTT results. Results are expressed as means of calculated cell viability ± standard deviations of each group in triplicate at absorbance 595 nm. To calculate time-dose effects, two-way ANOVA was performed using GraphPad Prism version 9.0. Significant differences between groups are marked with ns – non-significant, *p < 0.05, **p < 0.01, ***p < 0.001, ****p <0.0001. A nonlinear fit with log(inhibitor) vs. normalized response–variable slope analysis was performed using GraphPad Prism version 9.0.

We observed ISS's time and dose-dependent effect during treatment on all tested cell lines (Figure 25). The nonlinear regression analysis was performed to calculate IC50s of ISS in treated cell lines, which was around 70% in all cases. The results represent the percentage of time recommended to introduce serum starvation in the cell lines to reduce cell viability by 50%. This means we would need to introduce serum starvation for 16h (70%) out of 24 during five to ten days of treatment.

Next, to understand the possible mechanisms behind the action of ISS, we performed mRNA expression analysis of the HCT-116 CRC cell line, which resembles the MSI subtype of CRC.

Exploratory analysis

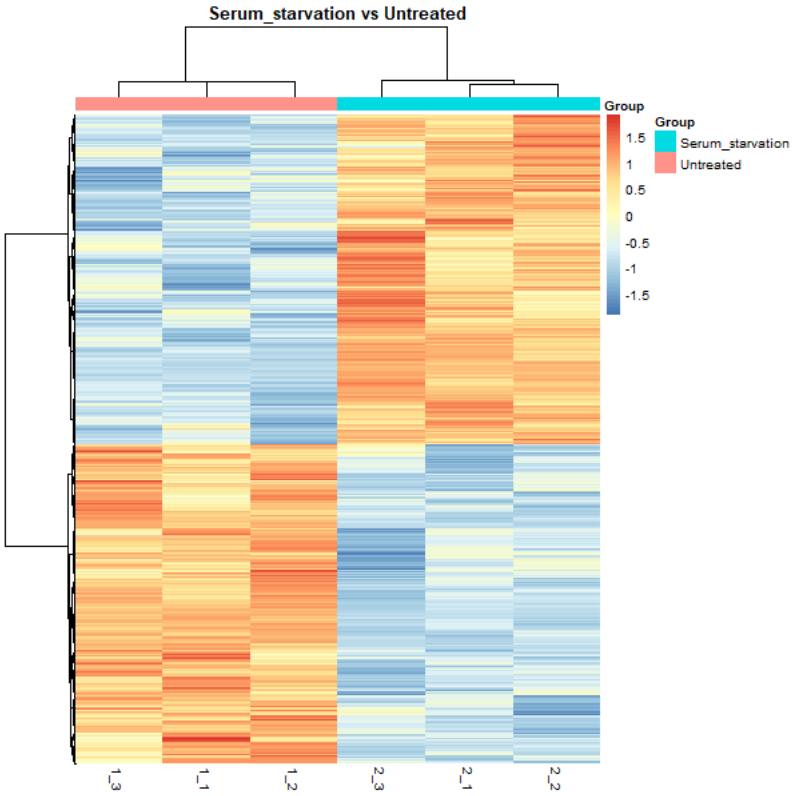

Figure 26. A hierarchical clustering heatmap analysis of the differentially expressed genes with fold change over 1.5 and adjusted p-values < 0.05 for untreated control versus ISS in the HCT-116 CRC cell line. The x-axis shows non-supervised clusters between the two treatment groups. The 1.1, 1.2, and 1.3 are independent replicates for untreated and 2.1, 2.2, and 2.3 are for ISS. The y-axis shows differentially expressed genes. The fold changes of up-regulated genes are in the red-orange colour spectrum, and the down-regulated genes are represented in the blue colour spectrum. The heatmap was generated using R software version 4.2.2.

A heatmap represents differentially expressed genes for untreated versus ISS in the HCT-116 CRC cell line. The unsupervised clustering based on the underlying data determined if there were sub-categories within untreated control and ISS treatment. As the figure shows, there were significant differences in gene expression between the groups. The differences were not substantial for the biological replicates within the same group, showing the treatment samples' good quality (Figure 26).

Pathway analysis

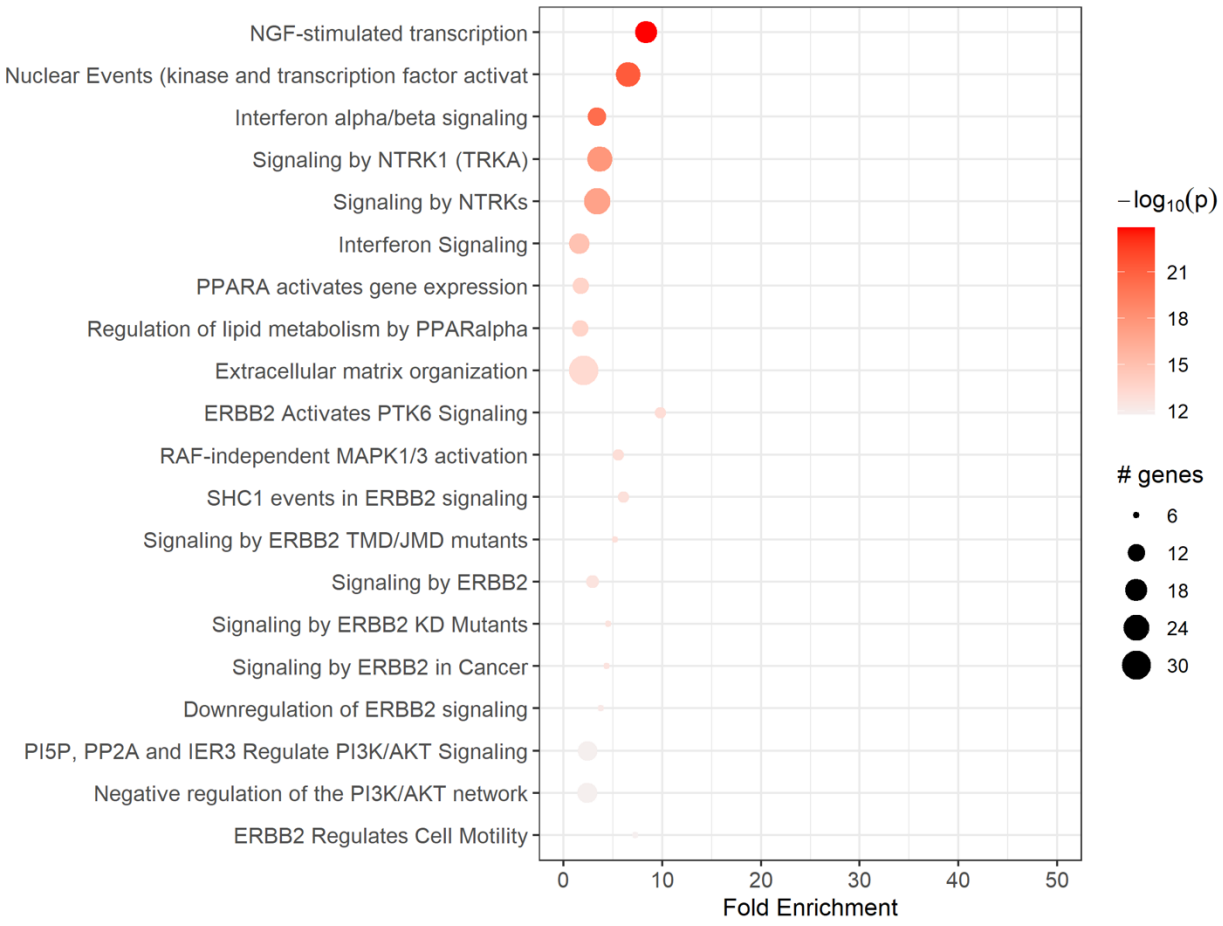

Figure 27. The Reactome dot plot of the top 20 terms for untreated versus ISS in the HCT-116 CRC cell line. The top 20 terms with the highest fold change are shown in this plot, with their corresponding Reactome pathways on the y-axis. The size of the dots represents the number of genes in each pathway, while the red colour's intensity indicates the enrichment's significance. The most enriched pathways are shown at the top of the plot. The figure was generated using pathfindR enrichment analysis software.

Based on dot plot analysis, the ISS changed multiple pathways involved in CRC cell survival, lipid metabolism, extracellular matrix organization, ERBB2 receptor signalling, as well as PI3K/AKT pathway (Figure 27).

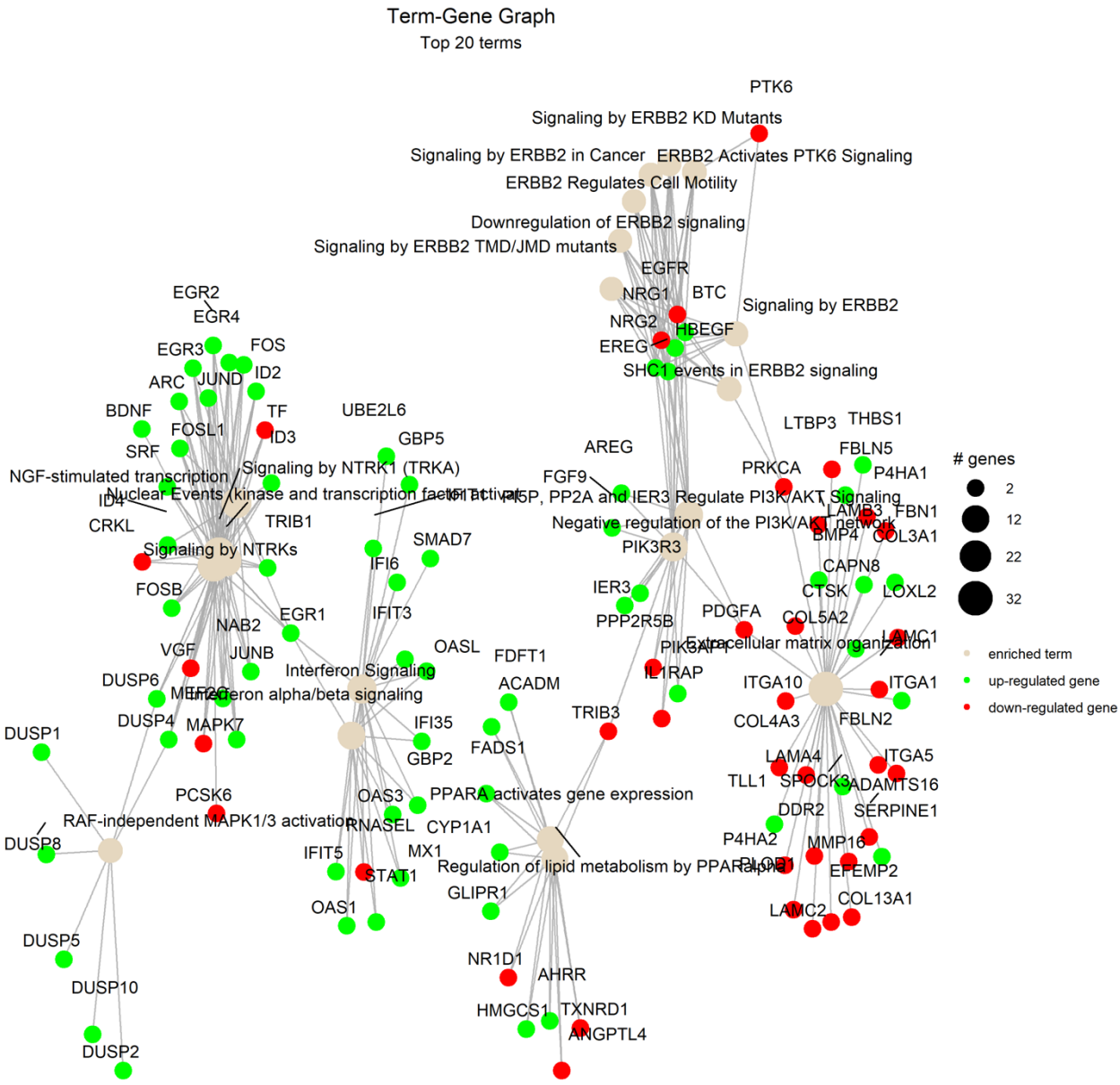

Figure 28. The Reactome Term-Gene Graph for Top 20 terms for untreated versus ISS treatment in the HCT-116 CRC cell line. The graph displays the top 20 Reactome terms and their corresponding gene sets. Each node represents a Reactome term, and the size of the node is proportional to the number of genes associated with that term. The edges between the nodes represent the overlap in gene sets between the terms. The edge's thickness represents the overlap's magnitude, and the edge's colour represents the direction of the overlap, with green for downregulated and red for upregulated genes. The figure was generated using pathfindR enrichment analysis software.

There was a strong upregulation of multiple genes that participate in NTRK1 signalling, including ARC, EGR1, EGR2, EGR3, EGR4, FOS, FOSB, FOSL1, ID2, ID3, ID4, JUNB, JUND, NAB2, SRF, TRIB1 (Figures 27 and 28). Most listed factors participate in cell proliferation, invasion, metastasis, and resistance to chemotherapy-induced apoptosis. There was an increased expression of ARC, which is an apoptosis repressor with CARD. The upregulation of ARC expression in CRC has been associated with increased resistance to chemotherapy-induced apoptosis. Next, the increased levels of EGR1-4, the early growth response genes, are involved in regulating cellular proliferation, differentiation, and survival. Upregulation of EGFR1-4 expression in CRC has been linked to increased cell proliferation, invasion, and metastasis. An increase in serum response factor (SRF), which is a transcription factor that regulates gene expression in response to extracellular signals, could indicate the activation of pro-survival mechanisms in tested cancer cells.

On the other hand, there was a downregulation of TF (coding for iron-binding factor) and VGF, a neuropeptide precursor implicated in cancer progression and metastasis. Downregulation of TF and VGF can have different effects on CRC, with TF downregulation potentially leading to reduced proliferation and increased apoptosis, while VGF downregulation may decrease migration and invasion of CRC cells.

There were multiple genes that were upregulated under RAF-independent MAPK1/3 activation term, which involved DUSP1, DUSP10, DUSP2, DUSP4, DUSP5, DUSP6, and DUSP8. The upregulation of listed DUSP genes in CRC can have different effects on MAPK signalling and may contribute to the development and progression of the disease. For instance, increased levels of DUSP1, which is a phosphatase that dedephosphorylates and inactivates ERK1/2, JNK, and p38 MAPKs. Overexpression of DUSP1 in CRC can inhibit the growth and proliferation of the cells and suppress the growth and proliferation by reducing the activity of MAPKs. The upregulation of DUSP6 may inhibit ERK1/2 activity and prevent apoptosis. DUSP8 is a phosphatase that dephosphorylates and inactivates JNK and p38 MAPKs, and it was shown to inhibit cell proliferation and migration of cancer cells. However, the upregulation of DUSP2 has been shown to have both pro- and anti-tumorigenic effects in different cancer types. Overall, the effects of upregulating DUSP in CRC can be complex and may depend on the specific DUSP isoform.

Multiple gene upregulation was responsible for interferon signalling, including EGR1, GBP2, GBP5, IFI35, IFI6, IFIT1, IFIT3, IFIT5, MX1, OAS1, OAS3, OASL, SMAD7, STAT1, and UBE2L6. Interferon signalling is thought to have anti-tumor effects by promoting apoptosis and inhibiting tumor cell proliferation and migration. On the other hand, some of the upregulated genes, such as STAT1 and SMAD7, could have pro-tumor effects. STAT1 is a transcription factor involved in immune system activation to viral infection, and it has been shown to promote tumor growth and survival. In contrast, SMAD7 is involved in the TGF-β signalling pathway and can promote tumor growth and metastasis.

Regulation of lipid metabolism by PPARα signalling was mainly increased with ISS. The genes responsible for making medium-chain acyl-CoA dehydrogenase (ACADM), long-chain fatty acids synthesis, and cholesterol metabolism, including the HMGCS1 gene, which is the first committed step in synthesizing ketone bodies, were increased. There were a few genes that were downregulated too. Decreased levels of ANGPTL4 expression of the gene coding for angiopoietin-like protein 4 that regulate lipid and glucose metabolism, as well as the growth of new blood vessels, could lead to inhibition of angiogenesis in cancer cells. Interestingly, there was inhibition of the NR1D1 (Nuclear Receptor Subfamily 1 Group D Member 1), which is involved in the regulation of circadian rhythms and forms a critical negative limb of the circadian clock by repressing the expression of core clock components. NR1D1 also regulates lipid metabolism, adipogenesis, gluconeogenesis and the macrophage inflammatory response.

The genes BTC, EREG, HBEGF, and NRG2 that take part in the epidermal growth factor receptor family were upregulated and take part in cancer proliferation and migration. On the other hand, the downregulation of EGFR (epidermal growth factor receptor), which takes part in the regulation of cell growth, proliferation, differentiation, and survival, could be one of the important targets in cancer therapy. Additionally, decreased levels of neuregulin 1 transcript could also decrease proliferation and survival. Moreover, lowering PRKCA (protein kinase C alpha) and PTK6 (protein tyrosine kinase 6) could also inhibit cell growth, proliferation, and cancer progression.

The following genes were upregulated in PI3K signalling under ISS treatment: AREG (amphiregulin), BTC (betaleucin), EREG (epiregulin), FGF9 (fibroblast growth factor 9), HBEGF (heparin-binding EGF-like growth factor), NRG2 (neuregulin 2), PIK3AP1 (phosphoinositide-3-kinase adaptor protein 1), and PIK3R3 (phosphoinositide-3-kinase regulatory subunit 3). All the

mentioned genes take part in the activation of cell growth, proliferation, insulin signalling, and cancer progression, which could result in the unwanted effects of cancer. On the other hand, the EGFR, NRG1, and PDGFA were downregulated under ISS. The epidermal growth factor receptor, coded by the EGFR gene, triggers a signalling pathway that promotes cell growth and proliferation of cancer cells. Thus, inhibition of EGFR by ISS could be beneficial in CRC therapy.

Many genes that code for the extracellular matrix organization were upregulated, including BMP4, CAPN8, COL3A1, COL5A2, FBLN5, ITGA1, SERPINE1, SPOCK3, THBS1, and TLL1. The bone morphogenic protein coded by the BMP4 gene was overexpressed under ISS. BMP4 plays a role in cell differentiation and proliferation. Next, the overexpressed gene was CAPN8, coding for calpain 8 protein, a calcium-dependent cysteine protease, which plays a role in cytoskeletal organization. The increased expression of genes responsible for coding for collagen type 3 and type 5, could indicate stimulation of connective tissue formation by cancer cells. Increased expression of the FBLN5 gene responsible for fibulin 5 could help promote the adhesion of endothelial cells and help develop new arteries. ITGA1 codes for an alpha 1 subunit of integrin receptors. SERPINE1 (plasminogen activator inhibitor 1) is responsible for inhibiting fibrinolysis; thus, it would help with the reorganization of extracellular tissue to the cancer cell's advantage. THBS1 is responsible for thrombospondin-1p180, which helps in cell-to-cell and cell-to-matrix interactions. TLL1 codes for tolloid-like protein 1 is a metalloprotease that helps process procollagen C-propeptides, which means that it also takes part in extracellular matrix reorganization.

On the other hand, multiple genes taking part in extracellular matrix organization were downregulation too, including ADAMTS16, COL13A1, COL4A3, CTSK, DDR2, EFEMP2, FBLN2, FBN1, ITGA10, ITGA5, LAMA4, LAMB3, LAMC1, LAMC2, LOXL2, LTBP3, MMP16, P4HA1, P4HA2, PDGFA, PLOD1, and PRKCA. ADAMTS16 gene codes for ADAM metallopeptidase with thrombospondin type 1. It is a disintegrin and metalloproteinase. COL13A1 and COL4A3 codes for collagen types 13 and 4, respectively. Collagen type 4 is a main structural component of basement membranes and would help in the formation of new vessels. CTSK coding for cathepsin K, a lysosomal cysteine proteinase that could contribute to tumor invasiveness, was also decreased. DDR2 is a gene encoding for discoidin domain receptor subclass of the receptor tyrosine kinase protein family. This protein is a collagen-induced receptor that activates signal transduction pathways involved in cell adhesion, proliferation, and extracellular matrix

remodelling. DDR2 could be involved in wound repair and regulate tumor growth and invasiveness. EFEMP2, a gene responsible for EGF-containing fibulin extracellular matrix protein 2, is part of many ECM proteins and has been implicated in elastic fiber formation and connective tissue development; particularly, it participates in terminal differentiation and maturation of smooth muscle cells. FBLN2 codes for fibulin 2, which is an ECM matrix protein that plays a role in organ development and can bind to fibrillin. The downregulation of FBN1 coding for fibrillin 1, an ECM glycoprotein that is a structural component of calcium-binding microfibrils, could lead to the inhibition of cancer invasion. ITGA10 and ITGA5 codes for integrin subunit alpha 10 and 5 are collagen-binding proteins involved in cell-matrix adhesion. LAMA4 (laminin-8 subunit alpha), LAMB3 (laminin B1k chain), LAMC1 (laminin subunit gamma 1), and LAMC2 (laminin subunit gamma 2) were downregulated too. Laminins, a family of ECM glycoproteins, are ones of the main noncollagenous constituents of basement membranes, which are implicated in cell adhesion, differentiation, migration, and metastasis. Decreased LOXL2 coding for lysyl oxidase-like 2 delta E13 essential to connective tissue biogenesis, encoding an extracellular copper-dependent amine oxidase that catalyzes the first step in forming crosslinks in collagen and elastin could contribute to the inhibition of cancer invasiveness. LTBP3 (latent TGF-β binding protein 3), which forms a complex with TGF- β and plays a structural role in the extracellular matrix was also reduced. MMP16 (matrix metalloproteinase 16) takes part in the breakdown of ECM, tissue remodeling, and metastasis. P4HA1 and 2 (prolyl 4-hydroxylase, alpha polypeptide 1 and 2) encode a key component of prolyl hydroxylase, which is a major enzyme in collagen synthesis. PDGFA (platelet-derived growth factor subunit A) this protein is a part of PDGF, which is essential for cell proliferation, cell migration, survival, angiogenesis, and chemotaxis. PLOD1 (Procollagen-lysine 1,2-Oxoglutarate-Dioxygenase) catalyzes the hydroxylation of lysyl residues in collagen-like peptides. PRKCA (Protein kinase C alpha) belongs to a family of serine-threonine protein kinases that calcium can activate. This protein takes part in cell adhesion, cell transformation, cell cycle checkpoint, cell volume control, tumorigenesis, and angiogenesis.

The top 10 up- and 10 down-regulated genes are presented in Table 6.

Table 6. Top 10 up-and 10 down-regulated genes for untreated versus ISS treatment in the HCT-116 CRC cell line based on mRNA expression analysis.

Top 10 up-regulated genes			
Gene name	Gene description	Gene biotype	Log2 Fold Change

NR4A3	nuclear receptor subfamily 4 group A member 3	Protein coding	6.2
EGR3	early growth response 3	Protein coding	4.2
EGR2	early growth response 2	Protein coding	3.8
NR4A1	nuclear receptor subfamily 4 group A member 1	Protein coding	3.7
OVOL2	Ovo like zinc finger 2	Protein coding	3.3
THBS1	thrombospondin 1	Protein coding	3.1
METTL7A	methyltransferase like 7A	Protein coding	2.9
HK2-DT	HK2 divergent transcript	Protein coding	2.8
LONRF2	LON peptidase N-terminal domain and ring finger 2	Protein coding	2.8
FGFBP1	fibroblast growth factor binding protein 1	Protein coding	2.8
Top 10 down-regulated genes			
Gene name	Gene description	Gene biotype	Log2 Fold Change
HKDC1	hexokinase domain containing 1	Protein coding	-3.1
SPX	spexin hormone	Protein coding	-3.1
PHF24	PHD finger protein 24	Protein coding	-2.8
XBP1P1	X-box binding protein 1 pseudogene 1	Processed pseudogene	-2.8
RBM46	RNA binding motif protein 46	Protein coding	-2.7
TBPL2	TATA-box binding protein like 2	Protein coding	-2.6
N/A	family with sequence similarity 151, member A (FAM151A) pseudogene	Processed pseudogene	-2.5
N/A	novel transcript	lncRNA	-2.5
CD68	CD68 molecule	Protein coding	-2.5

LINC02631	long intergenic non-protein coding RNA 2631	Protein coding	-2.4

Overall, the reduction of the vast majority of factors that take part in CRC's invasion and metastatic mechanisms could become beneficial effects of ISS.

1.4.4 Combination of intermittent serum starvation and CBD in colorectal cancer cell lines

Based on the literature review and data from mRNA expression pathway analysis, I combined different doses of CBD with ISS to see if there would be a synergistic interaction between these treatments.

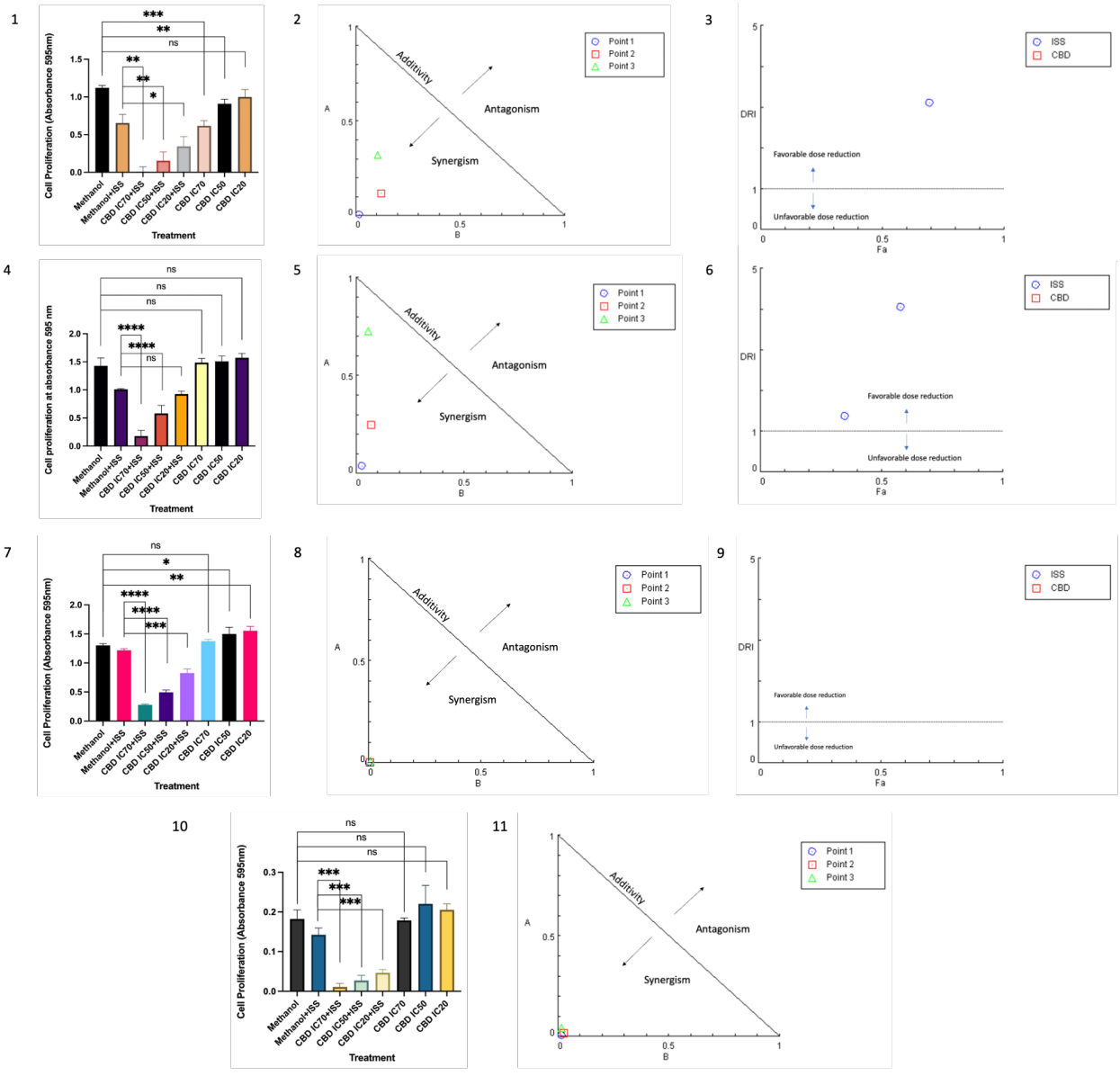

Figure 29. The changes of cell proliferation under ISS (FBS 10% for 8 h/FBS 0% for 16 h) combined with different doses of CBD treatment on the HCT-116 (1), HT-29 (4), LS-174T (7), and HCEC (10) cell lines based on MTT results. Results are expressed as means of calculated cell viability ± standard deviations of each group in triplicate. Multiple unpaired t-tests were performed using GraphPad Prism version 9.0. Significant differences between groups are marked with ns – non-significant, *p < 0.05, **p < 0.01, ***p < 0.001, ****p <0.0001. **Normalized isobologram for the combination of CBD and ISS with normalization of the dose with IC50 to the unity of both x and y axis in the HCT-116 (2), HT-29 (5), LS-14T (8), and HCEC (11).** All the combination points indicated the synergistic interaction. Normalized isobologram was generated using CompuSyn software. Abbreviations: A – ISS $(D)_1/(IC50)_1$; B – CBD $(D)_2/(IC50)_2$; D – dose; Point 1 – the combination of CBD IC70 and ISS IC50; Point 2 – the combination of CBD IC50 and ISS IC50; Point 3 – the combination of CBD IC20 and ISS IC50. **Fa – DRI plot for the combination of ISS with CBD in HCT-116 (3), HT-29 (6), and LS-174T (9) CRC cell lines.** Abbreviations: DRI – dose reduction index; Fa - fraction affected by the drug concentration (% of cell growth inhibition/100); CBD – CBD; ISS – intermittent serum starvation. The plot was generated using CompuSyn software.

When we combined different doses of CBD with intermittent serum starvation (ISS), we observed a significant difference between the controls and CBD combined with ISS (Figure 29).

To further analyze our results, whether we observed synergistic or antagonistic interaction, we calculated CI based on the median-effect equation (Chou) and combination index theorem (Chou-Talalay) as well as generated dose-effect curves using CompuSyn software (243–245).

Based on the results, we observed a strong synergistic interaction between CBD and ISS. The actual CI values are shown in Table 7. Furthermore, to see if we could reduce the dose of treatment and maintain the same cytotoxic effect, we calculated the dose reduction index (DRI). The DRI measures how many-fold the dose of each drug in a synergistic combination may be reduced at a given effect level compared with the doses of each drug alone (243). The DRI is important in clinical situations in which dose reduction leads to reduced toxicity toward the host while the therapeutic efficacy is retained. The greater the DRI value (DRI>1), the greater the dose reduction for a given therapeutic effect. However, it does not necessarily indicate synergism (243,244). The DRI values for CBD and ISS were all above 1, which indicates that we can reduce the dose of CBD or ISS when administered together.

Overall, we would recommend the combination of ISS with CBD due to its synergistic interaction and high DRI values for further testing on CRC.

Table 7. CI data for the combination of ISS with CBD in tested cell lines. Data was generated using CompuSyn software.

Dose of CBD (μM)	Dose of ISS (% of time under serum starvation)	Effect (fraction of cell growth inhibition)	CI	Interaction effect
HCT-116				
8.3	70	0.99	0.03	Very strong synergism
5.9	70	0.86	0.24	Strong synergism
2.4	70	0.69	0.43	Synergism
HT-29				
4.9	70	0.88	0.07	Very strong synergism
3.5	70	0.58	0.32	Synergism
1.4	70	0.35	0.78	Moderate synergism
LS-174T				
6.7	70	0.79	0.004	Very strong synergism
4.8	70	0.62	0.009	Very strong synergism
1.9	70	0.37	0.02	Very strong synergism

We performed mRNA sequencing and bioinformatic pathway analysis on the HCT-116 CRC cell line to further investigate the synergistic effect of combining CBD with ISS.

Exploratory analysis

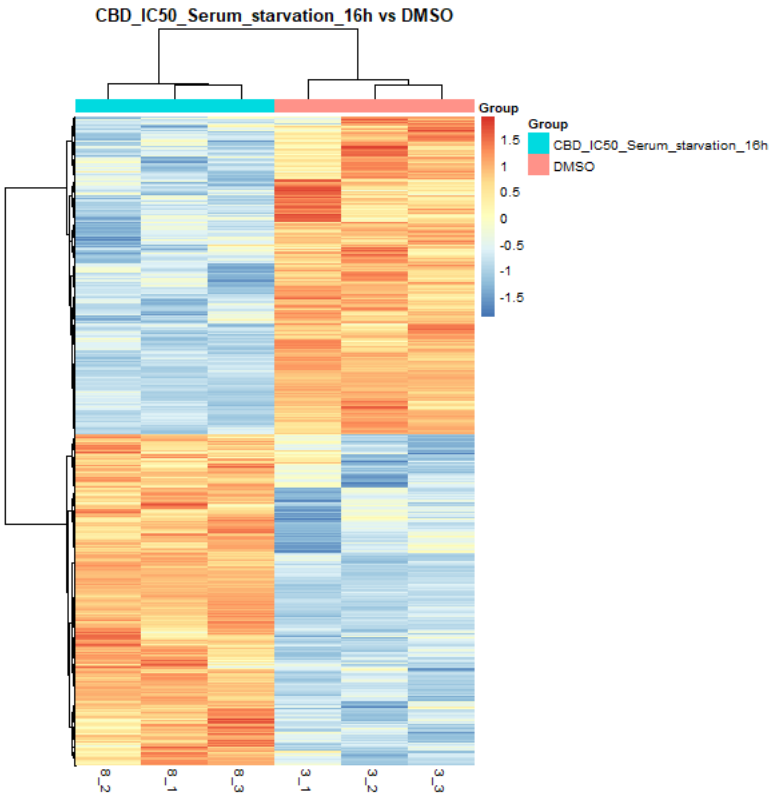

Figure 30. A hierarchical clustering heatmap analysis of the differentially expressed genes with fold change over 1.5 and adjusted p-values < 0.05 for DMSO control versus CBD IC50 and ISS in the HCT-116 CRC cell line. The x-axis shows non-supervised clusters between the two treatment groups. The 3.1, 3.2, and 3.3 are independent replicates for DMSO and 8.1, 8.2, and 8.3 are for CBD IC50 and ISS treatment. The y-axis shows differentially expressed genes. The fold changes of up-regulated genes are in the red-orange colour spectrum, and the down-regulated genes are represented in the blue colour spectrum. The heatmap was generated using R software version 4.2.2.

A heatmap represents differentially expressed genes for DMSO versus CBD IC50 combined with ISS in the HCT-116 CRC cell line. The unsupervised clustering based on the underlying data determined if there were sub-categories within untreated control and ISS treatment. As the figure shows, there were significant differences in gene expression between the groups. The differences were not substantial for the biological replicates within the same group, showing the treatment samples' good quality (Figure 30).

Pathway analysis

Figure 31. The Reactome dot plot of the top 20 terms for DMSO versus CBD IC50 and ISS in the HCT-116 CRC cell line. The top 20 terms with the highest fold change are shown in this plot, with their corresponding Reactome pathways on the y-axis. The size of the dots represents the number of genes in each pathway, while the red colour's intensity indicates the enrichment's significance. The most enriched pathways are shown at the top of the plot. The figure was generated using pathfindR enrichment analysis software.

Based on the Reactome dot plot, the genes that take part in MAPK and PI3K/AKT signalling, carbohydrate metabolism, NGF signalling, and apoptosis were differentially expressed when we compared the combination of CBD and ISS to DMSO control (Figure 31).

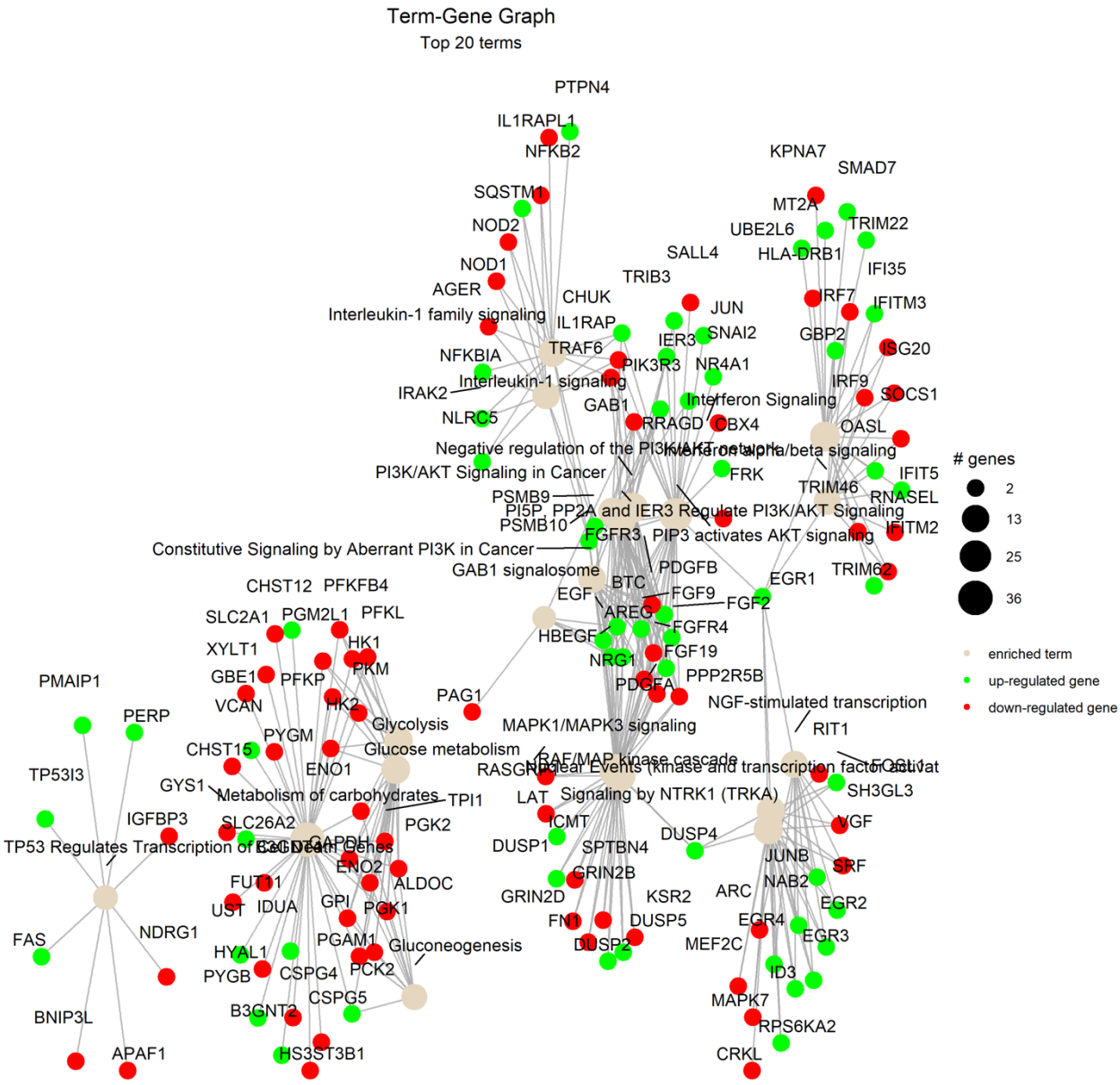

Figure 32. The Reactome Term-Gene Graph for Top 20 terms for DMSO versus CBD IC50 combined with ISS treatment in the HCT-116 CRC cell line. The graph displays the top 20 Reactome terms and their corresponding gene sets. Each node represents a Reactome term, and the size of the node is proportional to the number of genes associated with that term. The edges between the nodes represent the overlap in gene sets between the terms. The edge's thickness represents the overlap's magnitude, and the edge's colour represents the direction of the overlap, with green for downregulated and red for upregulated genes. The figure was generated using pathfindR enrichment analysis software.

When we analyzed each major Reactome term for differentially expressed genes, the multiple pathways of interest were changed (Figure 32). The following genes under the "TP53 regulate the transcription of cell death genes" term was upregulated – FAS, PERP, PMAIP1, and TP53I3. All the mentioned genes might help in the stimulation of apoptosis. FAS codes for the cell surface death receptor, which is a TNF-superfamily of receptors taking part in the extrinsic apoptotic pathway. PERP is a p53 apoptosis effector related to PMP22. PMAIP1 (Phorbol-12Myristate-13-Acetate-Induced Protein 1) is a pro-apoptotic subfamily within the BCL-2 protein family that determine whether a cell commits to apoptosis. Lastly, TP53I3 (tumor protein P53 inducible protein 3), this gene is involved in p53-mediated cell death. Additionally, decreased levels of IGFBP3 (insulin-like growth factor binding protein 3), which binds to IGF and prolongs its half-life, which is shown to promote cell growth effects of the IGF in cell culture, could further assist in the suppression of CRC cell growth.

Similarly to CBD alone, the combination of CBD and ISS inhibited multiple genes responsible for carbohydrate metabolism. The inhibition of hexokinases 1 and 2 and other enzymes that are part of glycolysis and gluconeogenesis were downregulated. It was shown that many tumors rely on glycolysis as a major source of energy production. Thus, carbohydrate metabolism inhibition could drastically affect cancer cells' survival (231).

The RAF/MAP kinase cascade genes were upregulated: AREG, BTC, DUSP1, DUSP2, DUSP4, DUSP5, EGF, FGF19, FGF2, FGF9, HBEGF, ICMT, PDGFB, PSMB10, PSMB9. The increased levels of amphiregulin (AREG), epidermal growth factors, fibroblast growth factors 19, 2, and 9, and platelet-derived growth factor subunit B transcripts, which play essential roles in the stimulation of cancer cell proliferation, survival, EMT, and invasion could be responsible for cell survival under CBD and ISS treatments. Increased transcripts of heparin binding EGF like growth factor (HBEGF), a positive regulator of epidermal growth factor receptor and protein kinase B might overstimulate stress response pathways and cell survival in a way that could be damaging to cancer cells. Additionally, the increased expression of dual specificity phosphatases 1, 2, 4 and 5 (DUSP1, DUSP2, DUSP4, DUSP5), negative regulators of MAP kinase MAPK1/ERK2 SAPK/JUN, p38, which results in its interference with several cellular processes such as response to environmental stress and negative regulation of cellular proliferation. Next, the downregulation of fibroblast growth factor receptor 3 and 4 (FGFR3 and FGFR4), which are genes coding for cell surface receptors that respond to fibroblast growth factors and regulate cell proliferation,

migration, lipid metabolism, glucose uptake, and activation of RAS, MAPK1/ERK2, MAPK3/ERK1, as well as AKT1 signalling cascades, would result in inhibition of cell proliferation. Furthermore, the decreased expression of kinase suppressor Ras 2 (KSR2) and RAS guanyl-releasing protein 1 (RASGRP1) that promotes BRAF-mediated phosphorylation of MAP2K1/MEK1 and helps in the activation of Ras would also contribute to the inhibition of cell proliferation. Additionally, inhibition of fibronectin 1 (FN1) involved in cell adhesion, migration, and invasion of cancer cells could suppress tumor progression.

Next, we analyzed changes in the "PI3K/AKT signalling in cancer" term. The increased levels of transcripts for a component of inhibitor of NFκB (CHUK) and NFκB inhibitor alpha (NFKBIA) would suggest inhibition of inflammatory cytokine formation. The phosphoinositide-3-kinase regulatory subunit 3 (PIK3R3), a regulatory subunit of PI3K, was also increased, which could point to the overactivation of the PI3K/AKT pathway. Moreover, the higher levels of the NR4A1 gene, nuclear receptor subfamily 4 group A member 1, which is the steroid-thyroid hormone-retinoid receptor superfamily, is a transcription factor induced by the serum stimulation could further indicate an attempt of cancer cells to stimulate cell proliferation. On the contrary, decreased levels of neuregulin 1 (NRG1), a direct ligand of ERBB3 and ERBB4 tyrosine kinase receptors, which activate ERBB receptors, could be responsible for the inhibition of cancer cell growth. Additionally, the downregulated fibroblast growth factor receptors 3 and 4, PDGFA, and GAB1 (GRB2-associated binding protein 1), which take part in FGF signalling, indicate downregulation of this pathway and possible suppression of tumor cell invasiveness and EMT.

The increased signalling by NTRK1 (Neurotrophic tyrosine receptor kinase gene fusion) term could promote cancer cell growth. The elevated levels of BDNF (brain-derived neurotrophic factor), EGR 1-4 (early growth response proteins 1-4), JUNB (transcription factor jun-B) that enables sequence-specific dsDNA binding activity and is a part of AP-1 transcription factors, SRF (serum response factor), which stimulates cell proliferation and takes part in immediate-early genes, might indicate stimulation of cell proliferation. Moreover, increased TIAM (T-lymphoma invasion and metastasis-inducing protein 1), a guanine nucleotide exchange factor (GEF), regulates RAC1 signalling pathways that affect cell shape, migration, adhesion, growth, survival, actin cytoskeleton formation, endocytosis and membrane trafficking could contribute to activation of cancer cell migration and metastasis.

On the other hand, lower levels of ARC (activity-regulated cytoskeleton-associated protein) involved in cell migration and cytoskeleton organization may indicate decreased cancer cell invasion. Additionally, decreased CRKL (CRK-like proto-oncogene adaptor protein) that has been shown to activate the RAS and JUN kinase signalling pathways and transform fibroblasts in a RAS-dependent fashion, MAPK7 (mitogen protein kinase 7), involved in cell proliferation and transcription regulation, and RIT1 (Ras-like without CAAX 1 – Ras-related GTPase), involved in regulating p38 MAPK-dependent signalling cascades related to cellular stress could support the hypothesis that combination of CBD and ISS can have an antiproliferative effect.

Based on the IL-1 signalling term, there was an overall inhibition of NFkB signalling. For instance, the increased expression of an NFkB kinase complex (CHUK) inhibitor component and NFKBIA suggests the downregulation of NFkB signalling. Higher levels of NLR family CARD domain containing 5, a caspase recruitment domain containing NLR family, play in cytokine response through inhibition of NFkB and negative regulation of IFN signalling could also contribute to inhibition of pro-inflammatory cascades.

Additionally, the downregulation of IL1RAP (IL1 receptor accessory protein), which helps in the activation of signalling events of IL-1-responsive genes, NFKB2 (NFkB subunit 2), NOD1, NOD2 (nucleotide binding oligomerization domain containing 1 and 2), members of Nod1/Apaf-1 family proteins that take part in the immune response to LPS and activation of NFkB, and TRAF6 (TNF receptor associated factor 6), which helps in the activation of NFkB and response to inflammation, suggest that NFkB signalling was substantially downregulated under our treatment.

Interferon signalling term. There was an increased expression of early growth response 1 transcript (EGR1), which is a transcriptional regulator required for differentiation and mitogenesis. Higher levels of GBP2 (guanylate binding protein 2), a GTPase, which induces IFN-induced proteins, IFI35 and IFIT5 (interferon-induced protein and interferon-induced protein with tetratricopeptide repeats 5) induce macrophage activation, antiviral defence, and negatively regulates NFkB.

The top 10 up- and 10 down-regulated genes are presented in Table 8.

Table 8. Top 10 up-and 10 down-regulated genes for DMSO versus ISS and CBD treatment in the HCT-116 CRC cell line based on mRNA expression analysis.

Top 10 up-regulated genes			
Gene name	Gene description	Gene biotype	Log2 Fold Change

NR4A3	nuclear receptor subfamily 4 group A member 3	Protein coding	4.1
THBS1	thrombospondin 1	Protein coding	3.3
SSTR5-AS1	SSTR5 antisense RNA 1	lncRNA	3.2
LINC01629	long intergenic non-protein coding RNA 1629	lncRNA	2.9
RNF39	ring finger protein 39	Protein coding	2.7
EDN1	endothelin 1	Protein coding	2.6
CCN1	cellular communication network factor 1	Protein coding	2.6
N/A	novel transcript	lncRNA	2.5
AHRR	aryl hydrocarbon receptor repressor	Protein coding	2.4
CCN2	cellular communication network factor 2	Protein coding	2.4
Top 10 down-regulated genes			
Gene name	Gene description	Gene biotype	Log2 Fold Change
CA9	carbonic anhydrase 9	Protein coding	-4.6
ARRDC4	arrestin domain containing 4	Protein coding	-3.9
UPK1A-AS1	UPK1A antisense RNA 1	lncRNA	-3.5
HLA-V	major histocompatibility complex, class I, V (pseudogene)	Transcribed unprocessed pseudogene	-3.4
PAG1	phosphoprotein membrane anchor with glycosphingolipid microdomains 1	Protein coding	-3.2
FAM13A-AS1	FAM13A antisense RNA 1	lncRNA	-3.2

PFKFB4	6-phosphofructo-2-kinase/fructose-2,6-biphosphatase 4	Protein coding	-3.1
	novel transcript	lncRNA	-3.0
PPFIA4	PTPRF interacting protein alpha 4	Protein coding	-23.0
FRZB	frizzled related protein	Protein coding	-2.9

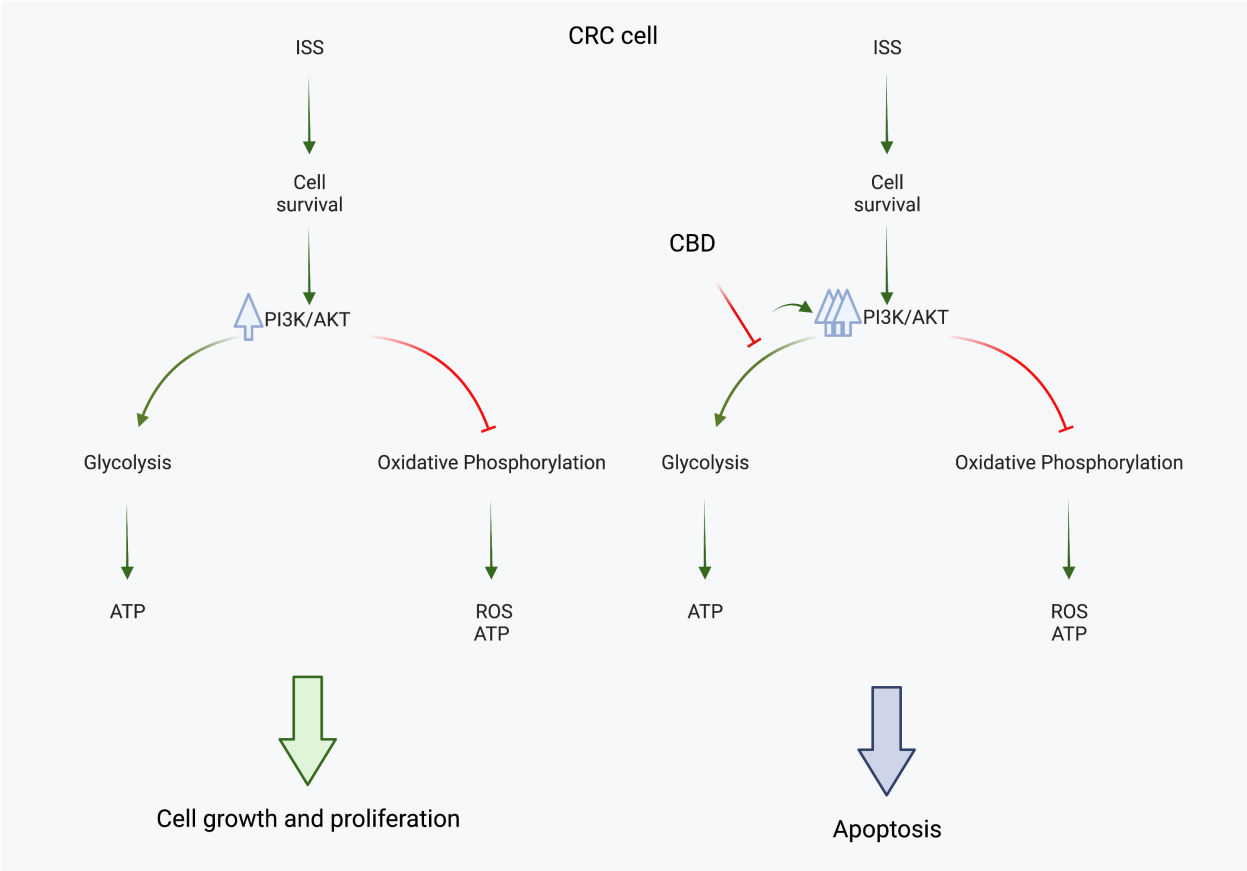

Figure 33. The synergistic effect of CBD and ISS in HCT-116 CRC cell line. Created with Biorender.com

In CRCs, the RAS-MAPK pathway is overactivated, with KRAS and BRAF being overexpressed in approximately 50% and 15% of cases (104,105). PI3K/AKT signalling is upregulated in almost 40% of colon malignancies (106). When AKT is activated, it can increase enzymes in the glycolytic pathway to generate ATP and some of the byproducts of glycolysis are

utilized for cancer cell growth (Figure 33). At the same time, AKT inhibits oxidative phosphorylation to reduce ROS formation in mitochondria. In this case, the only pathway to generate energy is glycolysis. Based on our results, our hypothesis behind the synergistic interaction between ISS and CBD is that ISS overactivated PI3K/AKT signalling, which on the one hand, makes cancer cells rely on glycolysis; however, CBD strongly inhibited carbohydrate metabolism. As a result, cancer cells were not able to generate ATP via pro-survival pathways, resulting in the stimulation of cell death.

1.4.5 Combination of cisplatin and cannabidiol in colorectal cancer cell lines

Based on the literature review and data from mRNA expression pathway analysis, I combined different doses of CBD with cisplatin to see if there would be a synergistic interaction between these treatments.

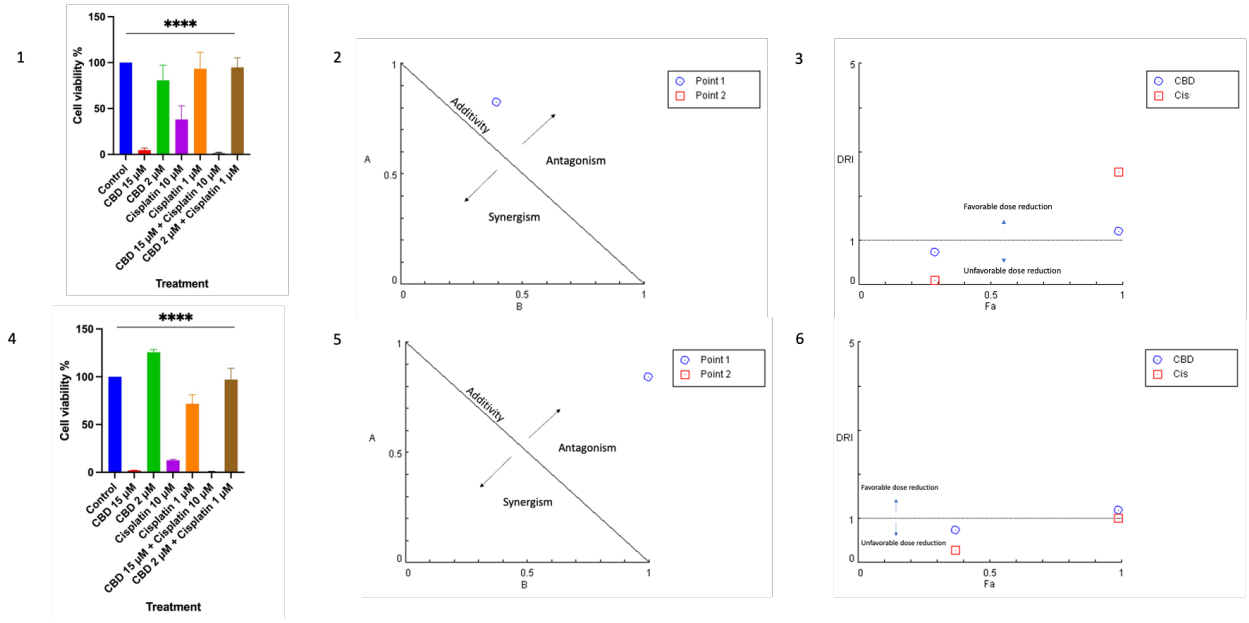

Figure 34. The percentage of cell viability changes under CBD combined with cisplatin at day 5 of treatment on the HCT-116 (1), and HT-29 (4) cell lines based on MTT results. Results are expressed as means of calculated cell viability ± standard deviations of each group in triplicate. One-way ANOVA was performed using GraphPad Prism version 9.0. Significant differences between groups are marked with ns – non-significant, *p < 0.05, **p < 0.01, ***p < 0.001, ****p <0.0001. **Normalized isobologram for the combination of CBD and cisplatin with normalization of the dose with IC50 to the unity of both x and y axis in the HCT-116 (2), HT-29 (5).** All the combination points indicated the antagonistic interaction.

Normalized isobologram was generated using CompuSyn software. Abbreviations: A – cisplatin $(D)_1/(IC50)_1$; B – CBD $(D)_2/(IC50)_2$; D – dose; Point 1 – the combination of CBD 15 μM and cisplatin 10 μM; Point 2 – the combination of CBD 2 μM and cisplatin 1 μM. **Fa – DRI plot for the combination of ISS with CBD in HCT-116 (3), and HT-29 (6) CRC cell line.** Abbreviations: DRI – dose reduction index; Fa - fraction affected by the drug concentration (% of cell growth inhibition/100); CBD – CBD; Cis – cisplatin. The plot was generated using CompuSyn software.

We observed a significant dose-dependent effect of cisplatin and CBD alone and in combination treatments compared to control in the HT-29 CRC cell line. At the concentration of 15 μM of CBD, cell viability was 2%. For 10 μM cisplatin – 12.6%. When these two concentrations were combined, cell growth decreased to 0.8% (Figure 34). We observed similar dose-dependent effects of cisplatin and CBD in the HCT-116 CRC cell line. At the concentration of 15 μM of CBD, cell viability was 4.7%. For 10 μM cisplatin – 38.1%. When these two concentrations were combined, cell growth decreased to 1.4%.

To further find out whether we observed synergistic or antagonistic interaction, we calculated CI based on the median-effect equation (Chou) and combination index theorem (Chou-Talalay) as well as generated dose-effect curves using CompuSyn software (243–245). Based on the normalized isobologram analysis, the combination of CBD and cisplatin had an antagonistic effect on CRC cell lines (Table 9). Moreover, as the results showed, the DRI values for CBD were all around 1, which indicates that we cannot reduce the dose of CBD when combined with cisplatin. Moreover, DRI for cisplatin was 1 and 0.3. Thus, the dose of cisplatin could not be reduced, even increased, to maintain its cell inhibitory effect on the HT-29 CRC cell line.

Table 9. CI data for the combination of CBD and cisplatin. Data was generated using CompuSyn software.

Dose of CBD (μM)	Dose of cisplatin (μM)	Effect (fraction of cell growth inhibition)	CI	Interaction effect
HCT-116				
15	10	0.99	1.2	Slight antagonism
7	7	0.29	12.1	Strong antagonism
HT-29				
15	10	0.99	1.84	Antagonism

7	7	0.37	4.95	Strong antagonism

We looked at mRNA sequencing data for DMSO vs. CBD and cisplatin in the HCT-116 CRC cell line to understand the possible mechanisms behind the antagonistic interaction between CBD and cisplatin.

Exploratory analysis

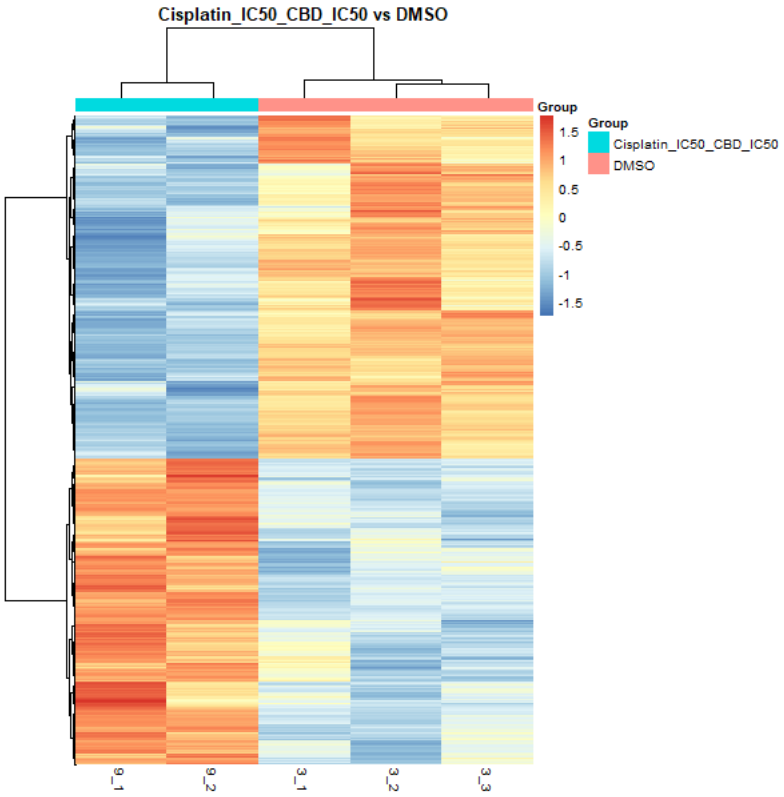

Figure 35. A hierarchical clustering heatmap analysis of the differentially expressed genes with fold change over 1.5 and adjusted p-values < 0.05 for DMSO control versus CBD IC50 and cisplatin in the HCT-116 CRC cell line. The x-axis shows non-supervised clusters between the two treatment groups. The 3.1, 3.2, and 3.3 are independent replicates for DMSO and 9.1, 9.2 are for CBD IC50 and cisplatin treatment. The y-axis shows differentially expressed genes. The fold changes of up-regulated genes are in the red-orange colour spectrum, and the down-regulated genes are represented in the blue colour spectrum. The heatmap was generated using R software version 4.2.2.

A heatmap represents differentially expressed genes for DMSO versus CBD IC50 combined with cisplatin in the HCT-116 CRC cell line. The unsupervised clustering based on the

underlying data determined if there were sub-categories within DMSO control and CBD with cisplatin treatment. As Figure 35 shows, there were significant differences in gene expression between the groups. The differences were not substantial for the biological replicates within the same group, showing the treatment samples' good quality (Figure 35).

Pathway analysis

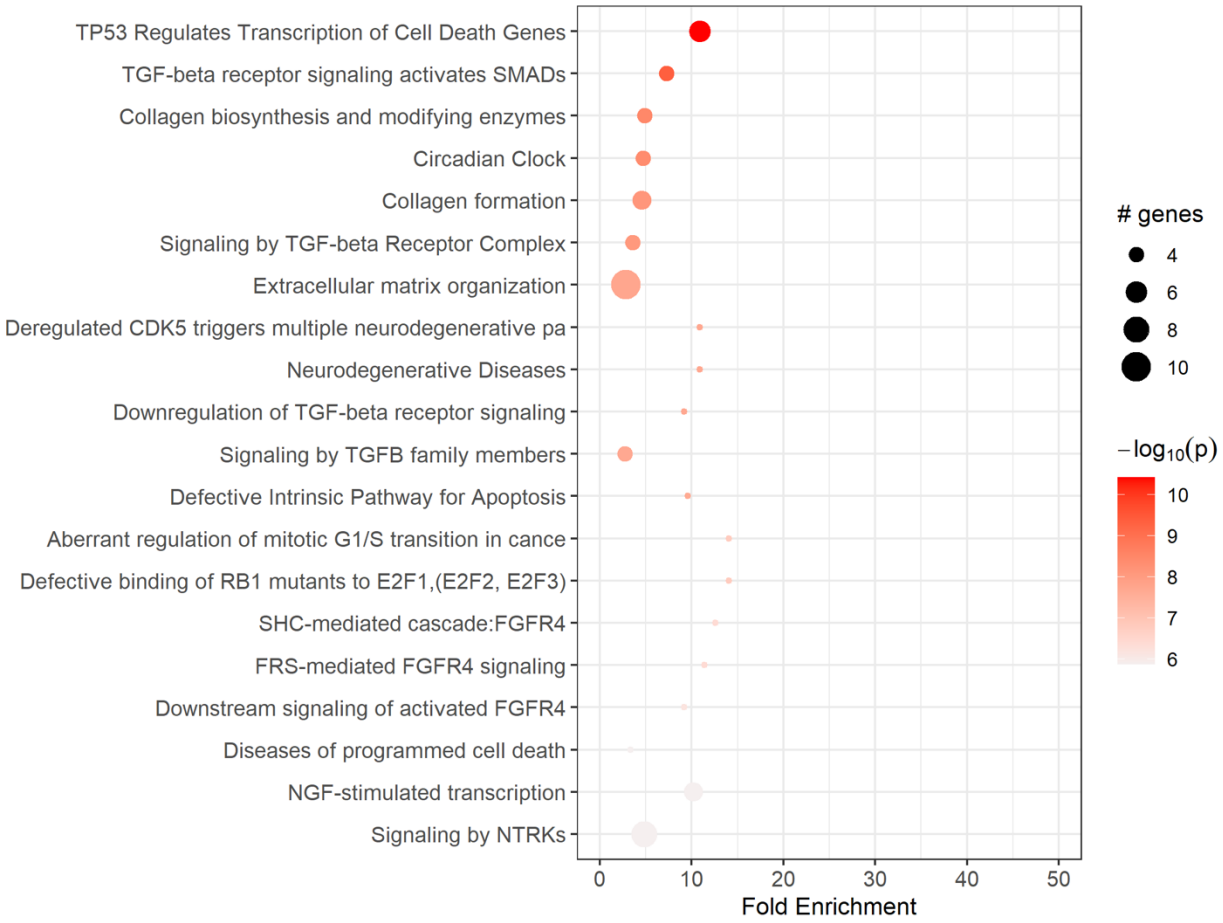

Figure 36. The Reactome dot plot of the top 20 terms for DMSO versus CBD IC50 and cisplatin in the HCT-116 CRC cell line. The top 20 terms with the highest fold change are shown in this plot, with their corresponding Reactome pathways on the y-axis. The size of the dots represents the number of genes in each pathway, while the red colour's intensity indicates the enrichment's significance. The most enriched pathways are shown at the top of the plot. The figure was generated using pathfindR enrichment analysis software.

The results based on the Reactome dot plot showed the differential gene expression in the TP53 regulation of apoptosis, TGF-β signalling, extracellular matrix organization, circadian clock regulation and checkpoints defects (Figure 36). When we compared dot plots for cisplatin alone

and cisplatin combined with CBD, it was visible that when cisplatin was administered alone, there was a much higher fold enrichment of genes responsible for TP53-mediated cell death. This could be one of the explanations for why CBD and cisplatin worked antagonistically.

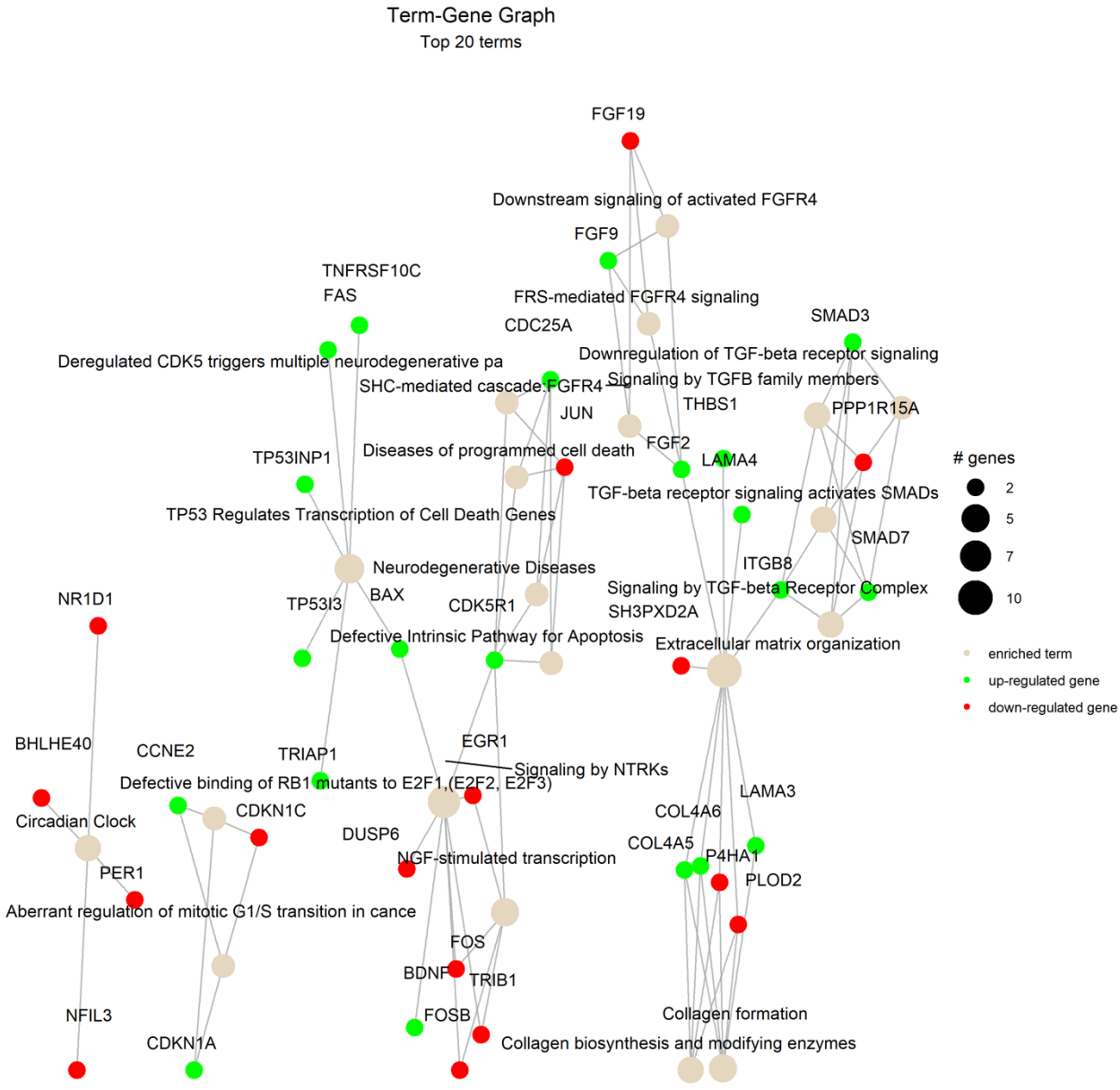

Figure 37. The Reactome Term-Gene Graph for Top 20 terms for DMSO versus CBD IC50 combined with cisplatin treatment in the HCT-116 CRC cell line. The graph displays the top 20 Reactome terms and their corresponding gene sets. Each node represents a Reactome term, and the size of the node is proportional to the number of genes associated with that term. The edges between the nodes represent the overlap in gene sets between the terms. The edge's thickness

represents the overlap's magnitude, and the edge's colour represents the direction of the overlap, with green for downregulated and red for upregulated genes. The figure was generated using pathfindR enrichment analysis software.

The BHLHE40 (basic helix-loop-helix family member E40) gene that controls the body's circadian clock was downregulated. BHLHE40 represses activation of PER1 and is believed to be involved in the circadian clock (Figure 37). Next, NFIL3 (nuclear factor, IL-3 regulated), which is a transcriptional regulator of genes responsible for the circadian clock, was also increased. These might indicate an increased regulation of circadian rhythms under the combination of CBD and cisplatin and are one of the rationales why we wanted to add ISS to our treatments.

There was an increased expression of genes responsible for the extracellular matrix organization and cancer cell invasiveness, including collagen, laminins, and FGF2 activation. On the other hand, the increased SMAD7 could prevent the activation of TGF-β and inhibit EMT in cancer cells.

Cisplatin is known to activate apoptosis due to its damaging effect on the DNA. However, our results showed that the increased levels of cyclin E2 (CCNE2) and CDC25A (cell division cycle 25A) and decreased transcripts for CDK inhibitor 1C (CDKN1C) could stimulate cell cycle progression even with damaged DNA. This could also be one of the reasons why CBD with cisplatin had antagonistic interaction.

Despite the upregulation of many genes responsible for cell survival, we observed increased levels of pro-apoptotic transcripts, BAX, FAS, TNFRSF10C, TP53I3, TP53INP1, and TRIAP. These genes were upregulated in a similar way under cisplatin treatment alone. However, as we already mentioned, when we looked at the dot plot analysis, we observed lower fold enrichment for CBD and cisplatin combination compared to cisplatin alone. Furthermore, the downregulation of FOS and JUN, the AP-1 transcription factor subunits, would indicate inhibition of cell proliferation.

Based on the Reactome data for differential expression analysis in HCT-116 CRC cells, CBD in combination with cisplatin decreased the expression of genes responsible for glucose metabolism, glycolysis, and gluconeogenesis, such as PFKFB4 that regulates fructose-2,6-bisphosphate, and responded to hypoxia to help cancer cells produce more ATP. There was also downregulation of hexokinase 2 (HK2) expression that is involved in the rapid activation of glycolysis in cancer cells. The transcript for glucose-6-phosphate isomerase (GPI) was decreased

too. The function of GPI, along with the regulation of glucose metabolism, is acting as an autocrine motility factor, a tumor-secreting cytokine, and an inducer of angiogenesis. This shows that the addition of CBD inhibited transcription of factors that help in the survival of cancer cells under energy and oxygen scarcity and might prevent cancer progression.

The top 10 up- and 10 down-regulated genes are presented in Table 10.

Table 10. Top 10 up-and 10 down-regulated genes for DMSO versus cisplatin and CBD treatment in the HCT-116 CRC cell line based on mRNA expression analysis.

Top 10 up-regulated genes			
Gene name	Gene description	Gene biotype	Log2 Fold Change
CYP1A1	cytochrome P450 family 1 subfamily A member 1	Protein coding	2.2
AHRR	aryl hydrocarbon receptor repressor	Protein coding	1.8
ALDH1A3	aldehyde dehydrogenase 1 family member A3	Protein coding	1.4
ZBED2	zinc finger BED-type containing 2	Protein coding	1.3
GALNT5	polypeptide N-acetylgalactosaminyltransferase 5	Protein coding	1.3
CYP1B1	cytochrome P450 family 1 subfamily B member 1	Protein coding	1.3
GDA	guanine deaminase	Protein coding	1.3
THBS1	thrombospondin 1	Protein coding	1.2
SULF2	sulfatase 2	Protein coding	1.2
N/A	novel transcript	lncRNA	1.2
Top 10 down-regulated genes			
Gene name	Gene description	Gene biotype	Log2 Fold Change
FOSB	FosB proto-oncogene, AP-1 transcription factor subunit	Protein coding	-2.9

ANKRD37	ankyrin repeat domain 37	Protein coding	-2.0
FOS	Fos proto-oncogene, AP-1 transcription factor subunit	lncRNA	-1.9
RAPGEF4	Rap guanine nucleotide exchange factor 4	Transcribed unprocessed pseudogene	-1.6
EGR1	early growth response 1	Protein coding	-1.5
SUSD2	sushi domain containing 2	lncRNA	-1.3
JUN	Jun proto-oncogene, AP-1 transcription factor subunit	Protein coding	-1.2
DDIT3	DNA damage inducible transcript 3	Protein coding	-1.1
	novel transcript, antisense to GAPDH	lncRNA	-1.1
ARRDC4	arrestin domain containing 4	Protein coding	-1.1

Overall, based on our mRNA expression results, we suggest that the antagonistic effect of combining CBD and cisplatin was the result of lower fold enrichment in genes responsible for apoptosis when compared to the cisplatin action alone in the HCT-116 CRC cell line.

1.4.6 Combination of intermittent serum starvation and cisplatin in colorectal cancer cell lines

To see if the addition of ISS to cisplatin could result in a synergistic effect, I combined the treatments and performed cell viability assays on four cell lines.

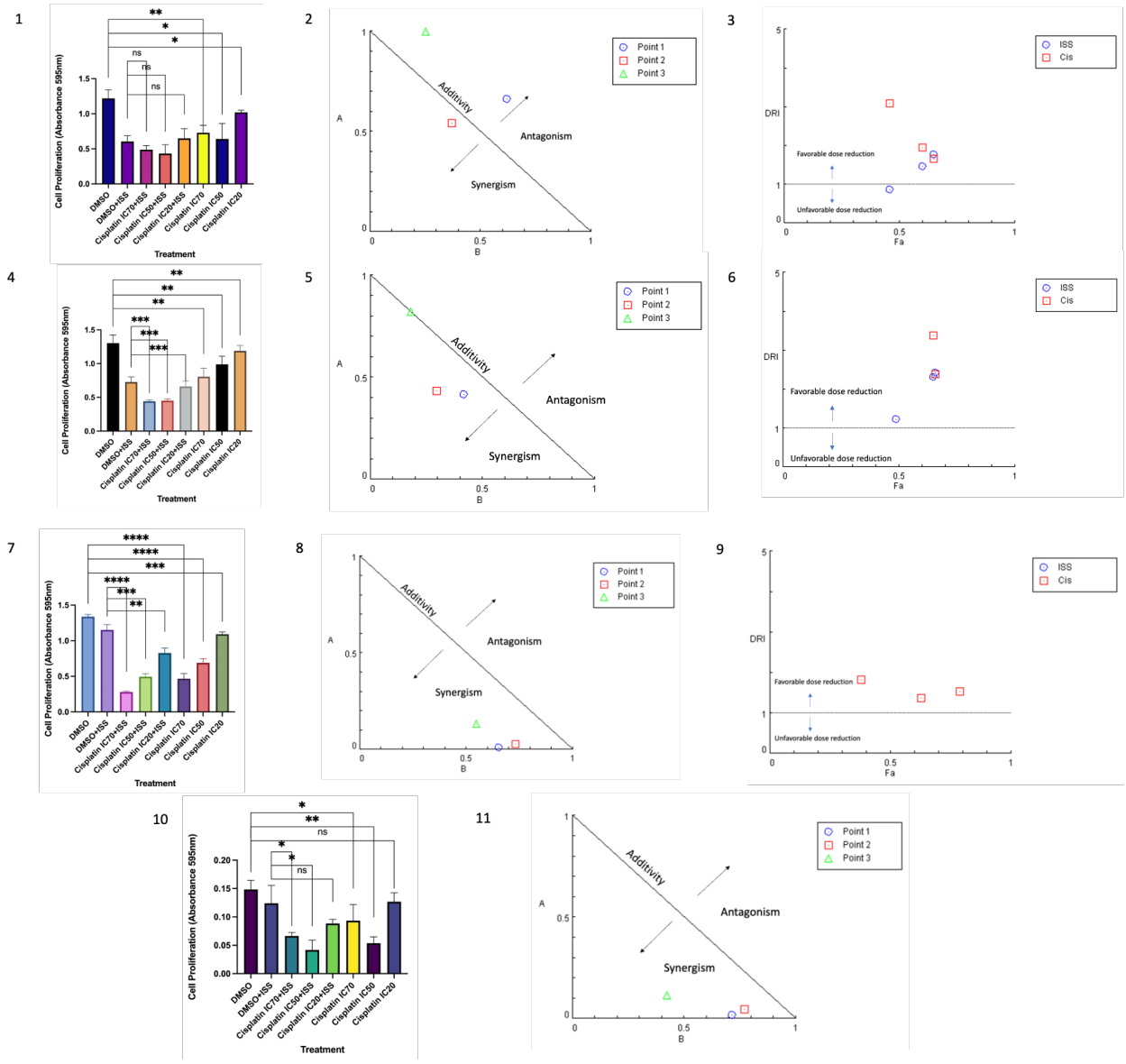

Figure 38. The changes of cell proliferation under ISS (FBS 10% for 8 h/FBS 0% for 16 h) combined with different doses of cisplatin treatment on the HCT-116 (1), HT-29 (4), LS-174T (7), and HCEC (10) cell lines based on MTT results. Results are expressed as means of calculated cell viability ± standard deviations of each group in triplicate. Multiple unpaired t-tests were performed using GraphPad Prism version 9.0. Significant differences between groups are marked with ns – non-significant, *p < 0.05, **p < 0.01, ***p < 0.001, ****p <0.0001. **Normalized isobologram for the combination of cisplatin and ISS with normalization of the dose with IC50 to the unity of both x and y axis in the HCT-116 (2), HT-29 (5), LS-174T (8), and HCEC (11).** Most of the combination points indicated a synergistic interaction. Normalized isobologram was generated using CompuSyn software. Abbreviations: A – ISS $(D)_1/(IC50)_1$; B –

Cisplatin $(D)_2/(IC50)_2$; D – dose; Point 1 – the combination of Cisplatin IC70 and ISS IC50; Point 2 – the combination of Cisplatin IC50 and ISS IC50; Point 3 – the combination of Cisplatin IC20 and ISS IC50. **Fa – DRI plot for the combination of ISS with Cisplatin in HCT-116 (3), HT-29 (6), and LS-174T (9) CRC cell lines.** Abbreviations: DRI – dose reduction index; Fa - fraction affected by the drug concentration (% of cell growth inhibition/100); Cis – Cisplatin; ISS – intermittent serum starvation. The plot was generated using CompuSyn software.

Based on the cell viability, when we combined different doses of cisplatin with intermittent serum starvation (ISS), we observed a significant difference between control ISS and all tested doses of cisplatin combined with ISS (Figure 38). To further test whether we observed synergistic or antagonistic interaction, we calculated CI based on the median-effect equation (Chou) and combination index theorem (Chou-Talalay) as well as generated dose-effect curves using CompuSyn software (243–245). The normalized isobologram showed that the combination of cisplatin and ISS had a synergistic effect in most CRC cells, except for the HCT-116 cell line (Table 11).

Table 11. CI data for the combination of ISS and cisplatin. Data was generated using CompuSyn software.

Dose of cisplatin (μM)	Dose of ISS (% of time under serum starvation)	Effect (fraction of cell growth inhibition)	CI	Interaction effect
HCT-116				
1.8	70	0.61	1.3	Moderate antagonism
1.3	70	0.66	0.9	Nearly additive
0.5	70	0.5	1.3	Moderate antagonism
HT-29				
1.9	70	0.66	0.72	Moderate synergism
1.3	70	0.65	0.83	Moderate synergism

0.5	70	0.49	1.0	Additive effect
LS-174T				
4.1	70	0.79	0.66	Synergism
2.9	70	0.63	0.76	Moderate synergism
1.2	70	0.38	0.68	Synergism
HCEC				
2.9	70	0.7	0.74	Moderate synergism
2.1	70	0.55	0.82	Moderate synergism
0.8	70	0.4	0.54	Synergism

As for DRI values, combining cisplatin and ISS would allow reducing the dose of cisplatin in each tested CRC cell line.

To understand the possible mechanisms behind the interaction between ISS and cisplatin we looked at mRNA sequencing data for DMSO vs. ISS and cisplatin in the HCT-116 CRC cell line.

Exploratory analysis

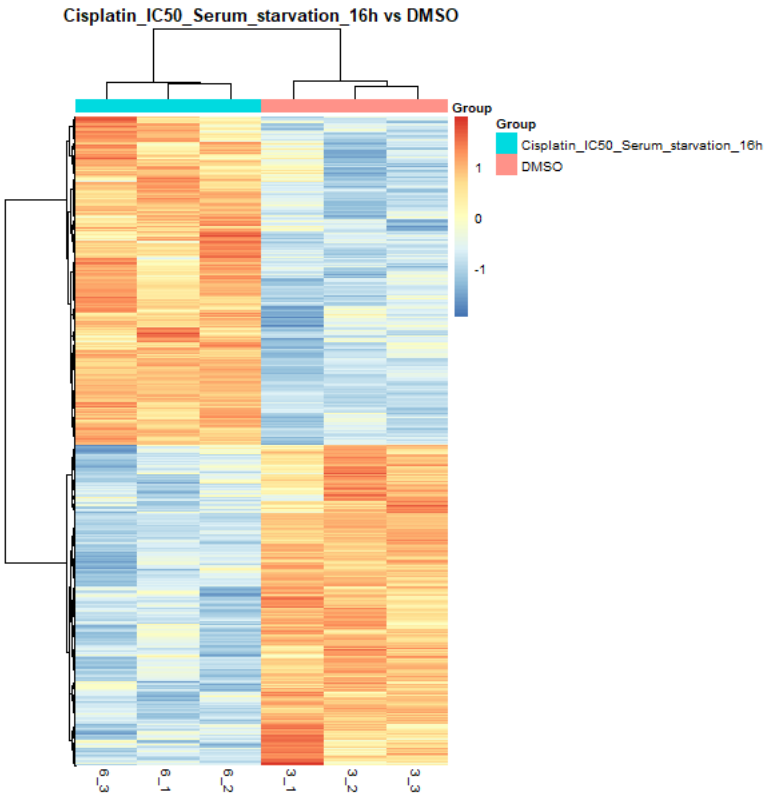

Figure 39. A hierarchical clustering heatmap analysis of the differentially expressed genes with fold change over 1.5 and adjusted p-values < 0.05 for DMSO control versus cisplatin and ISS in the HCT-116 CRC cell line. The x-axis shows non-supervised clusters between the two treatment groups. The 3.1, 3.2, and 3.3 are independent replicates for DMSO and 6.1, 6.2, and 6.3 are for ISS and cisplatin treatment. The y-axis shows differentially expressed genes. The fold changes of up-regulated genes are in the red-orange colour spectrum, and the down-regulated genes are represented in the blue colour spectrum. The heatmap was generated using R software version 4.2.2.

A heatmap represents differentially expressed genes for DMSO versus ISS combined with cisplatin in the HCT-116 CRC cell line (Figure 39). The unsupervised clustering based on the underlying data determined if there were sub-categories within DMSO control and ISS with cisplatin treatment. As the figure shows, there were significant differences in gene expression between the groups. The differences were not substantial for the biological replicates within the same group, showing the treatment samples' good quality.

Pathway analysis

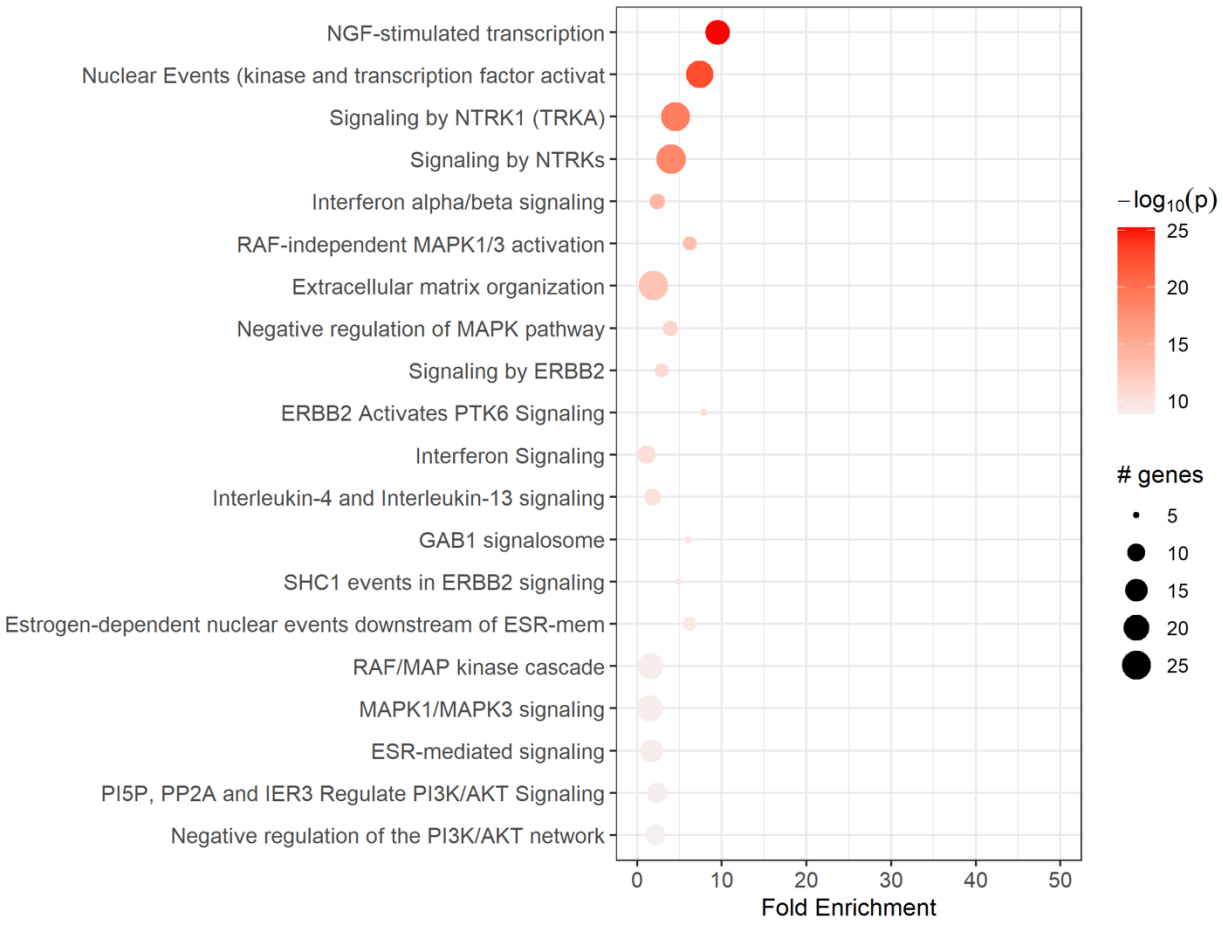

Figure 40. The Reactome dot plot of the top 20 terms for DMSO versus ISS and cisplatin in the HCT-116 CRC cell line. The top 20 terms with the highest fold change are shown in this plot, with their corresponding Reactome pathways on the y-axis. The size of the dots represents the number of genes in each pathway, while the red colour's intensity indicates the enrichment's significance. The most enriched pathways are shown at the top of the plot. The figure was generated using pathfindR enrichment analysis software.

Based on the dot plot analysis, the addition of ISS to cisplatin could have shifted the action of cisplatin from strongly pro-apoptotic toward pro-survival mechanisms (Figure 40). Possibly, because ISS could have reduced the speed of DNA replication, the important stage of the cell cycle for cisplatin's cytotoxic effects.

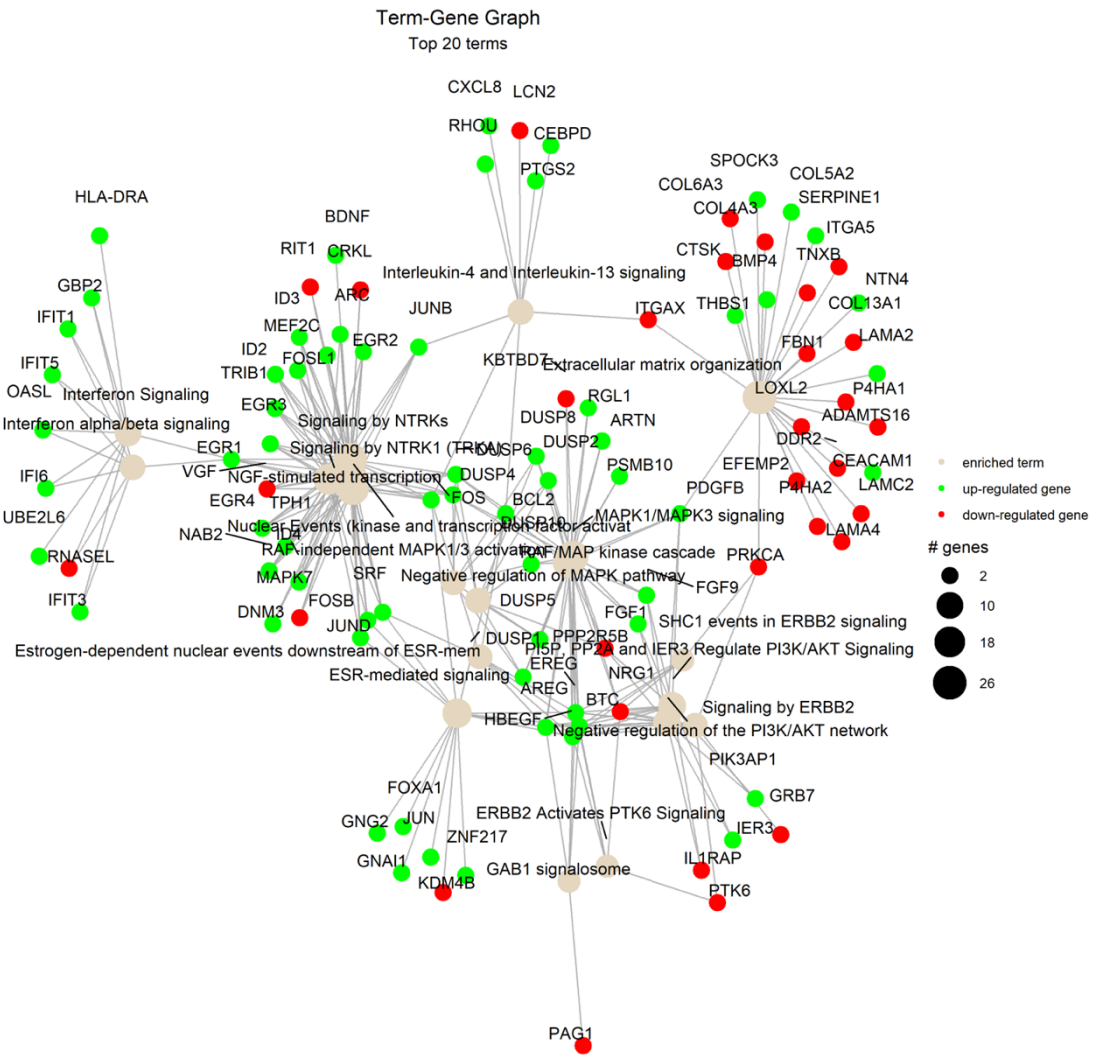

Figure 41. The Reactome Term-Gene Graph for the top 20 terms for DMSO versus ISS combined with cisplatin treatment in the HCT-116 CRC cell line. The graph displays the top 20 Reactome terms and their corresponding gene sets. Each node represents a Reactome term, and the size of the node is proportional to the number of genes associated with that term. The edges between the nodes represent the overlap in gene sets between the terms. The edge's thickness represents the overlap's magnitude, and the edge's colour represents the direction of the overlap, with green for downregulated and red for upregulated genes. The figure was generated using pathfindR enrichment analysis software.

The elevated levels of brain-derived neurotrophic factor (BDNF), early growth response proteins 1-4 (EGR1-4), and parts of AP-1 transcription factors (FOS and JUNB) indicated activation of cell survival mechanisms and cell proliferation. Increased levels of BCL2 would

indicate inhibition of apoptosis. A higher serum response factor (SRF) could also stimulate cell proliferation. SRF is a part of immediate-early genes that regulate the cell cycle, apoptosis and couples cellular gene expression to cytoskeletal dynamics could indicate strong pro-survival signals in cancer cells. More to that, increased levels of TP53I3 and its effector GADD45A indicated p53-mediated DNA repair (Figure 41).

The elevated HBEGF and PDGF indicated stimulation of growth factor signalling. Additionally, higher levels of MAP2K3 would indicate activation of MAP kinase signalling in response to insulin and is necessary for glucose transporter expression. Interestingly, oxidative phosphorylation could have been inhibited. Lower levels of PDK1, a pyruvate dehydrogenase, a mitochondrial enzyme that catalyzes the oxidative decarboxylation of pyruvate and is one of the major enzymes responsible for regulating the homeostasis of carbohydrate fuels in mammals, would suggest inhibition of oxidative phosphorylation in HCT-116 cells. As previously discussed, PI3K/AKT signalling could reduce mitochondrial oxidation yet stimulate glucose utilization as a main fuel for cancer cells, a common pro-survival mechanism in cancer cells.

The increased levels of BMP4 (bone morphogenic protein), CEACAM1 (CEA cell adhesion molecule), COL5A2 (collagen type V alpha 2 chain), LAMA2 (laminin subunit alpha 2), NTN4 (netrin 4), PDGFB (platelet derived GF subunit B), SERPINE1 (serpin family E member 1), SPOCK3 (osteonectin), and THBS1 (thrombospondin 1) indicated a wide variety of responses related to interactions with the extracellular matrix, which can represent an attempt of cancer cell to activate its invasive potential. Furthermore, the elevated levels of ARC, a gene coding for an activity-regulated cytoskeleton-associated protein involved in cell migration, could lead to cancer cell progression. Another protein regulating microtubular and vesicular transport that could cause cancer cell progression was dynamin 3 (DNM3).

However, with the lowering of proteins that take part in Ras signalling, CRK like proto-oncogene adaptor protein (CRKL) and Ras-like without CAAX 1 (RIT1), the GTPase regulating p38 MAPK-dependent signalling cascade that responds to cellular stress, as well as MAPK7 could reduce cancer cell proliferation and inhibit its survival mechanisms. Decreased MAPK7, PRKCA (protein kinase C alpha), and PTK6 (protein kinase 6) intracellular signal transducers responsible for cell proliferation could suppress cancer cell growth. Moreover, decreased levels of transcripts responsible for the formation of some collagens, laminins, and metalloproteases could lead to the suppression of cancer cell invasiveness.

The increased transcripts for EGR1, a few interferon-induced proteins (IFI6, IFIT1, IFIT3, IFIT5) and MHC class II (HLA-DRA) indicated strong stimulation of IFN signalling, which could result in activation of macrophages in the tumor microenvironment. Additionally, listed transcripts take part in the negative regulation of apoptosis and inhibition of cell proliferation by activating p21 and p27.

The top 10 up- and 10 down-regulated genes are presented in Table 12.

Table 12. Top 10 up-and 10 down-regulated genes for DMSO versus cisplatin and ISS treatment in the HCT-116 CRC cell line based on mRNA expression analysis.

Top 10 up-regulated genes			
Gene name	Gene description	Gene biotype	Log2 Fold Change
NR4A3	nuclear receptor subfamily 4 group A member 3	Protein coding	6.3
EGR3	early growth response 3	Protein coding	4.1
NR4A1	nuclear receptor subfamily 4 group A member 1	Protein coding	3.8
EGR2	early growth response 2	Protein coding	3.7
EDN1	endothelin 1	Protein coding	3.5
THBS1	thrombospondin 1	Protein coding	3.3
ATOH8	atonal bHLH transcription factor 8	Protein coding	3.0
FGFBP1	fibroblast growth factor binding protein 1	Protein coding	2.9
METTL7A	methyltransferase like 7A	Protein coding	2.8
NR4A2	nuclear receptor subfamily 4 group A member 2	Protein coding	2.8
Top 10 down-regulated genes			
Gene name	Gene description	Gene biotype	Log2 Fold Change
C1orf162	chromosome 1 open reading frame 162	Protein coding	-3.1
N/A	novel transcript, antisense to PET112L	lncRNA	-3.1

PHF24	PHD finger protein 24	Protein coding	-3.0
FRZB	frizzled related protein	Protein coding	-2.7
DNAJB13	DnaJ heat shock protein family (Hsp40) member B13	Protein coding	-2.4
THSD7A	thrombospondin type 1 domain containing 7A	Protein coding	-2.4
SNX31	sorting nexin 31	Protein coding	-2.4
TM4SF19	transmembrane 4 L six family member 19	Protein coding	-2.3
HKDC1	hexokinase domain containing 1	Protein coding	-2.3
PLSCR2	phospholipid scramblase 2	Protein coding	-2.2

Overall, based on the mRNA expression results, we observed an activation of multiple pro-survival and pro-invasive mechanisms under the combination of ISS and cisplatin in HCT-116. Thus, we would not recommend such a treatment combination in the MMR-deficient CRC, but we would suggest doing further experiments to support this notion.

1.4.7 Combination of intermittent serum starvation, cisplatin and cannabidiol in colorectal cancer cell lines

To see if the addition of ISS to cisplatin and CBD could synergize, I combined the treatments and performed cell viability assays on four cell lines.

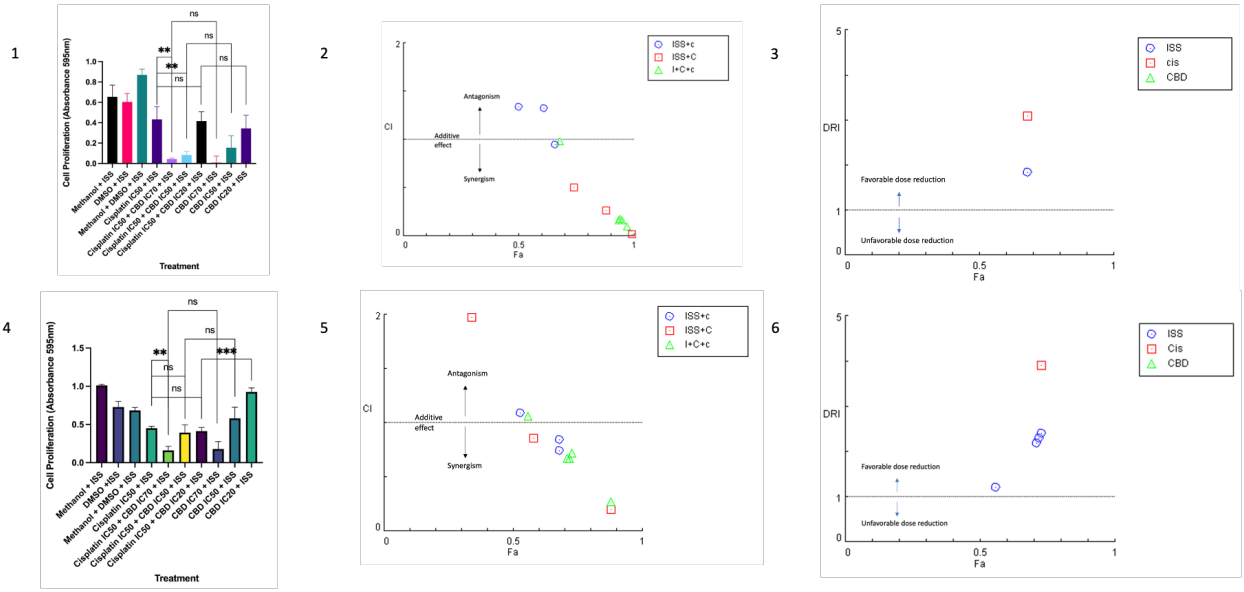

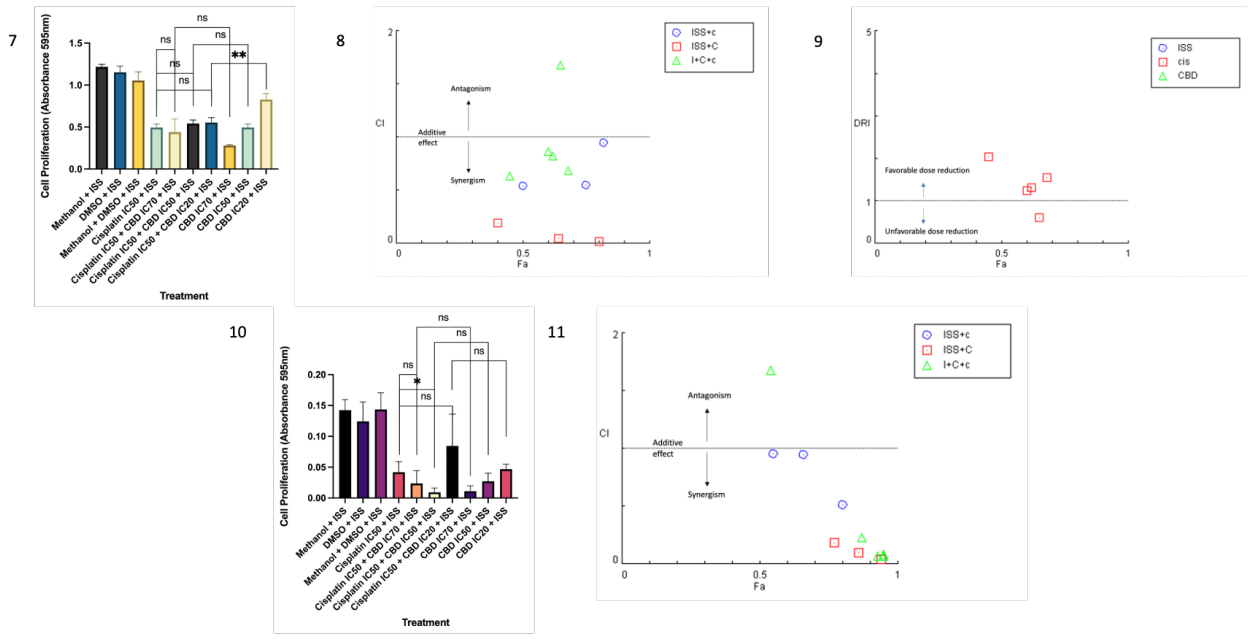

Figure 42. The changes of cell viability under ISS (FBS 10% for 8 h/FBS 0% for 16 h) combined with different doses of CBD and cisplatin treatment on the HCT-116 (1), HT-29 (4), LS-174T (7), and HCEC (10) CRC cell line based on MTT results. Results are expressed as means of calculated cell viability ± standard deviations of each group in triplicate. Multiple unpaired t-tests were performed using GraphPad Prism version 9.0. Significant differences between groups are marked with ns – non-significant, *p < 0.05, **p < 0.01, ***p < 0.001, ****p <0.0001. **Fa – CI plot for HCT-116 (2), HT-29 (5), LS-174T (8), and HCEC (11).** The combination index (CI) was calculated to quantify synergism and antagonism of the drugs, where CI<1 indicates synergism, CI=1 – additive effect, and CI>1 – antagonistic effect. Abbreviations: CI – combination index; Fa – fraction affected by the drug concentration (% of cell growth inhibition/100); ISS+c – the combination of ISS with cisplatin in different doses; ISS+C – the combination of ISS with CBD in different doses; I+C+c – the combination of ISS with CBD and cisplatin in different doses. The plot was generated using CompuSyn software. **Fa – DRI plot for the combination of ISS with CBD and cisplatin in HCT-116 (3), HT-29 (6), and LS-174T (11) CRC cell lines.** Abbreviations: DRI – dose reduction index; Fa - fraction affected by the drug concentration (% of cell growth inhibition/100); CBD – CBD; ISS – intermittent serum starvation. The plot was generated using CompuSyn software.

We observed the lowest cell viability when combining CBD with other treatments. However, in this case, calculating drug interactions is more important than the statistical significance between the treatments. Drug interactions such as synergism or antagonism are based on biophysical and biochemical interactions between treatments, not on statistical significance. To further analyze our results, whether we observed synergistic or antagonistic interaction, we calculated CI based on the median-effect equation (Chou) and combination index theorem (Chou-Talalay) as well as generated dose-effect curves using CompuSyn software (243–245). As shown on Fa-CI plots combining CBD, cisplatin, and ISS had a synergistic effect in most CRC cells (Figure 42, Table 13). Remarkably, by combining three treatments together, we were able to reverse the antagonistic interaction between CBD and cisplatin in tested CRC cell lines. Only in LS-174T and HCEC cells we observed an antagonistic effect when we combined higher doses of cisplatin with CBD and ISS. However, because the Fa values were relatively low, we would disregard this result as the desirable synergistic effects are when we observe Fa higher than 0.9.

As for DRI values, combining cisplatin with CBD and ISS would allow reducing the dose of cisplatin in each tested CRC cell line.

Table 13. CI data for the combination of ISS, CBD, and cisplatin. Data was generated using CompuSyn software.

Dose of ISS (% of time under serum starvation)	Dose of cisplatin (μM)	Dose of ISS CBD (μM)	Fa (fraction of cell growth inhibition)	CI	Interaction effect
HCT-116					
70	1.3	8.3	0.97	0.097	Very strong synergism
70	1.3	5.9	0.94	0.17	Strong synergism
70	1.3	2.4	0.68	0.98	Nearly additive
70	1.9	5.9	0.95	0.16	Strong synergism
70	0.5	5.9	0.94	0.16	Strong synergism
HT-29					
70	1.3	4.9	0.88	0.27	Strong synergism
70	1.3	3.5	0.72	0.67	Synergism

70	1.3	1.4	0.71	0.67	Synergism
70	1.9	3.5	0.73	0.72	Moderate synergism
70	0.5	3.5	0.56	1.06	Nearly additive
LS-174T					
70.0	2.9	6.7	0.68	0.7	Synergism
70.0	2.9	4.8	0.62	0.8	Moderate synergism
70.0	2.9	1.9	0.6	0.87	Slight synergism
70.0	6.7	4.8	0.65	1.7	Antagonism
70.0	1.2	4.8	0.45	0.6	Synergism
HCEC					
70.0	2.1	8.3	0.87	0.2	Strong synergism
70.0	2.1	5.9	0.95	0.07	Very strong synergism
70.0	2.1	2.4	0.54	1.7	Antagonism
70.0	2.9	5.9	0.95	0.09	Very strong synergism
70.0	0.84	5.9	0.93	0.07	Very strong synergism

Next, to understand the possible synergistic mechanisms behind the interaction between ISS, CBD, and cisplatin, we looked at mRNA sequencing data for DMSO vs. ISS, CBD, and cisplatin in the HCT-116 CRC cell line.

Exploratory analysis

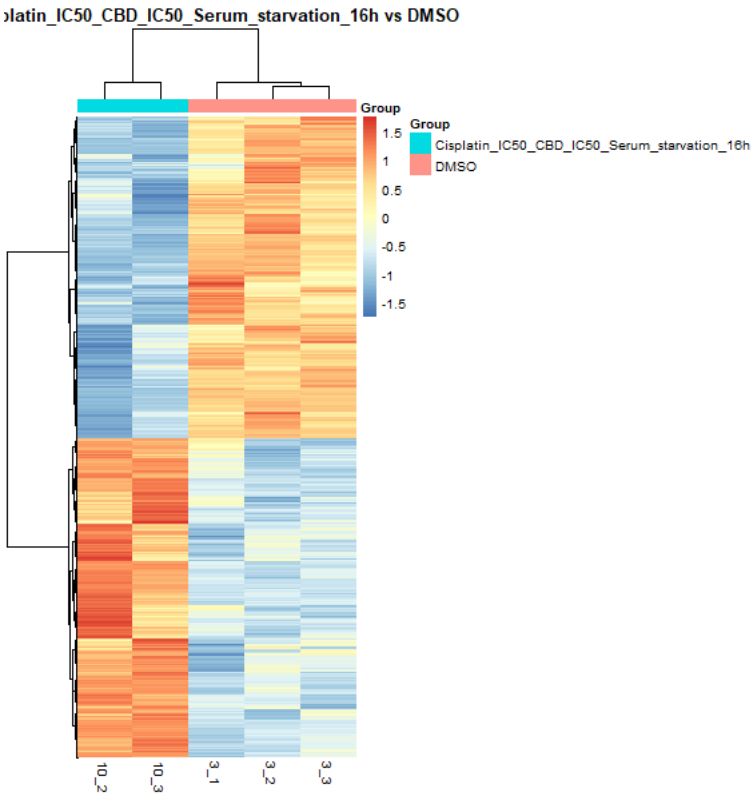

Figure 43. A hierarchical clustering heatmap analysis of the differentially expressed genes with fold change over 1.5 and adjusted p-values < 0.05 for DMSO control versus cisplatin, CBD and ISS in the HCT-116 CRC cell line. The x-axis shows non-supervised clusters between the two treatment groups. The 3.1, 3.2, and 3.3 are independent replicates for DMSO and 10.2, and 10.3 are for ISS, CBD and cisplatin treatment. The y-axis shows differentially expressed genes. The fold changes of up-regulated genes are in the red-orange colour spectrum, and the down-regulated genes are represented in the blue colour spectrum. The heatmap was generated using R software version 4.2.2.

A heatmap represents differentially expressed genes for DMSO versus ISS combined with cisplatin and CBD in the HCT-116 CRC cell line (Figure 43). The unsupervised clustering based on the underlying data determined if there were sub-categories within DMSO control and ISS with cisplatin and CBD treatment. As the figure shows, there were significant differences in gene expression between the groups. The differences were not substantial for the biological replicates within the same group, showing the treatment samples' good quality.

Pathway analysis

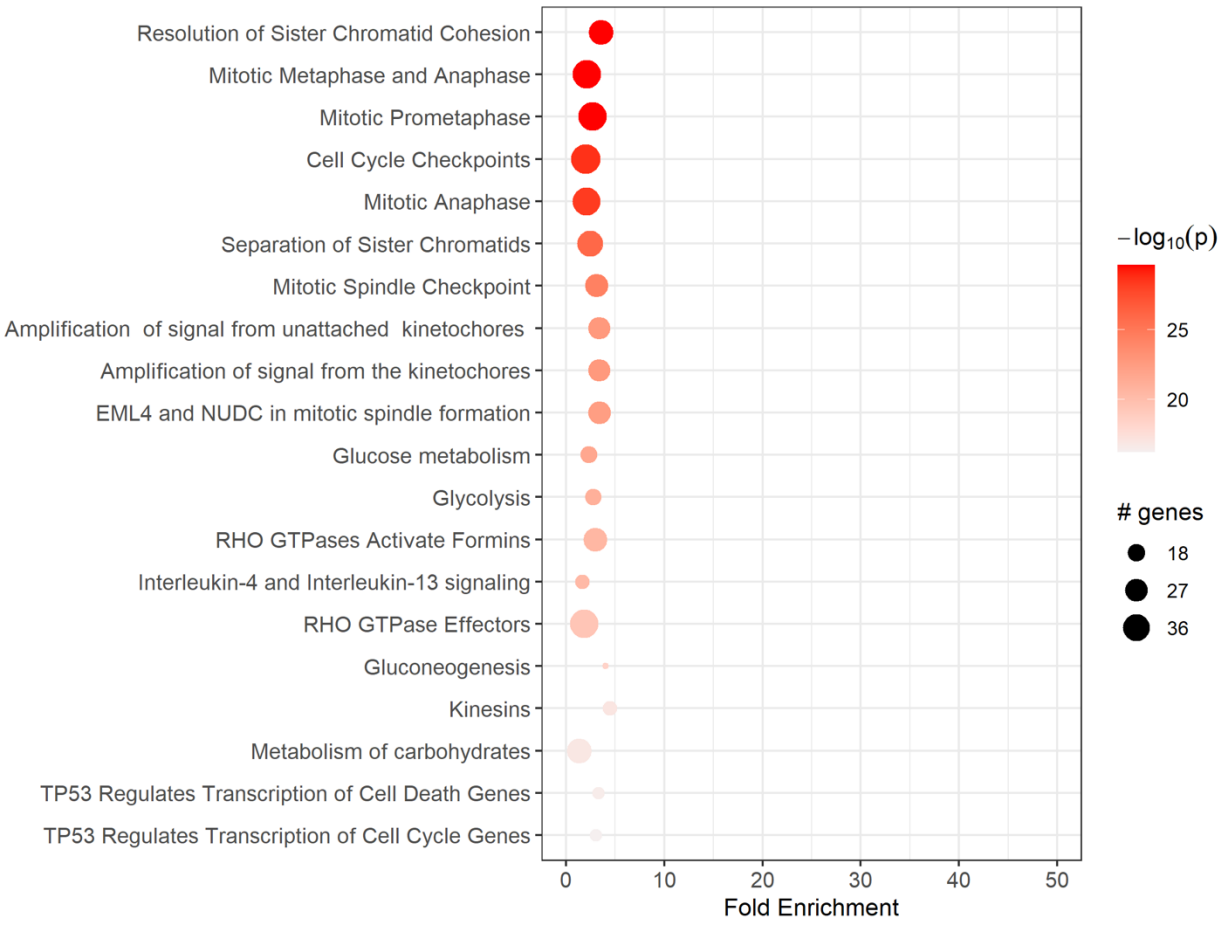

Figure 44. The Reactome dot plot of the top 20 terms for DMSO versus ISS, CBD and cisplatin in the HCT-116 CRC cell line. The top 20 terms with the highest fold change are shown in this plot, with their corresponding Reactome pathways on the y-axis. The size of the dots represents the number of genes in each pathway, while the red colour's intensity indicates the enrichment's significance. The most enriched pathways are shown at the top of the plot. The figure was generated using pathfindR enrichment analysis software.

The dot plot analysis showed a strong upregulation of genes that are responsible for sister chromatid cohesion, mitotic spindle checkpoint, amplification of signals from kinetochores, activation of TP53-mediated apoptosis and disorders of carbohydrate metabolism (Figure 44). I suggest that the combination of CBD and ISS caused strong inhibition of energetic reserves in CRC cells, which could assist in cisplatin's cytotoxic effect. I already mentioned in the literature review that cisplatin often causes cell cycle arrest in the G2/M phase, which we also could see in our pathway analysis.

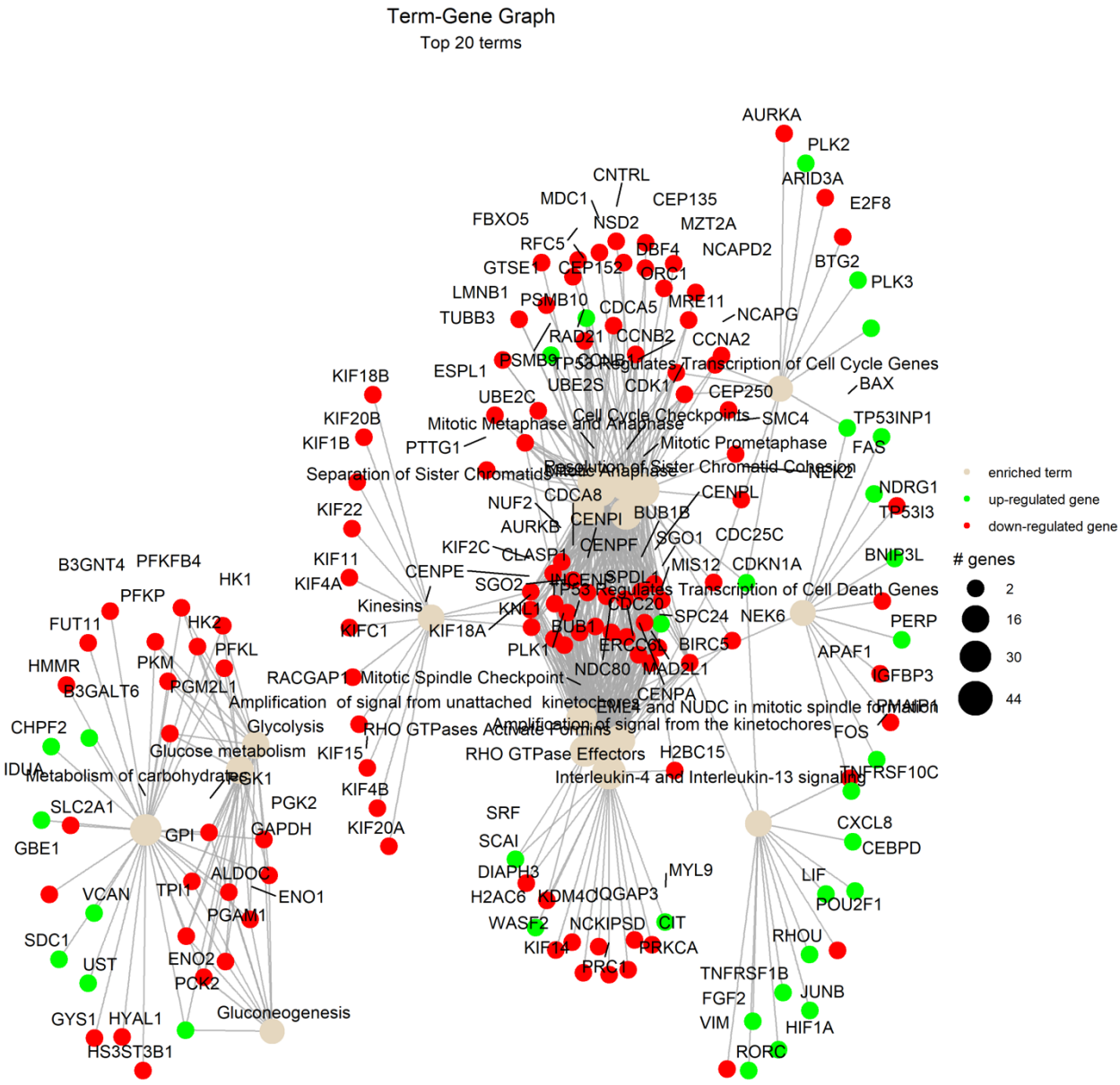

Figure 45. The Reactome Term-Gene Graph for Top 20 terms for DMSO versus ISS combined with cisplatin treatment in the HCT-116 CRC cell line. The graph displays the top 20 Reactome terms and their corresponding gene sets. Each node represents a Reactome term, and the size of the node is proportional to the number of genes associated with that term. The edges between the nodes represent the overlap in gene sets between the terms. The edge's thickness represents the overlap's magnitude, and the edge's colour represents the direction of the overlap, with green for upregulated and red for downregulated genes. The figure was generated using pathfindR enrichment analysis software.

Under the combination of ISS, cisplatin, and CBD, there was a massive decrease in transcripts responsible for the resolution of sister chromatid cohesion, genes involved in metaphase and anaphase, separation of sister chromatids, and amplification of signals from kinetochores (Figure 45).

The increased levels of CDKN1A, a gene coding for cyclin-dependent kinase inhibitor 1 A, indicated cell cycle arrest. The decreased levels of AURKB – aurora B kinases responsible for the alignment and chromosome segregation during mitosis through association with microtubules could also indicate cell cycle arrest in the M phase. Moreover, decreased BUB1, a gene coding for mitotic checkpoint serine/threonine kinase B that has been localized in kinetochores and plays an important role in inhibiting the anaphase-promoting complex/cyclosome (APC/C), delaying the onset of anaphase. The decreased levels of centromere proteins A, F, E, I, and L would disturb the proper mitotic behaviour of chromosomes leading to improper centromere structures. A decrease of CLASP1, a nonmotor microtubule-associated protein involved in regulating microtubule dynamics at the kinetochores, also indicated a disturbance of proper mitosis. Lower levels of NUF2, the NUF2 component of the NDC80 kinetochore complex, would suggest improper chromosome segregation and spindle checkpoint activity. Additionally, MAD2L1, mitotic arrest deficient 2 like 1, a component of the mitotic spindle assembly checkpoint that prevents anaphase onset until all chromosomes are properly aligned, was decreased, suggesting arrest in the M phase. A highly expressed during mitosis PLK1 coding for polo-like kinase 1 that regulates centrosome maturation and spindle assembly, removing cohesins from chromosome arms, inactivating APC/C inhibitors, and regulation of mitotic exit and cytokinesis was also decreased. Furthermore, decreased expression of RAD21, a gene involved in the repair of DNA-double strand breaks and chromatin cohesion during mitosis, would suggest disorders in HR repair systems.

The lowering of cyclin-dependent kinase 1 (CDK1), cell division cycle 20 (CDC20), and cyclin B1 and B2 (CCNB1 and CCNB2) would suggest strong inhibition of cell cycle progression in the G2/M phase.

Similarly to cisplatin alone, p53-mediated pro-apoptotic factors such as FAS and BAX were upregulated. Additionally, decreased levels of survivin and N-myc downstream regulated NDRG1, a stress response protein involved in hormone response, would further suggest inhibiting pro-survival mechanisms and activation of apoptosis.

There were increased levels of JUNB protooncogene, an AP-1 transcription factor subunit which regulates cell proliferation. Additionally, the increased levels of HIF1α and FGF2 indicated activation of survival pathways in cancer cells and possible stimulation of EMT, which would be unwanted effects of combinational treatment. Additionally, increased Ras homolog family member U, a Rho GTPase activating PAK1 and JNK1, can induce the formation of filopodium and dissolving stress fibers. It also mediates the effects of Wnt signalling in regulating cell morphology, cytoskeletal organization, and cell proliferation. Moreover, an increase in TNFRSF1B, a gene encoding a member of the TNF-receptor superfamily, together with TNFR1, forms a heterocomplex that mediates the recruitment of c-IAP1 and c-IAP2, which could help in cancer cell survival.

The increased betacellulin (BTC) levels could indicate the increased production of EGF-like proteins to stimulate cancer cell growth. Additionally, higher levels of FGF1, FGF2, FGF9 and FGF19 indicate a strong stimulation of FGF signalling, which could stimulate broad mitogenic and cell survival mechanisms, including angiogenesis, invasion, and metastasis. Heparin-binding EGF Like growth factor (HBEGF), when elevated, could stimulate PI3K/AKT pro-survival signalling. Moreover, elevated levels of PDGF, TGF-α and PI3K regulatory subunit 3 also indicated activation of the PI3K/AKT signalling and possible stimulation of EMT.

On the other hand, reduced fibroblast growth factor receptor 4 (FGFR4) and EGFR could decrease cell proliferation, migration, and lipid and glucose metabolism. Lower levels of IL-1 receptor accessory protein could reduce IL-1-dependent activation of NFkB and result in an anti-inflammatory effect. Additionally, SNAIL1, a strong inductor of EMT, was also decreased, which would indicate inhibition of tumour cell progression. Decreased Ras-related GTP binding D, which takes part in AKT/mTOR signalling and activation and relocation of mTORC1 to the lysosomes, could inhibit CRC cell growth.

The increased expression of different types of collagen components such as collagen type I alpha 1 chain, collagen type IV alpha 5 chain, collagen type XI alpha 2 chain, as well as CEA adhesion molecule 1, integrin subunits alpha 1 and 10, laminin subunits, and syndecan 1 indicated a strong formation of ECM connections between cancer cells and the environment that could lead to invasion and metastasis. On the other hand, the downregulation of ADAMTS2, ADAMTS14, MMP11, and MMP7, metalloproteases which help in cancer cell invasiveness by dissolving the ECM components, could prevent cancer invasive potential.

The top 10 up- and 10 down-regulated genes are presented in Table 14.

Table 14. Top 10 up-and 10 down-regulated genes for DMSO versus cisplatin, ISS, and CBD treatment in the HCT-116 CRC cell line based on mRNA expression analysis.

Top 10 up-regulated genes			
Gene name	Gene description	Gene biotype	Log2 Fold Change
NR4A3	nuclear receptor subfamily 4 group A member 3	Protein coding	4.1
THBS1	thrombospondin 1	Protein coding	3.9
SSTR5-AS1	SSTR5 antisense RNA 1	lncRNA	3.2
ABCA12	ATP binding cassette subfamily A member 12	Protein coding	3.2
EDN1	endothelin 1	Protein coding	3.1
AHRR	aryl hydrocarbon receptor repressor	Protein coding	2.67
CCN1	cellular communication network factor 1	Protein coding	2.6
GDF15	growth differentiation factor 15	Protein coding	2.6
CCN2	cellular communication network factor 2	Protein coding	2.6
CD7	CD7 molecule	lncRNA	2.5
Top 10 down-regulated genes			
Gene name	Gene description	Gene biotype	Log2 Fold Change
UPK1A-AS1	UPK1A antisense RNA 1	lncRNA	-3.3
CA9	carbonic anhydrase 9	Protein coding	-3.3

ARRDC4	arrestin domain containing 4	Protein coding	-3.3
PFKFB4	6-phosphofructo-2-kinase/fructose-2,6-biphosphatase 4	Protein coding	-3.2
LINC00640	long intergenic non-protein coding RNA 640	lncRNA	-2.9
RPL17P50	ribosomal protein L17 pseudogene 50	processed_pseudogene	-2.8
KLHL2P1	kelch like family member 2 pseudogene 1	unprocessed_pseudogene	-2.8
HLA-V	major histocompatibility complex, class I, V (pseudogene)	transcribed_unprocessed_pseudogene	-2.7
ZNF101P2	zinc finger protein 101 pseudogene 2	processed_pseudogene	-2.7
KDM4A-AS1	KDM4A antisense RNA 1	lncRNA	-2.7

Overall, we observed a strong activation of G2/M cell cycle arrest and apoptosis in HCT-116 CRC cells under the combination of CBD, cisplatin, and ISS. However, despite the strong cytotoxic effects of combinational treatment, there was an upregulation of transcripts that take part in cancer cell EMT and invasive potential.

1.5. Discussion, limitations and future perspectives

1.5.1. Cisplatin

Cisplatin is an effective chemotherapy agent that is used for the treatment of multiple cancers (144). It is often used in combination with other anticancer therapies (145). Unfortunately, the development of resistance to cisplatin and, as a result, cancer progression occuroccurs often (146,147).

Cisplatin has a strong pro-apoptotic effect (155,156), which coincided with our data on the HT-29 and the HCT-116 CRC cell lines. Cisplatin's cytotoxic action is explained that by forming

DNA crosslinks, it can cause DNA- damage and apoptosis (144). Additionally, when administered, cisplatin induces oxidative stress primarily in mitochondria, reducing membrane potential (143) and ultimately leading to cell death (149).

According to the mRNA expression data obtained from the HT-29 CRC cell line, cisplatin had multiple effects on cancer cells. Cisplatin hindered various biosynthetic pathways, including aminoacyl-tRNA and rRNA, thereby inhibiting global translation. Furthermore, it reduced multiple metabolic pathways that cancer cells depend on for growth and proliferation, such as glycolysis, gluconeogenesis, and oxidative phosphorylation. Cisplatin induced cytotoxic effects by increasing the expression of several genes involved in both the intrinsic and extrinsic pathways of apoptosis. Another effect of cisplatin was the increased expression of p21, which can lead to cell cycle arrest in the G1/S phase. Nonetheless, cell cycle arrest may not be a beneficial effect of chemotherapy as it may lead to cell survival (152). Our data also showed that under cisplatin, multiple unwanted mechanisms were activated that could result in CRC cell survival and progression, which are often observed in clinical settings as a disease relapses.

1.5.2 CBD

As we previously mentioned, the mechanisms of anticancer effects of cannabinoids include the activation of apoptosis, endoplasmic reticulum (ER) stress response, downregulation of survivin (inhibitor of apoptosis), a decrease of RAS/MAPK and PI3K/AKT signalling (22,26,35,37,40). However, our data on the HCT-116 CRC cell line did not show such a variety of mechanisms involved. We suggest that perhaps the dose of IC50 was not sufficient to activate the full spectrum of cytotoxic effects of CBD, at least when it was administered alone. It is also possible that the effect of CBD depends on the cancer type and tissues involved.

Adding CBD modulated TGF- β signalling via SMAD7 and SMAD3 upregulation, which resulted in the inhibition of TGF- β, a common pathway affected in CRCs (19,20) responsible for EMT and cell survival. Interestingly, CBD also inhibited ABCA1 transcript, which belongs to the ABC family of transporters that commonly contribute to chemotherapy drug resistance. Thus, CBD could possibly reduce the development of drug resistance via decreasing drug efflux pumps.

A persistent chronic inflammatory response in some CRCs with increased levels of TNF, IL-17, IL-23, IFN-γ, and IL-6 due to the activation of NFkB and STAT3 can lead to the formation of aberrant cryptic foci (ACF) and adenomas that eventually can develop into adenocarcinomas. Moreover, continuous activation of COX-2 increases KRAS signalling and promotes tumor

survival, progression, and metastatic potential (13–15). As our results showed, CBD decreased levels of MAP3K8 transcript, an oncogene coding for Mitogen-Activated Protein Kinase Kinase Kinase 8, which can activate both MAP and JNK pathways as well as proinflammatory pathways involving activation of NFκB. This could be one of the mechanisms of CBDs preventive action on CRCs development.

Additionally, we observed the decreased the expression of genes responsible for glucose metabolism, glycolysis, and gluconeogenesis, such as PFKFB4 that regulates fructose-2,6-bisphosphate and respond to hypoxia to help cancer cells produce more ATP. There was also downregulation of hexokinase 2, which is involved in the rapid activation of glycolysis in cancer cells. Our data also showed that the addition of CBD inhibited the transcription of factors that help cancer cells with energy and oxygen scarcity. Thus, it could prevent cancer cell survival and the development of cancer progression. The observed mechanisms of CBD regarding glucose metabolism were of high interest to us because they could assist with the mechanisms of serum deprivation when two treatments were combined together.

Overall, the Reactome data for differential expression analysis in the HCT-116 CRC cells showed that CBD had a range of effects on gene expression. CBD was observed to decrease the expression of genes responsible for glucose metabolism, glycolysis, and gluconeogenesis, which could impede cancer growth. Additionally, CBD downregulated cell mitogenesis and differentiation gene, specifically FOSB, EGR3, and EGR1. CBD had an impact on TGF-β signalling pathways and decreased the expression of ABCA1 and ANGPTL4, potentially reducing the development of drug resistance. Conversely, CBD increased the expression of oncogenes like JUN and MAPK3K8. In summary, these results suggest that CBD may have therapeutic potential for the MSI subtype of CRC. However, further experimental data would be required to support this idea, such as apoptosis assay, protein expression analysis of selected pathways, and animal models.

1.5.3 ISS

Studies have demonstrated that both serum starvation *in vitro* and short-term food deprivation *in vivo* can decrease growth factor stimulation levels (167–169). When growth signals are depleted in normal cells, it can reduce proliferation-stimulating signalling activity and metabolism (170). However, cancer cells respond differently to starvation, as it can trigger cellular stress due to their metabolic reprogramming to ensure continuous proliferation (171) and activate

the DNA damage response (162). In mice models, short-term fasting protected normal cells while sensitizing malignant cells to chemotherapy drugs, which depends on reduced levels of IGF-1 and glucose (185). This was one of the reasons why we decided to test 0% FBS ISS. FBS is known to contain a high number of growth-stimulating factors that would boost cancer cell growth. We wanted to see how pro-survival signalling in CRC cells will respond to ISS because multiple oncogenic pathways play a role in decreased stress resistance in cancer cells, which results in their inability to switch into a stress-protective mode (183).

The mRNA expression analysis of ISSs' effects in the HCT-116 showed that serum deprivation activated multiple survival pathways, including PI3K/AKT signalling. ISS downregulated the expression of EGFR, which could inhibit cell growth, proliferation, and survival of cancer cells. On the other hand, increased levels of serum response factor and PI3K signalling may indicate the activation of survival pathways in CRC cells. Multiple genes that take part in the downregulation of MAPK/ERK1/2 signalling were increased, which could lead to the prevention of apoptosis. The numerous genes taking part in extracellular matrix reorganization were changed too. The decreased levels of some integrins, laminins, MMPs and PDGFs could point to reduced invasiveness of HCT-116 cells under ISS treatment. Interestingly, ISS also inhibited carbohydrate and modulated lipid metabolism similarly to the CBD treatment alone.

Based on the literature review, MTT and mRNA expression data we decided to test CBD, cisplatin, and ISS in different combinations to see if we could achieve a synergistic effect. Thus, our next step was to look at different treatment interactions (Figure 46) and their molecular mechanisms.

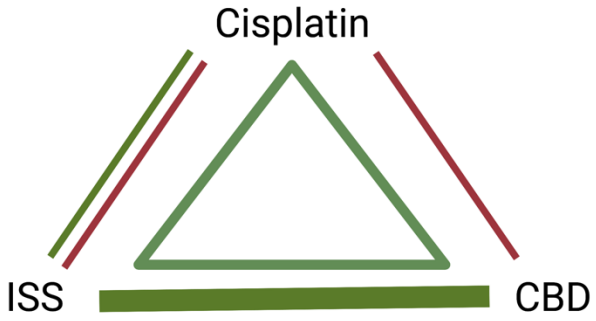

Figure 46. The treatment interactions between intermittent serum starvation, CBD, and cisplatin in CRC cell lines. Green lines indicated synergistic interactions, and red lines indicated antagonistic effects. The line thickness indicated the strength of the interaction. Figure created with BioRender.com

1.5.4 ISS and CBD

As previously mentioned, many cancer cells have higher glucose uptake rates and rely on glycolysis and lactic acid fermentation even when oxygen is present, known as the Warburg effect (216). The PI3K/AKT/mTOR pathway is a key regulator of aerobic glycolysis and cellular biosynthesis, involving enhanced glucose uptake, essential amino acids, and protein translation (207). In cancer, hyperactivation of AKT prevents apoptosis and boosts uncontrolled cell proliferation. The signalling from growth factors and cytokine receptors can inhibit the activation of apoptosis by stimulating PI3K/AKT signalling (221).

The potential of modulating tumor metabolism for therapeutic purposes has not been extensively studied. However, there are several methods for influencing tumor metabolism that could have therapeutic implications and normalize cell metabolism. These methods include inhibiting HIF-1α from decreasing angiogenesis, re-establishing p53 to activate apoptosis, and suppressing PI3K/AKT/mTOR signalling pathway to inhibit cell growth and proliferation (223,224). Additionally, AKT may inhibit apoptosis via the activation of mitochondria-bound

hexokinase (234). In summary, low-nutrient conditions and glycolysis inhibitors may enhance the activation of apoptosis for glucose-addicted cancer cells with overactivated oncogenes.

Based on our results, we suggest that the strong synergistic effect between ISS and CBD was due to the hyperactivation of AKT signalling and simultaneous inhibition of glycolysis and oxidative phosphorylation (Figure 33), which pushed cancer cells toward the stimulation of pro-apoptotic factors.

1.5.5 Cisplatin and CBD

As mentioned previously, the activation of p38 MAPK pathway plays a crucial role in cisplatin-induced apoptotic death, as it triggers the transcription of PUMA and NOXA via p53 activation (155,156). According to Hayakawa et al. (2000) (157), cisplatin-induced DNA damage leads to phosphorylation of BAD via the pro-survival AKT pathway. Other studies have also indicated that BAD protein is phosphorylated by ERK cascade in response to cisplatin treatment (158). Our mRNA sequencing results also indicated a strong upregulation of p-53 mediated transcription of genes involved in apoptosis and based on the literature review, these mechanisms were similarly modulated by cannabinoids, which is why we combined cisplatin and CBD to explore the possibility of a synergistic interaction.

Unfortunately, the combination of CBD and cisplatin had an antagonistic effect. Although we observed an activation of pro-apoptotic genes, the fold enrichment of cell death transcripts was much higher in cisplatin alone compared to cisplatin with CBD. We suggest that one of the reasons might be an increased basal activity of pro-survival pathways under CBD treatment due to its modulative role in carbohydrate and lipid metabolism.

1.5.6 Cisplatin and ISS

It was previously shown that serum starvation sensitized cancer cells to cisplatin while protecting normal cells. In normal cells, serum starvation caused cell cycle arrest in G0/G1 phase due to p53/p21 activation, which depended on AMPK but not on the activation of ATM. However, but in cancer cells, serum starvation-activated p53 was both AMPK- and ATM-dependent. Additionally, the combination of cisplatin with serum starvation led to the activation of the ATM/CHK2/p53 pathway, compared to cisplatin alone, which indicated that the combination therapy sensitized cancer cells to chemotherapy. As a result, short-term starvation sensitized tumor xenografts to cisplatin, as indicated by significant tumor growth delay and the induction of complete remission in 60% of mesotheliomas and 40% of lung carcinoma xenografts. Thus,

combining starvation with cisplatin may enhance the therapeutic index of cisplatin-based chemotherapy (162). However, our results were different. Based on the cell viability, the combination of ISS and cisplatin had various effects on different CRC cell lines. In the MMR deficient, p53-positive HCT-116 CRC cell line, we observed antagonistic interaction with the strong activation of pro-survival mechanisms, such as increase in AP-1 transcription factors, stimulation of growth factor signalling, and upregulation of transcripts that take part in cancer cell invasiveness. On the other hand, in APC mutated HT-29 CRC cell line, we observed a synergistic effect. However, without mRNA pathway analysis of the HT-29 cell line, we cannot suggest any molecular mechanisms behind such an effect and would not recommend combining ISS with cisplatin to inhibit the CRC cell growth at this stage of experimental research.

1.5.7. Cisplatin, CBD, and ISS

The capacity of cisplatin to create DNA crosslinks results in the activation of cell cycle checkpoints. Cisplatin leads to a temporary pause in the S phase of the cell cycle, aided by p16. Cdc2-cyclin A or B kinase is strongly inhibited, resulting in more noticeable G2/M cell cycle arrest. In addition, cisplatin triggers the activation of ATM and ATR, which includes the phosphorylation of the p53 protein (154). Our results showed that when CBD, cisplatin, and ISS were combined, we observed synergistic interaction between the treatments. Interestingly, the differential gene expression analysis revealed a strong activation of multiple transcripts taking part in G2/M cell cycle arrest and p53-mediated transcription of cell death genes. We observed a massive decrease in transcripts responsible for the resolution of sister chromatids cohesion, genes involved in metaphase and anaphase regulation, and kinetochore signalling. We suggest that ISS and CBD, which acted by suppressing metabolic pathways in the HCT-116 CRC cell line, aided the cytotoxic effects of cisplatin, resulting in the upregulation of pro-apoptotic genes and G2/M arrest. It would be interesting to check if this combination could result in mitotic catastrophe and cell death in multiple CRC cell lines.

1.5.8. Conclusions

Based on our hypotheses, we could propose that CBD did modulate cell metabolism and stress survival pathways in the HCT-116 CRC cell line. Our second hypothesis stated that CBD and cisplatin would act in synergy. However, our results showed an antagonistic interaction between those two treatments. Our third hypothesis stated that ISS might induce cytotoxicity in CRC cells via reprogramming and activation of stress signalling, which we observed in the HCT-

116 CRC cell line. The fourth hypothesis suggested the synergistic effect between cisplatin and ISS. Here, the data were controversial. We did show a synergistic effect of ISS and cisplatin on HT-29 and LS-174T cell lines, but not in the MMR-deficient HCT-116 cell line. The next hypothesis was about the synergistic interaction between CBD and ISS, which we supported with our MTT results and mRNA expression data. The last hypothesis on the synergistic effect of CBD, cisplatin and ISS was also supported. We indeed showed a synergistic interaction between cisplatin, CBD, and ISS. Surprisingly, differential gene expression analysis showed strong activation of transcripts responsible for G2/M arrest and possible mitotic catastrophe.

Overall, based on our cell viability results and mRNA expression analysis, we established treatment interactions in CRC cell lines and understood some of the molecular mechanisms behind those drug interactions. However, more experiments would be needed to support our statements. We hope that we have established the basics for further research in this field. However, we understand that the major limitation of our study is that we made suggestions based on cell viability and mRNA expression analysis, and more confirmatory studies would be needed to support our notions. As a future perspective, we would suggest checking the protein expression of selected pathways, performing apoptosis assays for different treatments and their combinations, and animal models with intermittent fasting and drug combinations, which could provide more reliable data and become clinically applicable.

CHAPTER 2: THE EFFECTS OF EXTRACT #18 AND CISPLATIN ON COLORECTAL CANCER CELL LINES

2.1. Introduction

The molecular effects of cannabinoids and cisplatin on colorectal cancer were described in chapter 1 of this thesis. In this introduction, we will mainly focus on cannabinoid extracts and some of the anticancer effects of terpenes present in the cannabis plant that could be relevant to our research.

2.1.1 The anticancer effects of cannabis extracts

Experiments on the CRC cell lines DLD-1 and HCT-116 indicate the significant inhibition of proliferation by high-CBD *Cannabis sativa* extracts (38). These studies also indicate a higher affinity of CBD extract to CB1 and CB2 receptors than purified CBD. In addition, the same extract decreases polyp formation in an AOM animal model and reduces neoplastic growth in xenograft tumor models (38).

Nallathambi et al. (2017) showed synergistic interaction within different fractions of *C. sativa* extract, resulting in colon cancer G0/G1 cell cycle arrest and apoptosis (43). This study shows that the extracts high in cannabigerolic acid (CBGA) and THCA exerts the most potent anticancer effect. THCA shows immunomodulatory, anti-inflammatory, and antineoplastic activity, whereas CBGA has predominantly cytotoxic activity. The suppressed expression of genes, such as cyclin E2 and cyclin E1, causes cell cycle arrest. In addition, TRAIL and PUMA genes are stimulated under the combination of extracts, which results in the apoptosis of CRC cells (43).

On the contrary, Raup-Konsavage et al. (2020) indicated that full-spectrum CBD oils did not reduce cell viability of CRC, melanoma and glioblastoma cell lines more effectively than pure CBD. Purified CBD showed lower IC_{50} concentrations than CBD oils (246).

The controversial data regarding the effectiveness of cannabinoids vs. cannabinoid extracts show that the variabilities in concentrations of cannabinoids, terpenes and other molecules present in the cannabis plant may impact their therapeutic effects. Moreover, these active ingredients' levels may often vary within the same strain and be influenced by growth conditions (247). The solution could be to test the combinations of pure cannabinoids, terpenes, or other molecules of interest in known doses and on specific molecular subtypes of CRC.

2.1.2. Cannabis sativa and effects of terpenes on cancer

The following section was discussed in the review article by Cherkasova et al. (2022) (248).

The cannabis plant is rich in terpenes and flavonoids, biologically active substances which can also be used in cancer treatment (249,250). There are more than 20,000 terpenes in nature, with around 200 found in *Cannabis* plants (251). The monoterpene myrcene, sesquiterpenes β-caryophyllene, and α-humulene are often present in *Cannabis* chemovars. However, the spectrum of terpenes can vary from plant to plant. We described some of the common terpenes that have anti-neoplastic effects and can be one of the components in *Cannabis* extracts.

Myrcene is present in hop, bay, verbena, lemongrass, citrus, and even carrot. Surprisingly, in some animal studies, myrcene showed to be carcinogenic, causing kidney cancer in rats and liver cancer in mice (252). Another study showed that myrcene protected human B lymphocytes from DNA damage caused by hydroperoxides (253). However, it also had cytotoxic effects on breast, colon, cervical, lung cancer cell lines, and leukemia cells (251,254). There is not much knowledge about the mechanisms of action of myrcene, and more studies should be undertaken considering its controversial effects on cancer cells.

β-caryophyllene is a sesquiterpenoid commonly present in black pepper, oregano, basil, and rosemary. This terpene can induce apoptosis and cause cell cycle arrest in lung and ovarian cancer cell lines (255,256). It can also influence the production of free radicals and have antiapoptotic and antiproliferative effects via activation of the JAK1/STAT3 pathway in osteosarcoma cells (257). Importantly, β-caryophyllene may sensitize different cancer cell lines to the conventional chemotherapy drug doxorubicin (258–261). Additionally, it attenuated doxorubicin-induced chronic cardiotoxicity in rats via the activation of CB2 receptors (262). Moreover, the combination of β-caryophyllene with 5-fluorouracil (5-FU) or oxaliplatin on colorectal cancer cells sensitized those cells to chemotherapeutics (263) as well as the addition of it to sorafenib treatment in liver cancer cells (264). Thus, combining different cannabinoids with β-caryophyllene may become advantageous in cancer therapy and needs further investigation.

The monocyclic sesquiterpene, humulene, is also present in the cannabis plant. Humulene has cytotoxic activity on multiple cancer cell lines via increasing production of reactive oxygen species (265,266), inhibition of AKT in hepatocellular carcinoma cells with activation of apoptosis (267). In *in vitro* models, humulene enhanced 5-fluorouracil, oxaliplatin, and doxorubicin cytotoxic effects (260,263).

Another terpene, limonene, is a cyclic monoterpene mainly present in citrus plants and can also be present in *Cannabis*. In the bladder cancer cell line, limonene caused G2/M cell cycle

arrest, decreased migration and metastasis, and increased Bax and caspase 3, thus, inducing apoptosis (268). It inhibited PI3K/AKT, induced autophagy and enhanced sensitivity to docetaxel in *in vitro* cancer cell models (269–272). In *in vivo* models, limonene decreased tumor growth, induced apoptosis, and reduced c-Jun and c-myc expression (272–280). There was one small clinical trial regarding breast cancer patients that received limonene for a short period of time. This study evaluated the metabolomic profiles of breast cancer patients, which showed decreased cell cycle regulatory protein expression, including cyclin D1 (281).

The next terpene that appears in *Cannabis* is pinene. It is present in pine resins, rosemary, basil, and parsley. As multiple preclinical data show, pinene was able to reduce the cell viability, stimulate apoptosis and induce cell cycle arrest in numerous cancer cell lines (282–288). Moreover, it can act synergistically with paclitaxel in tested lung cancer (286). In *in vivo* animal models showed reduced growth and number of tumors under pinene treatment (289). These data could also support the advantageous action of *Cannabis* extracts rich in terpenes versus purified cannabinoids in fighting against different malignancies. Different entourage effects of cannabinoids and other substances in the *Cannabis* plant were extensively reviewed (290).

Based on the literature review, there is a strong rationale to test the effectiveness of *Cannabis sativa* extracts with different terpenoid profiles to see if some specific combinations of cannabinoids with terpenoids could be more beneficial in the treatment of CRC cell lines compared to cannabinoids alone. Moreover, testing selected extracts together with conventional chemotherapy drugs, including cisplatin, could also be advantageous, as many cancer patients are taking cannabis extracts for cancer-related symptom relief.

2.2. Hypotheses

Based on the literature review and initial data from our laboratory, we formulated the following hypotheses:

1. Whole-plant *Cannabis sativa* extracts are more potent than pure cannabinoids due to their entourage effect with plant terpenes.
2. Whole plant *Cannabis sativa* extracts potentiate cisplatin-mediated cell killing, reducing the necessary therapeutic/cytotoxic doses of cisplatin.

2.3. Materials and methods

2.3.1. Main reagents

Activated *Cannabis sativa* extract #18 was prepared in Dr. Kovalchuk's Laboratory at the University of Lethbridge. Plants and some *Cannabis sativa* extracts were provided by the "Pathway Rx" and "Sundial Growers" companies. Stocks were prepared in a 60 mg/ml concentration, a DMSO concentration of 0.25%, and kept at -20°C.

2.3.2. Cell culture and maintenance

It was the same as described in chapter 1.

2.3.3. Treatments

Exposure of CRC cells to cannabis extracts

The cannabis plants were grown, flowers were harvested, and extracted with ethanol in a licensed facility at the University of Lethbridge. After evaporation, the resin was dissolved in DMSO to the 60 mg/ml concentration and kept at -20°C. For the treatments, the resuspended extracts were diluted accordingly for cell cultures.

2.3.4. Terpene analysis

The terpenes of extract #18 were analyzed on dry flowers with the help of 8610C GC coupled with a flame ionization detector (SRI Instruments at Canvas Labs, Vancouver, BC, Canada). The extract was sent to Canvas Labs for the analysis.

2.3.5. High-performance liquid chromatography (HPLC)

High-performance liquid chromatography (HPLC) and mass spectrometry were performed to detect the levels of cannabinoids in cannabis extracts. The system had the G1315C DAD, G1316B column compartment, autosampler (G1367D), and the binary pump (G1312B). The Phenomenex Kinetex EVO C18 column with a Phenomenex SecurityGuard ULTRA guard column was used for the separation. The data acquisition, control of the instrument, and integration were performed with help of software, ChemStation LC 3D Rev B.04.02 (Agilent Technologies). For calibrating the standards and analysis of samples, the injection volume of 2 µL was usedThe injection volume of 2 µL was used to calibrate the standards and analyze samples. The detection of compound peaks was done for 230 nm and 280 nm. On the A side, the mobile phases included 50 mM ammonium formate (Sigma-Aldrich) in HPLC grade water (Fisher Chemical), and 100% methanol on the B side. The flow rate was 0.3 ml/min.

Per each cultivar, two samples were analyzed, with two technical repeats for each sample. The crude extracts were resuspended in 1 mL of methanol and filtered through a 0.22-lm syringe PTFE filter. The filtered extracts were diluted ten times with methanol and then separated by HPLC. The extracts were fractionated in the fraction collector (Agilent Technologies serial #DE63056961) and nine fractions were collected according to the obtained chromatogram. CBD and THC were used as external calibration standards for quantifying cannabinoids at suitable concentrations ranging from 5–50 μg.

2.3.6. Cell viability assay (MTT)

It was the same as described in chapter 1.

2.3.7. RNA extraction and gene expression analysis

RNA isolation was described in chapter 1.

The library preparation of mRNA samples from the HT-29 CRC cell line was performed using NEBNext® Ultra™ RNA Library Prep Kit for Illumina® (New England BioLabs). Next-generation sequencing was performed using Illumina NovaSeq500 PE 100 bp at the University of Lethbridge.

Pathway analysis of the HT-29 CRC cell line

For the HT-29 CRC samples, the global transcriptome profiling included library preparation (mRNA libraries were prepared using Illumina TruSeq Directional (Poly(A) Selection), sequencing of libraries (NextSeq500, Illumina) with the configuration of single-end 75 bp, and subsequent pathway analysis. The reference genome was Human GRCh37 (Ensembl) downloaded from Illumina iGENOME. Base calling and demultiplexing were done using Illumina CASAVA 1.9 pipeline.

Bioinformatics workflow

Initial sequencing library quality control was analyzed with FastQC 0.11.8. Reads were mapped to the human genome (Ensembl, GRCh37) using hisat2 version 2.0.5. Read mapping to genes was counted using featureCounts version 1.6.1 from the Subread package. Additional summary statistics and additional quality control was performed using MultiQC.

The exploratory analysis included non-supervised hierarchical clustering and principal component analysis (PCA). Raw count data was loaded into R version 3.6.1. Genes with a low expression level defined as less than 1 count per million in at least 2 samples were removed from the analysis. Normalization and variance stabilizing transformation was applied to raw count data

as described in the DESeq2 manual. Relationships between samples were explored using non-supervised hierarchical clustering and PCA. The results of the exploratory analysis were visualized as heatmaps and principal component plots. Clustering and PCA were based on the top 1500 of genes with the highest median absolute deviation (MAD). In the case of hierarchical clustering, the distance measure was euclidean and the clustering algorithm - ward.D.

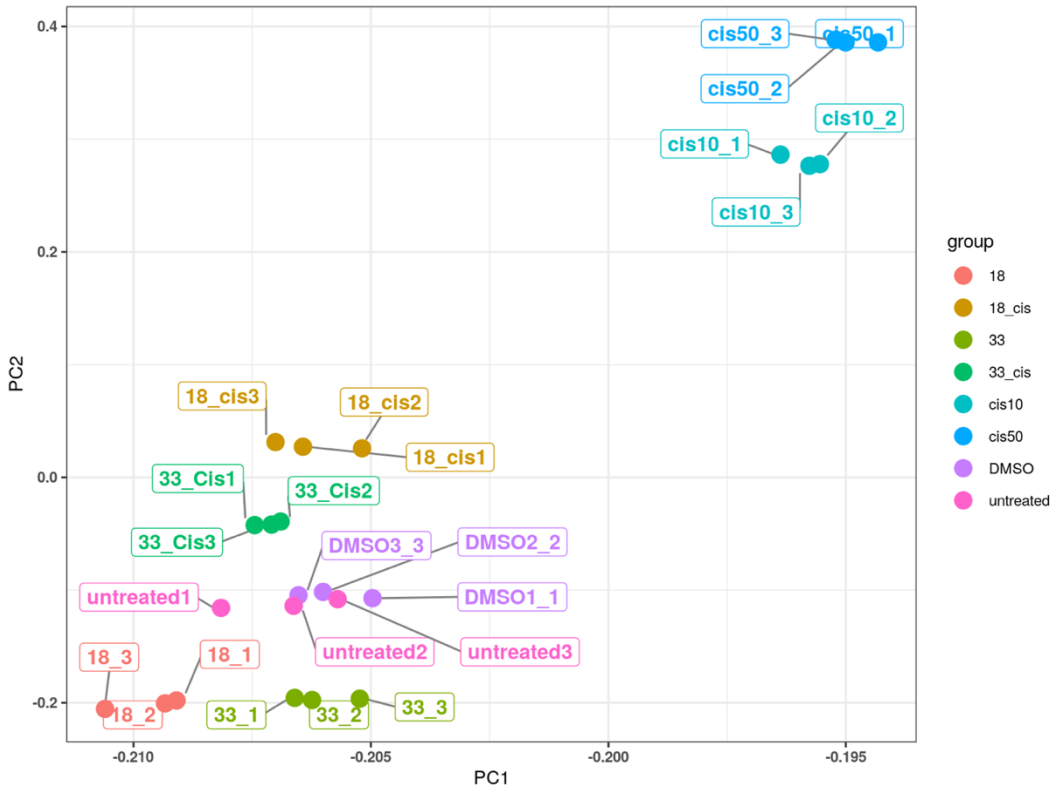

Figure 47. Principal component analysis (PCA) plot based on the top 1500 genes with the highest variance for multiple treatments in the HT-29 CRC cell line. Each treatment group (biological triplicate) is represented in a different colour. The x-axis represents the values of the first principal component (PC1), and the y-axis represents the values for the second principal component (PC2). The PCA plot was generated using R software version 4.2.2.

PCA is a statistical procedure that uses an orthogonal transformation to convert a set of observations of possibly correlated variables into a set of values of linearly uncorrelated variables called principal components. We expected the biological replicates to cluster closely in the PCA plot, which reflected the similarity of their gene expression profiles. Since inter-individual variance is not expected within the same cell line, the biological replicates belonging to separate clusters in the case of cell lines indicate a high degree of technical variance. All samples clustered

perfectly according to the experimental treatments. No samples were excluded as statistical outliers (Figure 47).

Differential expression analysis

Raw count values for each sequencing sample were loaded into R version 3.6.1. Normalization was conducted using DESeq function with default parameters. Differentially expressed genes were detected using DESeq2 1.24.0 Bioconductor package as described in the package vignette. Genes with adjusted p-values (Bonferroni-Hochberg adjustment for multiple comparisons) less than 0.05 (5% chance of gene being a false positive) and over 1.5-fold change in either direction were selected as differentially expressed. The results were annotated with gene symbols, entrez ids and gene descriptions using biomaRt 2.40.3 Bioconductor package.

Over-represented gene ontology (GO) terms were detected using TopGO v2.36.0 Bioconductor package. Over-represented Kyoto Encyclopedia of Genes and Genomes (KEGG) pathways were detected using GOstats v2.50.0 Bioconductor package. Lists of differentially expressed genes (adjusted p-value < 0.05 and log2FC > 0.59) detected with DESeq2 were used to find significantly over-represented GO categories and KEGG pathways. The analysis was done separately on up- and down-regulated genes. The results were saved in each of the comparisons sub-folders. Over-represented GO categories were detected using the topGO 2.36.0 Bioconductor package. GO term analysis was conducted against the biological process (BP) category using an elimination test to focus on the most specific terms. Significantly enriched KEGG pathways were detected using GOstats 2.50.0 Bioconductor package and GAGE 2.34.0 Bioconductor packages. Pathview 1.24.0 Bioconductor package displayed the top 30 pathways in uni-directional GAGE analysis. The uni-directional (up- or down-regulation) GAGE analysis results are saved in the files with the following naming scheme: **vs*_kegg.p.txt. Bi-directional analysis detects perturbed pathways with no regard to the overall direction of the change. The results of the bi-directional analysis are saved in **vs*_kegg.2d.txt.

Perturbed (activated/inhibited) pathways were determined with the SPIA v2.36.0 Bioconductor package. SPIA method combines classical over-representation analysis with the measurement of pathway perturbation under a given condition. The bootstrap procedure is used to estimate the significance of total pathway perturbation. The global pathway significance p-value combines the enrichment and perturbated p-values. The SPIA analysis was conducted for each of the comparisons following the instructions in the package's vignette. The list of differentially

expressed genes consisted of the genes with adjusted p-value less than 0.05, the background list included all the genes in the DESeq2 results table. SPIA results were saved as tab-delimited file in each of the comparisons sub-directories.

The data were visualized using plotting functions implemented in R. The results were represented using MA plots, volcano plots and heatmaps. Heatmaps were built using the heatmap.2 function from gplots package 2.13.0, volcano plot – ggplot2_0.9.3.1. Heatmaps showing the pathway analysis results were output using the SigGeneSet function with the option 'heatmap=TRUE.' Significantly enriched pathways were drawn using a Bioconductor package Pathview version 1.2.4.

2.3.8. Statistical analysis

Statistical analysis was described in chapter 1.

2.3.9. Calculation of combination index (CI).

It was described in chapter 1.

2.4 Results and discussion

2.4.1 Cannabinoid extract #18 and colorectal cancer cell lines.

More than 40 *Cannabis sativa* extracts were tested using cell viability assay (Table 15) on the HT-29 CRC cell line. To select the most active cannabis extracts, the cultivars - 4, 6, 8, 10, 11, 14, 18, 20, 24, 27, 28, 29, 30, 33, 38, 40, 41, 45, 47, 52, 81, 90, 98, 130, 131, 132, 133, 134, 135, 136, 137, 138, 139, 140, 141, 142, 147, 148, 149, 154, 155, and 156 were tested on the HT-29 CRC cell line using cell viability assay (MTT). All extracts were treated in concentrations 0.007 µg/ml and 0.015 µg/ml for 5 days, which were shown to be previously effective on various breast cancer cell lines in our laboratory. Based on the cell growth inhibition capacity, extract #18 was selected for further studies.

Table 15. The phenotypic screening of *Cannabis sativa* extracts in dose of 0.015 µg/µl on the HT-29 CRC cell line based on day 4 of cell viability assay.

Cannabis sativa extract #	Fold change of cell viability compared to DMSO control
4	Inhibited 2 times
6	Inhibited less than 1.5 times
8	Inhibited 2 times

10	Inhibited less than 1.5 times
11	Inhibited 3 times
14	Inhibited 2.5 times
18	**Inhibited 5.8 times**
20	Inhibited 2.8 times
24	Inhibited 3.7 times
27	Inhibited 1.9 times
28	Inhibited 2.4 times
29	Inhibited 1.7 times
30	Inhibited 2.5 times
33	Inhibited 5.7 times
38	Inhibited 2.7 times
40	Inhibited 2.5 times
41	Inhibited 3.3 times
45	Inhibited less than 1.5 times
47	Inhibited 4.7 times
52	Inhibited 2.4 times
81	Inhibited 3 times
90	Inhibited less than 1.5 times
98	Inhibited less than 1.5 times
130	Inhibited 2.1 times
131	Inhibited less than 1.5 times
132	Inhibited 2 times
133	Inhibited less than 1.5 times
134	Inhibited less than 1.5 times
135	Inhibited 2 times
136	Inhibited 2 times
137	Inhibited 2 times
138	Inhibited 2 times
139	Inhibited 2.7 times

140	Inhibited 1.8 times
141	Inhibited less than 1.5 times
142	Inhibited less than 1.5 times
147	Inhibited less than 1.5 times
148	Inhibited less than 1.5 times
149	Inhibited less than 1.5 times
154	Inhibited less than 1.5 times
155	Inhibited less than 1.5 times
156	Inhibited less than 1.5 times

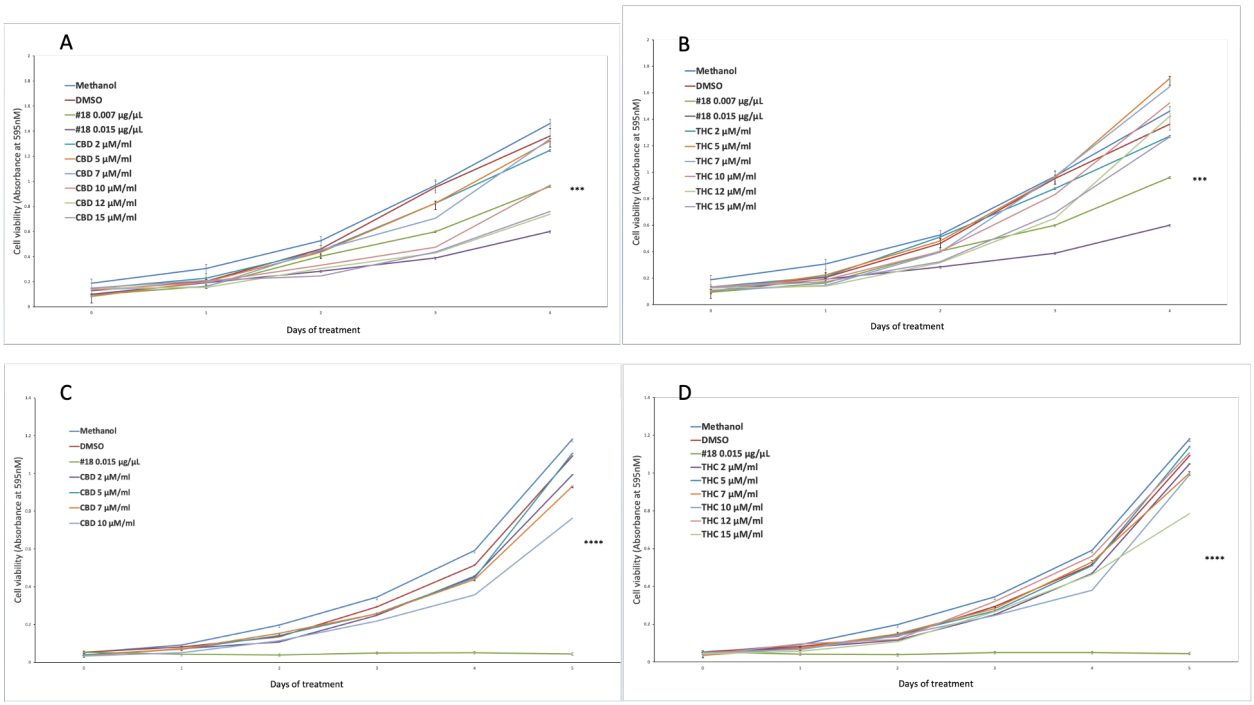

Figure 48. The time-dose-dependent effect of Extract #18, THC and CBD on HCT-116 (A, B) and HT-29 (C, B) CRC cell lines based on MTT results. Results are expressed as means of calculated cell viability ± standard deviations of each group in triplicate at absorbance 595 nm. To calculate time-dose effects, two-way ANOVA was performed using Microsoft Excel. Significant differences between groups are marked with ns – non-significant, *p < 0.05, **p < 0.01, ***p < 0.001, ****p <0.0001.

Extract #18 had higher potency than the others; thus, it was selected for further analysis. Next, to see if extract #18 is more effective than pure cannabinoids, we compared the changes in

cell viability between extract #18 and THC and CBD on HCT-116 and the HT-29 CRC cell lines (Figure 48).

Based on HPLC data, as is shown in Table 16, extract #18 is high in THC (~10%) and low in CBD (< 1%). Thus, the results indicated that extract #18 was much more effective in inhibiting CRC cell growth than THC alone. Additionally, extract #18 had high levels of β-myrcene and α-pinene as indicated in the terpenoid profile.

Table 16. Terpenoid profile of extract#18 based on HPLC results.

Terpene levels in extract #18	Parts Per Million (PPM)
alpha-Pinene	0.309
beta-Pinene	0.109
beta-Myrcene	0.42
Limonene	0.035
Terpinolene	0.03
Linalool	0.017
Fenchyl Alcohol	N/A
alpha-Bisabolol	0.003
alpha-Terpineol	N/A
trans-Caryophyllene	0.052
alpha-Humulene	0.035
trans-Nerolidol	0.003
cis-Nerolidol	0
Borneol isomers	N/A
Camphene	N/A
beta-Ocimene	0.003
Fenchone isomers	N/A
Sabinene	N/A
p-Mentha-1,5-diene	N/A
(+)-3-Carene	0.002
alpha-Terpinene	0.07
Eucalyptol	N/A
gamma-Terpinene	0.005
p-Cymene	0.082
Camphor isomers	N/A
Isopulegol	0.002
Caryophyllene oxide	0.107
Valencene	N/A
Geraniol	0.007
Guaiol	0.002
trans-beta-Ocimene	N/A
Sabinene Hydrate	N/A

Isoborneol	N/A
Hexahydrothymol	N/A
gamma-Terpineol	N/A
Geranyl Acetate	N/A
Pulegone	N/A
Nerol	N/A
alpha-Cedrene	N/A
Cedrol	N/A
a-Humulene	0.035
b-Eudesmol	N/A
Total Terpene content	**1.328**

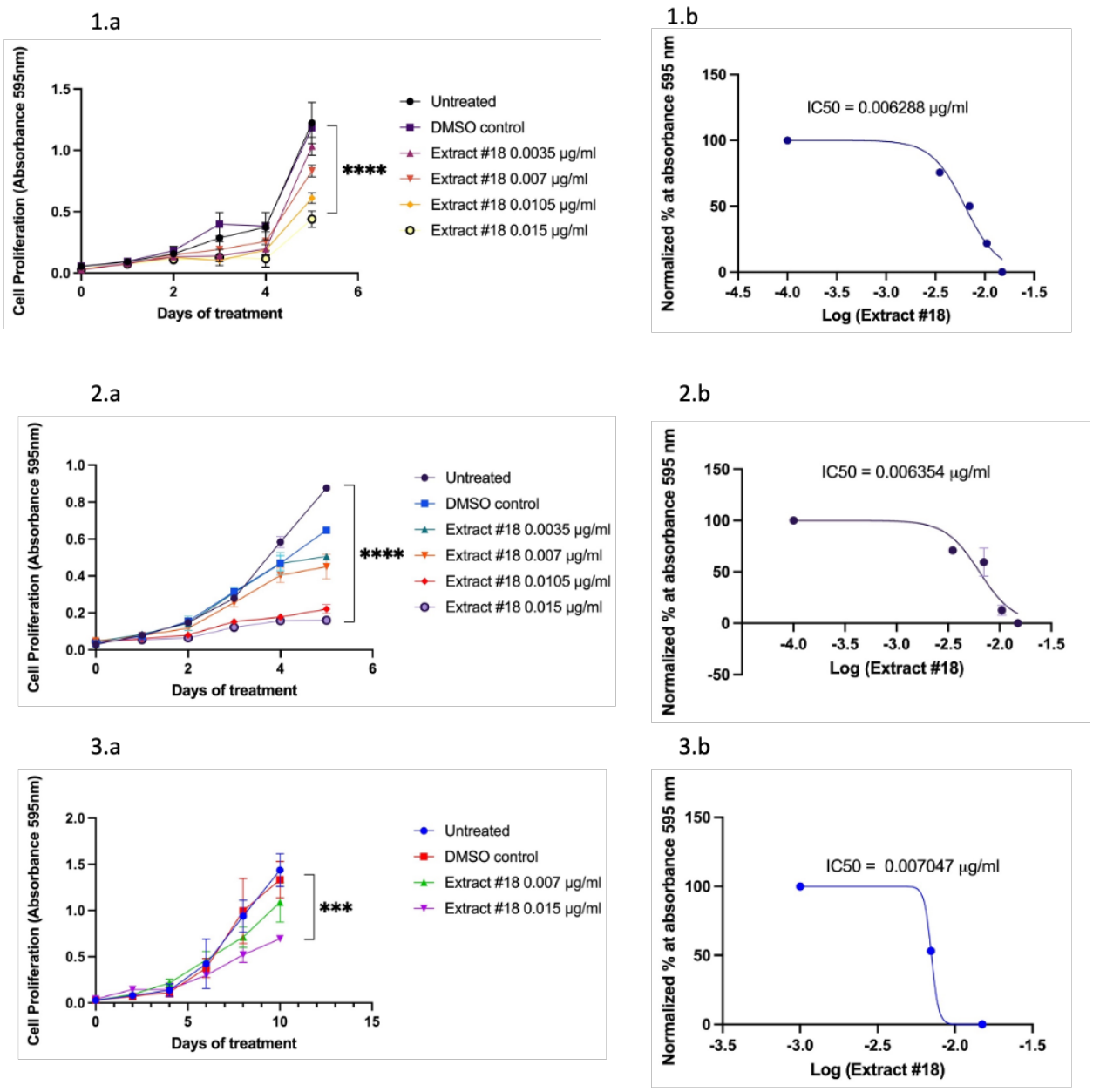

Figure 49. The time-dose-dependent effect and nonlinear regression analysis of the dose-effect curve with calculated IC50 values of extract #18 on HCT-116 (1.a, 1.b), HT-29 (2.a, 2.b), and LS-174T (3.a, 3.b), cell lines based on MTT results. Results are expressed as means of calculated cell viability ± standard deviations of each group in triplicate at absorbance 595 nm. To calculate time-dose effects, two-way ANOVA was performed using GraphPad Prism version 9.0. Significant differences between groups are marked with ns – non-significant, *p <

0.05, **p < 0.01, ***p < 0.001, ****p <0.0001. A nonlinear fit with log(inhibitor) vs. normalized response–variable slope analysis was performed using GraphPad Prism version 9.0.

Based on the cell viability, the time and dose-dependent effect of extract#18 was visible in each tested CRC cell line (Figure 49). Cell proliferation was significantly inhibited throughout tested concentrations. The non-linear regression analysis showed that IC50s for each cell line were in a similar range, around 0.0065 µg/ml. Considering that the THC concentration was 10%, we assumed that in the extract's half-maximal inhibitory concentration, the THC concentration was 0.00065 µg/ml, equivalent to 20.4 µM.

We analyzed mRNA expression pathway to establish possible molecular mechanisms behind extract#18 effectiveness.

Exploratory analysis

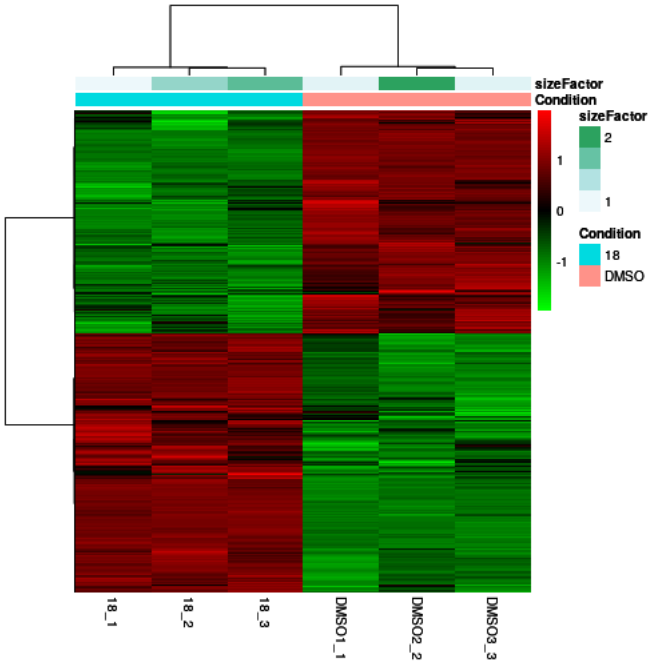

Figure 50. A hierarchical clustering heatmap analysis of the differentially expressed genes with fold change over 1.5 and adjusted p-values < 0.05 for DMSO control versus extract #18 in the HT-29 CRC cell line. The x-axis shows non-supervised clusters between the two treatment groups. The DMSO_1, DMSO_2, and DMSO_3 are independent replicates for DMSO and 18_1, 18_2, and 18_3 is for extract #18. The y-axis shows differentially expressed genes. The fold changes of up-regulated genes are in the red-orange colour spectrum, and the down-regulated genes are represented in the blue colour spectrum. The heatmap was generated using R software version 4.2.2.

A heatmap represents differentially expressed genes for DMSO versus extract #18 in the HT-29 CRC cell line (Figure 50). The unsupervised clustering based on the underlying data determined if there were sub-categories within DMSO control and extract #18 treatment. As the figure shows, there were significant differences in gene expression between treatment groups. The differences were not substantial for the biological replicates within the same group, showing the treatment samples' good quality.

Pathway analysis

A

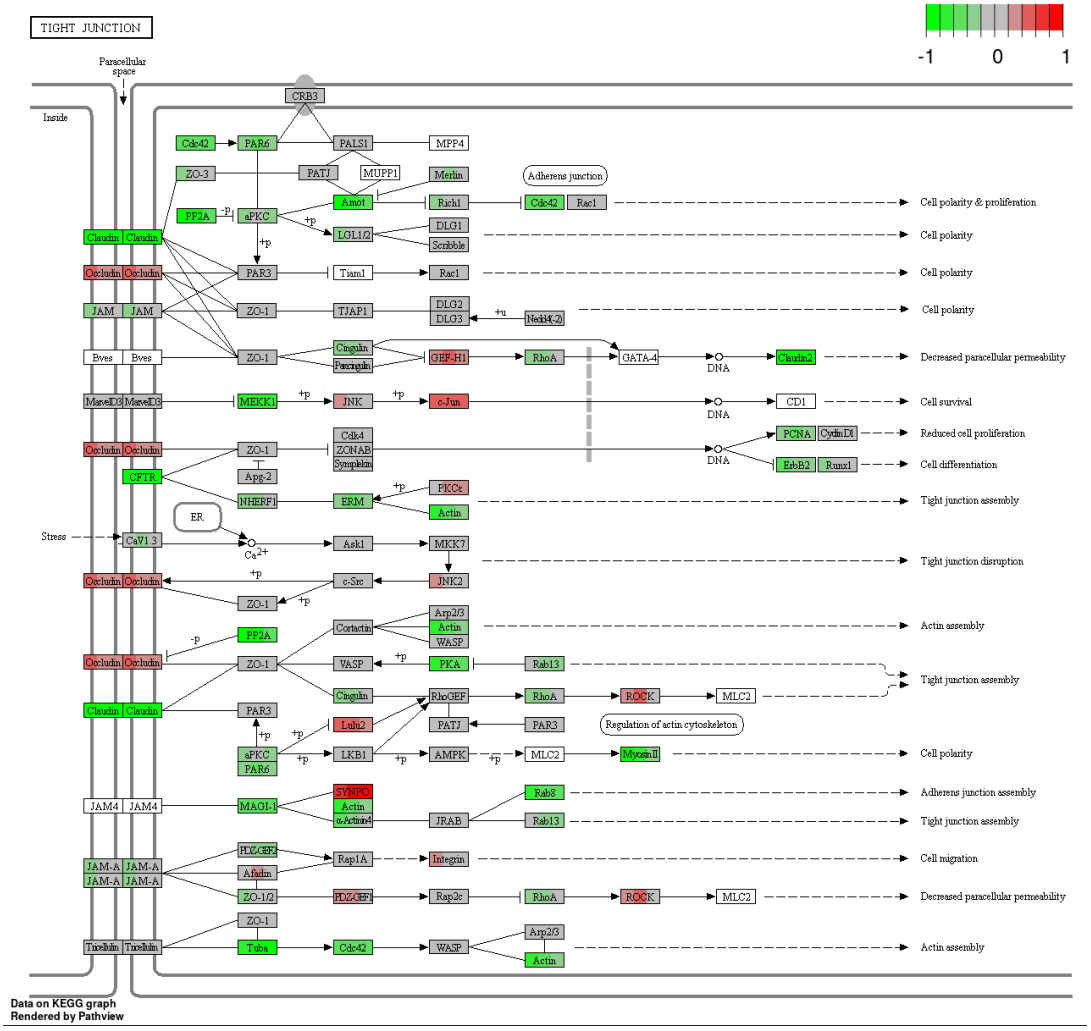

B

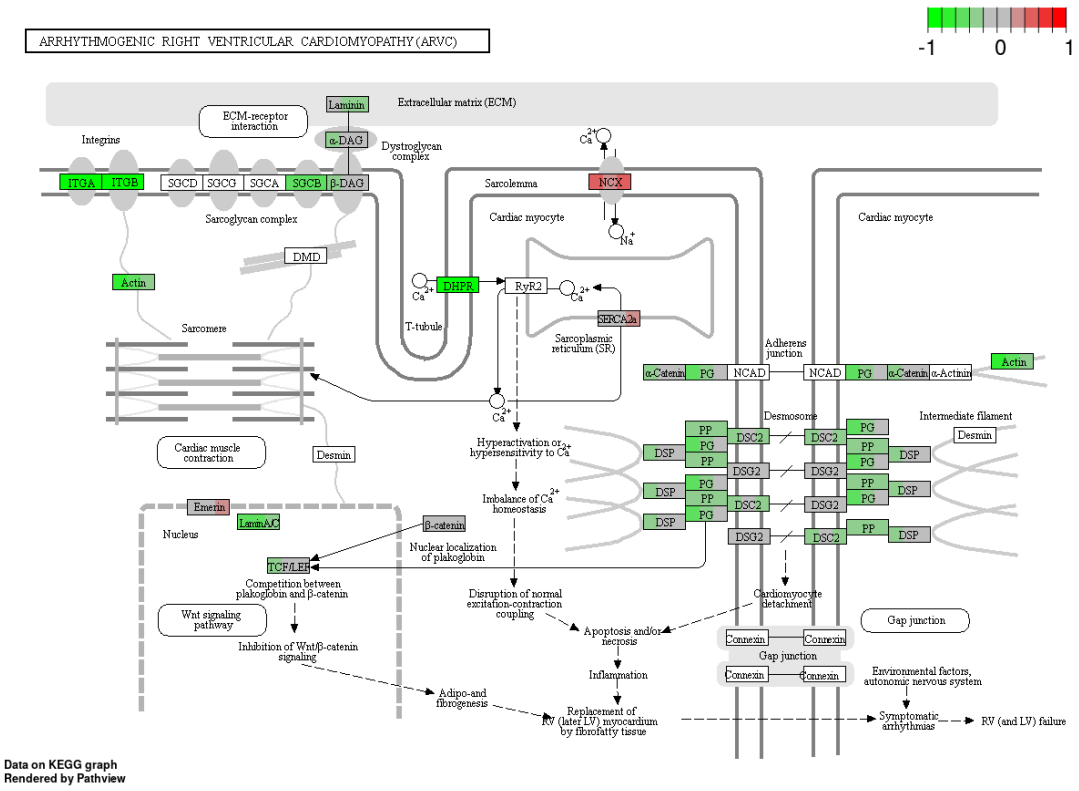

Figure 51. Changes of tight junctions (A) and cell adhesion and Wnt signalling pathway (B) under extract #18 compared to DMSO control. The genes are coloured according to the difference in expression level between treatment and control for each individual sample. Red colour shows up- and green down-regulation relative to the treatment group. Data based on GAGE uni-directional analysis.

As Figure 510A shows, high-THC cannabinoid extract#18 caused multiple changes in the expression of genes responsible for tight junctions in the HT-29 cell line. The decreased claudin and its downstream signalling proteins could inhibit cell polarity and proliferation of cancer cells. Overexpressed occludin can control paracellular diffusion in tested cells and, with decreased claudin 2, can decrease paracellular permeability. However, the overactivation of c-Jun, a widely studied protein in the AP-1 complex, may promote cell survival and tumorigenesis in HT-29 cells. Next, there was a decrease in PCNA and ERBB2 levels, which further may reduce cell proliferation and differentiation. Previous figures already indicated that tested extract inhibited actin and adherent junction assemblies.

Hight-THC cannabinoid extract #18 downregulated the genes that took part in adherent junctions' formation in HT-29 CRC cells (Figure 51B). There is a downregulation of most proteins

that form desmosomal and adherent junctions and some of the integrins. There was also decreased expression of actin and laminin. Such changes might indicate the loss of contact inhibition in cancer cells. However, decreased levels of integrins and laminins, which assist in cancer cell invasiveness, could suggest inhibition of tumor invasion. Additionally, extract #18 inhibited TCF/LEF transcription factor, which is an effector in the Wnt signalling pathway. As HT-29 has a mutation in the APC gene, we could suggest that Wnt signalling is upregulated. Thus, adding extract #18 may alter the oncogenic signalling of this pathway and have an anti-cancer effect.

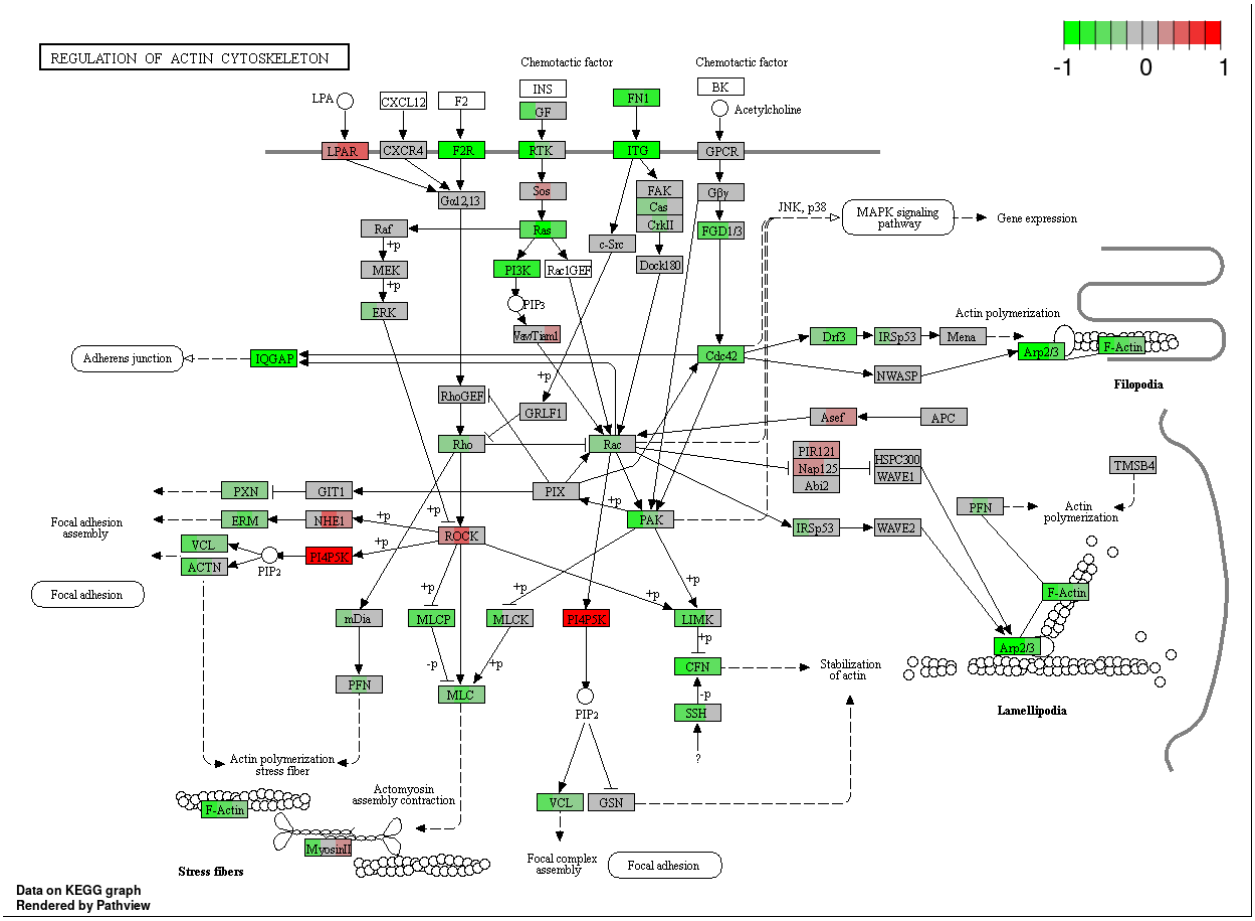

Figure 52. Changes of actin cytoskeleton regulation under high-THC extract #18 compared to DMSO control. The genes are coloured according to the difference in expression level between treatment and control for each individual sample. Red colour shows up- and green down-regulation relative to the treatment group. Data based on GAGE uni-directional analysis.

Hight-THC cannabinoid extract #18 decreased the expression of PI3K, a part of the Ras/PI3K/AKT signalling pathway, and often upregulated in CRCs (Figure 52). We also know that the HT-29 cell line is mutated in PI3K, which may indicate an anticancer effect of tested

cannabinoid extract. There was decreased expression of fibronectin which decreases extracellular matrix interactions in cancer cells. Moreover, extract #18 inhibited Rho A, Rho G, and Rho GTPases that regulate cytoskeletal dynamics, cell migration, and cell-cycle progression, relay extracellular signals, and translate them into intracellular responses.

There was an inhibition of the formation of adherent junctions, focal adhesion, actin stabilization and actin polymerization, as well as Ras/MAPK pathway and cell signals responsible for the activation of chemotaxis towards chemotactic factors in the cancer microenvironment. This might imply that extract#18 can inhibit the invasion and migration of cancer cells, which could prevent metastasis formation in a classical subtype of CRC.

A

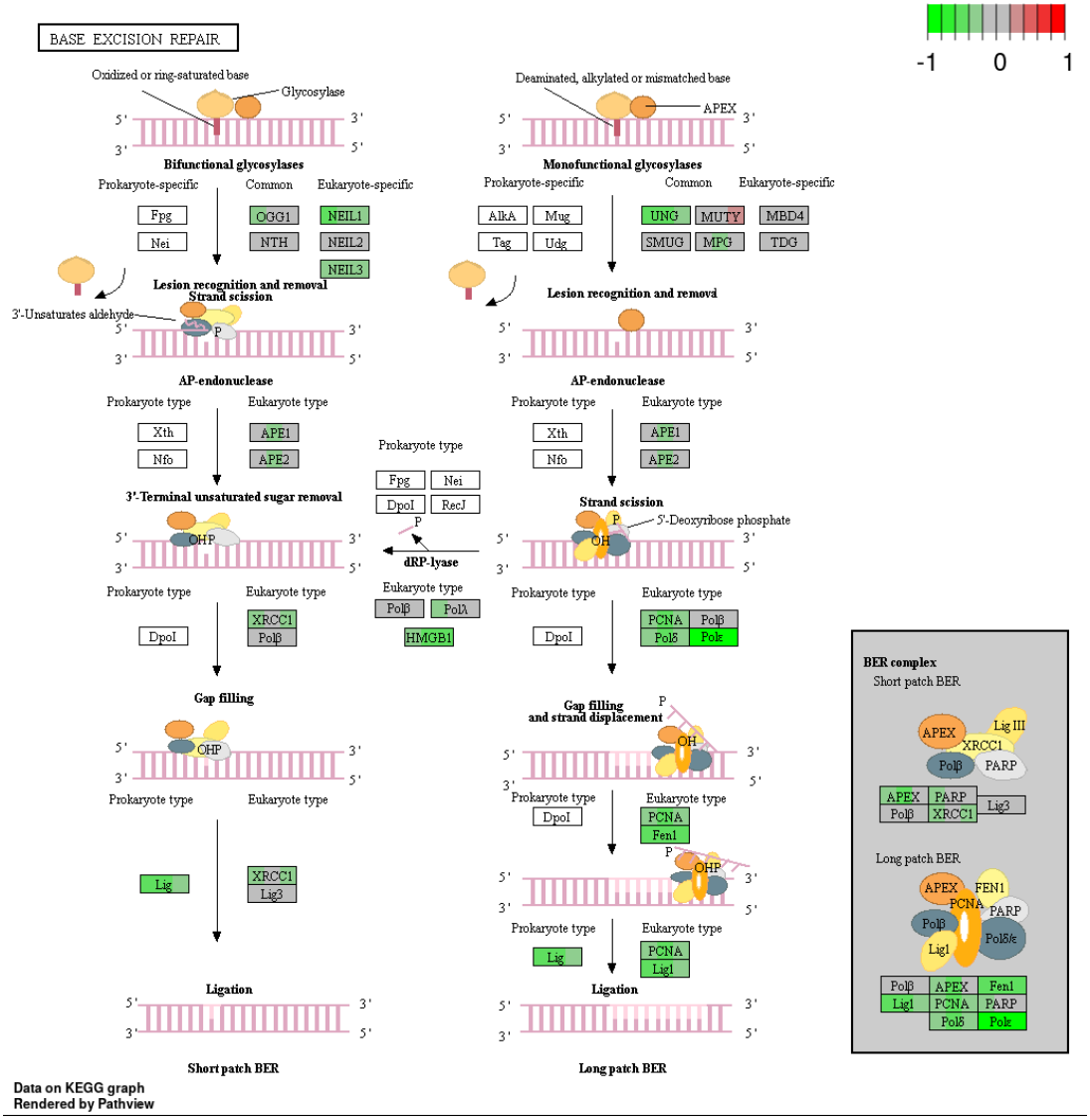

B

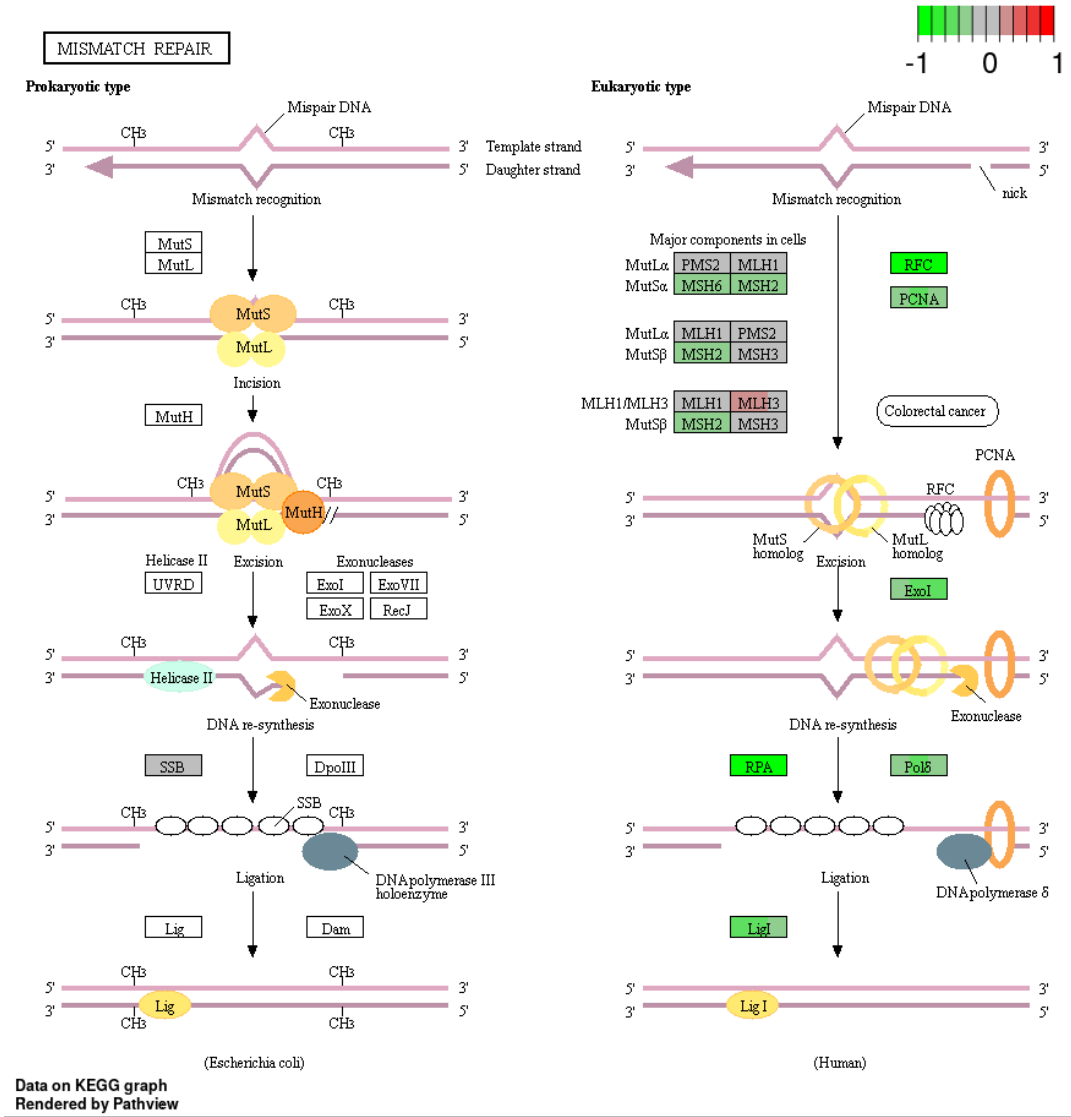
MISMATCH REPAIR
-1
0
1
Prokaryotic type
Mispair DNA
CH3
5'
3'
Template strand
Daughter strand
Mismatch recognition
MutS
MutL
Incision
MutH
Helicase II
UVRD
Excision
Exonucleases
ExoI
ExoVII
ExoX
RecJ
Exonuclease
DNA re-synthesis
SSB
DpoIII
Ligation
DNA polymerase III holoenzyme
Lig
Dam
(Escherichia coli)
Eukaryotic type
nick
Major components in cells
MutLα
MutSα
PMS2
MLH1
MSH6
MSH2
MutLα
MutSβ
MSH2
MSH3
MLH1/MLH3
MutSβ
MLH3
RFC
PCNA
Colorectal cancer
MutS homolog
MutL homolog
Pol δ
RPA
LigI
Lig I
(Human)
Data on KEGG graph
Rendered by Pathview

C

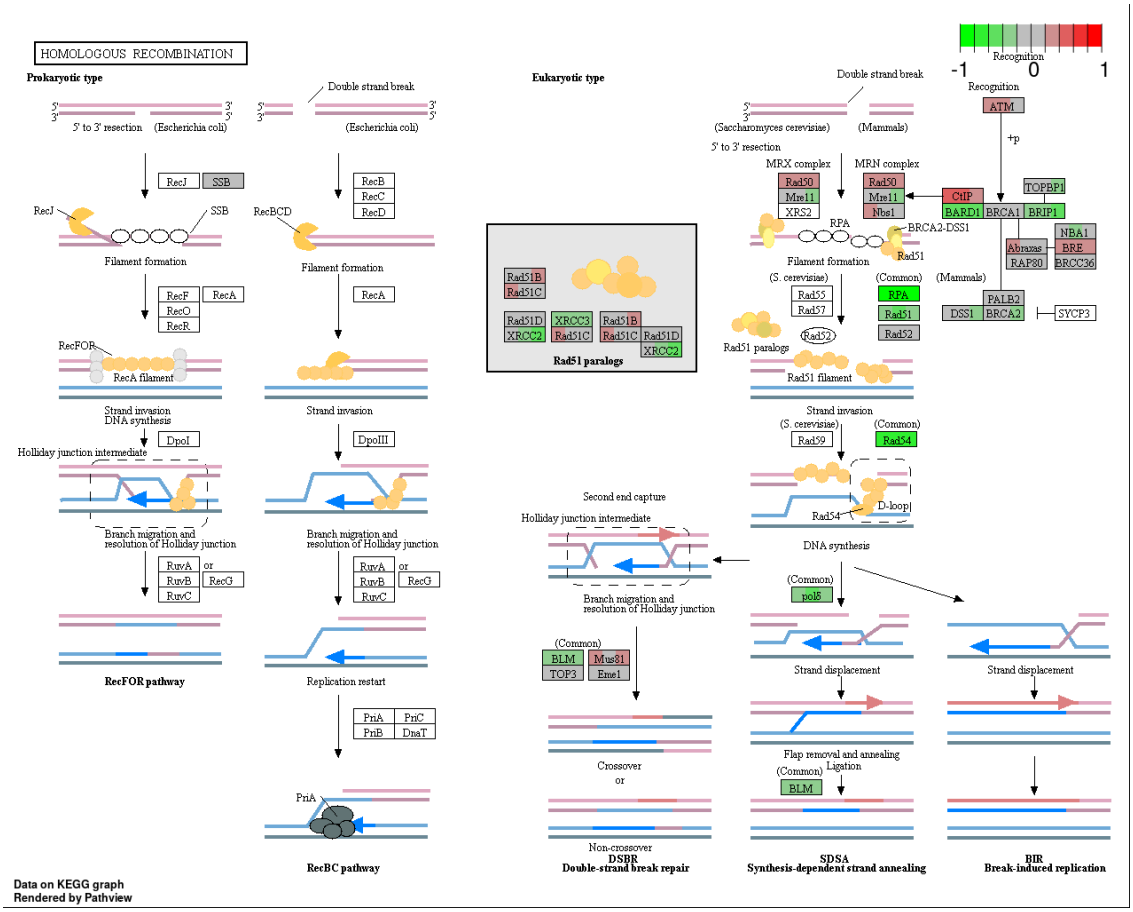

Figure 53. Changes of base excision repair (A), mismatch repair (B), and homologous recombination (C) under high-THC extract #18 compared to DMSO control in the HT-29 CRC cell line. The genes are coloured according to the difference in expression level between treatment and control for each individual sample. Red colour shows up- and green down-regulation relative to the treatment group. Data based on GAGE uni-directional analysis.

Hight-THC cannabinoid extract #18 decreased the expression of most of the genes in the short and long patch base excision repair (BER) pathway (Figure 53A). There was a downregulation of bifunctional and monofunctional glycosylases. The tested extract also decreased levels of AP-endonucleases, the genes responsible for gap filling, strand displacement, and ligation, including PCNA and polymerases δ and ε. Such strong inhibition of the DNA repair pathway may indicate one of the major anticancer effects of cannabinoid extracts in the HT-29 cell line. Cancer cells encounter high stress on their genetic apparatus. If the DNA-repair systems are off, it might induce drastic chromosomal instabilities and cancer cell death.

Figure 53B represents a decrease in the expression of most of the genes present in the mismatch repair (MMR) pathway by adding high-THC cannabinoid extract #18. There was a lower expression of *MSH6*, *MSH2*, and *RFC* genes responsible for recognizing bulky DNA lesions. Exonuclease I, polymerase δ, and ligase I was also inhibited, which ceased the excision, DNA re-synthesis and ligation of the mismatched DNA.

The microsatellite unstable subtype of CRC often has mutated genes in the MMR system. In the early stages of tumor development, such genetic changes can promote the formation of driver mutations beneficial for cancer progression. However, in the later stages of carcinogenesis, tumors rely on DNA repair systems to keep them alive due to the huge genotoxic stress encountered by cancer cells. Thus, the inhibition of the MMR system by tested cannabinoid extract can be a double-edged sword in cancer cytotoxicity. It is possible that adding the extract prior tumor development might promote carcinogenesis. Still, if added after the CRC becomes a full-blown disease, it might push cancer cells toward death due to the inability to repair irreversible DNA damage. In this case, we tested the cell line representing the classical subtype of CRC. However, it would be interesting to test cannabinoid extracts or cannabinoids alone on microsatellite unstable CRC and see if the treatment is as effective as in the canonical subtype.

Figure 53C represents changes in the expression of multiple genes responsible for homologous recombination (HR) in the HT-29 cell line under high-THC cannabinoid extract #18 treatment. We observed changes in either direction, but we suggest HR was overall suppressed. The expression data showed an increase in ATM, Rad50, Rad51B, Rad51C, and BRE, the genes needed in the initial stages of HR, including double-strand break recognition, formation of MRX complexes and filaments. However, the genes encoding downstream signalling proteins responsible for strand invasion, DNA synthesis, strand displacement, flap removal and ligation, such as RPA, Rad51, Rad54, polymerase δ and BLM, were decreased.

The expression data regarding DNA repair systems showed that extract #18 suppressed almost every DNA damage response pathway in the HT-29 CRC cell line. Simultaneous disorder of multiple DNA repair systems could be an Achilles' heel of many cancers, especially ones under high genotoxic stress. It may be one of the major anticancer mechanisms used by cannabinoids. However, more experimental data would be needed to confirm such a statement.

A

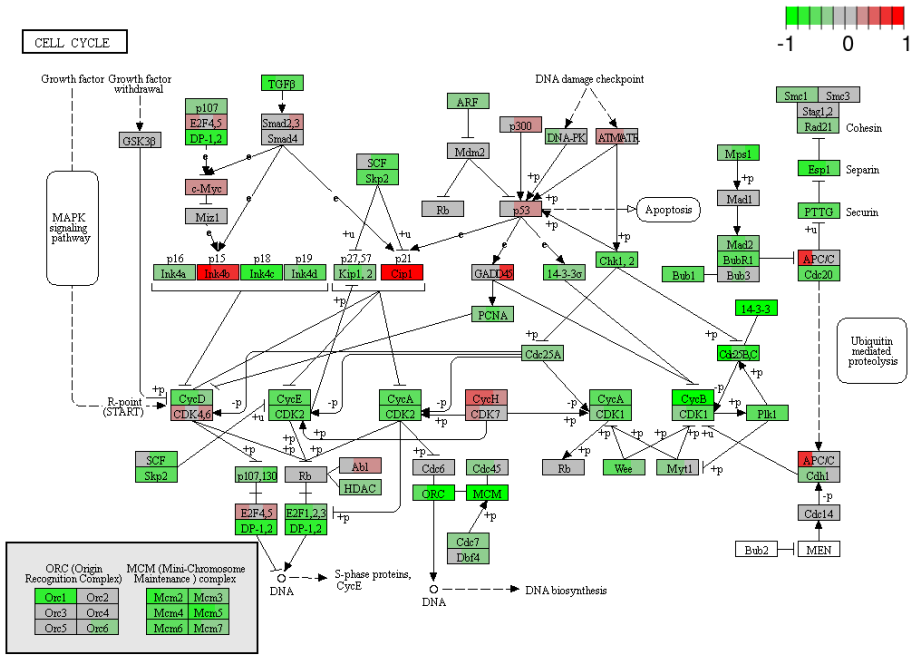
CELL CYCLE
-1 0 1
Growth factor
Growth factor withdrawal
TGFβ
p107
E2F4,5
DP-1,2
Smad2,3
Smad4
GSK3β
c-Myc
Miz1
SCF
Skp2
ARF
p300
DNA-PK
ATM&ATR
DNA damage checkpoint
Mdm2
Rb
p53
Apoptosis
Mps1
Mad1
Mad2
BubR1
Bub3
Bub1
Smc1
Smc3
Stag1,2
Rad21
Cohesin
Esp1
Separin
PTTG
Securin
APC/C
Cdc20
MAPK signaling pathway
p16 Ink4a
p15 Ink4b
p18 Ink4c
p19 Ink4d
p27,57 Kip1, 2
p21 Cip1
GADD45
14-3-3σ
Chk1, 2
PCNA
14-3-3
Cdc25A
Cdc25C
Ubiquitin mediated proteolysis
R-point (START)
CycD
CDK4,6
CycE
CDK2
CycA
CDK2
CycH
CDK7
CycA
CDK1
CycB
CDK1
Plk1
SCF
Skp2
p107,130
Rb
Abl
HDAC
Cdc6
Cdc45
ORC
MCM
Rb
Wee
Myt1
APC/C
Cdh1
Cdc14
E2F4,5
DP-1,2
E2F1,2,3
DP-1,2
Cdc7
Dbf4
Bub2
MEN
ORC (Origin Recognition Complex)
Orc1
Orc2
Orc3
Orc4
Orc5
Orc6
MCM (Mini-Chromosome Maintenance) complex
Mcm2
Mcm3
Mcm4
Mcm5
Mcm6
Mcm7
DNA
S-phase proteins, CycE
DNA
DNA biosynthesis
G1
S
G2
M
Data on KEGG graph
Rendered by Pathview

B

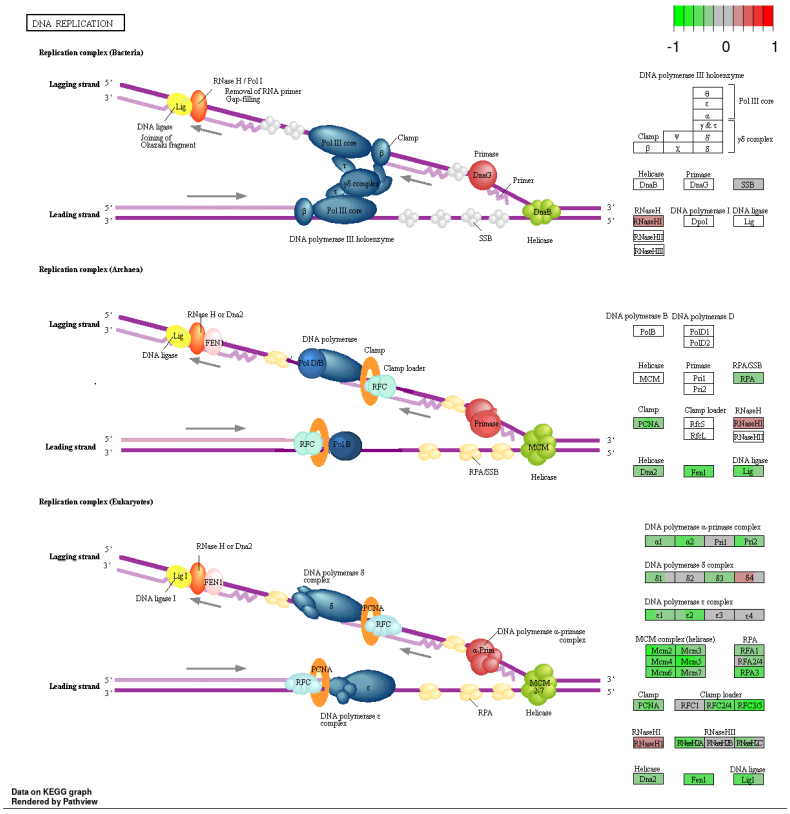
DNA REPLICATION
-1 0 1
Replication complex (Bacteria)
Lagging strand
Leading strand
RNase H / Pol I
Removal of RNA primer
Okip-filling
Lig
DNA ligase
Joining of Okazaki fragment
Pol III core
Clamp
β
γδ complex
Primer
Dna3
DnaB
Helicase
SSB
DNA polymerase III holoenzyme
DNA polymerase III holoenzyme
Pol III core
γδ complex
Helicase
DnaB
Primase
DnaG
SSB
RNaseH
RNaseHII
RNaseHIII
DNA polymerase I
PolI
DNA ligase
Lig
Replication complex (Archaea)
RNase H or Dna2
FEN1
DNA ligase
DNA polymerase
PolD/B
Clamp
Clamp loader
RFC
Primase
RPA/SSB
MCM
Helicase
DNA polymerase B
DNA polymerase D
PolB
PolD1
PolD2
Helicase
MCM
Primase
Pri1
Pri2
RPA/SSB
RPA
Clamp
PCNA
Clamp loader
RfcS
RfcL
RNaseH
RNaseHI
RNaseHII
Helicase
Dna2
Fen1
DNA ligase
Lig
Replication complex (Eukaryotes)
RNase H or Dna2
Lag1
FEN1
DNA ligase I
DNA polymerase δ complex
δ
PCNA
RFC
DNA polymerase α-primase complex
α-Prim
RPA
DNA polymerase ε complex
ε
MCM 2/7
Helicase
DNA polymerase α-primase complex
α1
α2
Pri1
Pri2
DNA polymerase δ complex
δ1
δ2
δ3
δ4
DNA polymerase ε complex
ε1
ε2
ε3
ε4
MCM complex (helicase)
Mcm2
Mcm3
Mcm4
Mcm5
Mcm6
Mcm7
RPA
RPA1
RPA2/4
RPA3
Clamp
PCNA
Clamp loader
RFC1
RFC2/4
RFC3/5
RNaseHI
RNaseHII
Helicase
Dna2
Fen1
DNA ligase
Lig1
Data on KEGG graph
Rendered by Pathview

Figure 54. Inhibition of cell cycle (A) and DNA replication (B) under high-THC extract #18 compared to DMSO control in the HT-29 CRC cell line. The genes are coloured according to the difference in expression level between treatment and control for each individual sample. Red colour shows up- and green - down-regulation, relative to the treatment group. Data based on GAGE uni-directional analysis.

Hight-THC cannabinoid extract #18 significantly decreased the expression of most of the genes that participate in cell cycle regulation, with a few exceptions (Figure 54A). The strong inhibition of merely every promoter of cell cycle progression and upregulation of tumor suppressors such as p53, p21, p15, and APC/C would cause cell cycle arrest at every checkpoint. First, the downregulation of cyclin D, E, and A together with CDK 2 would cause arrest in the G1/S stage, lowering the protein synthesis necessary for DNA replication. Next, the downregulation of cyclin A, B and CDK1 could stop the cell cycle in the G2 checkpoint. Lastly, the decreased expression of cell division control 20 (Cdc20) and separins would lead to the arrest in the M checkpoint, being catastrophic for cancer cells. Moreover, there was decreased expression of TGF-β, a well-known protein taking part in the epithelial-to-mesenchymal transition of cancer cells. Thus, tested cannabinoid extract could inhibit cancer invasiveness.

Additionally, extract #18 upregulated ATM/ATR, the DNA damage response, together with p53 tumor suppressor and GADD45. Subsequently, our treatment inhibited multiple cyclins and cyclin-dependent kinases, which resulted in cell cycle arrest.

Our data also indicated increased expression of c-Myc and E2F4,5 genes, encoding transcription factors, which might be an attempt by cancer cells to stimulate their growth. However, the downstream effectors of those proteins are downregulated, which would not be enough to promote the growth of the HT-29 cell line, and our MTT results have shown this.

Cell cycle arrest gives cancer cells time to repair DNA under genotoxic stress. However, we also have seen inhibition of DNA repair pathways, which would not let the HT-29 cells recover and might push them toward apoptosis.

Hight-THC cannabinoid extract #18 significantly decreased the expression of most of the genes that participate in DNA replication (Figure 54B). The levels of DNA polymerase α-primase complex, DNA polymerases δ and ε complexes were down. Furthermore, levels of PCNA, helicase (MCM complex), RPA and DNA ligases were also decreased, which indicates that DNA

replication is strongly inhibited in the HT-29 CRC cell line. These results further support the notion that the tested extract has a major effect on cell cycle progression.

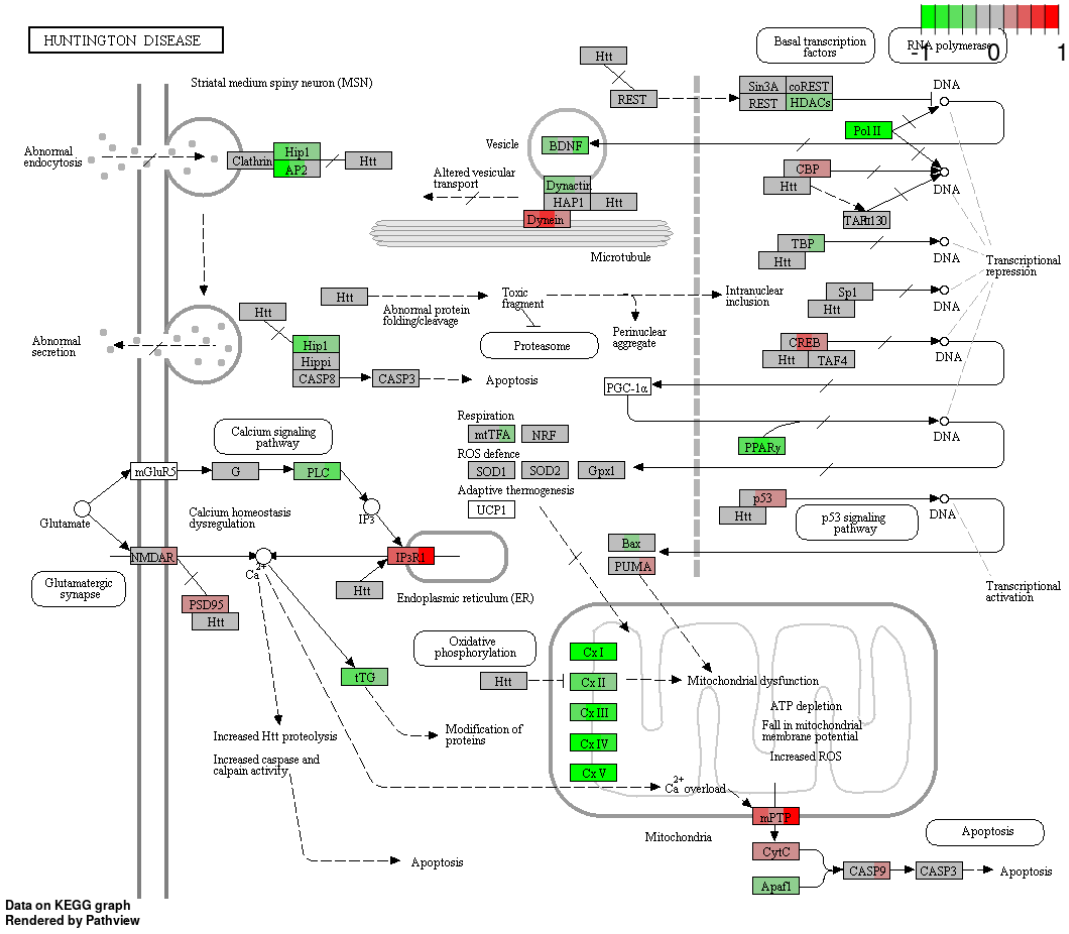

Figure 55. Inhibition of transcription, exocytosis and oxidative phosphorylation under high-THC extract #18 compared to DMSO control in HT-29 CRC cell line. The genes are coloured according to the difference in expression level between treatment and control for each individual sample. Red colour shows up- and green - down-regulation, relative to the treatment group. Data based on GAGE uni-directional analysis.

Similar to cisplatin action, high-THC cannabinoid extract #18 significantly decreased the expression of complexes I to V, which are essential for oxidative phosphorylation (Figure 55). Moreover, there was an increase of p53, mPTP, cytochrome C, and caspase 9, indicating an apoptosis activation in the HT-29 CRC cell line. In addition, the treatment strongly inhibited polymerase II, which takes part in gene transcription.

Abnormal exocytosis is enhanced in cancer cells to transport different molecules, such as growth factors and mRNAs, to distant organs to prepare future metastatic niches. Thus, inhibition of microvesicular transport is important in the prevention of metastasis. The tested extract inhibited vesicular transport, endo- and exocytosis, which was directly opposite to the effect of cisplatin. As a result, cannabinoid extract #18 might prevent metastasis formation in the canonical subtype of CRC.

Finally, there was a strong downregulation of PPARγ, essential for insulin sensitization, glucose uptake and an enhancement of energy metabolism in HT-29 cancer cells. The inhibition of PPARγ might impair multiple metabolic pathways that cancer cells utilize for their growth and proliferation. Thus, the addition of nutrient deprivation potentially would further affect cancer metabolism and push it towards self-destruction.

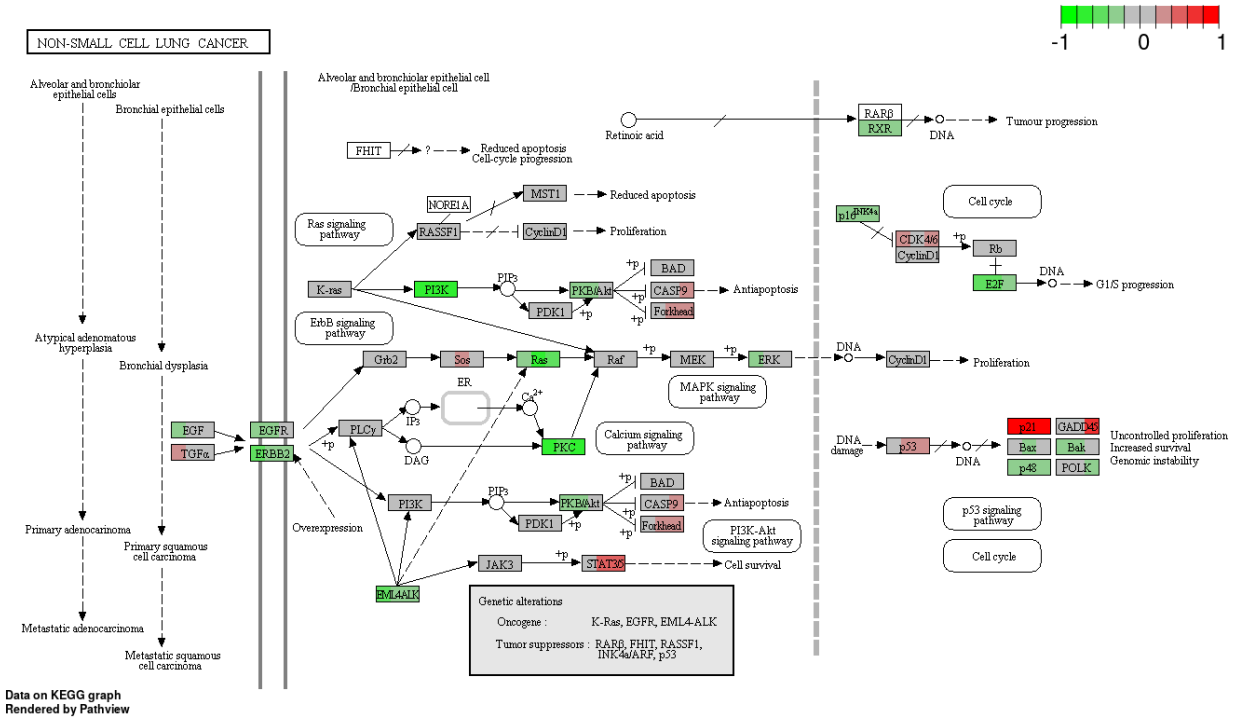

Figure 56. The alteration of oncogenic signalling pathways with high-THC extract #18 compared to DMSO control in HT-29 CRC cell line. The genes are coloured according to the difference in expression level between treatment and control for each individual sample. Red colour shows up- and green – down-regulation, relative to the treatment group. Data based on GAGE uni-directional analysis.

Extract #18 decreased the expression of multiple cancer signalling pathways, as presented in Figure 56. Among downregulated genes, there were EGF, EGFR and ERBB2, often overexpressed in some cancers. Also, oncogenes EML4-ALK, Ras, ERK, PI3K, PKB/Akt, and PKC mRNA formation was inhibited. Thus, the tested extract inhibited Ras, MAPK and PI3K cascades, the major signalling pathways regulating cell growth, survival and apoptosis. Additionally, proapoptotic, p53, caspase 9, and Forkhead increased their expression. However, the decreased levels of E2F, Bax and Bak, along with increased p21, might push cancer cells toward cell cycle arrest in G1/S instead of cell death. In that case, adding another treatment with a strong proapoptotic effect, such as cisplatin, might be beneficial.

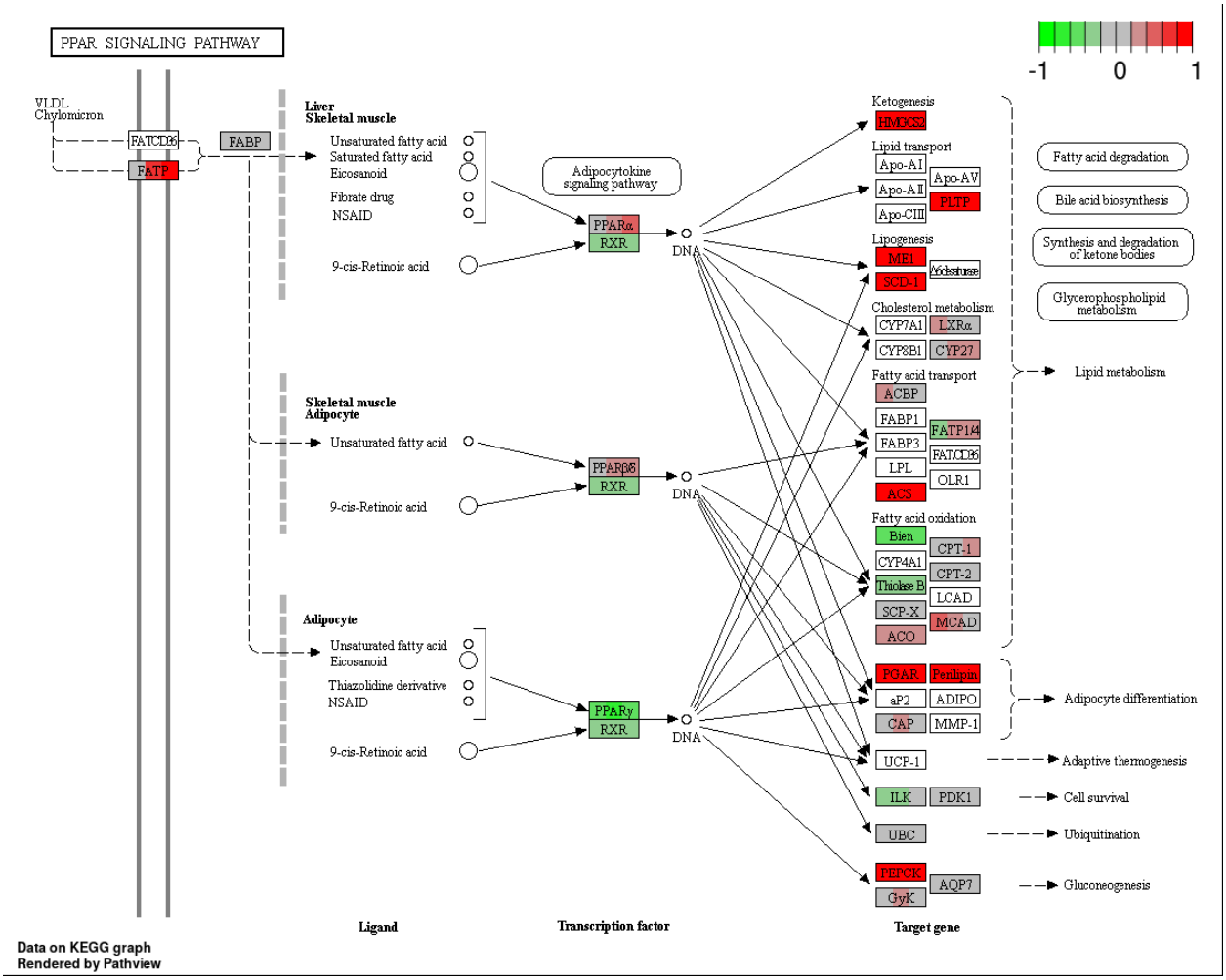

Figure 57. Changes of PPAR signalling under high-THC extract #18 compared to DMSO control in HT-29 CRC cell line. The genes are coloured according to the difference in expression level between treatment and control for each individual sample. Red colour shows up-

and green – down-regulation, relative to the treatment group. Data based on GAGE uni-directional analysis.

Hight-THC cannabinoid extract #18 significantly decreased the expression of PPARγ and retinoid acid receptor RXR, which regulate lipid metabolism, inflammation, cell differentiation, and apoptosis (Figure 57). Interestingly, PPARα and PPARβ/δ expression was increased with many of their target genes that regulate ketogenesis, lipid transport, lipogenesis, cholesterol metabolism, adipocyte differentiation, and gluconeogenesis. On the contrary, some genes responsible for fatty acid oxidation were down-regulated. These data may indicate that tested cannabinoid extract increased lipid biosynthesis and decreased lipid katabolism. Thus, it increased lipid formation and storage in cancer cells via PPARα and PPARβ/δ. However, the treatment decreased glucose metabolism in the HT-29 CRC cell line via inhibition of PPARγ.

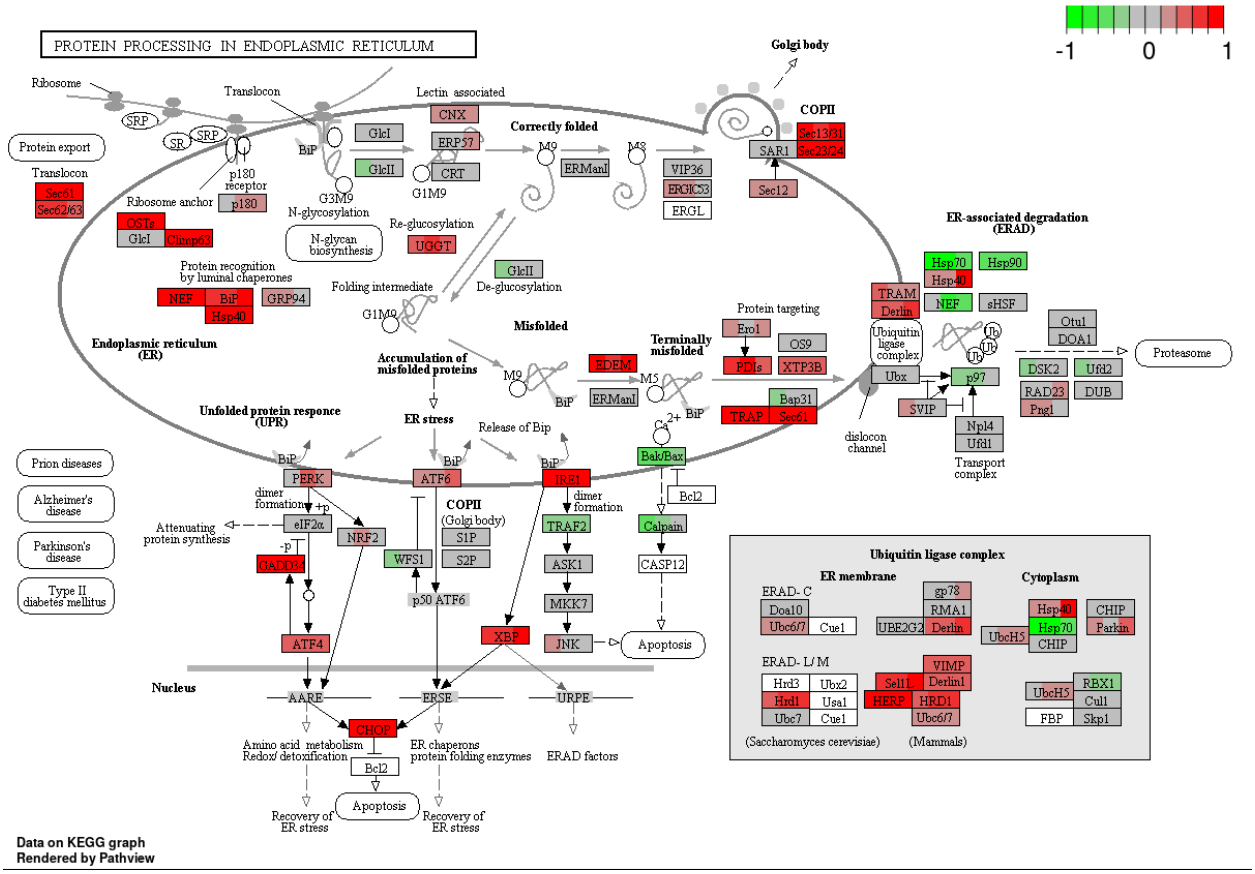

Figure 58. Changes of protein processing in endoplasmic reticulum under high-THC extract #18 compared to DMSO control in the HT-29 CRC cell line. The genes are coloured according to the difference in expression level between treatment and control for each individual

sample. Red colour shows up- and green - down-regulation, relative to the treatment group. Data based on GAGE uni-directional analysis.

High-THC cannabinoid extract #18 significantly increased protein processing in the endoplasmic reticulum (ER), which triggered the accumulation of misfolded proteins, ER stress and unfolded protein response (Figure 58). As a result, the strong upregulation of *ATF4* and *CHOP* could lead to pro-apoptotic signalling by downregulating *Bcl2*. In parallel, there was a decreased expression of *Bak*/*Bax* and *calpain*, which might have an anti-apoptotic effect and give the cancer cells time to recover from ER stress. This could be one of the unwanted effects of tested cannabinoid extract on CRC cancer cells and could promote its survival.

2.4.2. Cannabinoid extract #18 and cisplatin in colorectal cancer cell lines

Next, I analyzed the cell viability of CRC cells to test if extract #18 could act in synergy with cisplatin.

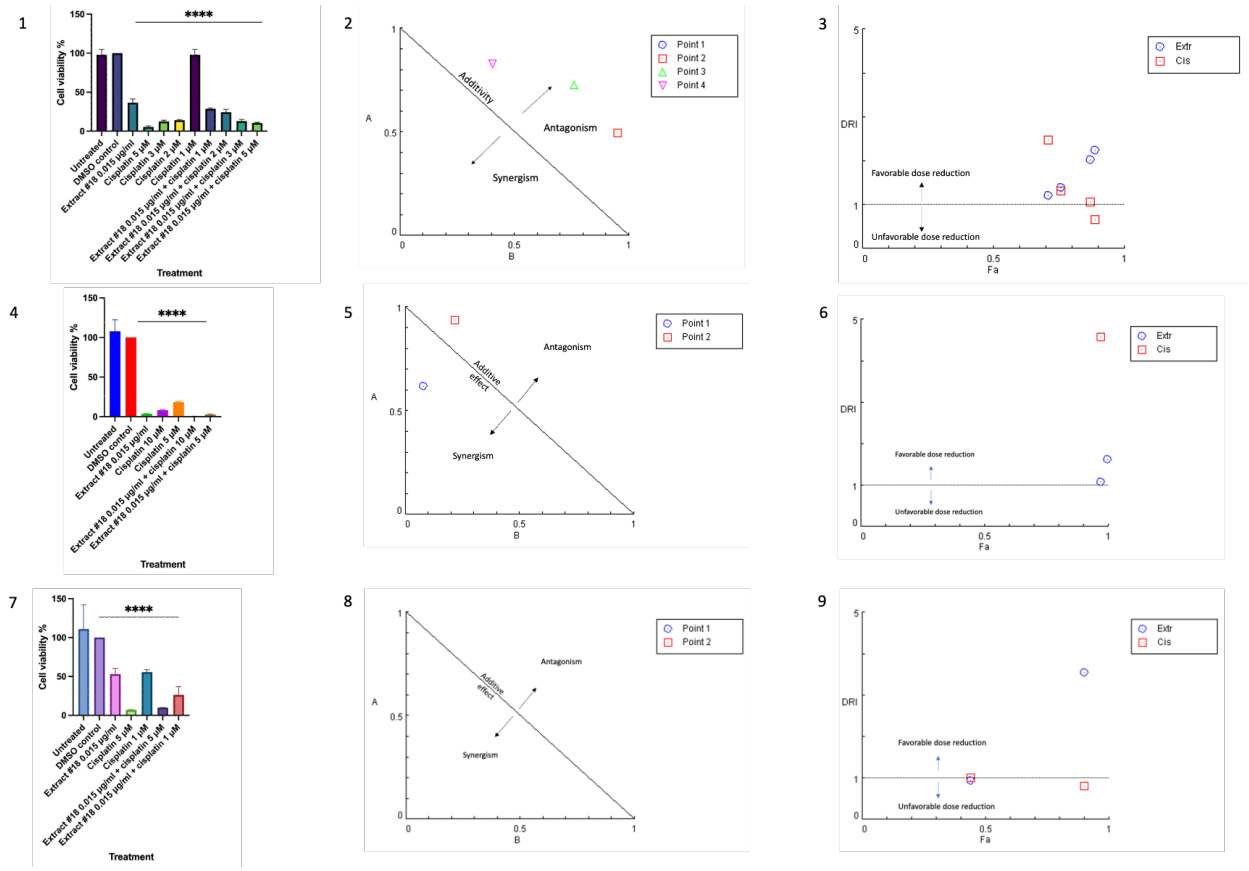

Figure 59. The changes in cell viability under extract #18 combined with different doses of cisplatin on the HCT-116 (1), HT-29 (4), and LS-174T (7) CRC cell line based on MTT results. Results are expressed as means of calculated cell viability ± standard deviations of

each group in triplicate. To calculate time-dose effects, two-way ANOVA was performed using GraphPad Prism version 9.0. Significant differences between groups are marked with ns – non-significant, *p < 0.05, **p < 0.01, ***p < 0.001, ****p <0.0001. **Normalized isobologram for the combination of extract #18 and cisplatin with normalization of the dose with IC50 to the unity of both x and y axis in the HCT-116 (2), HT-29 (5), and LS-174T (8).** Most of the combination points indicated an antagonistic interaction. Normalized isobologram was generated using CompuSyn software. Abbreviations: A – Extract#18 $(D)_1/(IC50)_1$; B – Cisplatin $(D)_2/(IC50)_2$; D – dose; Point 1 – the combination of extract #18 (0.015 μg/mL) and cisplatin (5 μM); Point 2 – the combination of extract #18 (0.015 μg/mL) and cisplatin (10 μM). **Fa – DRI plot for the combination of extract#18 and cisplatin in different doses in CRC cell lines.** Abbreviations: DRI – dose reduction index; Fa - fraction affected by the drug concentration (% of cell growth inhibition/100); Extr – extract #18; Cis - cisplatin. The plot was generated using CompuSyn software.

Based on the cell viability (Figure 59), the combination of extract #18 with cisplatin resulted in antagonistic interaction in most tested CRC cell lines, except for the HT-29, which represents the canonical subtype of CRC (Table 17). The DRI values for cisplatin were higher than 1 in the HCT-116 and the HT-29 cell lines, indicating the possibility of cisplatin dose reduction.

Table 17. CI data for the combination of extract#18 and cisplatin. Data was generated using CompuSyn software.

Dose of extract#18 (μg/mL)	Dose of cisplatin (μM)	Effect (fraction of cell growth inhibition)	CI	Interaction effect
HCT-116				
0.015	5.0	0.89	1.96	Antagonism
0.015	3.0	0.87	1.44	Moderate antagonism
0.015	2.0	0.76	1.49	Antagonism
0.015	1.0	0.71	1.23	Moderate antagonism
HT-29				
0.015	10.0	0.997	0.70	Synergism
0.015	5.0	0.972	1.15	Slight antagonism
LS-174T				

0.015	5.0	0.9	1.5	Antagonism
0.015	1.0	0.44	2.1	Antagonism

Next, we performed gene expression analysis to understand the mechanisms behind the combination of extract #18 with cisplatin in the HT-29 CRC cell line.

Exploratory analysis

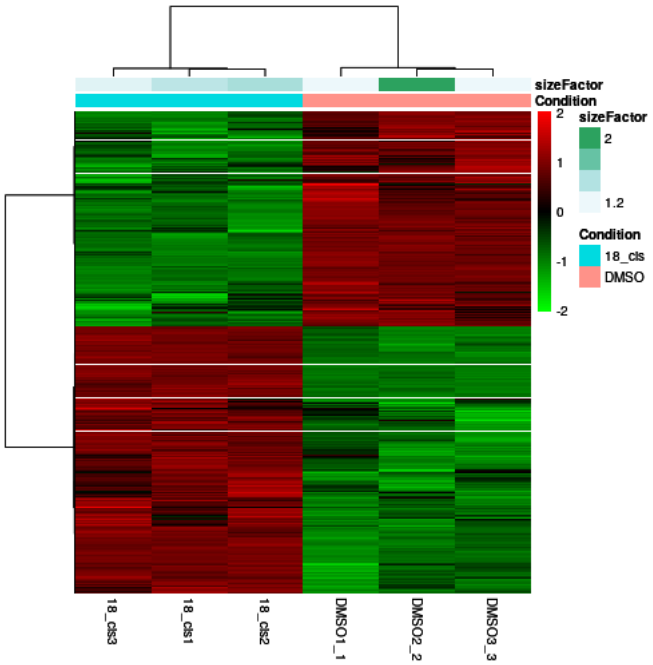

Figure 60. A hierarchical clustering heatmap analysis of the differentially expressed genes with fold change over 1.5 and adjusted p-values < 0.05 for DMSO control versus extract #18 in the HT-29 CRC cell line. The x-axis shows non-supervised clusters between the two treatment groups. The DMSO_1, DMSO_2, and DMSO_3 are independent replicates for DMSO and 18_1, 18_2, and 18_3 are for extract #18. The y-axis shows differentially expressed genes. The fold changes of up-regulated genes are in the red-orange colour spectrum, and the down-regulated genes are represented in the blue colour spectrum. The heatmap was generated using R software version 4.2.2.

A heatmap represents differentially expressed genes for DMSO versus extract #18 in the HT-29 CRC cell line. The unsupervised clustering based on the underlying data determined if there were sub-categories within DMSO control and extract #18 treatment. As the figure shows, there were significant differences in gene expression between treatment groups. The differences were

not substantial for the biological replicates within the same group, showing the treatment samples' good quality (Figure 60).

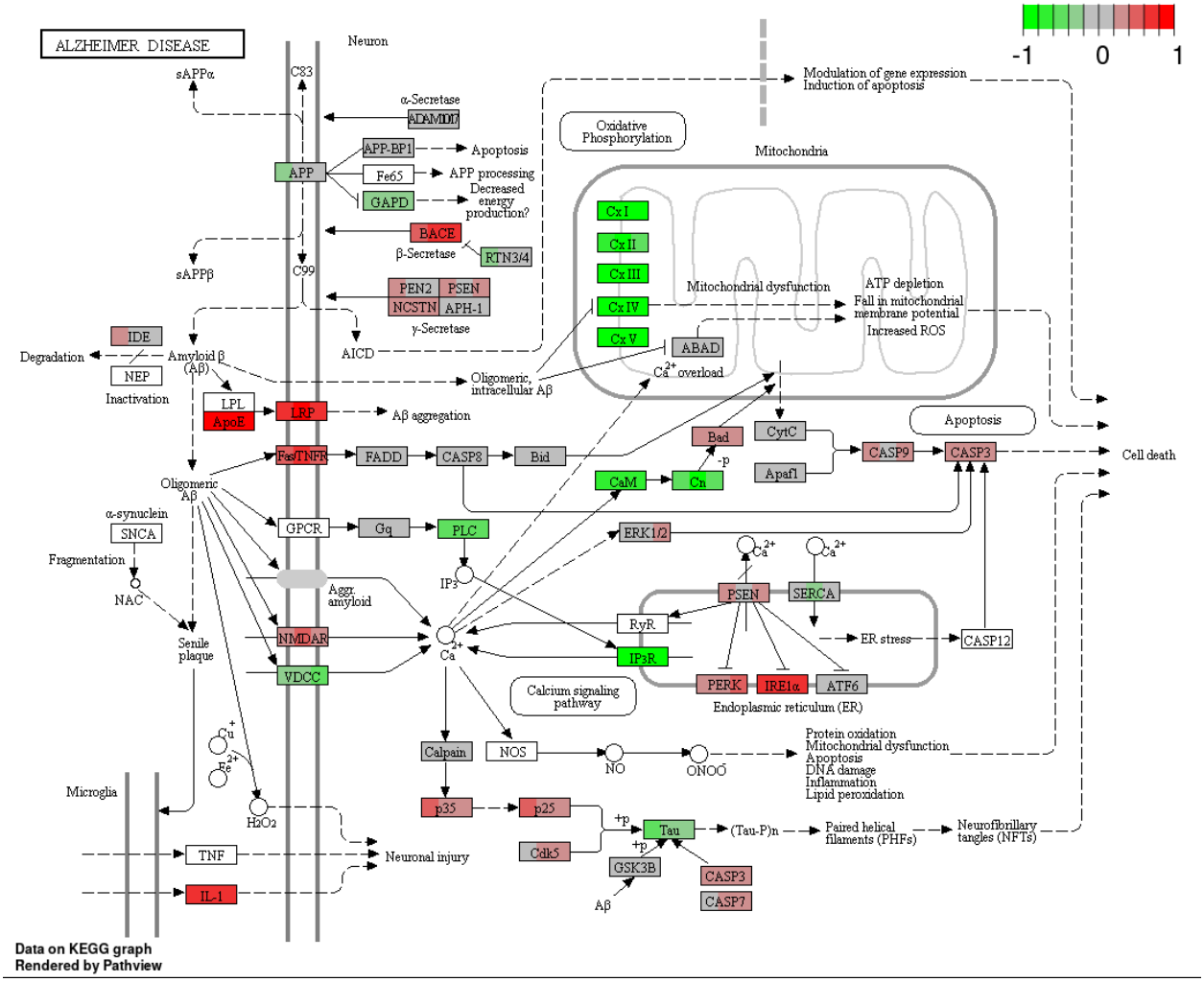

Figure 61. Inhibition of oxidative phosphorylation and activation of apoptosis under the combination of cisplatin and high-THC extract #18 compared to DMSO control in the HT-29 CRC cell line. The genes are coloured according to the difference in expression level between treatment and control for each individual sample. Red colour shows up- and green down-regulation relative to the treatment group. Data based on GAGE uni-directional analysis.

The combination of cisplatin with extract #18 had an inhibitory effect on oxidative phosphorylation (Figure 61). It decreased the expression of all five complexes and inhibited ATP production in the HT-29 cancer cells. The combination therapy also increases the expression levels of genes responsible for apoptosis. There was a significant elevation of ERK1/2, Fas/TNFR, Bad, and caspases 9, 7, and 3. Moreover, the increased expression of the genes that take part in ER

stress responses, such as PERK, PSEN and IRE1α, also might potentiate apoptosis signalling. Additionally, we observed lowered GAPD, which could indicate decreased energy production in cancer cells. There was also an increased expression of pro-inflammatory cytokine *IL-1*, which would be one of the unwanted effects in tested treatment, as inflammation is a well-known process promoting CRC carcinogenesis.

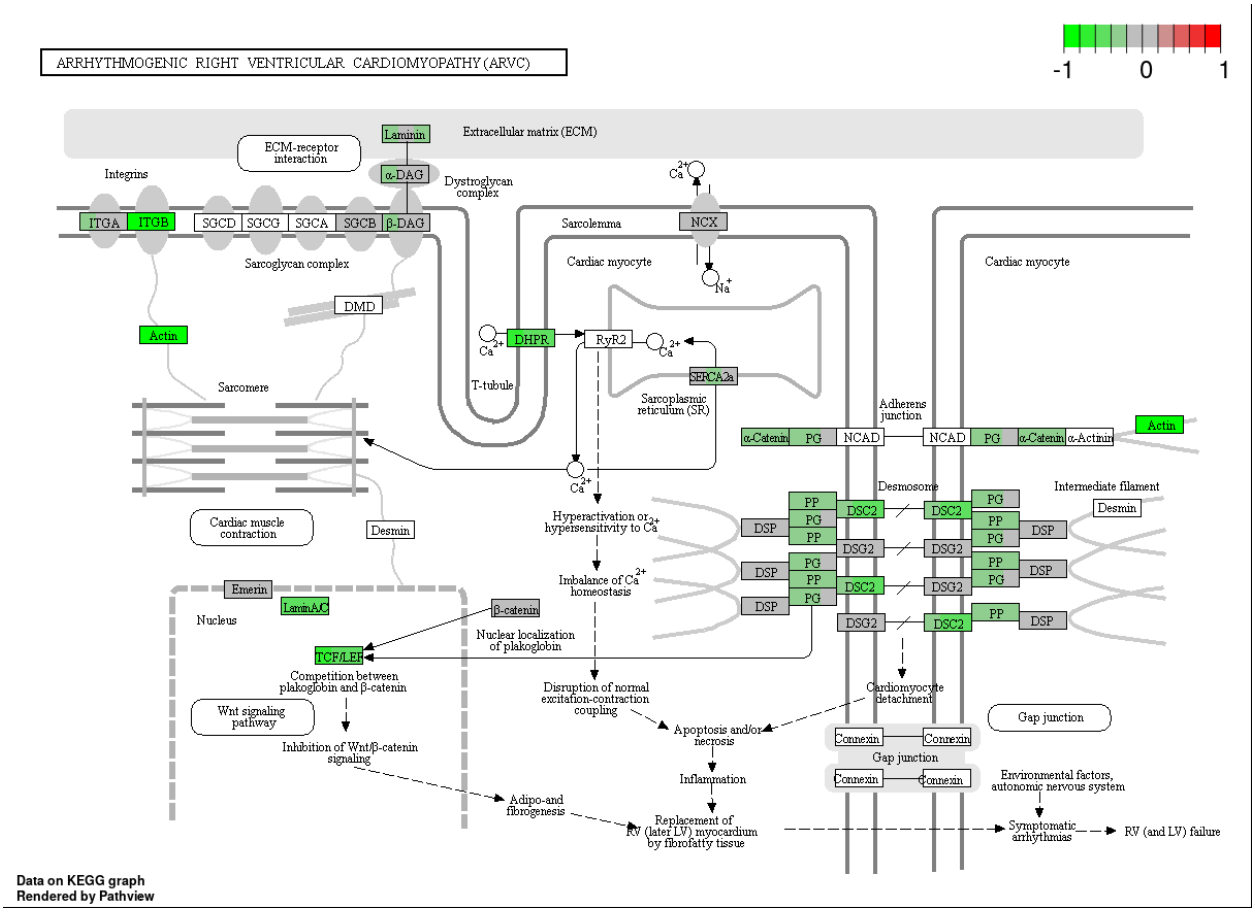

Figure 62. Inhibition of actin cytoskeleton regulation, adherent junction formation, and Wnt signalling pathway under cisplatin and high-THC extract #18 compared to DMSO control in the HT-29 CRC cell line. The genes are coloured according to the difference in expression level between treatment and control for each individual sample. Red colour shows up- and green down-regulation relative to the treatment group. Data based on GAGE uni-directional analysis.

The combination of cisplatin with extract#18 had an inhibitory effect on TCF/LEF (Figure 62). These transcription factors are a part of Wnt signalling and are dysregulated in a canonical subtype of CRC. Our treatment significantly inhibited mRNAs that encoded integrins, laminin,

and actin, which interact with cells and the extracellular matrix. Additionally, there was a decreased expression of multiple proteins forming adherent and desmosomal junctions, which are important components in cell-to-cell interactions. The dysregulation of cytoskeletal structures and junction formation could prevent the EMT of cancer cells and inhibit their invasive potential.

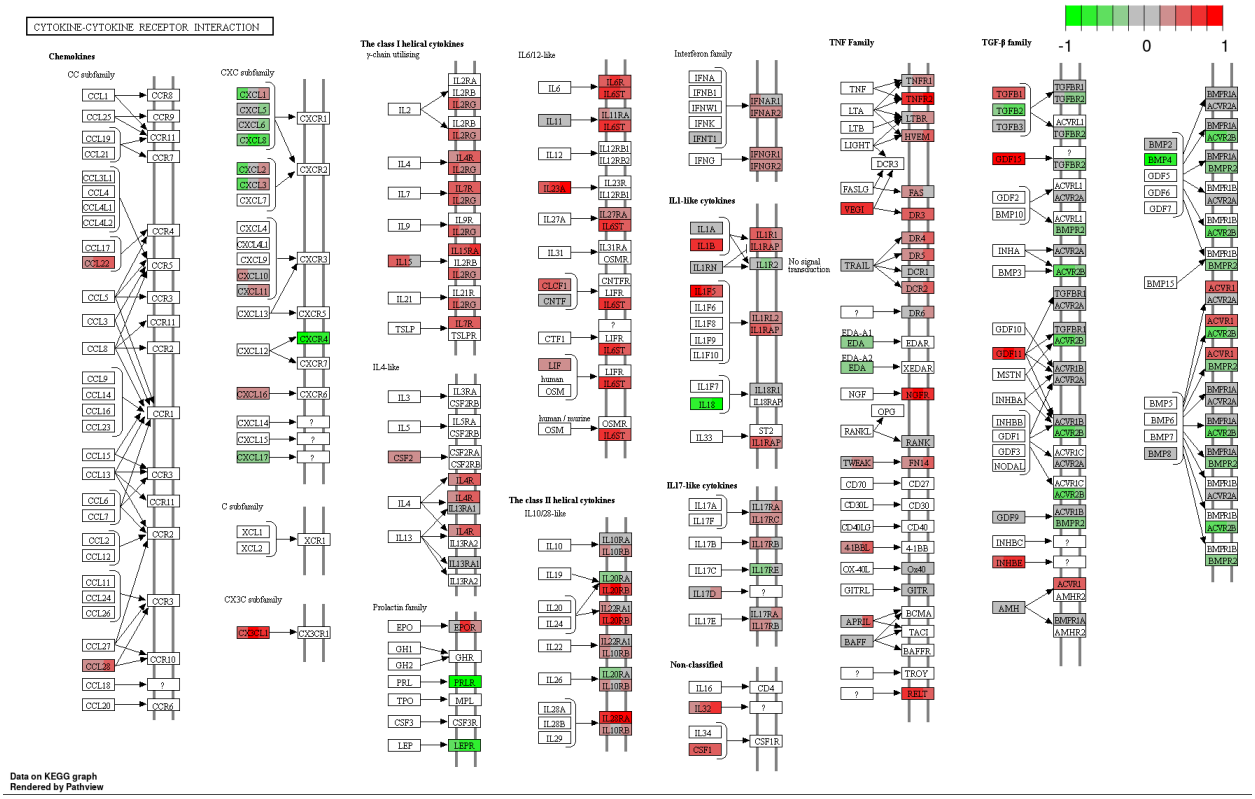

Figure 63. Changes of cytokine-cytokine receptor interactions under cisplatin and high-THC extract #18 compared to DMSO control in the HT-29 CRC cell line. The genes are coloured according to the difference in expression level between treatment and control for each individual sample. Red colour shows up- and green – down-regulation, relative to the treatment group. Data based on GAGE uni-directional analysis.

The combination of cisplatin with extract #18 didn't show many differences in expression data when compared to the expression data of cisplatin alone in the HT-29 CRC cell line.

The combination therapy increased the expression of multiple genes responsible for the cytokine-cytokine receptor interaction in CRC cell line HT-29 compared to DMSO control. As the figure shows, mRNAs are increased for chemokines CCL22 from the CC subfamily and CXC subfamily with decreased expression of the CXCR4 receptor gene. There was also an increased expression of the genes encoding receptors reacting to IL2, IL4, IL6, IL7, IL9, IL10, IL15 and

IL17, which participate in the humoral immune response (Figure 63). Moreover, the expression of IL18, which facilitates type 1 immune response, was significantly lower. As we mentioned previously, shifting cellular immune response to humoral helps cancer cells in immune response evasion.

On the other hand, an increased TNF family receptor expression could help activate the extrinsic apoptotic pathway. The decreased expression of TGF-β family receptors might prevent the EMT activation, which would decrease the invasive potential of the CRC cell line.

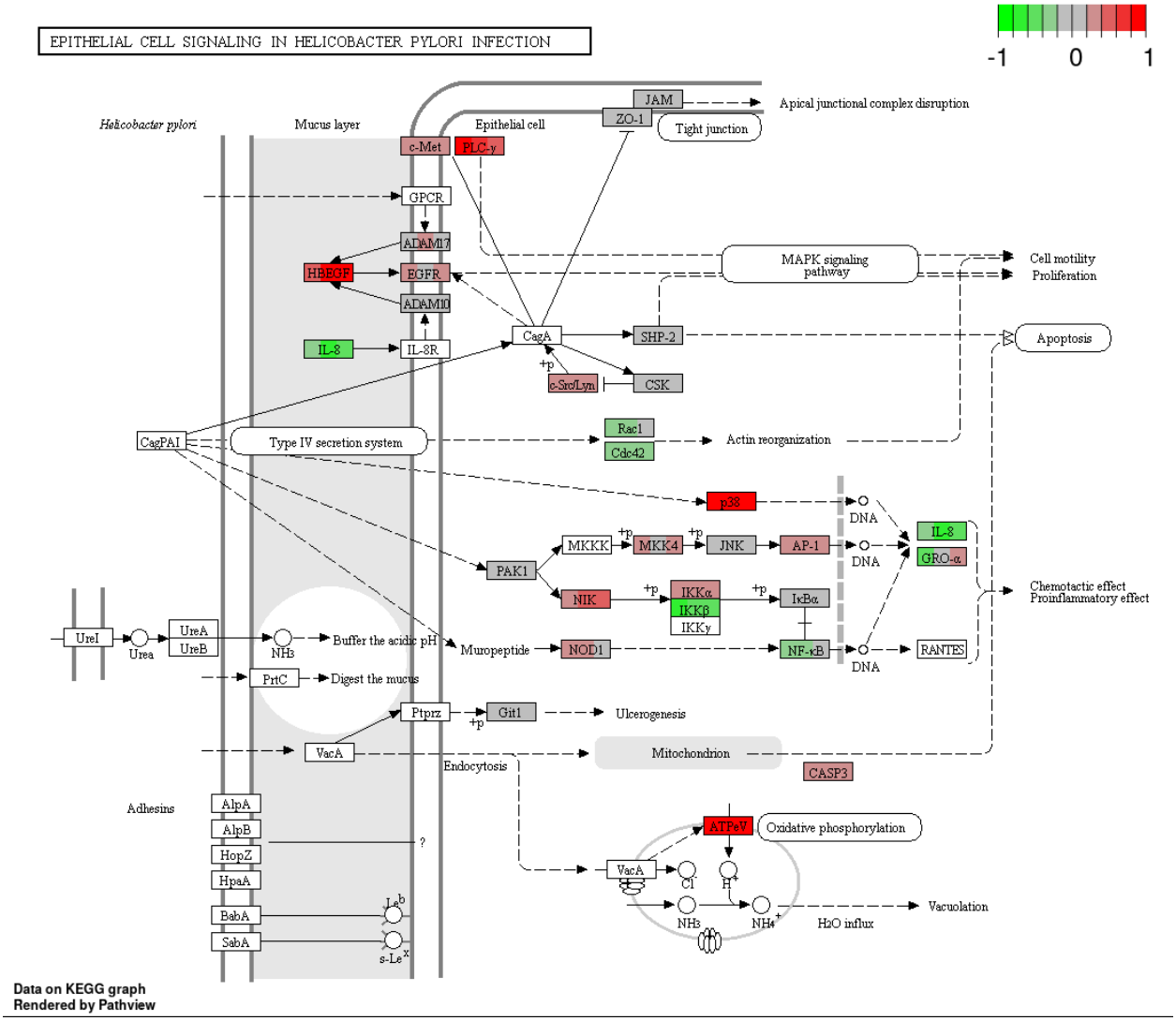

Figure 64. MAPK and proinflammatory pathways signalling changes under cisplatin and high-THC extract #18 compared to DMSO control in the HT-29 CRC cell line. The genes are coloured according to the difference in expression level between treatment and control for each

individual sample. Red colour shows up- and green down-regulation relative to the treatment group. Data based on GAGE uni-directional analysis.

Combining cisplatin with extract #18 increased MAPK signalling via increased HBEGF, EGFR, and p38 expression (Figure 64). While the increased growth factors and their receptors might have a stimulatory effect on tumor cell growth, the strong upregulation of p38 with increased caspase 3 could direct cancer cells toward apoptosis. Moreover, the decreased levels of NFκB and IL8 indicated the lowering of proinflammatory signalling.

There was also decreased expression of Rac1 and Cdc-42, which decreased actin reorganization, causing reduced cell motility, and as a result, lowered invasiveness of the HT-29 cell line.

However, increased levels of hepatocyte growth factor receptor cMet might stimulate tumor growth and metastasis. Together with PLCγ, it could promote cell growth, migration, and proliferation of cancer cells.

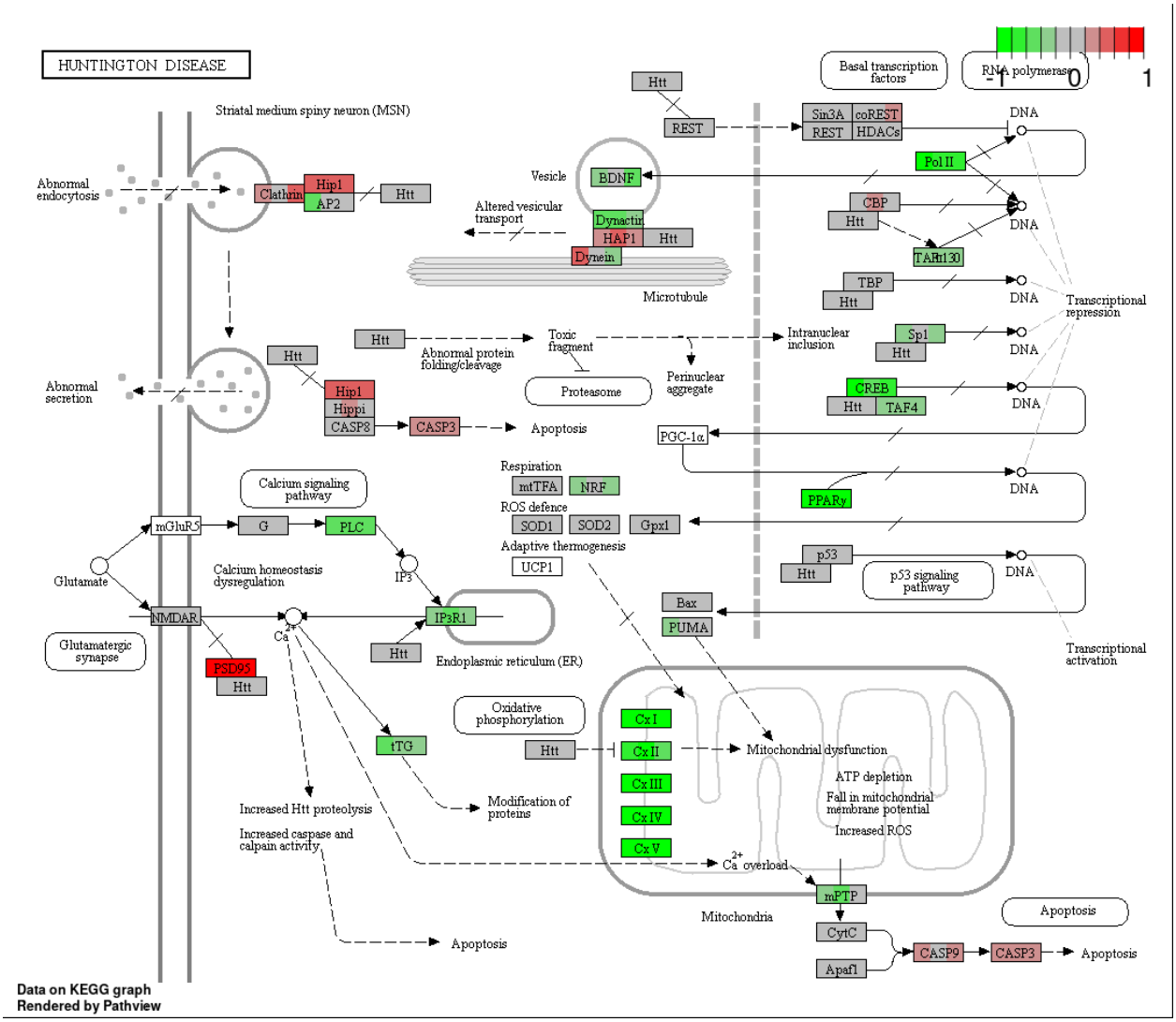

Figure 65. Transcriptional repression, changes of microvesicular transport, oxidative phosphorylation under cisplatin in combination with high-THC extract #18 compared to DMSO control in HT-29 CRC cell line. The genes are coloured according to the difference in expression level between treatment and control for each individual sample. Red colour shows up- and green down-regulation relative to the treatment group. Data based on GAGE uni-directional analysis.

The combination of cisplatin with high-THC cannabinoid extract #18 had similar effects as extract #18 alone. There was a significant decrease in the expression of complexes I to V, which are part of oxidative phosphorylation (Figure 65). However, compared to extract #18 alone, there was no increase of p53, decreased mPTP and no change in *cytochrome C* levels. Combining

cisplatin and high-THC cannabinoid extract #18 increased caspases 9 and 3 more significantly than the extract alone, indicating a stronger apoptosis activation in the HT-29 cell line.

Moreover, the tested treatment upregulated some genes involved in vesicular transport, endo- and exocytosis, which might help with the stimulation of the formation of metastatic niches in the canonical subtype of CRC. Additionally, there was a strong downregulation of PPARγ, essential for insulin sensitization, glucose uptake and an enhancement of energy metabolism in the HT-29 cancer cells. The interesting effect was the inhibition of NRF expression, which takes part in cellular respiration and mitochondrial DNA transcription and replication.

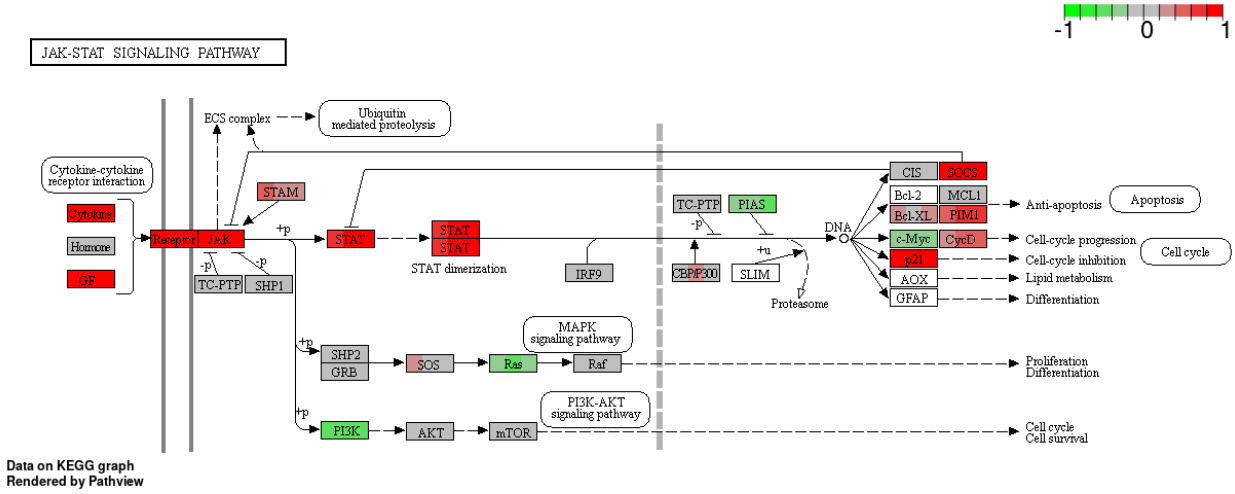

Figure 66. JAK/STAT signalling changes under the combination of cisplatin with high-THC extract #18 compared to DMSO control in the HT-29 CRC cell line. The genes are coloured according to the difference in expression level between treatment and control for each individual sample. Red colour shows up- and green down-regulation relative to the treatment group. Data based on GAGE uni-directional analysis.

In the HT-29 cell line, the combination of cisplatin and extract #18 downregulated Ras and PI3K expression, major oncogenes that are often increased in multiple cancers (Figure 66). Also, it upregulated p21 and downregulated transcription factor cMyc, which can be responsible for cell cycle arrest, inhibition of proliferation and cell survival mechanisms. However, there was a strong increase in JAK/STAT signalling, which could lead to the inhibition of apoptosis and cell cycle progression via upregulated cyclin D, Bcl-XL and PIM. Except for downregulated cMyc, these effects were similar to the action of cisplatin alone.

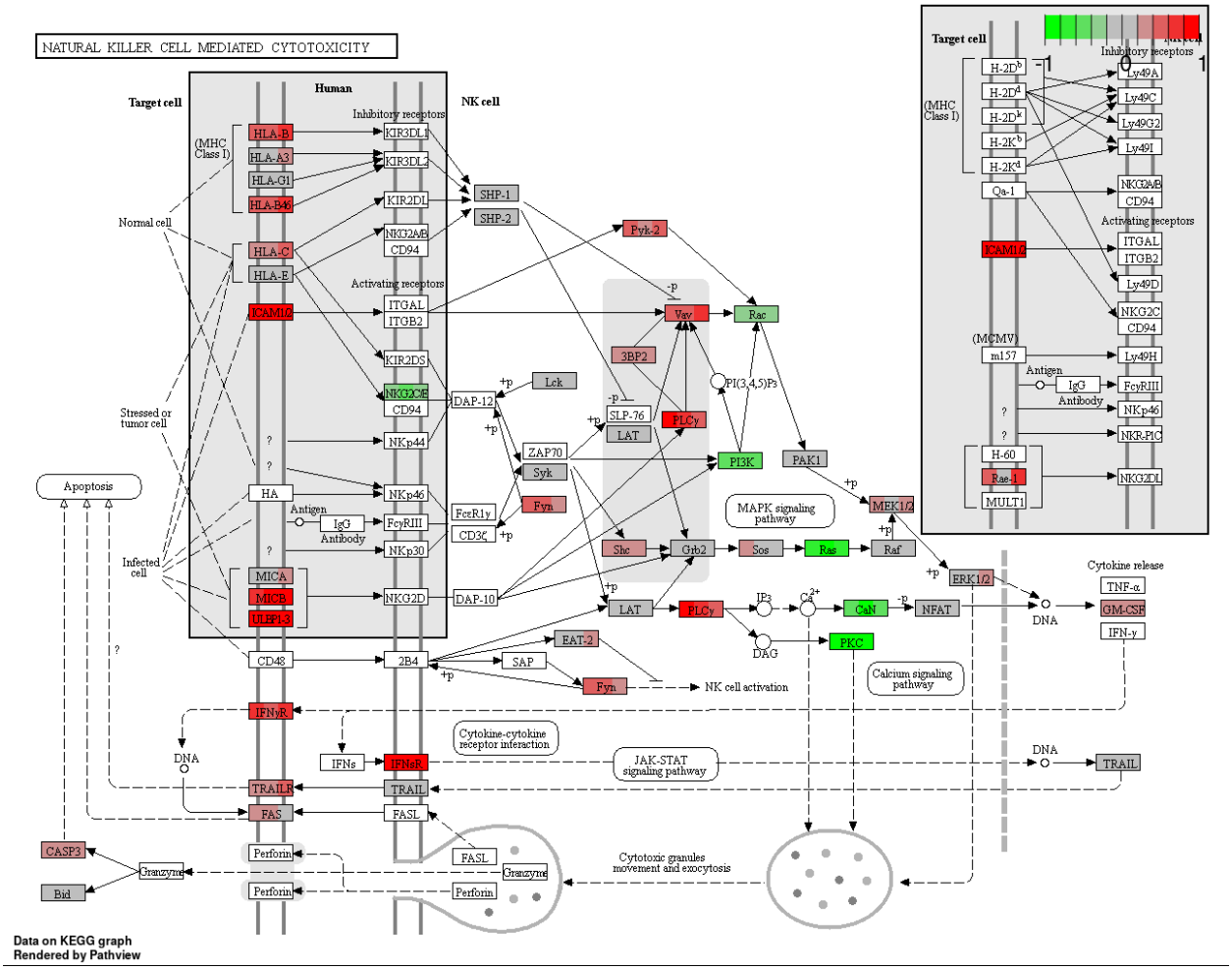

Figure 67. Activation of natural killer cell-mediated immunity under cisplatin in combination with high-THC extract #18 compared to DMSO control in HT-29 CRC cell line. The genes are coloured according to the difference in expression level between treatment and control for each individual sample. Red colour shows up- and green down-regulation relative to the treatment group. Data based on GAGE uni-directional analysis.

The combination of cisplatin with high-THC cannabinoid extract #18 caused the upheaval of the expression of genes responsible for activating NK against cancer cells in the HT-29 CRC cell line (Figure 67). As we previously mentioned, the upregulation of MHC class I helps with the recognition of cancer cells by the immune system. Moreover, the combinational treatment caused the upregulation of ICAM1/2, the cell adhesion molecules, which activated PLCγ, a part of the Ca signalling pathway, and helps with the cancer cell's recognition by NKs. However, the downstream signalling gene expression in Ca signalling, such as CaN and PKC, was significantly downregulated. Although Ras was down-regulated, the higher MEK1/2 and ERK1/2 MAPK

signalling molecules were increased, subsequently increasing the granulocyte-macrophage colony-stimulating factor (GM-CSF). GM-CSF is responsible for the stimulation of the production of granulocytes, such as neutrophils, eosinophils, and macrophages. However, in this case, it activated JAK/STAT pathway in cancer cells leading to increased expression of interferon receptors causing upregulation of TRAIL and FAS, which would activate the extrinsic apoptosis pathway. Moreover, an increased Fyn would enhance NK cell activation and subsequent killing of cancer cells. These effects of combinational treatment might activate immune system surveillance of cancer cells and cancel the effects of cisplatin, which was the evasion of the immune response.

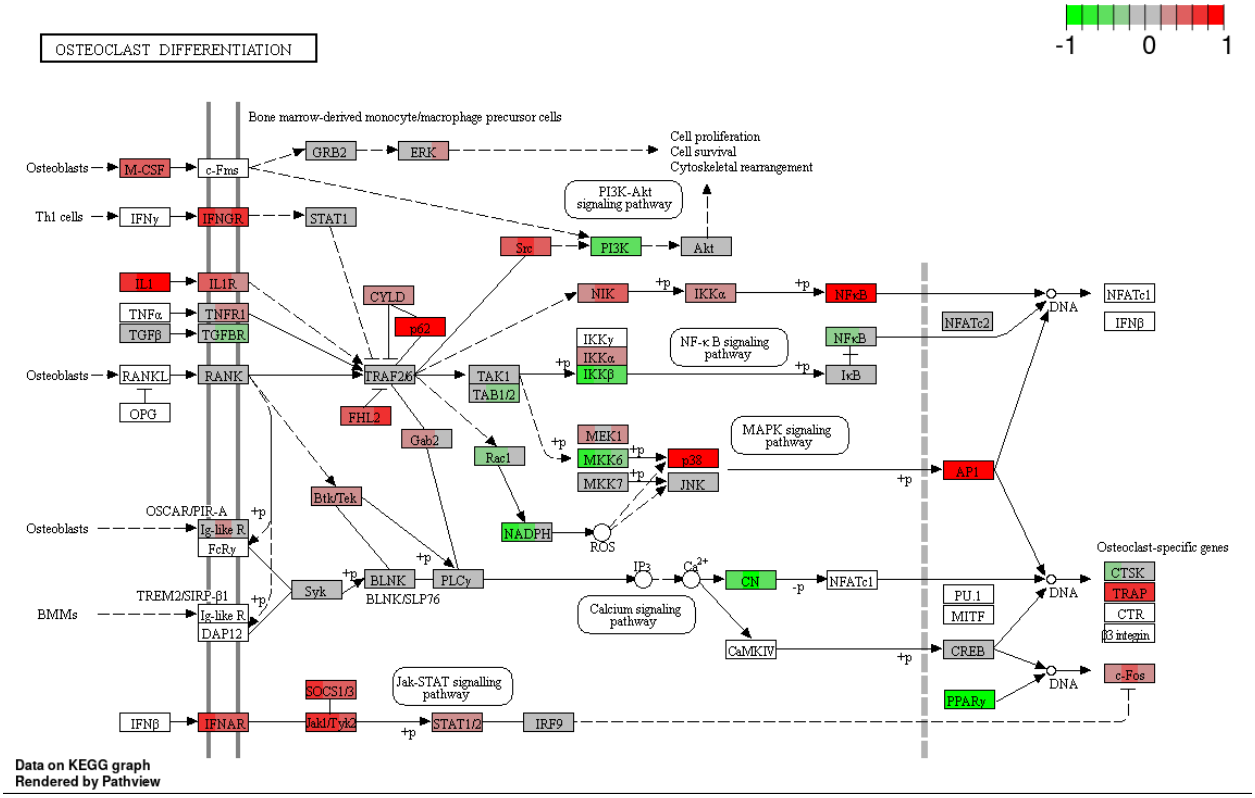

Figure 68. Changes of PI3K/AKT, NFκB, MAPK, JAK/STAT, and Ca signaling pathways under cisplatin combined with high-THC extract #18 compared to DMSO control in HT-29 CRC cell line. The genes are coloured according to the difference in expression level between treatment and control for each individual sample. Red colour shows up- and green down-regulation relative to the treatment group. Data based on GAGE uni-directional analysis.

The figure above represents the dysregulation of multiple oncogenic-stimulating pathways under the combination of cisplatin with high-THC cannabinoid extract #18 in the HT-29 CRC cell line (Figure 68). There was increased expression of macrophage-colony stimulating factor (M-

CSF), IL-1, and IFNAR, which might activate macrophages' proliferation, differentiation, and activation in a tumor microenvironment. As already mentioned, activating the JAK/STAT signalling pathway with the help of IFNAR caused the upregulation of c-Fos, a transcription factor involved in cell proliferation after extracellular stimuli. Additionally, there was a decreased signalling via the calcium pathway due to the inhibition of calcineurin (CN) expression.

Another pathway affected by our combinational treatment was MAPK, which caused increased expression of p38 that could activate apoptosis in cancer cells. However, increased expression of transcription factor AP-1 that regulates gene response in various exogenous stimuli, including cytokines and growth factors, could stimulate the expression of genes responsible for cancer cell proliferation. Moreover, there was a decreased expression of PI3K, which could lead to decreased cell proliferation, survival, and dysregulation of cytoskeletal rearrangement. Interestingly, there was an upregulation of p62, a protein involved in the degradation of misfolded protein through ubiquitin or autophagy-lysosomal pathway. The upregulation of p62 often occurs due to nutrient status change, oxidative stress, and inflammation (291).

The combination of cisplatin with extract #18 also increased the expression of TNFR1, NIK, IKKα, and NFκB, which is responsible for activating the transcription of multiple proinflammatory cytokines and anti-apoptotic factors. This mechanism would contradict the anticancer effects of our treatments and might be responsible for the mechanisms of survival of cancer cells.

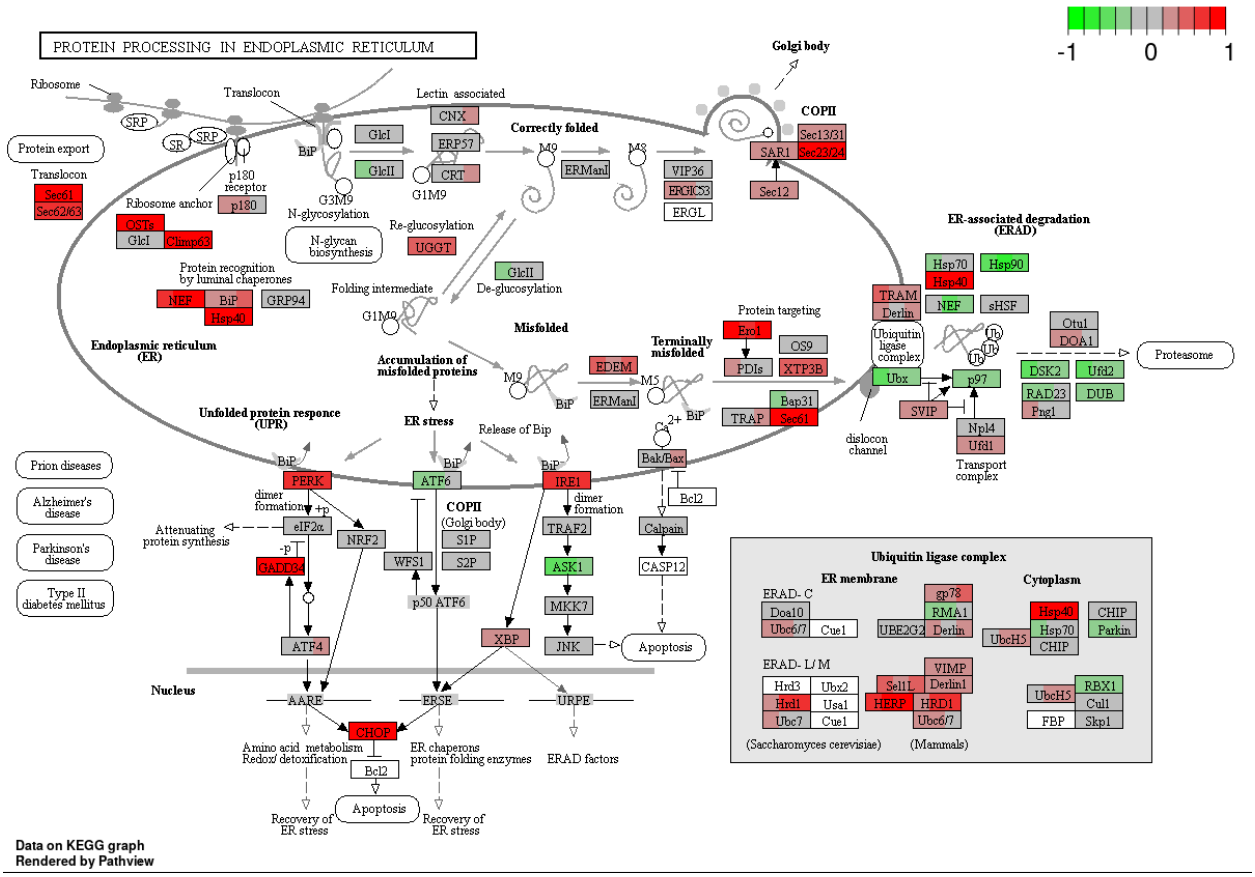

Figure 69. Changes of protein processing in the endoplasmic reticulum under cisplatin combined with high-THC extract #18 compared to DMSO control in HT-29 CRC cell line. The genes are coloured according to the difference in expression level between treatment and control for each individual sample. Red colour shows up- and green – down-regulation, relative to the treatment group. Data based on GAGE uni-directional analysis.

The combination of cisplatin with high-THC cannabinoid extract #18 significantly increased the expression of genes encoding protein processing in the endoplasmic reticulum (ER), which likely triggered the accumulation of misfolded proteins, ER stress and unfolded protein response (Figure 69). The expression data did not differ much from the treatment with extract #18 alone. There was a strong upregulation of proteins in the endoplasmic reticulum that are designed to deal with the misfolded protein response indicating ER stress response. However, the expression of genes that target misfolded proteins for proteasomal degradation was decreased, which could indicate further accumulation of the misfolded proteins in ER. Moreover, increased expression of PERK and IRE1 genes with the downstream increase of the expression of CHOP were possibly strong signals for the activation of apoptosis in cancer cells. Additionally, the increased expression

of GADD34, which could potentially lead to the suppression of eIF2α, might indicate inhibition of global translation in treated cancer cells.

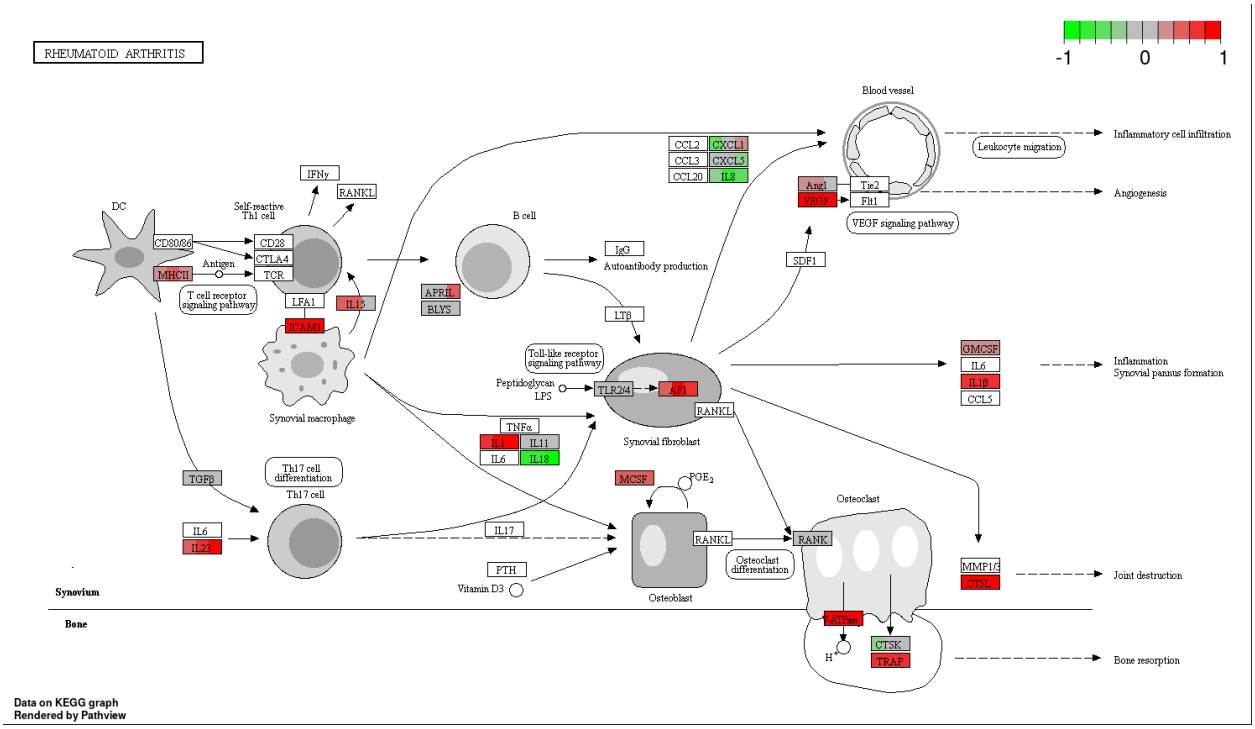

Figure 70. Changes of cytokine production under cisplatin combined with high-THC extract #18 compared to DMSO control in HT-29 CRC cell line. The genes are coloured according to the difference in expression level between treatment and control for each individual sample. Red colour shows up- and green - down-regulation, relative to the treatment group. Data based on GAGE uni-directional analysis.

Figure 70 presents the action of cisplatin in the combination of extract #18 on multiple pathways involved in immune system response. The action was very similar to the action of cisplatin alone. There was an increased expression of MHC class II responsible for antigen presentation, ICAM1, enhancing cellular adhesion, and pro-inflammatory IL-1β. There was also upregulation of VEGF, which is responsible for angiogenesis. Moreover, upregulation of IL-23 may stimulate Th17 cells, inhibiting the cellular immune response of cancer cells. The interesting effect of treatment was the downregulation of IL-18 and IL-8, responsible for cytotoxic T-cell activation and chemotaxis of the immune cells. These results may indicate an attempt by CRC cells to avoid immune destruction and activate angiogenesis. These mechanisms were not present in the action of extract #18 alone.

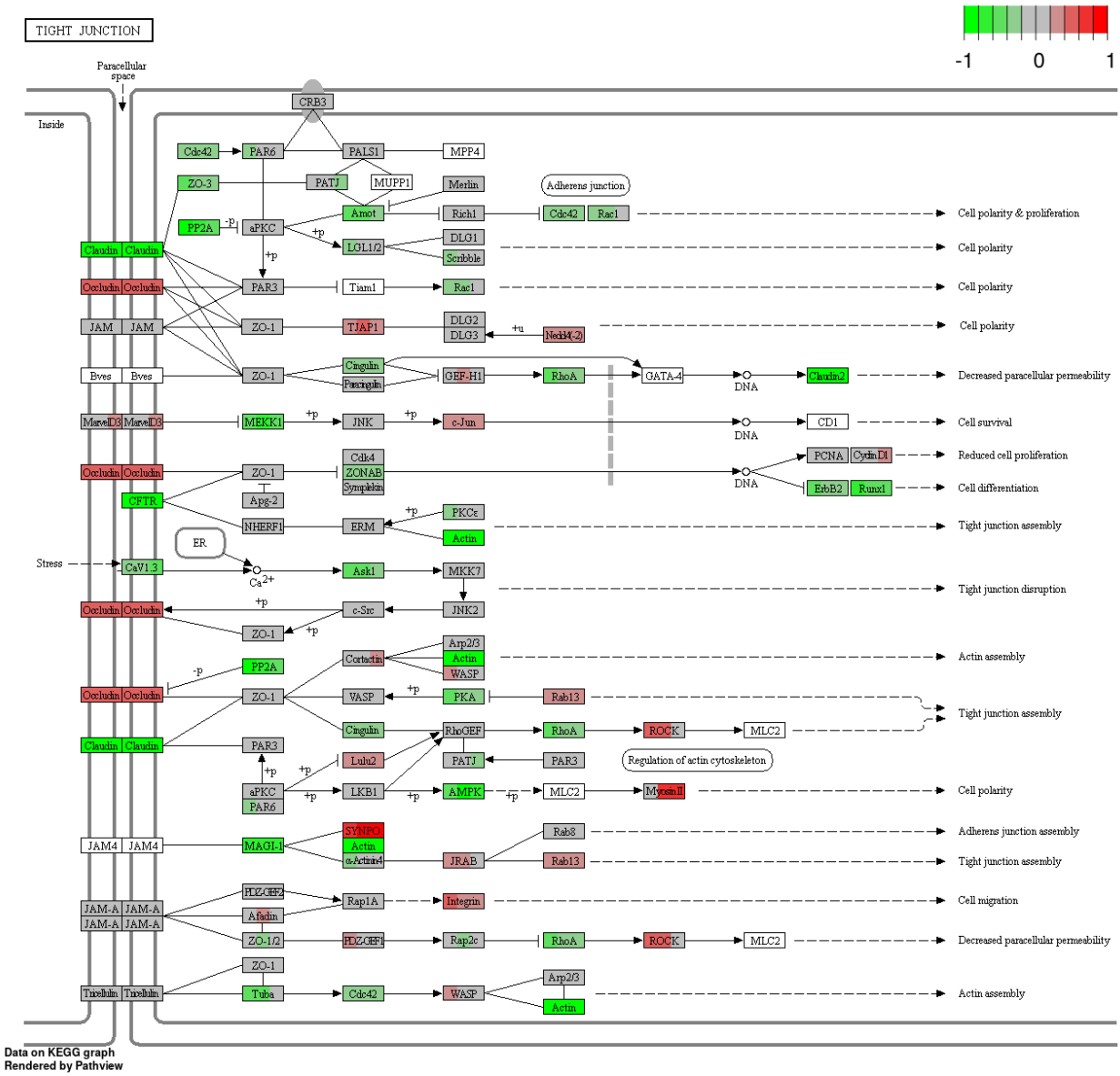

Figure 71. Changes of tight junction regulation under cisplatin in combination with high-THC extract #18 compared to DMSO control in HT-29 CRC cell line. The genes are coloured according to the difference in expression level between treatment and control for each individual sample. Red colour shows up- and green - down-regulation, relative to the treatment group. Data based on GAGE uni-directional analysis.

As the figure above shows, the combination treatments were very similar to the action of high-THC cannabinoid extract #18 alone. Overall, inhibition of actin cytoskeleton formation might decrease the ability of cancer cells to invade (Figure 71).

2.5. Discussion, limitations, and future perspectives.

2.5.1. Effect of extract #18 on CRC

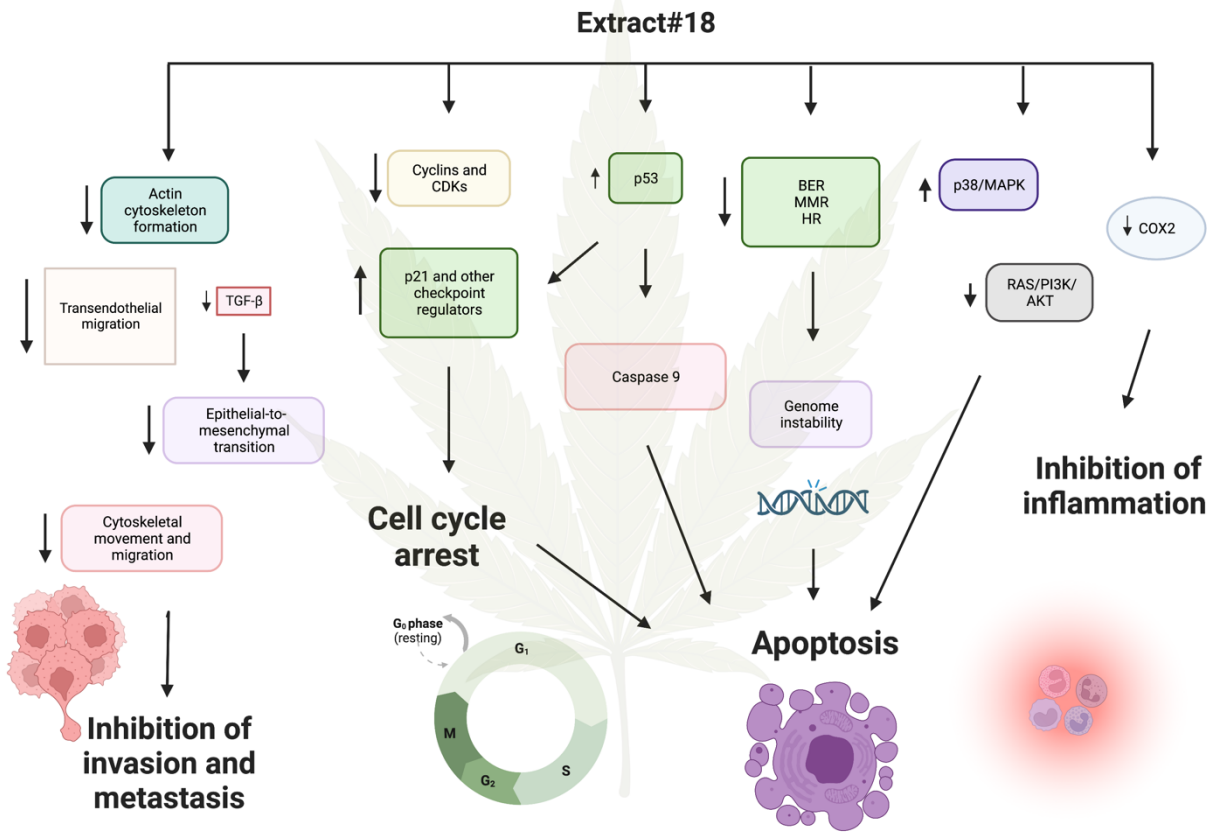

Figure 72. Likely mechanisms of the cytotoxic effects of high-THC cannabis extract #18 in the HT-29 CRC cell line. Created with BioRender.com

Based on our mRNA expression data analysis, high-THC cannabis extract #18 had a strong cytotoxic effect on the classical molecular subtype of CRC, represented by the HT-29 cell line (Figure 72). The tested extract caused cell cycle arrest via decreased expression of most genes that participate in cell cycle progression, DNA replication, and increased expression of tumor suppressors such as p53 and p21. Additionally, MMR, BER, and HR inhibition could cause genotoxic stress in cancer cells. Thus, even if tumor cells stopped their proliferation and had time to fix their DNA, DNA repair was inhibited, which can also contribute to cell death. Moreover, an increased expression of caspase 9, inhibition of oxidative phosphorylation, decreased glucose uptake, suppression of Ras/PI3K/AKT, and activation of MAPK/p38 would further assist in the activation of apoptosis.

Another anti-cancer mechanism of extract #18 was the possible inhibition of cancer cell invasion and metastasis. The expression analysis showed decreased expression of adherent junction formation, deregulation of the actin cytoskeleton, and decreased Rho signalling, which regulates cytoskeletal dynamics, cell migration, and cell cycle progression. There was decreased expression of cell adhesion molecules taking part in transendothelial migration, which might indicate inhibition of cell invasion. What is more, the lowered expression of TGF-β could prevent the epithelial-to-mesenchymal transition of cancer cells, which is a pertinent mechanism in tumor invasiveness. Interestingly, there was also decreased extracellular vesicle formation, an important mechanism for preparing metastatic niches in carcinogenesis. Furthermore, cannabis extract #18 decreased COX-2 expression, which could have an anti-inflammatory effect on the tested CRC cell line.

Although multiple pieces of evidence indicated a strong cytotoxic effect of high-THC cannabinoid extract on the HT-29 CRC cell line, which was supported by our MTT results, changes in a few pathways could raise our concern. For instance, there was a strong upregulation of the protein turnover in ER, which caused ER stress response and decreased levels of pro-apoptotic proteins Bax and Bak. Thus, it would be logical to combine cannabinoid extracts with strong apoptosis activators, for example, cisplatin.

2.5.2. Combination of extract #18 and cisplatin

The combination of cisplatin with high-THC cannabis extract #18 changed the expression of multiple genes in the HT-29 cell line. Most of the changes were similar to cisplatin or extract #18 alone, but there were few cancelling effects of cisplatin on the anticancer action of extract #18. Moreover, new qualitative changes under the combinational treatment might explain the survival HT-29 cell line under combinational treatment than cisplatin or extract #18 separately.

The following was similar between the effect of extract #18 alone and in combination with cisplatin: there was decreased oxidative phosphorylation, decreased translation and transcription, activation of ER stress, decreased Ras/PI3K and PPARγ signalling, and increased expression of p21, which could lead to activation of cell cycle arrest. Additionally, the caspases 9, 7 and 3 were increased, which may indicate the activation of apoptosis under the combination of cisplatin with extract #18.

Interestingly, the combinational treatment cancelled a strong inhibition of the cell cycle gene expression and down-regulation of DNA repair pathways by extract #18 alone. This might

be one of the mechanisms of the better survival of HT-29 cancer cells under the addition of cisplatin to the tested extract #18, as supported by our MTT results. Moreover, there was no inhibition of inflammation. On the contrary, because of the strong activation of the JAK/STAT and NFκB pathways, the levels of proinflammatory cytokines, for instance, IL1β were higher.

When we compared the effects of combining cisplatin with extract #18, we still observed the unwanted effects of cisplatin alone, such as immune response evasion, angiogenesis activation and microvesicular transport (Figure 73). We suggest that extract #18 overcame the effect of cisplatin on epithelial-to-mesenchymal transition by inhibiting levels of TGFβ. However, the combination treatment showed no PDL-1 expression changes and no activation of lysosomal hydrolases, opposing the effects of cisplatin alone.

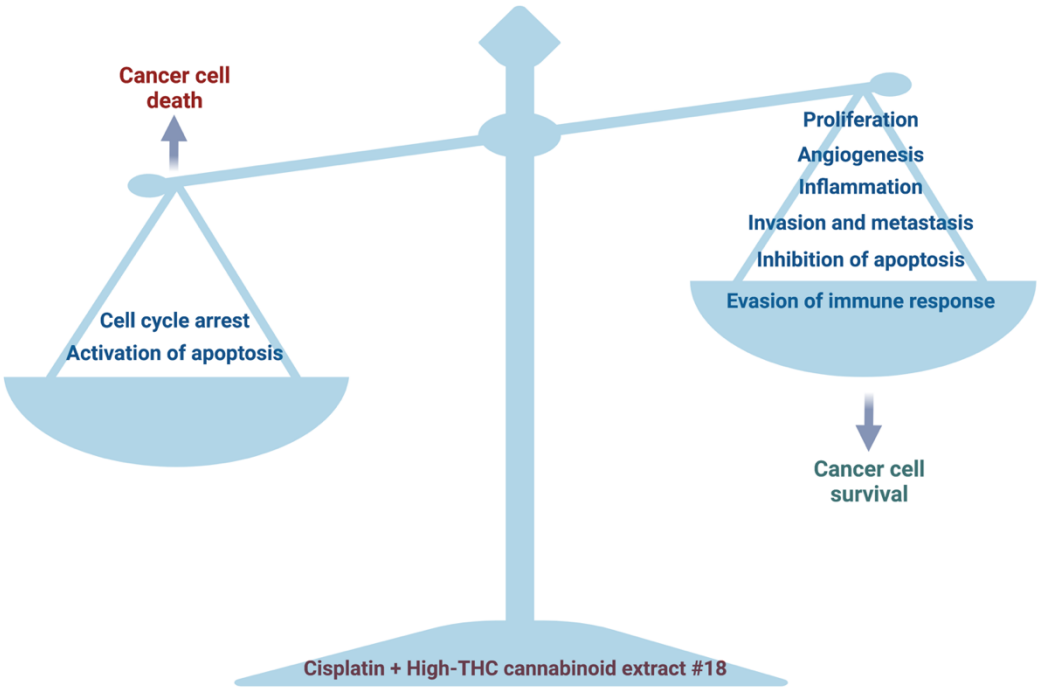

Figure 73. The cytotoxic vs. pro-survival effects of cisplatin and high-THC cannabis extract #18 on the HT-29 CRC cell line. Created with BioRender.com

Other surprising results were that combinational treatment had more pro-oncogenic changes than the treatments separately. For example, there was an increased expression of cMet oncogene, which could stimulate cancer cell proliferation with elevated levels of cyclin D. Moreover, the levels of genes encoding anti-apoptotic proteins, BclXL and PIM, were also higher, which indicated that pro-survival pathways were kicking in. In addition, increased mRNA expression of proteins responsible for activating NK cells could be one of the beneficial effects of

our combinational treatment. However, upregulated levels of GM-CSF and M-CSF could increase the production of granulocytes and activation of macrophages, which may support the inflammatory microenvironment surrounding CRC cells.

Overall, the combination of cisplatin and high-THC cannabis extract #18 cancelled some of the possible cytotoxic effects on the HT-29 cancer cells than the cisplatin and extract #18 treatments alone and activated pro-survival mechanisms, which allowed tested cancer cells to survive our treatment.

Our hypotheses stated that whole-plant *Cannabis sativa* extracts would be more potent than pure cannabinoids. However, during the phenotypic screening of over 40 extracts, the most effective was the high-THC cannabis extract, with an IC50 dose of THC of around 22 μM in it. Additionally, the terpenoid profile of extract #18 showed high levels of α-pinene and β-myrcene that could have contributed to the cytotoxic effects of the tested extract. Based on mRNA differential gene expression of the HT-29 CRC cell line, the molecular mechanisms involved in cell cytotoxicity were similar to the described actions of cannabinoids in our literature review (35,76,78,89–91). Thus, to further test if terpenoids had a significant effect on CRC cell lines, we suggest performing experiments combining purified α-pinene and β-myrcene with THC and comparing the results with extract #18.

Our second hypothesis stated that *Cannabis sativa* extracts potentiate cisplatin-mediated cell killing. We did not support this hypothesis, as we observed an antagonistic interaction between extract #18 and cisplatin.

Overall, based on our cell viability results and mRNA expression analysis, we established treatment interactions in CRC cell lines and understood some of the molecular mechanisms behind those drug interactions. However, we understand that the major limitation of our study is that we made suggestions based on cell viability and mRNA expression analysis, and more confirmatory studies would be needed to support our suggestions. However, more experiments would be needed to support our data. We hope that we have established the basics for further research in this field. As a future perspective, we would suggest supporting our data by testing more cannabinoid extracts, protein expression, apoptosis assays, and animal models.

References

1. Canadian Cancer Statistics Advisory Committee. Canadian cancer statistics 2019. Toronto ON: Canadian Cancer Society. Available at: cancer.ca/Canadian-Cancer-Statistics-2019-EN. 2019.

2. WHO. Global status report on noncommunicable diseases. https://www.who.int/nmh/publications/ncd_report_full_en.pdf. 2020;1–162.

3. Sung H, Ferlay J, Siegel RL, Laversanne M, Soerjomataram I, Jemal A, et al. Global cancer statistics 2020: GLOBOCAN estimates of incidence and mortality worldwide for 36 cancers in 185 countries. CA Cancer J Clin. 2021;0(0):1–41.

4. Testa U, Pelosi E, Castelli G. Colorectal Cancer: Genetic Abnormalities, Tumor Progression, Tumor Heterogeneity, Clonal Evolution and Tumor-Initiating Cells. Medical Sciences. 2018;6(2):31.

5. Fearon ER;, Vogelstein B. A genetic model for colorectal tumorigenesis. Cell. 1990;61:759–67.

6. Funkhouser WK, Lubin IM, Monzon FA, Zehnbauer BA, Evans JP, Ogino S, et al. Relevance, Pathogenesis, and testing algorithm for mismatch repair-defective colorectal carcinomas: A report of the association for molecular pathology. Journal of Molecular Diagnostics. 2012;14(2):91–103.

7. Guinney J, Dienstmann R, Wang X, De Reyniès A, Schlicker A, Soneson C, et al. The consensus molecular subtypes of colorectal cancer. Nat Med. 2015;21(11):1350–6.

8. Rodriguez-Salas N, Dominguez G, Barderas R, Mendiola M, García-Albéniz X, Maurel J, et al. Clinical relevance of colorectal cancer molecular subtypes. Crit Rev Oncol Hematol. 2017;109:9–19.

9. Nallathambi R, Mazuz M, Ion A, Selvaraj G, Weininger S, Fridlender M, et al. Anti-Inflammatory Activity in Colon Models Is Derived from Δ9-Tetrahydrocannabinolic Acid That Interacts with Additional Compounds in *Cannabis* Extracts. Cannabis Cannabinoid Res. 2017;2(1):167–82.

10. Li SKH, Martin A. Mismatch Repair and Colon Cancer: Mechanisms and Therapies Explored. Trends Mol Med. 2016;22(4):274–89.

11. Hall W, Christie M, Currow D. Cannabinoids and cancer: Causation, remediation, and palliation. Lancet Oncology. 2005;6(1):35–42.

12. Lakatos PL, Lakatos L. Risk for colorectal cancer in ulcerative colitis: Changes, causes and management strategies. World J Gastroenterol. 2008;14(25):3937–47.

13. Sakamoto K, Maeda S, Hikiba Y, Nakagawa H, Hayakawa Y, Shibata W, et al. Constitutive NF-κB activation in colorectal carcinoma plays a key role in angiogenesis, promoting tumor growth. Clinical Cancer Research. 2009;15(7):2248–58.

14. Yu H, Pardoll D, Jove R. STATs in cancer inflammation and immunity: A leading role for STAT3. Nat Rev Cancer. 2009;9(11):798–809.

15. Terzić J, Grivennikov S, Karin E, Karin M. Inflammation and Colon Cancer. Gastroenterology. 2010;138(6):2101–14.

16. Castellone MD, Teramoto H, Williams BO, Druey KM, Gutkind JS. Prostaglandin E2 promotes colon cancer cell growth through a Gs-axin-β-catenin signaling axis. Science (1979). 2005;310(5753):1504–10.

17. Kaler P, Augenlicht L, Klampfer L. Macrophage-derived IL-1B stimulates Wnt signaling and growth of colon cancer cells: A crosstalk interrupted by vitamin D3. Oncogene. 2009;28(44):3892–902.

18. Leedham SJ, Graham TA, Oukrif D, McDonald SAC, Rodriguez-Justo M, Harrison RF, et al. Clonality, Founder Mutations, and Field Cancerization in Human Ulcerative Colitis-Associated Neoplasia. Gastroenterology. 2009;136(2):542-550.e6.

19. Takaku K, Oshima M, Miyoshi H, Matsui M, Seldin MF, Taketo MM. Intestinal tumorigenesis in compound mutant mice of both Dpc4 (Smad4) and Apc genes. Cell. 1998;92(5):645–56.

20. Oshima M, Dinchuk JE, Kargman SL, Oshima H, Hancock B, Kwong E, et al. Suppression of intestinal polyposis in Apc(Δ716) knockout mice by inhibition of cyclooxygenase 2 (COX-2). Cell. 1996;87(5):803–9.

21. Atreya I, Neurath MF. Immune cells in colorectal cancer: Prognostic relevance and therapeutic strategies. Expert Rev Anticancer Ther. 2008;8(4):561–72.

22. Cianchi F, Papucci L, Schiavone N, Lulli M, Magnelli L, Vinci MC, et al. Cannabinoid receptor activation induces apoptosis through tumor necrosis factor α-mediated ceramide de novo synthesis in colon cancer cells. Clinical Cancer Research. 2008;14(23):7691–700.

23. Nallathambi R, Mazuz M, Namdar D, Shik M, Namintzer D, Vinayaka AC, et al. Identification of Synergistic Interaction Between Cannabis-Derived Compounds for Cytotoxic Activity in Colorectal Cancer Cell Lines and Colon Polyps That Induces Apoptosis-Related Cell Death and Distinct Gene Expression. 2018;3:120–35.

24. Javid FA, Phillips RM, Afshinjavid S, Verde R, Ligresti A. Cannabinoid pharmacology in cancer research : A new hope for cancer patients ? Eur J Pharmacol. 2016;775:1–14.

25. Raup-Konsavage WM, Johnson M, Legare CA, Yochum GS, Morgan DJ, Vrana KE. Synthetic cannabinoid activity against colorectal cancer cells. Cannabis Cannabinoid Res. 2018;3(1):272–81.

26. Wang D, Wang H, Ning W, Backlund MG, Dey SK, Dubois RN. Loss of cannabinoid receptor 1 accelerates intestinal tumor growth. 2009;68(15):6468–76.

27. Tutino V, Caruso MG, De Nunzio V, Lorusso D, Veronese N, Gigante I, et al. Down-regulation of cannabinoid type 1 (CB1) receptor and its downstream signaling pathways in metastatic colorectal cancer. Cancers (Basel). 2019;11(5).

28. Ligresti A, Bisogno T, Matias I, De Petrocellis L, Cascio MG, Cosenza V, et al. Possible endocannabinoid control of colorectal cancer growth. Gastroenterology. 2003;125(3):677–87.

29. Anderson SP, Zylla DM, McGriff DM, Arneson TJ. Impact of Medical Cannabis on Patient-Reported Symptoms for Patients With Cancer Enrolled in Minnesota's Medical Cannabis Program. J Oncol Pract. 2019;15(4):e338–45.

30. Grill M, Högenauer C, Blesl A, Haybaeck J, Golob-Schwarzl N, Ferreirós N, et al. Members of the endocannabinoid system are distinctly regulated in inflammatory bowel disease and colorectal cancer. Sci Rep. 2019;9(1):1–13.

31. Madras BK. Update of Cannabis and its medical use. Alcohol and drug abuse research. 2015;5(37):1–41.

32. Hoffenberg EJ, McWilliams S, Mikulich-Gilbertson S, Murphy B, Hoffenberg A, Hopfer CJ. Cannabis oil use by adolescents and young adults with inflammatory bowel disease. J Pediatr Gastroenterol Nutr. 2019;68(3):348–52.

33. Couch DG, Cook H, Ortori C, Barrett D, Lund JN, O'Sullivan SE. Palmitoylethanolamide and Cannabidiol Prevent Inflammation-induced Hyperpermeability of the Human Gut in Vitro and in Vivo-A Randomized, Placebo-controlled, Double-blind Controlled Trial. Inflamm Bowel Dis. 2019;25(6):1006–18.

34. Sanger GJ. Endocannabinoids and the gastrointestinal tract: What are the key questions? Br J Pharmacol. 2007;152(5):663–70.

35. Greenhough A, Patsos HA, Williams AC, Paraskeva C. The cannabinoid Δ9-tetrahydrocannabinol inhibits RAS-MAPK and PI3K-AKT survival signalling and induces BAD-mediated apoptosis in colorectal cancer cells. Int J Cancer. 2007;121(10):2172–80.

36. Pellerito O, Notaro A, Sabella S, de Blasio A, Vento R, Calvaruso G, et al. WIN induces apoptotic cell death in human colon cancer cells through a block of autophagic flux dependent on PPARγ down-regulation. Apoptosis. 2014;19(6):1029–42.

37. Jeong S, Yun HK, Jeong YA, Jo MJ, Kang SH, Kim JL, et al. Cannabidiol-induced apoptosis is mediated by activation of Noxa in human colorectal cancer cells. Cancer Lett [Internet]. 2019;447(December 2018):12–23. Available from: https://doi.org/10.1016/j.canlet.2019.01.011

38. Romano B, Borrelli F, Pagano E, Cascio MG, Pertwee RG, Izzo AA. Inhibition of colon carcinogenesis by a standardized Cannabis sativa extract with high content of cannabidiol. Phytomedicine [Internet]. 2014;21(5):631–9. Available from: http://dx.doi.org/10.1016/j.phymed.2013.11.006

39. Pagano E, Capasso R, Piscitelli F, Romano B, Parisi OA, Finizio S, et al. An orally active Cannabis extract with high content in cannabidiol attenuates chemically-induced intestinal inflammation and hypermotility in the mouse. Front Pharmacol. 2016;7(OCT):1–12.

40. Orrego-González E, Londoño-Tobón L, Ardila-González J, Polania-Tovar D, Valencia-Cárdenas A, Velez-Van Meerbeke A. Cannabinoid Effects on Experimental Colorectal Cancer Models Reduce Aberrant Crypt Foci (ACF) and Tumor Volume: A Systematic Review. Evidence-based Complementary and Alternative Medicine. 2020;2020.

41. Izzo AA, Aviello G, Petrosino S, Orlando P, Marsicano G, Lutz B, et al. Increased endocannabinoid levels reduce the development of precancerous lesions in the mouse colon. J Mol Med. 2008;86(1):89–98.

42. De Petrocellis L, Ligresti A, Moriello AS, Allarà M, Bisogno T, Petrosino S, et al. Effects of cannabinoids and cannabinoid-enriched Cannabis extracts on TRP channels and endocannabinoid metabolic enzymes. Br J Pharmacol. 2011;163(7):1479–94.

43. Nallathambi R, Mazuz M, Ion A, Selvaraj G, Weininger S, Fridlender M, et al. Anti-Inflammatory Activity in Colon Models Is Derived from Δ9-Tetrahydrocannabinolic Acid That Interacts with Additional Compounds in Cannabis Extracts . Cannabis Cannabinoid Res. 2017;2(1):167–82.

44. Ryberg E, Larsson N, Sjögren S, Hjorth S, Hermansson NO, Leonova J, et al. The orphan receptor GPR55 is a novel cannabinoid receptor. Br J Pharmacol. 2007;152(7):1092–101.

45. Hasenoehrl C, Feuersinger D, Sturm EM, Bärnthaler T, Graf R, Grill M, et al. G protein-coupled receptor GPR55 promotes colorectal cancer and has opposing effects to cannabinoid receptor 1. Int J Cancer. 2018;142(1):121–32.

46. Dall'Stella PB, Docema MFL, Maldaun MVC, Feher O, Lancellotti CLP. Case report: Clinical outcome and image response of two patients with secondary high-grade glioma treated with chemoradiation, PCV, and cannabidiol. Front Oncol. 2019;9(JAN):1–7.

47. Sulé-Suso J, Watson NA, van Pittius DG, Jegannathen A. Striking lung cancer response to self-administration of cannabidiol: A case report and literature review. SAGE Open Med Case Rep. 2019;7:2050313X1983216.

48. Erices JI, Torres Á, Niechi I, Bernales I, Quezada C. Current natural therapies in the treatment against glioblastoma. Phytotherapy Research. 2018;32(11):2191–201.

49. Zhang MW, Ho RCM. The Cannabis Dilemma: A Review of Its Associated Risks and Clinical Efficacy. J Addict. 2015;2015:1–6.

50. Howlett AC. The cannabinoid receptors. Prostaglandins Other Lipid Mediat. 2002;68–69:619–31.

51. Lutz B. Molecular biology of cannabinoid receptors. Prostaglandins Leukot Essent Fatty Acids. 2002;66(2–3):123–42.

52. Glass M, Northup JK. Agonist selective regulation of G proteins by cannabinoid CB1 and CB2 receptors. Mol Pharmacol. 1999;56(6):1362–9.

53. Jin W, Brown S, Roche JP, Hsieh C, Celver JP, Kovoor A, et al. Distinct domains of the CB1 cannabinoid receptor mediate desensitization and internalization. Journal of Neuroscience. 1999;19(10):3773–80.

54. Mackie K, Hille B. Cannabinoids inhibit N-type calcium channels in neuroblastoma-glioma cells. Proc Natl Acad Sci U S A. 1992;89(9):3825–9.

55. Caulfield MP, Brown DA. Cannabinoid receptor agonists inhibit Ca current in NG108–15 neuroblastoma cells via a Pertussis toxin-sensitive mechanism. Br J Pharmacol. 1992;106(2):231–2.

56. Mackie K, Lai Y, Westenbroek R, Mitchell R. Cannabinoids activate an inwardly rectifying potassium conductance and inhibit Q-type calcium currents in AtT20 cells transfected with rat brain cannabinoid receptor. Journal of Neuroscience. 1995;15(10):6552–61.

57. Henry DJ, Chavkin C. Activation of inwardly rectifying potassium channels (GIRK1) by co- expressed rat brain cannabinoid receptors in Xenopus oocytes. Neuroscience letterse. 1995;186:91–4.

58. Watkins AR. Cannabinoid interactions with ion channels and receptors. Channels. 2019;13(1):162–7.

59. Sun Y, Bennett A. Cannabinoids: A new group of agonists of PPARs. PPAR Res. 2007;2007.

60. Pacher P, Bátkai S, Kunos G. The endocannabinoid system as an emerging target of pharmacotherapy. Pharmacol Rev. 2006;58(3):389–462.

61. Cristino L, Bisogno T, Di Marzo V. Cannabinoids and the expanded endocannabinoid system in neurological disorders. Nat Rev Neurol. 2020;16(1):9–29.

62. Di Marzo V. New approaches and challenges to targeting the endocannabinoid system. Nat Rev Drug Discov. 2018;17(9):623–39.

63. Monsalve FA, Pyarasani RD, Delgado-Lopez F, Moore-Carrasco R. Peroxisome proliferator-activated receptor targets for the treatment of metabolic diseases. Mediators Inflamm. 2013;2013.

64. Marquéz L, Suárez J, Iglesias M, Bermudez-Silva FJ, de Fonseca FR, Andreu M. Ulcerative colitis induces changes on the expression of the endocannabinoid system in the human colonic tissue. PLoS ONE. 2009;4(9).

65. Kulkarni-Narla A, Brown DR. Localization of CB1-cannabinoid receptor immunoreactivity in the porcine enteric nervous system. Cell and Tissue Research. 2000;302(1):73–80.

66. Argaw A, Duff G, Zabouri N, Cecyre B, Chaine N, Cherif H, et al. Concerted Action of CB1 Cannabinoid Receptor and Deleted in Colorectal Cancer in Axon Guidance. Journal of Neuroscience. 2011;31(4):1489–99.

67. Gyires K, S. Zádori Z. Role of Cannabinoids in Gastrointestinal Mucosal Defense and Inflammation. Curr Neuropharmacol. 2016;14(8):935–51.

68. Duncan M, Davison JS, Sharkey KA. Review article: Endocannabinoids and their receptors in the enteric nervous system. Alimentary Pharmacology and Therapeutics. 2005;22(8):667–83.

69. Starowicz K, Nigam S, Di Marzo V. Biochemistry and pharmacology of endovanilloids. Pharmacology and Therapeutics. 2007;114(1):13–33.

70. Ward SM, Bayguinov J, Won KJ, Grundy D, Berthoud HR. Distribution of the vanilloid receptor (VR1) in the gastrointestinal tract. Journal of Comparative Neurology. 2003;465(1):121–35.

71. Hasenoehrl C, Taschler U, Storr M. The gastrointestinal tract – a central organ of cannabinoid signaling in health and disease. 2016;1765–80.

72. Di Marzo V. Targeting the endocannabinoid system: To enhance or reduce? Nat Rev Drug Discov. 2008;7(5):438–55.

73. Cani PD, Plovier H, Van Hul M, Geurts L, Delzenne NM, Druart C, et al. Endocannabinoids-at the crossroads between the gut microbiota and host metabolism. Nat Rev Endocrinol. 2016;12(3):133–43.

74. Storr MA, Sharkey KA. The endocannabinoid system and gut-brain signalling. Curr Opin Pharmacol. 2007;7(6):575–82.

75. Wang D, Wang H, Ning W, Backlund MG, Dey SK, DuBois RN. Loss of cannabinoid receptor 1 accelerates intestinal tumor growth. Cancer Res. 2008;68(15):6468–76.

76. Cianchi F, Papucci L, Schiavone N, Lulli M, Magnelli L, Vinci MC, et al. Cannabinoid receptor activation induces apoptosis through tumor necrosis factor α-mediated ceramide de novo synthesis in colon cancer cells. Clinical Cancer Research. 2008;14(23):7691–700.

77. Izzo AA, Camilleri M. Cannabinoids in intestinal inflammation and cancer. Pharmacol Res. 2009;60(2):117–25.

78. Martinez-Martinez E, Gomez I, Martin P, Sanchez A, Roman L, Tejerina E, et al. Cannabinoids receptor type 2, CB2, expression correlates with human colon cancer progression and predicts patient survival. Oncoscience. 2015;2(2):131.

79. Gustafsson SB, Palmqvist R, Henriksson ML, Dahlin AM, Edin S, Jacobsson SOP, et al. High tumour cannabinoid CB 1 receptor immunoreactivity negatively impacts disease-specific survival in stage II microsatellite stable colorectal cancer. PLoS One. 2011;6(8).

80. Cudaback E, Marrs W, Moeller T, Stella N. The expression level of CB1 and CB2 receptors determines their efficacy at inducing apoptosis in astrocytomas. PLoS One. 2010;5(1).

81. Pertwee RG, Cascio MG. Known Pharmacological Actions of Delta-9-Tetrahydrocannabinol and of Four Other Chemical Constituents of Cannabis that Activate Cannabinoid Receptors. Handbook of Cannabis. 2015;115–36.

82. Henstridge CM, Balenga NAB, Kargl J, Andradas C, Brown AJ, Irving A, et al. Minireview: Recent developments in the physiology and pathology of the lysophosphatidylinositol-sensitive receptor GPR55. Molecular Endocrinology. 2011;25(11):1835–48.

83. Ross RA. L-α-Lysophosphatidylinositol meets GPR55: A deadly relationship. Trends Pharmacol Sci. 2011;32(5):265–9.

84. Henstidge CM, Balenga NAB, Ford LA, Ross RA, Waldhoer M, Irving AJ. The GPR55 ligand L-α-lysophosphatidylinositol promotes RhoA-dependent Ca 2+ signaling and NFAT activation . The FASEB Journal. 2009;23(1):183–93.

85. Andradas C, Caffarel MM, Pérez-Gómez E, Salazar M, Lorente M, Velasco G, et al. The orphan G protein-coupled receptor GPR55 promotes cancer cell proliferation via ERK. Oncogene. 2011;30(2):245–52.

86. Kargl J, Andersen L, Hasenöhrl C, Feuersinger D, Stančic A, Fauland A, et al. GPR55 promotes migration and adhesion of colon cancer cells indicating a role in metastasis. Br J Pharmacol. 2016;173(1):142–54.

87. Stančić A, Jandl K, Hasenöhrl C, Reichmann F, Marsche G, Schuligoi R, et al. The GPR55 antagonist CID16020046 protects against intestinal inflammation. Neurogastroenterology and Motility. 2015;27(10):1432–45.

88. Balenga NAB, Aflaki E, Kargl J, Platzer W, Schröder R, Blättermann S, et al. GPR55 regulates cannabinoid 2 receptor-mediated responses in human neutrophils. Cell Res. 2011;21(10):1452–69.

89. Izzo AA, Muccioli GG, Ruggieri MR, Schicho R. Endocannabinoids and the Digestive Tract and Bladder in Health and Disease. Handb Exp Pharmacol. 2015;231:423–47.

90. Chen L, Chen H, Li Y, Li L, Qiu Y, Ren J. Endocannabinoid and ceramide levels are altered in patients with colorectal cancer. Oncol Rep. 2015;34(1):447–54.

91. Jeong S, Yun HK, Jeong YA, Jo MJ, Kang SH, Kim JL, et al. Cannabidiol-induced apoptosis is mediated by activation of Noxa in human colorectal cancer cells. Cancer Lett. 2019;447(December 2018):12–23.

92. Sreevalsan S, Joseph S, Jutooru I, Chadalapaka G, Safe SH. Induction of Apoptosis by Cannabinoids in Prostate and Colon Cancer Cells Is Phosphatase Dependent. Anticancer Res. 2011;31(11):3799–807.

93. Mullen TD, Hannun YA, Obeid LM. Ceramide synthases at the centre of sphingolipid metabolism and biology. Biochemical Journal. 2012;441(3):789–802.

94. Tidhar R, Ben-Dor S, Wang E, Kelly S, Merrill AH, Futerman AH. Acyl chain specificity of ceramide synthases is determined within a region of 150 residues in the tram-lag-CLN8 (TLC) domain. Journal of Biological Chemistry. 2012;287(5):3197–206.

95. Morad SAF, Cabot MC. Ceramide-orchestrated signalling in cancer cells. Nat Rev Cancer. 2013;13(1):51–65.

96. Sánchez C, Galve-Roperh I, Rueda D, Guzmán M. Involvement of sphingomyelin hydrolysis and the mitogen-activated protein kinase cascade in the Δ9-Tetrahydrocannabinol-induced stimulation of glucose metabolism in primary astrocytes. Mol Pharmacol. 1998;54(5):834–43.

97. Ogretmen B, Hannun YA. Biologically active sphingolipids in cancer pathogenesis and treatment. Nat Rev Cancer. 2004;4(8):604–16.

98. Velasco G, Sánchez C, Guzmán M. Towards the use of cannabinoids as antitumour agents. Nat Rev Cancer [Internet]. 2012;12(6):436–44. Available from: http://dx.doi.org/10.1038/nrc3247

99. Wang D, Wang H, Ning W, Backlund MG, Dey SK, DuBois RN. Loss of cannabinoid receptor 1 accelerates intestinal tumor growth. Cancer Res. 2008;68(15):6468–76.

100. Hasenoehrl C, Taschler U, Storr M, Schicho R. The gastrointestinal tract – a central organ of cannabinoid signaling in health and disease. Neurogastroenterology and Motility. 2016;28(12):1765–80.

101. Adam-Klages S, Adam D, Wiegmann K, Struve S, Kolanus W, Schneider-Mergener J, et al. FAN, a novel WD-repeat protein, couples the p55 TNF-receptor to neutral sphingomyelinase. Cell. 1996;86(6):937–47.

102. White-Gilbertson S, Mullen T, Senkal C, Lu P, Ogretmen B, Obeid L, et al. Ceramide synthase 6 modulates TRAIL sensitivity and nuclear translocation of active caspase-3 in colon cancer cells. Oncogene. 2009;28(8):1132–41.

103. Osawa Y, Uchinami H, Bielawski J, Schwabe RF, Hannun YA, Brenner DA. Roles for C16-ceramide and sphingosine 1-phosphate in regulating hepatocyte apoptosis in response to tumor necrosis factor-α. Journal of Biological Chemistry. 2005;280(30):27879–87.

104. Bos JL, Vries MV de, Van Der Eb AJ, Fearon ER, Vogelstein B, Hamilton SR, et al. Prevalence of ras gene mutations in human colorectal cancers. Nature. 1987;327(6120):293–7.

105. Davies H, Bignell GR, Cox C, Stephens P, Edkins S, Clegg S, et al. Mutations of the BRAF gene in human cancer. Nature. 2002;417(6892):949–54.

106. Parsons DW, Wang TL, Samuels Y, Bardelli A, Cummins JM, DeLong L, et al. Colorectal cancer: Mutations in a signalling pathway. Nature. 2005;436(7052):792.

107. Hart S, Fischer OM, Ullrich A. Cannabinoids Induce Cancer Cell Proliferation via Tumor Necrosis Factor α-Converting Enzyme (TACE/ADAM17)-Mediated Transactivation of the Epidermal Growth Factor Receptor. Cancer Res. 2004;64(6):1943–50.

108. Premoli M, Aria F, Bonini SA, Maccarinelli G, Gianoncelli A, Pina S Della, et al. Cannabidiol: Recent advances and new insights for neuropsychiatric disorders treatment. Life Sci. 2019;224(February):120–7.

109. McCarberg BH, Barkin RL. The future of cannabinoids as analgesic agents: A pharmacologic, pharmacokinetic, and pharmacodynamic overview. Am J Ther. 2007;14(5):475–83.

110. Johansson E, Ohlsson A, Lindgren J -E, Agurell S, Gillespie H, Hollister LE. Single-dose kinetics of deuterium-labelled cannabinol in man after intravenous administration and smoking. Biomed Environ Mass Spectrom. 1987;14(9):495–9.

111. Yuan Y, Xu X, Zhao C, Zhao M, Wang H, Zhang B, et al. The roles of oxidative stress, endoplasmic reticulum stress, and autophagy in aldosterone/mineralocorticoid receptor-induced podocyte injury. Laboratory Investigation. 2015;95(12):1374–86.

112. Sano R, Reed JC. ER stress-induced cell death mechanisms. Biochim Biophys Acta. 2013;1833(12):1–26.

113. Narita T, Ri M, Masaki A, Mori F, Ito A, Kusumoto S, et al. Lower expression of activating transcription factors 3 and 4 correlates with shorter progression-free survival in multiple myeloma patients receiving bortezomib plus dexamethasone therapy. Blood Cancer J. 2015;5(November 2014).

114. Kim JL, Kim BR, Kim DY, Jeong YA, Jeong S, Na YJ, et al. Cannabidiol enhances the therapeutic effects of TRAIL by upregulating DR5 in colorectal cancer. Cancers (Basel). 2019;11(5):1–14.

115. Salvesen GS, Duckett CS. IAP proteins: Blocking the road to death's door. Nat Rev Mol Cell Biol. 2002;3(6):401–10.

116. Altieri DC. Validating survivin as a cancer therapeutic target. Nat Rev Cancer. 2003;3(1):46–54.

117. György B, Szabó TG, Pásztói M, Pál Z, Misják P, Aradi B, et al. Membrane vesicles, current state-of-the-art: Emerging role of extracellular vesicles. Cellular and Molecular Life Sciences. 2011;68(16):2667–88.

118. Ansa-Addo EA, Lange S, Stratton D, Antwi-Baffour S, Cestari I, Ramirez MI, et al. Human Plasma Membrane-Derived Vesicles Halt Proliferation and Induce Differentiation of THP-1 Acute Monocytic Leukemia Cells. The Journal of Immunology. 2010;185(9):5236–46.

119. Muralidharan-Chari V, Clancy JW, Sedgwick A, D'Souza-Schorey C. Microvesicles: Mediators of extracellular communication during cancer progression. J Cell Sci. 2010;123(10):1603–11.

120. Turola E, Furlan R, Bianco F, Matteoli M, Verderio C. Microglial microvesicle secretion and intercellular signaling. Front Physiol. 2012;3(May):1–11.

121. Baroni M, Pizzirani C, Pinotti M, Ferrari D, Adinolfi E, Calzavarini S, et al. Stimulation of P2 (P2X 7) receptors in human dendritic cells induces the release of tissue factor-bearing microparticles . The FASEB Journal. 2007;21(8):1926–33.

122. Bergsmedh A, Szeles A, Henriksson M, Bratt A, Folkman MJ, Spetz AL, et al. Horizontal transfer of oncogenes by uptake of apoptotic bodies. Proc Natl Acad Sci U S A. 2001;98(11):6407–11.

123. Hoshino A, Costa-Silva B, Shen TL, Rodrigues G, Hashimoto A, Tesic Mark M, et al. Tumour exosome integrins determine organotropic metastasis. Nature. 2015;527(7578):329–35.

124. Kosgodage US, Mould R, Henley AB, Nunn A V., Guy GW, Thomas EL, et al. Cannabidiol (CBD) is a novel inhibitor for exosome and microvesicle (EMV) release in cancer. Front Pharmacol. 2018;9(AUG).

125. Choi AMK, Ryter SW, Levine B. Mechanisms of disease: Autophagy in human health and disease. New England Journal of Medicine. 2013;368(7):651–62.

126. Hua Y, Zhu Y, Zhang J, Zhu Z, Ning Z, Chen H, et al. MiR-122 targets X-linked inhibitor of apoptosis protein to sensitize oxaliplatin-resistant colorectal cancer cells to oxaliplatin-mediated cytotoxicity. Cellular Physiology and Biochemistry. 2018;51(5):2148–59.

127. Tan S, Peng X, Peng W, Zhao Y, Wei Y. Enhancement of oxaliplatin-induced cell apoptosis and tumor suppression by 3-methyladenine in colon cancer. Oncol Lett. 2015;9(5):2056–62.

128. Jeong S, Kim BG, Kim DY, Kim BR, Kim JL, Park SH, et al. Cannabidiol overcomes oxaliplatin resistance by enhancing NOS3- and SOD2-Induced autophagy in human colorectal cancer cells. Cancers (Basel). 2019;11(6):1–18.

129. Schläfli AM, Berezowska S, Adams O, Langer R, Tschan MP. Reliable LC3 and p62 autophagy marker detection in formalin fixed paraffin embedded human tissue by immunohistochemistry. European Journal of Histochemistry. 2015;59(2):137–44.

130. Tournier N, Chevillard L, Megarbane B, Pirnay S, Scherrmann JM, Declèves X. Interaction of drugs of abuse and maintenance treatments with human P-glycoprotein (ABCB1) and breast cancer resistance protein (ABCG2). International Journal of Neuropsychopharmacology. 2010;13(7):905–15.

131. Holland ML, Allen JD, Arnold JC. Interaction of plant cannabinoids with the multidrug transporter ABCC1 (MRP1). Eur J Pharmacol. 2008;591(1–3):128–31.

132. Holland ML, Lau DTT, Allen JD, Arnold JC. The multidrug transporter ABCG2 (BCRP) is inhibited by plant-derived cannabinoids. Br J Pharmacol. 2007;152(5):815–24.

133. Stout SM, Cimino NM. Exogenous cannabinoids as substrates, inhibitors, and inducers of human drug metabolizing enzymes: A systematic review. Drug Metab Rev. 2014;46(1):86–95.

134. Pagano E, Borrelli F, Orlando P, Romano B, Monti M, Morbidelli L, et al. Pharmacological inhibition of MAGL attenuates experimental colon carcinogenesis. Pharmacol Res [Internet]. 2017;119:227–36. Available from: http://dx.doi.org/10.1016/j.phrs.2017.02.002

135. Notarnicola M, Messa C, Orlando A, Bifulco M, Laezza C, Gazzerro P, et al. Estrogenic induction of cannabinoid CB1 receptor in human colon cancer cell lines. Scand J Gastroenterol. 2008;43(1):66–72.

136. Thapa D, Kang Y, Park PH, Noh SK, Lee YR, Han SS, et al. Anti-tumor activity of the novel hexahydrocannabinol analog LYR-8 in human colorectal tumor xenograft is mediated through the inhibition of Akt and hypoxia-inducible factor-1α activation. Biol Pharm Bull. 2012;35(6):924–32.

137. Peters M, Kogan NM. HU-331: A cannabinoid quinone, with uncommon cytotoxic properties and low toxicity. Expert Opin Investig Drugs. 2007;16(9):1405–13.

138. Solinas M, Massi P, Cinquina V, Valenti M, Bolognini D, Gariboldi M, et al. Cannabidiol, a Non-Psychoactive Cannabinoid Compound, Inhibits Proliferation and Invasion in U87-MG and T98G Glioma Cells through a Multitarget Effect. PLoS One. 2013;8(10).

139. Solinas M, Massi P, Cantelmo AR, Cattaneo MG, Cammarota R, Bartolini D, et al. Cannabidiol inhibits angiogenesis by multiple mechanisms. Br J Pharmacol. 2012;167(6):1218–31.

140. Stanley CP, Hind WH, Tufarelli C, O'Sullivan SE. Cannabidiol causes endothelium-dependent vasorelaxation of human mesenteric arteries via CB1 activation. Cardiovasc Res. 2015;107(4):568–78.

141. Joseph J, Niggemann B, Zaenker KS, Entschladen F. Anandamide is an endogenous inhibitor for the migration of tumor cells and T lymphocytes. Cancer Immunology, Immunotherapy. 2004;53(8):723–8.

142. Rosenberg B., van Camp L., Krigas T. Inhibition of cell division in escherichia coli by electrolysis products from a platinum electrode. Nature. 1965;205:698–9.

143. Kelland L. The resurgence of platinum-based cancer chemotherapy. Vol. 7, Nature Reviews Cancer. 2007. p. 573–84.

144. Dasari S, Bernard Tchounwou P. Cisplatin in cancer therapy: Molecular mechanisms of action. Eur J Pharmacol. 2014 Oct 5;740:364–78.

145. Milczarek M, Rosinska S, Psurski M, Maciejewska M. Combined Colonic Cancer Treatment with Vitamin D Analogs and Irinotecan or Oxaliplatin. Anticancer Res [Internet]. 2013;33:433–44. Available from: https://www.researchgate.net/publication/235423262

146. Kosmas C, Tsavaris NB, Malamos NA, Vadiaka M, Koufos C. Phase II study of paclitaxel, ifosfamide, and cisplatin as second-line treatment in relapsed small-cell lung cancer. Journal of Clinical Oncology. 2001;19(1):119–26.

147. Iwasaki Y, Nagata K, Nakanishi M, Natuhara A, Kubota Y, Ueda M, et al. Double-cycle, high-dose ifosfamide, carboplatin, and etoposide followed by peripheral blood stem-cell transplantation for small cell lung cancer. Chest. 2005;128(4):2268–73.

148. Saad SY, Najjar TA, Alashari M. Role Of Non-Selective Adenosine Receptor Blockade And Phosphodiesterase Inhibition In Cisplatin-Induced Nephrogonadal Toxicity In Rats. Clin Exp Pharmacol Physiol. 2004;31:862–7.

149. Desoize B. Cancer and Metals and Metal Compounds:Part I — Carcinogenesis. Critical Reviewes in Oncology/Hematology [Internet]. 2002;42:1–3. Available from: www.elsevier.com/locate/critrevonc

150. Aggarwal SK. A Histochemical Approach to the Mechanism of Action of Cisplatin and Its Analogues. The Journal of Histochemistry and Cytochemistry. 1993;41(7):1013–73.

151. Aggarwal SK. Calcium Modulation of Toxicities due to Cisplatin. Met Based Drugs. 1998;5(2):77–81.

152. Dehaan RD, Yazlovitskaya EM, Persons DL. Regulation of p53 target gene expression by cisplatin-induced extracellular signal-regulated kinase. Cancer Chemother Pharmacol. 2001;48(5):383–8.

153. Siddik ZH. Cisplatin: Mode of cytotoxic action and molecular basis of resistance. Vol. 22, Oncogene. 2003. p. 7265–79.

154. Persons DL, Yazlovitskaya EM, Pelling JC. Effect of extracellular signal-regulated kinase on p53 accumulation in response to cisplatin. Journal of Biological Chemistry. 2000 Nov 17;275(46):35778–85.

155. Cuadrado A, Lafarga V, Cheung PCF, Dolado I, Llanos S, Cohen P, et al. A new p38 MAP kinase-regulated transcriptional coactivator that stimulates p53-dependent apoptosis. EMBO Journal. 2007 Apr 18;26(8):2115–26.

156. Winograd-Katz SE, Levitzki A. Cisplatin induces PKB/Akt activation and p38MAPK phosphorylation of the EGF receptor. Oncogene. 2006 Nov 30;25(56):7381–90.

157. Jun Hayakawa, Masahide Ohmichi, Hirohisa Kurachi, Yuki Kanda, Koji Hisamoto, Yukihiro Nishio, et al. Inhibition of BAD Phosphorylation Either at Serine 112 via Extracellular Signal-regulated Protein Kinase Cascade or at Serine 136 via Akt Cascade Sensitizes Human Ovarian Cancer Cells to Cisplatin. Cancer Res [Internet]. 2000;60:5988–94. Available from: https://www.researchgate.net/publication/12241334

158. Hayakawa J, Mittal S, Wang Y, Korkmaz KS, Adamson E, English C, et al. Identification of promoters bound by c-Jun/ATF2 during rapid large-scale gene activation following genotoxic stress. Vol. 17, Molecular Cell. 2004. p. 521–35.

159. Mitsuuchi Y JSSMWSHTTJ. The phosphatidylinositol 3-kinase/AKT signal transduction pathway plays a critical role in the expression of p21WAF1/CIP1/SDI1 induced by cisplatin and paclitaxel. Cancer Res . 2000;60(19):5390–4.

160. Donner DB, Mayo LD. The PTEN, Mdm2, p53 tumor suppressor-oncoprotein network [Internet]. Vol. 27, TRENDS in Biochemical Sciences. 2002. Available from: http://tibs.trends.com

161. Asselin E MGTB. XIAP regulates Akt activity and caspase-3-dependent cleavage during cisplatin-induced apoptosis in human ovarian epithelial cancer cells. Cancer Res. 2001;61(5):1862–8.

162. Shi Y, Felley-Bosco E, Marti TM, Orlowski K, Pruschy M, Stahel RA. Starvation-induced activation of ATM/Chk2/p53 signaling sensitizes cancer cells to cisplatin. BMC Cancer [Internet]. 2012;12(571). Available from: http://www.biomedcentral.com/1471-2407/12/571

163. Kaeberlein TL, Smith ED, Tsuchiya M, Welton KL, Thomas JH, Fields S, et al. Lifespan extension in Caenorhabditis elegans by complete removal of food. Aging Cell. 2006 Dec;5(6):487–94.

164. Wei M, Fabrizio P, Hu J, Ge H, Cheng C, Li L, et al. Life span extension by calorie restriction depends on Rim15 and transcription factors downstream of Ras/PKA, Tor, and Sch9. PLoS Genet. 2008;4(1):0139–49.

165. Gonidakis S, Finkel SE, Longo VD. Genome-wide screen identifies Escherichia coli TCA-cycle-related mutants with extended chronological lifespan dependent on acetate

metabolism and the hypoxia-inducible transcription factor ArcA. Aging Cell. 2010 Oct;9(5):868–81.

166. Goodrick C.L., Ingram D.K., Reynolds M.A., Freeman J.R., Cider N. Effects of intermittent feeding upon body weight and lifespan in inbred mice- interaction of genotype and age. Mechanisms of Aging and Development. 1990;55:69–87.

167. Gjedsted J, Gormsen LC, Nielsen S, Schmitz O, Djurhuus CB, Keiding S, et al. Effects of a 3-day fast on regional lipid and glucose metabolism in human skeletal muscle and adipose tissue. Acta Physiologica. 2007 Nov;191(3):205–16.

168. Thissen JP, Ketelslegers JM, Underwood LE. Nutritional Regulation of the Insulin-Like Growth Factors. Endocr Rev. 1994;15(1):80–101.

169. Flemström G, Bengtsson MW, Mäkelä K, Herzig KH. Effects of short-term food deprivation on orexin-A-induced intestinal bicarbonate secretion in comparison with related secretagogues. In: Acta Physiologica. 2010. p. 373–80.

170. Raff Martin C. Social controls on cell survival and cell death. Nature. 1992;356(6368):397–400.

171. Hanahan D, Weinberg RA. Hallmarks of cancer: The next generation. Cell [Internet]. 2011;144(5):646–74. Available from: http://dx.doi.org/10.1016/j.cell.2011.02.013

172. Thissent JP, Pucilowska JB, Underwood LE. Differential Regulation of Insulin-Like Growth Factor I (IGF-I) and IGF Binding Protein-l Messenger Ribonucleic Acids by Amino Acid Availability and Growth Hormone in Rat Hepatocyte Primary Culture. Endocrinology [Internet]. 1994;134(3):1570–6. Available from: https://academic.oup.com/endo/article-abstract/134/3/1570/2496989

173. Thissen JP, Ketelslegers JM, Underwood LE. Nutritional regulation of the insulin-like growth factors. Endocr Rev. 1994;15(1):80–101.

174. Raffaghello L, Lee C, Safdie FM, Wei M, Madia F, Bianchi G, et al. Starvation-dependent differential stress resistance protects normal but not cancer cells against high-dose chemotherapy. PNAS [Internet]. 2008;105(24):8215–20. Available from: www.pnas.org/cgi/content/full/

175. Lee C, Raffaghello L, Brandhorst S, Safdie FM, Bianchi G, Martin-Montalvo A, et al. Fasting cycles retard growth of tumors and sensitize a range of cancer cell types to chemotherapy. Sci Transl Med. 2012 Mar 7;4(124).

176. Cahill George F. Jr. Fuel metabolism in starvation. Annu Rev Nutr. 2006;26(1):1–22.

177. Chan JM, Stampfer MJ, Giovannucci E, Ma J, Pollak M. Insulin-like growth factor I (IGF-I), IGF-binding protein-3 and prostate cancer risk: Epidemiological studies. In: Growth Hormone and IGF Research. Churchill Livingstone; 2000.

178. Giovannucci E, Pollak M, Platz EA, Willett WC, Stampfer MJ, Majeed N, et al. Insulin-like growth factor I (IGF-I), IGF-binding protein-3 and the risk of colorectal adenoma and cancer in the nurses' health study. In: Growth Hormone and IGF Research. Churchill Livingstone; 2000.

179. Prisco M, Romano G, Peruzzi F, Valentinis B, Baserga R. Insulin and IGF-l Receptors Signaling in Protection from Apoptosis. Horm Metab Res. 1999;31:80–9.

180. Flototto T., Djahansouzi S., Glaser M., Hanstein B., Niederacher D., Brumm C., et al. Hormones and hormone antagonists: mechanisms of action in carcinogenesis of endometrial and breast cancer. Horm Metab Res. 2001;33:451–7.

181. Giovannucci E, Pollak M, Liu Y, Platz EA, Majeed N, Rimm EB, et al. Nutritional Predictors of Insulin-like Growth Factor I and Their Relationships to Cancer in Men 1. Cancer Epidemiology, Biomarkers and Prevention [Internet]. 2003;12:84–9. Available from: http://aacrjournals.org/cebp/article-pdf/12/2/84/1742975/ce0203000084.pdf

182. Ramsey MM, Ingram RL, Cashion AB, Amy HNG, Mark Cline J, Parlow AF, et al. Growth hormone-deficient dwarf animals are resistant to dimethylbenzanthracine (DMBA)-induced mammary carcinogenesis. Endocrinology. 2002 Oct 1;143(10):4139–42.

183. Longo VD, Mattson MP. Fasting: Molecular mechanisms and clinical applications. Vol. 19, Cell Metabolism. 2014. p. 181–92.

184. Guevara-Aguirre J, Priya Balasubramanian †, Guevara-Aguirre M, Wei M, Madia F, Cheng CW, et al. Growth Hormone Receptor Deficiency Is Associated with a Major Reduction in Pro-Aging Signaling, Cancer, and Diabetes in Humans. Sci Transl Med [Internet]. 2013;3(70). Available from: http://stm.sciencemag.org/content/3/70/70ra13.full.htmlhttp://stm.sciencemag.org/content/suppl/2011/02/11/3.70.70ra13.DC1.htmlhttp://www.sciencemag.org/content/sci/331/6019/837.full.htmlcanbefoundonlineat:

185. Brandhorst S, Wei M, Hwang S, Morgan TE, Longo VD. Short-term calorie and protein restriction provide partial protection from chemotoxicity but do not delay glioma progression. Exp Gerontol. 2013 Oct;48(10):1120–8.

186. Descamps O, Riondel J, Ducros V, Roussel AM. Mitochondrial production of reactive oxygen species and incidence of age-associated lymphoma in OF1 mice: Effect of alternate-day fasting. Mech Ageing Dev. 2005 Nov;126(11):1185–91.

187. Berrigan D, Perkins SN, Haines DC, Hursting SD. Adult-onset calorie restriction and fasting delay spontaneous tumorigenesis in p53-deficient mice. Vol. 23, Carcinogenesis. 2002.

188. Tessitore L, Tomasi C, Greco M, Sesca E, Laconi E, Maccioni O, et al. A subnecrogenic dose of diethylnitrosamine is able to initiate hepatocarcinogenesis in the rat when coupled

with fasting/ refeeding. Carcinogenesis [Internet]. 1996;17(2):289–92. Available from: http://carcin.oxfordjournals.org/

189. Kirkwood TBL. Understanding the odd science of aging. Vol. 120, Cell. Elsevier B.V.; 2005. p. 437–47.

190. Blagosklonny M v. Calorie restriction: Decelerating mTOR-driven aging from cells to organisms (including humans). Vol. 9, Cell Cycle. Taylor and Francis Inc.; 2010. p. 683–8.

191. Arumugam T v., Phillips TM, Cheng A, Morrell CH, Mattson MP, Wan R. Age and energy intake interact to modify cell stress pathways and stroke outcome. Ann Neurol. 2010;67(1):41–52.

192. Harvie MN, Pegington M, Mattson MP, Frystyk J, Dillon B, Evans G, et al. The effects of intermittent or continuous energy restriction on weight loss and metabolic disease risk markers: A randomized trial in young overweight women. Int J Obes. 2011 May;35(5):714–27.

193. Sengupta S, Peterson TR, Laplante M, Oh S, Sabatini DM. mTORC1 controls fasting-induced ketogenesis and its modulation by ageing. Nature. 2010 Dec 23;468(7327):1100–6.

194. Fernando M. Safdie, Tanya Dorff, David Quinn, Luigi Fontana, Min Wei, Changhan Lee, et al. Fasting and cancer treatment in humans- A case series report. Aging. 2009;1(12).

195. Savvidis C, Koutsilieris M. Circadian rhythm disruption in cancer biology. Molecular Medicine. 2012;18(9):1249–60.

196. Grundy A, Richardson H, Burstyn I, Lohrisch C, SenGupta SK, Lai AS, et al. Increased risk of breast cancer associated with long-term shift work in Canada. Occup Environ Med. 2013 Dec;70(12):831–8.

197. Pierce JP, Natarajan L, Caan BJ, Parker BA, Robert Greenberg E, Flatt SW, et al. Influence of a Diet Very High in Vegetables, Fruit, and Fiber and Low in Fat on Prognosis Following Treatment for Breast Cancer: The Women's Healthy Eating and Living (WHEL) Randomized Trial. Vol. 298, JAMA. 2007.

198. Patterson RE, Sears DD. Metabolic Effects of Intermittent Fasting. Annu Rev Nutr [Internet]. 2017;37:371–93. Available from: https://doi.org/10.1146/annurev-nutr-071816-

199. Johnson JB, Summer W, Cutler RG, Martin B, Hyun DH, Dixit VD, et al. Alternate day calorie restriction improves clinical findings and reduces markers of oxidative stress and inflammation in overweight adults with moderate asthma. Free Radic Biol Med. 2007 Mar 1;42(5):665–74.

200. Hartwell LH, Kastan MB. Cell Cycle Control and Cancer. Science (1979) [Internet]. 1994;266(5192):1821–8. Available from: www.sciencemag.org

201. Bartkova J, Hořejší Z, Koed K, Krä Mer A, Tort F, Zieger K, et al. DNA damage response as a candidate anti-cancer barrier in early human tumorigenesis. Nature [Internet]. 2005;434(7035):864–70. Available from: www.nature.com/nature

202. Luo J, Solimini NL, Elledge SJ. Principles of Cancer Therapy: Oncogene and Non-oncogene Addiction. Vol. 136, Cell. Elsevier B.V.; 2009. p. 823–37.

203. Ganem NJ, Storchova Z, Pellman D. Tetraploidy, aneuploidy and cancer. Curr Opin Genet Dev. 2007 Apr;17(2):157–62.

204. Weaver BAA, Cleveland DW. Decoding the links between mitosis, cancer, and chemotherapy: The mitotic checkpoint, adaptation, and cell death. Vol. 8, Cancer Cell. Cell Press; 2005. p. 7–12.

205. Warburg O. On the Origin of Cancer Cells. Science (1979) [Internet]. 1956;123(3191):309–14. Available from: http://science.sciencemag.org/

206. Kroemer G, Pouyssegur J. Tumor Cell Metabolism: Cancer's Achilles' Heel. Vol. 13, Cancer Cell. Cell Press; 2008. p. 472–82.

207. DeBerardinis RJ, Lum JJ, Hatzivassiliou G, Thompson CB. The Biology of Cancer: Metabolic Reprogramming Fuels Cell Growth and Proliferation. Vol. 7, Cell Metabolism. 2008. p. 11–20.

208. Moll UM, Schramm LM. P53 - An Acrobat in Tumorigenesis. Crit Rev Oral Biol Med. 1998;9(1):23–7.

209. vander Heiden MG, Plas DR, Rathmell JC, Fox CJ, Harris MH, Thompson CB. Growth Factors Can Influence Cell Growth and Survival through Effects on Glucose Metabolism. Mol Cell Biol. 2001 Sep;21(17):5899–912.

210. Gogvadze V, Orrenius S, Zhivotovsky B. Mitochondria in cancer cells: what is so special about them? Vol. 18, Trends in Cell Biology. 2008. p. 165–73.

211. Plas DR, Thompson CB. Akt-dependent transformation: There is more to growth than just surviving. Vol. 24, Oncogene. 2005. p. 7435–42.

212. Hatzivassiliou G, Zhao F, Bauer DE, Andreadis C, Shaw AN, Dhanak D, et al. ATP citrate lyase inhibition can suppress tumor cell growth. Cancer Cell. 2005;8(4):311–21.

213. Mathew R, Kongara S, Beaudoin B, Karp CM, Bray K, Degenhardt K, et al. Autophagy suppresses tumor progression by limiting chromosomal instability. Genes Dev. 2007 Jun 1;21(11):1367–81.

214. Halazonetis TD, Gorgoulis VG, Bartek J. An Oncogene-Induced DNA Damage Model for Cancer Development. Science (1979) [Internet]. 2008;319(5968):1352–5. Available from: http://science.sciencemag.org/

215. Szatrowski TP, Nathan CF. Production of Large Amounts of Hydrogen Peroxide by Human Tumor Cells. Cancer Res [Internet]. 1991;51:794–8. Available from: http://aacrjournals.org/cancerres/article-pdf/51/3/794/2446515/cr0510030794.pdf

216. Weinhouse S., Warburg O., Burg D., Schade A. L. On respiratory impairment in cancer cells. Science (1979) [Internet]. 1956;124(3215):267–72. Available from: www.sciencemag.org

217. Raj L, Ide T, Gurkar AU, Foley M, Schenone M, Li X, et al. Selective killing of cancer cells by a small molecule targeting the stress response to ROS. Nature. 2011 Jul 14;475(7355):231–4.

218. Murga M, Campaner S, Lopez-Contreras AJ, Toledo LI, Soria R, Montaña MF, et al. Exploiting oncogene-induced replicative stress for the selective killing of Myc-driven tumors. Nat Struct Mol Biol. 2011 Dec;18(12):1331–5.

219. Pickering MT, Stadler BM, Kowalik TF. miR-17 and miR-20a temper an E2F1-induced G1 checkpoint to regulate cell cycle progression. Oncogene. 2009 Jan 8;28(1):140–5.

220. Dominguez-Sola D, Ying CY, Grandori C, Ruggiero L, Chen B, Li M, et al. Non-transcriptional control of DNA replication by c-Myc. Nature. 2007 Jul 26;448(7152):445–51.

221. Kandel ES, Skeen J, Majewski N, di Cristofano A, Pandolfi PP, Feliciano CS, et al. Activation of Akt/Protein Kinase B Overcomes a G 2 /M Cell Cycle Checkpoint Induced by DNA Damage . Mol Cell Biol. 2002 Nov 15;22(22):7831–41.

222. Raff Martin C. Social Controls on Cell Survival and Cell Death. Nature. 1992;356(6368):397–400.

223. Datta SR, Brunet A, Greenberg ME. Cellular survival: a play in three Akts. Genes Dev [Internet]. 1999;13:2905–27. Available from: www.genesdev.org

224. Kandel ES, Hay N. The Regulation and Activities of the Multifunctional Serine/Threonine Kinase Akt/PKB Introduction And Historical Perspective. Exp Cell Res [Internet]. 1999;253(1):210–29. Available from: http://www.idealibrary.com

225. Xu RH, Pelicano H, Zhang H, Giles FJ, Keating MJ, Huang P. Synergistic effect of targeting mTOR by rapamycin and depleting ATP by inhibition of glycolysis in lymphoma and leukemia cells. Leukemia. 2005;19(12):2153–8.

226. Wieman HL, Wofford JA, Rathmell JC. Cytokine Stimulation Promotes Glucose Uptake via Phosphatidylinositol-3 Kinase/Akt Regulation of Glut1 Activity and Trafficking. Mol Biol Cell [Internet]. 2007;18:1437–46. Available from: http://www.molbiolcell.org/cgi/doi/10.1091/mbc.E06

227. Roos S, Jansson N, Palmberg I, Säljö K, Powell TL, Jansson T. Mammalian target of rapamycin in the human placenta regulates leucine transport and is down-regulated in restricted fetal growth. Journal of Physiology. 2007 Jul 1;582(1):449–59.

228. Edinger AL, Thompson CB. Akt maintains cell size and survival by increasing mTOR-dependent nutrient uptake. Mol Biol Cell. 2002;13(7):2276–88.

229. Barata JT, Silva A, Brandao JG, Nadler LM, Cardoso AA, Boussiotis VA. Activation of PI3K is indispensable for interleukin 7-mediated viability, proliferation, glucose use, and growth of T cell acute lymphoblastic leukemia cells. Journal of Experimental Medicine. 2004 Sep 6;200(5):659–69.

230. Plas DR, Talapatra S, Edinger AL, Rathmell JC, Thompson CB. Akt and Bcl-xL Promote Growth Factor-independent Survival through Distinct Effects on Mitochondrial Physiology. Journal of Biological Chemistry. 2001 Apr 13;276(15):12041–8.

231. Elstrom RL, Bauer DE, Buzzai M, Karnauskas R, Harris MH, Plas DR, et al. Akt stimulates aerobic glycolysis in cancer cells. Cancer Res [Internet]. 2004;64(11):3892–9. Available from: http://cancerres.aacrjournals.org/content/64/11/3892http://cancerres.aacrjournals.org/content/64/11/3892.full.html#ref-list-1http://cancerres.aacrjournals.org/content/64/11/3892.full.html#related-urls

232. Gingras AC, Raught B, Sonenberg N. Regulation of translation initiation by FRAP/mTOR. Vol. 15, Genes and Development. 2001. p. 807–26.

233. Buzzai M, Bauer DE, Jones RG, DeBerardinis RJ, Hatzivassiliou G, Elstrom RL, et al. The glucose dependence of Akt-transformed cells can be reversed by pharmacologic activation of fatty acid β-oxidation. Oncogene. 2005 Jun 16;24(26):4165–73.

234. Gottlob K, Majewski N, Kennedy S, Kandel E, Robey RB, Hay N. Inhibition of early apoptotic events by Akt/PKB is dependent on the first committed step of glycolysis and mitochondrial hexokinase. Genes Dev. 2001;15(11):1406–18.

235. Greer EL, Brunet A. FOXO transcription factors at the interface between longevity and tumor suppression. Vol. 24, Oncogene. 2005. p. 7410–25.

236. Essers MAG, de Vries-Smits LMM, Barker N, Polderman PE, Burgering BMT, Korswagen HC. Functional interaction between β-catenin and FOXO in oxidative stress signaling. Science (1979). 2005 May 20;308(5725):1181–4.

237. Nogueira V, Park Y, Chen CC, Xu PZ, Chen ML, Tonic I, et al. Akt Determines Replicative Senescence and Oxidative or Oncogenic Premature Senescence and Sensitizes Cells to Oxidative Apoptosis. Cancer Cell. 2008 Dec 9;14(6):458–70.

238. Adhikary S, Eilers M. Transcriptional regulation and transformation by Myc proteins. Vol. 6, Nature Reviews Molecular Cell Biology. 2005. p. 635–45.

239. Bolger AM, Lohse M, Usadel B. Trimmomatic: a flexible trimmer for Illumina sequence data. Bioinformatics [Internet]. 2014 Aug 1;30(15):2114–20. Available from: https://doi.org/10.1093/bioinformatics/btu170

240. Ulgen E, Ozisik O, Sezerman OU. pathfindR: An R Package for Comprehensive Identification of Enriched Pathways in Omics Data Through Active Subnetworks. Front Genet [Internet]. 2019;10. Available from: https://www.frontiersin.org/articles/10.3389/fgene.2019.00858

241. Safran M, Rosen N, Twik M, BarShir R, Stein TI, Dahary D, et al. The GeneCards Suite. In: Practical Guide to Life Science Databases. Springer Nature Singapore; 2021. p. 27–56.

242. Stelzer G, Rosen N, Plaschkes I, Zimmerman S, Twik M, Fishilevich S, et al. The GeneCards suite: From gene data mining to disease genome sequence analyses. Curr Protoc Bioinformatics. 2016;2016:1.30.1-1.30.33.

243. Chou TC. Theoretical basis, experimental design, and computerized simulation of synergism and antagonism in drug combination studies. Vol. 58, Pharmacological Reviews. 2006. p. 621–81.

244. Chou TC, Martin N. CompuSyn for Drug Combinations and for General Dose-Effect Analysis User's Guide A Computer Program for Quantitation of Synergism and Antagonism in Drug Combinations, and the Determination of IC 50 , ED 50 , and LD 50 Values. ComboSyn Inc, Paramus, NJ [Internet]. 2005; Available from: www.combosyn.com

245. Chou TC, Talalayi P. Quantitative analysis of Dose-Effect Relationships: The Combined Effects of Multiple Drugs or Enzyme Inhibitors. Adv Enzyme Regul. 1984;22:27–55.

246. Raup-Konsavage WM, Carkaci-Salli N, Greenland K, Gearhart R, Vrana KE. Cannabidiol (CBD) Oil Does Not Display an Entourage Effect in Reducing Cancer Cell Viability in vitro. Med Cannabis Cannabinoids. 2020;3(2):95–102.

247. Booth JK, Bohlmann J. Terpenes in Cannabis sativa – From plant genome to humans. Plant Science. 2019;284(January):67–72.

248. Cherkasova V, Wang B, Gerasymchuk M, Fiselier A, Kovalchuk O, Kovalchuk I. Use of Cannabis and Cannabinoids for Treatment of Cancer. Vol. 14, Cancers. MDPI; 2022.

249. Huang M, Lu JJ, Huang MQ, Bao JL, Chen XP, Wang YT. Terpenoids: Natural products for cancer therapy. Vol. 21, Expert Opinion on Investigational Drugs. 2012. p. 1801–18.

250. Abotaleb M, Samuel SM, Varghese E, Varghese S, Kubatka P, Liskova A, et al. Flavonoids in cancer and apoptosis. Vol. 11, Cancers. MDPI AG; 2019.

251. Tomko AM, Whynot EG, Ellis LD, Dupré DJ. Anti-cancer potential of cannabinoids, terpenes, and flavonoids present in cannabis. Vol. 12, Cancers. MDPI AG; 2020. p. 1–81.

252. National Toxicology Program. NTP technical report on the toxicology and carcinogenesis studies of beta-myrcene (CAS No. 123-35-3) in F344/N rats and B6C3F1 mice (Gavage studies). Natl Toxicol Program Tech Rep Ser [Internet]. 2010;557:1–163. Available from: http://ntp.niehs.nih.gov

253. Mitić-Ćulafić D, Žegura B, Nikolić B, Vuković-Gačić B, Knežević-Vukčević J, Filipič M. Protective effect of linalool, myrcene and eucalyptol against t-butyl hydroperoxide induced genotoxicity in bacteria and cultured human cells. Food and Chemical Toxicology. 2009 Jan;47(1):260–6.

254. Luis Da Silva S, Figueiredo PM, Yano T. Cytotoxic evaluation of essential oil from Zanthoxylum rhoifolium Lam. leaves. Acta Amazon. 2007;37(2):281–6.

255. Chung KS, Hong JY, Lee JH, Lee HJ, Park JY, Choi JH, et al. B-Caryophyllene in the essential oil from chrysanthemum boreale induces G1 phase cell cycle arrest in human lung cancer cells. Molecules. 2019 Oct 18;24(20).

256. Arul S RHRJDH. Beta-Caryophyllene Suppresses Ovarian Cancer Proliferation by Inducing Cell Cycle Arrest and Apoptosis. Anticancer Agents Med Chem. 2020;20(13):1530–7.

257. Annamalai V, Kotakonda M, Periyannan V. JAK1/STAT3 regulatory effect of β-caryophyllene on MG-63 osteosarcoma cells via ROS-induced apoptotic mitochondrial pathway by DNA fragmentation. J Biochem Mol Toxicol. 2020 Aug 1;34(8).

258. di Giacomo S, di Sotto A, Mazzanti G, Wink M. Chemosensitizing properties of β-caryophyllene and β-caryophyllene oxide in combination with doxorubicin in human cancer cells. Anticancer Res. 2017 Mar 1;37(3):1191–6.

259. di Sotto A, Irannejad H, Eufemi M, Mancinelli R, Abete L, Mammola CL, et al. Potentiation of low-dose doxorubicin cytotoxicity by affecting p-glycoprotein through caryophyllane sesquiterpenes in hepg2 cells: An in vitro and in silico study. Int J Mol Sci. 2020 Jan 2;21(2).

260. Ambrož M, Matoušková P, Skarka A, Zajdlová M, Žáková K, Skálová L. The effects of selected sesquiterpenes from myrica rubra essential oil on the efficacy of doxorubicin in sensitive and resistant cancer cell lines. Molecules. 2017 Jun 1;22(6).

261. Hanušová V, Caltová K, Svobodová H, Ambrož M, Skarka A, Murínová N, et al. The effects of β-caryophyllene oxide and trans-nerolidol on the efficacy of doxorubicin in breast cancer cells and breast tumor-bearing mice. Biomedicine and Pharmacotherapy. 2017 Nov 1;95:828–36.

262. Meeran MFN, al Taee H, Azimullah S, Tariq S, Adeghate E, Ojha S. β-Caryophyllene, a natural bicyclic sesquiterpene attenuates doxorubicin-induced chronic cardiotoxicity via activation of myocardial cannabinoid type-2 (CB2) receptors in rats. Chem Biol Interact. 2019 May 1;304:158–67.

263. Ambrož M, Šmatová M, Šadibolová M, Pospíšilová E, Hadravská P, Kašparová M, et al. Sesquiterpenes α-humulene and β-caryophyllene oxide enhance the efficacy of 5-fluorouracil and oxaliplatin in colon cancer cells. Acta Pharmaceutica. 2019 Mar 1;69(1):121–8.

264. di Giacomo S, Briz O, Monte MJ, Sanchez-Vicente L, Abete L, Lozano E, et al. Chemosensitization of hepatocellular carcinoma cells to sorafenib by β-caryophyllene oxide-induced inhibition of ABC export pumps. Arch Toxicol. 2019 Mar 6;93(3):623–34.

265. Legault J, Dahl Wivecke, Debiton E, Pichette A, Madelmont JC. Antitumor activity of balsam fir oil- Production of reactive oxygen species induced by α-humulene as possible mechanism of action. Planta Med. 2003;69:402–7.

266. Tundis R, Loizzo MR, Bonesi M, Menichini F, Dodaro D, Passalacqua NG, et al. In vitro cytotoxic effects of Senecio stabianus Lacaita (Asteraceae) on human cancer cell lines. Nat Prod Res. 2009 Dec;23(18):1707–18.

267. Chen H, Yuan J, Hao J, Wen Y, Lv Y, Chen L, et al. α-Humulene inhibits hepatocellular carcinoma cell proliferation and induces apoptosis through the inhibition of Akt signaling. Food and Chemical Toxicology. 2019 Dec 1;134.

268. Ye Z, Liang Z, Mi Q, Guo Y. Limonene terpenoid obstructs human bladder cancer cell (T24 cell line) growth by inducing cellular apoptosis, caspase activation, G2/M phase cell cycle arrest and stops cancer metastasis. JBUON. 2020;25(1):280–5.

269. Jia SS, Xi GP, Zhang M, Chen YB, Lei B, Dong XS, et al. Induction of apoptosis by D-limonene is mediated by inactivation of Akt in LS174T human colon cancer cells. Oncol Rep. 2013 Jan;29(1):349–54.

270. Berliocchi L, Chiappini C, Adornetto A, Gentile D, Cerri S, Russo R, et al. Early LC3 lipidation induced by D-limonene does not rely on mTOR inhibition, ERK activation and ROS production and it is associated with reduced clonogenic capacity of SH-SY5Y neuroblastoma cells. Phytomedicine. 2018 Feb 1;40:98–105.

271. Russo R, Cassiano MGV, Ciociaro A, Adornetto A, Varano GP, Chiappini C, et al. Role of d-limonene in autophagy induced by bergamot essential oil in SH-SY5Y neuroblastoma cells. PLoS One. 2014 Nov 24;9(11).

272. Yu X, Lin H, Wang Y, Lv W, Zhang S, Qian Y, et al. D-limonene exhibits antitumor activity by inducing autophagy and apoptosis in lung cancer. Onco Targets Ther. 2018 Apr 4;11:1833–47.

273. Haag JD LMGM. Limonene-induced regression of mammary carcinomas. Cancer Res. 1992;52(14):4021–7.

274. Gould MN, Moore CJ, Zhang R, Wang B, Kennan WS, Haag JD. Limonene Chemoprevention of Mammary Carcinoma Induction following Direct in Situ Transfer of

v-Ha-ras1. Cancer Res [Internet]. 1994;54:3540–3. Available from: http://aacrjournals.org/cancerres/article-pdf/54/13/3540/2454461/cr0540133540.pdf

275. Elegbede JA, Elson CE, Tanner MA, Qureshi A, Gould MN. Regression of Rat Primary Mammary Tumors Following Dietary d-Limonene. J Natl Cancer Inst. 1986;76(2):323–5.

276. Nakaizumi A, Baba M, Uehara H, Iishi H, Tatsuta M. d-Limonene inhibits N-nitrosobis(2-oxopropyl)amine induced hamster pancreatic carcinogenesis. Cancer Lett. 1997;117(1):99–103.

277. Manuele MG, Arcos Barreiro ML, Davicino R, Ferraro G, Cremaschi G, Anesini C. Limonene exerts antiproliferative effects and increases nitric oxide levels on a lymphoma cell line by dual mechanism of the ERK pathway: Relationship with oxidative stress. Cancer Invest. 2010;28(2):135–45.

278. Lu XG, Zhan LB, Feng BA, Qu MY, Yu LH, Xie JH. Inhibition of growth and metastasis of human gastric cancer implanted in nude mice by d-limonene. World J Gastroenterol [Internet]. 2004 Jul 15;10(14):2140–4. Available from: https://pubmed.ncbi.nlm.nih.gov/15237454

279. Uedo N, Tatsuta M, Iishi H, Baba M, Sakai N, Yano H, et al. Inhibition by d-limonene of gastric carcinogenesis induced by N-methyl-N H-nitro-N-nitrosoguanidine in Wistar rats. Cancer Lett. 1999;137:131–6.

280. Kumar Giri R, Paru T, Das BR. d-limonene chemoprevention of hepatocarcinogenesis in AKR mice: Inhibition of c-jun and c-myc. Vol. 6, ONCOLOGY REPORTS. 1999.

281. Miller JA, Pappan K, Thompson PA, Want EJ, Siskos AP, Keun HC, et al. Plasma metabolomic profiles of breast cancer patients after short-term limonene intervention. Cancer Prevention Research. 2015 Jan 1;8(1):86–93.

282. Hou J, Zhang Y, Zhu Y, Zhou B, Ren C, Liang S, et al. A-Pinene induces apoptotic cell death via caspase activation in human ovarian cancer cells. Medical Science Monitor. 2019 Sep 4;25:6631–8.

283. Xu Q, Li M, Yang M, Yang J, Xie J, Lu X, et al. α-pinene regulates miR-221 and induces G2/M phase cell cycle arrest in human hepatocellular carcinoma cells. Biosci Rep. 2018 Dec 11;38(6).

284. Zhao Y, Chen R, Wang Y, Yang Y. α-pinene inhibits human prostate cancer growth in a mouse xenograft model. Chemotherapy. 2018 Feb 1;63(1):1–7.

285. Li YL, Yeung CM, Chiu LCM, Cen YZ, Ooi VEC. Chemical Composition and Antiproliferative Activity of Essential Oil from the Leaves of a Medicinal Herb, Schefflera heptaphylla. Phytother Res [Internet]. 2009;23:140–2. Available from: www.interscience.wiley.com

286. Zhang Z, Guo S, Liu X, Gao X. Synergistic antitumor effect of α-pinene and β-pinene with paclitaxel against non-small-cell lung carcinoma (NSCLC). Drug Res. 2015 Apr 1;65(4):214–8.

287. Chen WQ, Xu B, Mao JW, Wei FX, Li M, Liu T, et al. Inhibitory effects of α-pinene on hepatoma carcinoma cell proliferation. Asian Pacific Journal of Cancer Prevention. 2014;15(7):3293–7.

288. Chen W, Liu Y, Li M, Mao J, Zhang L, Huang R, et al. Anti-tumor effect of α-pinene on human hepatoma cell lines through inducing G2/M cell cycle arrest. J Pharmacol Sci. 2015;127(3):332–8.

289. Matsuo AL, Figueiredo CR, Arruda DC, Pereira F v., Borin Scutti JA, Massaoka MH, et al. α-Pinene isolated from Schinus terebinthifolius Raddi (Anacardiaceae) induces apoptosis and confers antimetastatic protection in a melanoma model. Biochem Biophys Res Commun. 2011 Jul 29;411(2):449–54.

290. Russo EB. Taming THC: potential cannabis synergy and phytocannabinoid-terpenoid entourage effects. Br J Pharmacol [Internet]. 2011;163:1344–64. Available from: http://dx.doi.org/10.1111/bph.2011.163.issue-7www.brjpharmacol.org

291. Komatsu M, Kurokawa H, Waguri S, Taguchi K, Kobayashi A, Ichimura Y, et al. The selective autophagy substrate p62 activates the stress responsive transcription factor Nrf2 through inactivation of Keap1. Nat Cell Biol. 2010 Mar;12(3):213–23.